



**DOTTORATO DI RICERCA IN INGEGNERIA CIVILE PER
L'AMBIENTE ED IL TERRITORIO**
XII Ciclo - Nuova Serie (2011-2013)
DIPARTIMENTO DI INGEGNERIA CIVILE, UNIVERSITÀ DEGLI STUDI DI SALERNO

TESI DI DOTTORATO

**QUANTIFYING THE RISK TO LIFE POSED
BY HYPERCONCENTRATED FLOWS**

**(ANALISI QUANTITATIVA DEL RISCHIO PER LA VITA
UMANA DA FLUSSI IPERCONCENTRATI)**

ING. GIOVANNA DE CHIARA

Relatore:
PROF. ING. LEONARDO CASCINI

Coordinatore
PROF. ING. VINCENZO BELGIORNO

Correlatore:
PROF. ING. SETTIMIO FERLISI

QUANTIFYING THE RISK TO LIFE POSED BY HYPERCONCENTRATED FLOWS

Copyright © 2014 Università degli Studi di Salerno – via Giovanni Paolo II, 132 – 84084 Fisciano (SA), Italy – web: www.unisa.it

Proprietà letteraria, tutti i diritti riservati. La struttura ed il contenuto del presente volume non possono essere riprodotti, neppure parzialmente, salvo espressa autorizzazione. Non ne è altresì consentita la memorizzazione su qualsiasi supporto (magnetico, magnetico-ottico, ottico, cartaceo, etc.).

Benché l'autore abbia curato con la massima attenzione la preparazione del presente volume, Egli declina ogni responsabilità per possibili errori ed omissioni, nonché per eventuali danni dall'uso delle informazione ivi contenute.

Finito di stampare il 31/01/2014

To Professor Sorbino

TABLE OF CONTENTS

Table of contents.....	i
List of figures	v
List of tables	xi
Sommario	xiii
Abstract.....	xvii
Acknowledgements	xxi
About the author	xxiii
1 Introduction	1
2 The flow-like phenomena	5
2.1 Classification and general features	7
2.2 Debris flows	14
2.3 Hyperconcentrated flows	16
3 Risk analysis.....	21
3.1 General framework of the risk management process.....	23
3.2 Risk analysis.....	25
3.2.1 Scope definition.....	25
3.2.2 Hazard analysis	26
3.2.3 Consequence analysis.....	28
3.2.4 Risk estimation.....	34
3.2.1 Qualitative or Quantitative risk estimation.....	34
4 Risk zoning.....	39
4.1 General tools	40
4.2 The italian case study	45
4.3 Risk zoning in Italy.....	47
4.4 From qualitative to quantitative risk analisys and zoning.....	49
5 Quantitative risk analysis at medium scale: the Campania Region case study.....	51
5.1 The Campania Region.....	53
5.2 The historical database.....	54
5.3 F-N curves for the Campania Region.....	55
5.4 Features of different flow-like phenomena	58
5.5 Frequency analysis at regional scale of the two considered classes of flow-like phenomena	69

6	Investigation at site-specific scale for QRA	77
6.1	The test site.....	78
6.2	Geological and Hydrogeological settings.....	79
6.3	Geomorphological setting.....	82
6.4	In situ tests.....	84
6.5	Laboratory test results.....	87
6.6	In situ test results.....	88
6.6.1	Spatial distribution of the pyroclastic soils and their thickness	88
6.6.1	Soil suction regime.....	94
6.7	Analysis of historical incident data.....	95
6.7.1	Results of the historical analysis.....	96
7	Slope evolution model of Monte Albino massif.....	101
7.1	Analysis of geomorphological processes.....	101
7.2	Characterisation of morphological units.....	103
7.3	Characterisation of mountain catchments	106
7.4	Characterisation and classification of alluvial fans.....	112
7.5	Empirical analysis of field surveys results	115
7.6	Geomorphological slope evolution.....	118
7.7	General features of the prevailing slope instabilities	126
8	Geotechnical model and hazard analysis at site-specific scale.....	129
8.1	Susceptibility analysis	129
8.2	The frequency analysis	131
8.3	Modelling the triggering mechanisms.....	133
8.3.1	Modelling of surface erosion phenomena: The LISEM MODEL.....	135
8.3.2	Modelling of surface erosion phenomena: The input parameters	140
8.3.3	Modelling of the channel's sides instability	147
8.4	Hazard analysis.....	151
8.5	Run-out analysis.....	156
9	Quantitative estimation of the risk for life loss at the site-specific scale	165
9.1	The adopted procedure.....	165
9.2	Consequences analysis	166
9.2.1	Element at risk and their temporal-spatial probability....	166
9.2.1	Vulnerability of the elements at risk	169
9.3	Quantitative estimation of the risk for life loss.....	171
10	Concluding remarks	177

References181

LIST OF FIGURES

Figure 2.1 Number of natural disasters between 1900 - 2011 (source EM-DAT www.emdat.be).....	6
Figure 2.2 Main type of flow-like phenomena (Hutchinson, 1988).....	9
Figure 2.3 Continuous spectrum of sediment concentration. (Hutchinson, 1988).....	10
Figure 2.4 Classification of flow-like phenomena as a function of solid fraction and material type (Coussot and Meunier, 1996).	11
Figure 2.5 Processes causing dilution of mass and hyperconcentrated flows (Svendsen et al., 2003).....	19
Figure 3.1 Framework for landslide risk management (Fell et. al, 2008).24	
Figure 3.2 Vulnerability curves adopted in the QRA process by the Engineering Control Office in Hong Kong (Wong et al., 2005).....	34
Figure 4.1 Landslide Index (%). Calculated on a mesh size of 1 km expresses the landslides incidence on the regional territory potentially affected by landsliding phenomena (www.isprambiente.gov.it).....	46
Figure 5.1 a) The territory of the Campania region (southern Italy); b) Map of the areas of the Campania region where pyroclastic soils cover different bedrocks (modified from Vitolo, 2009).....	53
Figure 5.2 F-N curves related to fatal landslides in the territory of Campania region and Italy (Cascini et al., 2008 b, modified).	56
Figure 5.3 F-N curves related to fatal landslides in the Campania region and in different geo-environmental contexts. All curves refer to a 366-year period between 1640 and 2006 (Cascini et al., 2008 b).	57
Figure 5.4 Cumulative curve of flow-like phenomena occurred a) in the territory of Campania region and b) in the geological contexts (A1, A2, B, C) from the 16 th century to 2011.....	59
Figure 5.5 Montly distribution of a) debris flows and b) hyperconcentrated flows in the geo-environmental context A1 of the Campania region.....	61
Figure 5.6 Example of frontal rainfall events triggering debris flows (reconstruction obtained by CERIOUS, 2003).....	63

Figure 5.7 Rain events monitored at a) Lauro Town for the debris flows occurred in May 1998 and at b) S. Martino Valle Caudina Town for the debris flows occurred in December 1999 (reconstruction obtained by CERIUS, 2003).....	64
Figure 5.8 Example of meteorological structures attributable to the occurrence of hyperconcentrated flows: a) Isolated convective cells; b) Hurricane - like rainfall.....	65
Figure 5.9 Rain events monitored at a) Nocera Inferiore Town for the hyperconcentrated flows occurred in September 1955 and at b) Salerno Town for the hyperconcentrated flows occurred in October 1954.....	66
Figure 5.10 Spatial distribution in the geological context A1 of municipal territories historically affected by hyperconcentrated flows.	67
Figure 5.11 Spatial distribution in the geological context A1 of municipal territories historically affected by debris flows.....	68
Figure 5.12. F-I _n curves for hyperconcentrated flows and debris flows.	70
Figure 5.13 F-I _a curves for hyperconcentrated flows and debris flows... ..	71
Figure 5.14 Cumulative curves of hyperconcentrated flows events and Vesuvius eruptions interesting the geological context A1.....	72
Figure 5.15 F-I _n curves for hyperconcentrated flows with reference to different time periods.	73
Figure 5.16 F-N curve for hyperconcentrated flows with reference to the 20 th century.....	74
Figure 5.17 F-N curves for hyperconcentrated flows and debris flows..	74
Figure 6.1 a) Geographical setting of the test site of Monte Albino (Google Earth image); b) General overview of Monte Albino slope (photo dated 2011).....	78
Figure 6.2 Geological map of Monte Albino.	80
Figure 6.3 Hydrogeological map of Monte Albino.	82
Figure 6.4 DTM obtained on the basis of the data achieved via a LIDAR survey technique (Avioriprese s.r.l., edition of 2005, 1:1,000 scale), with indication of the sites where the in-situ tests were carried out.....	85
Figure 6.5 In-situ tests: a) Iron-rod drilling; b) Man-made pit; c) Suction measurement; d) Seismic field test; e) Seismograph; d) Dynamic Penetration test.	85
Figure 6.6 Grain size distribution of the investigated pyroclastic soil specimens.	88
Figure 6.7 Soil cover thickness map.	90
Figure 6.8 Typical trend of vertical stratigraphic intervals.	91
Figure 6.9 Areal distribution of vertical stratigraphic trend.....	92

Figure 6.10 Areal distribution of the class A' lithotype.	93
Figure 6.11 Areal distribution of the class B' lithotype.....	93
Figure 6.12 Soil suction measurements.....	94
Figure 6.13 Suction value for Pizzo d'Alvano massif (Cascini and Sorbino, 2002).....	95
Figure 6.14 Urbanised areas affected by hyperconcentrated flows occurred during the 18 th and the 19 th centuries.....	97
Figure 6.15 Cumulative distributions of: i) Vesuvius explosive eruptions occurred from 1631 up to now; ii) hyperconcentrated flow incident data (events occurred after the Vesuvius eruptions are circled in red).	99
Figure 6.16. Monthly distribution of the hyperconcentrated flows which, in the past, interested the Monte Albino hillslope.....	100
Figure 7.1 Morphotypes map.	102
Figure 7.2 Slope angle map.	104
Figure 7.3 Exposure map.	105
Figure 7.4 Morphological zoning map.	106
Figure 7.5 Mountain catchments along the Monte Albino hillslopes superimposed to a DTM derived from 1-m resolution data achieved via a LiDAR survey.	107
Figure 7.6 Longitudinal and transversal track section.....	108
Figure 7.7 Typical longitudinal profile.	109
Figure 7.8 Typical transversal profile.	111
Figure 7.9 Transversal profile type distribution.....	111
Figure 7.10 Alluvial fan distribution.	113
Figure 7.11 Field surveys deriving from ISPRA and Nocera Inferiore Municipality.....	114
Figure 7.12 Iron-rod drillings data correlation with a) slope angle, b) slope angle with N-E exposure, c) elevation and d) curvature.....	116
Figure 7.13 Dynamic penetration tests correlation with a) slope angle, b) exposure towards the North, c) elevation and d) curvature.....	116
Figure 7.14 Correlation between the real thickness of the pyroclastic soils and the slope angle.....	117
Figure 7.15 Map of theoretical thickness of the pyroclastic soils.....	118
Figure 7.16 Ranking of $E_{s,bi}$ index.	120
Figure 7.17 Ranking of $E_{m,bi}$ index.	121
Figure 7.18 Ranking of $E_{m,ui}$ index.....	122
Figure 7.19 Frontal view of the landslide occurred on March 2005.....	128
Figure 8.1 Susceptibility map of triggering area of hyperconcentrated flows.	131

Figure 8.2 Cumulative distributions of hyperconcentrated flow events and Vesuvius explosive eruptions.....	132
Figure 8.3 Pluviometric probabilistic curves for the Monte Albino test site.....	134
Figure 8.4 Flowchart of the LISEM model (from De Roo and Jetten, 1999).....	137
Figure 8.5 Different scenarios of rainfall event.	140
Figure 8.6 The adopted soil-water retention relationships (adapted from Bilotta et al., 2005).....	142
Figure 8.7 Computational slope section constituted of a) pyroclastic soils belonging to class B' and b) pyroclastic soils belonging both lithotypes (A' and B').....	143
Figure 8.8 Soil loss volume value per unit area for different rainfall scenario.	145
Figure 8.9 Mixture hydrograph and relative volumetric concentrations at the outlet of mountain catchment B1 for different return period T.	146
Figure 8.10 Examined cross-section tracks.	147
Figure 8.11 Local coordinate system.	148
Figure 8.12 Instability analysis for a) T=50 years, b) T=100 years, c) T=200 years.....	150
Figure 8.13 F-M curves for Monte Albino slope.....	152
Figure 8.14 Hazard maps of hyperconcentrated flows: a) T= 50 years, b) T=100 years and c) T=200 years.	154
Figure 8.15 Relationship between hazard and susceptibility in terms of mobilised normalised volumes.	155
Figure 8.16 Map of the run-out simulation, via the use of FLO-2D numerical code, of hyperconcentrated flows occurred on 12 September 1955.....	161
Figure 8.17 Maps of the maximum flow depth (d) reached by the FLO-2D simulated flowing mixtures in each of the computational grid cells for the three considered hazard scenarios (T = 50, 100 and 200 years).	163
Figure 8.18 Maps of the maximum flow velocity (v) reached by the FLO-2D simulated flowing mixtures in each of the computational grid cells for the three considered hazard scenarios (T = 50, 100 and 200 years).	164
Figure 9.1 Map of the census tracts (data from the Italian National Institute of Statistics-ISTAT 2001 census).....	168

Figure 9.2 Individual total risk map for the average exposed people in open space posed by hyperconcentrated flows.....171
Figure 9.3 Individual total risk map for the most exposed people living within buildings potentially impacted by hyperconcentrated flows.....172
Figure 9.4 Urbanised sectors at risk.....173
Figure 9.5 Ranking of the urbanised sectors at risk.174

LIST OF TABLES

Table 2.1 Global landslides statistics between 1900-2011 (source EM-DAT www.emdat.be).....	6
Table 2.2 Abbreviated classification of Slope Movements (Cruden, 1978).....	8
Table 2.3 Landslides velocity scale (Cruden and Varnes, 1996).....	8
Table 2.4 General Rheologic Classification of Water and Sediment Flows in Channels (Costa, 1988).	11
Table 2.5 Classification of flow-like phenomena (Hungr et al., 2001). ...	13
Table 2.6 Observed or measured characteristics of hyperconcentrated flows to approximate times of peak sediment (Pierson, 2005).....	17
Table 3.1 Example of assessment by a direct approach of Vulnerability for person in open space (extracted from Finlay et al., 1997).	33
Table 3.2 Example of a method for qualitative risk estimation to property (Extracted from AGS, 2000).	35
Table 4.1 Methods, levels, and types of zoning at different scales (Cascini, 2008 mod.).	43
Table 4.2 Landslide zoning mapping scales and their application (Fell et al., 2008 mod.).....	44
Table 5.1 Classification of area at risk with reference to flow-like phenomena.....	57
Table 5.2. Fatal events of hyperconcentrated flows recovered in the 20 th century.....	73
Table 6.1 Range of main physical properties of A' and B' ashy soils.	87
Table 6.2 Average values of shear strength parameters of A' and B' ashy soils.....	87
Table 6.3 Recorded incident data of hyperconcentrated flows occurred from 1707 to 1846, with indication of the affected areas.....	97
Table 7.1 Morphometric characteristics of the mountain catchments..	107
Table 7.2 Active alluvial fan volume.....	115
Table 7.3 $E_{s,bi}$ index value for each mountain catchment of Monte Albino hillslope.....	119
Table 7.4 $E_{m,bi}$ index value for each mountain catchment of Monte Albino hillslope.....	121

Table 7.5 Residual pyroclastic soil volumes per unit area.	123
Table 7.6 V_m Index value.....	124
Table 7.7 Comparison of morphological indices at the mountain catchment scale.....	125
Table 8.1 Susceptibility matrix for the triggering of hyperconcentrated flows.	130
Table 8.2 Main data on the critical rainfalls that triggered hyperconcentrated flows over Monte Albino hillslope.	133
Table 8.3 Rainfall characteristics for Monte Albino test site.	134
Table 8.4 Input parameter values of LISEM for the different types of use of land.	143
Table 8.5 Sediment concentration by volume and soil loss volume at the outlet of mountain catchments for different return period 'T'.	144
Table 8.6 Instability channel's sides volumes and volumetric concentration of sediments.....	151
Table 8.7 Hazard matrix for the triggering of hyperconcentrated flows.	153
Table 8.8 An overview of several 2D dynamic numerical run-out models (from Quan Luna, 2012)	158
Table 9.1 Global indicator values (GI_k) associated to the different census tracts and the corresponding temporal-spatial probabilities pertaining to the average persons at risk living within.	168
Table 9.2 Temporal-spatial probability value adopted on the basis of the age of the inhabitants for most exposed persons.	169
Table 9.3 $V_{(D:T)}$ values adopted with reference to the vulnerability of the average person in open space exposed at the hyperconcentrated flow risk.	170
Table 9.4 $V_{(D:T)}$ values adopted with reference to the vulnerability of the person most exposed at the hyperconcentrated flow risk.....	170
Table 9.5. Average number of expected casualties per event for each of the considered urbanised sector at risk.	173

SOMMARIO

Nei ultimi anni, a causa del notevole incremento della pressione demografica e dell'uso indiscriminato del territorio, i disastri causati dai fenomeni franosi sono risultati in tragico aumento.

Nell'ambito delle diverse tipologie di frane, alla categoria dei "flussi" - che in molti casi affliggono aree vaste - si associano le più gravi conseguenze in termini di perdita di vita umana e di danni economici. Pertanto, la comprensione dei meccanismi che si associano alle loro diverse fasi di movimento, come pure la previsione e la mitigazione del rischio ad esse associato, rappresentano aspetti conoscitivi e applicativi di fondamentale importanza nelle iniziative mirate alla salvaguardia della vita umana. Per la rilevanza del tema, si è assistito ad un crescente interesse da parte della Comunità tecnica e scientifica verso lo sviluppo di criteri volti all'analisi del rischio da frana, promuovendo il ricorso a metodologie di tipo quantitativo (Corominas et al., 2013).

La presente Tesi si concentra sull'utilizzo di procedure di analisi quantitative del rischio (QRA) finalizzate, nello specifico, alla stima del rischio di perdita di vita da fenomeni franosi di flusso.

Le forti ricadute applicative del QRA risiedono nella possibilità di superare alcuni limiti insiti nelle procedure di stima qualitativa, permettendo di affrontare in maniera compiuta e semplice i problemi legati alla gestione del rischio (ad esempio, la classificazione delle aree che prioritariamente necessitano di azioni di mitigazione del rischio o l'allocazione delle risorse finanziarie ed economiche ad esse associate). Tuttavia, a livello internazionale sono forniti principalmente contributi di carattere teorico sull'argomento. Tale circostanza è da legare alla intrinseca complessità delle procedure da adottare nel QRA e alla significativa mole di dati di input necessari (sia di natura tecnica e sia di natura socio-economica). A tal proposito, la presente Tesi si pone il principale obiettivo di superare le difficoltà insite nel QRA applicando, migliorando ed ottimizzando il suo impiego come strumento formale e strutturato utile ai professionisti coinvolti nel complesso processo di gestione del rischio da frana.

A tal riguardo, le attività di ricerca si sono concentrate sulla stima quantitativa del rischio di perdita di vita umana, a scala media e di sito, a seguito del verificarsi di flussi iperconcentrati.

La Tesi fornisce, preliminarmente, una descrizione delle principali caratteristiche dei fenomeni di flusso, rivolgendo particolare attenzione alle colate e ai flussi iperconcentrati. Vengono, nel seguito, discussi i fondamenti teorici e gli approcci metodologici (con i loro limiti e potenzialità) dell'analisi del rischio e della conseguente zonazione condotta con procedure di stima qualitativa e quantitativa. Si presenta, quindi, un inquadramento generale della zonazione del rischio vigente in Italia, condotta attraverso procedure di stima qualitativa.

Sulla base di tali premesse, si evidenziano i benefici rilevanti che, a livello regionale e a scala di sito, possono derivare dall'impiego di una procedura di stima quantitativa del rischio rispetto ad una qualitativa.

A scala media, l'analisi di documenti storici di eventi franosi occorsi nella regione Campania (sud Italia) ha consentito l'individuazione e la caratterizzazione delle differenti fenomenologie di flusso rapido che in essa possono manifestarsi. In particolare, queste ultime sono state individuate in un contesto geologico omogeneo, i cui versanti carbonatici sono ricoperti da terreni piroclastici sistematicamente affetti da fenomeni di instabilità, legati ad eventi pluviometrici critici, evoluti - spesso con catastrofiche conseguenze in termini di perdita di vita e di proprietà - in colate o flussi iperconcentrati.

Studi così approfonditi hanno consentito il raggiungimento di risultati originali dai quali sono scaturite considerazioni di grande interesse applicativo sulla distribuzione spaziale e temporale (in termini di frequenza) delle fenomenologie di interesse e sulle condizioni iniziali e al contorno che preludono al loro accadimento.

A scala di dettaglio, l'attività di ricerca si è incentrata sulla stima quantitativa del rischio di perdita di vita con riferimento alla popolazione residente nell'area urbanizzata ai piedi del Monte Albino (ubicato nel Comune di Nocera Inferiore (SA), Regione Campania), a seguito del verificarsi di flussi iperconcentrati.

L'originalità delle procedure proposte consiste nel coniugare i fondamenti della teoria del rischio con l'approccio geotecnico, puntando alla profonda comprensione della meccanica che presiede alle diverse e complesse fasi di movimento dei fenomeni oggetto d'interesse.

A tal fine, si sono condotte indagini in sito molto approfondite (aventi lo scopo di inquadrare le caratteristiche geologiche e geomorfologiche del

versante e di identificare i fattori che lo predispongono a differenti fenomeni di instabilità, di caratterizzare la distribuzione areale delle coltri piroclastiche e il loro assetto lito-stratigrafico) ed analisi di laboratorio (al fine di avere una completa caratterizzazione fisica e meccanica dei terreni coinvolti). Tale studio ha rappresentato il presupposto indispensabile per la corretta modellazione ingegneristica dei fenomeni a scala di dettaglio - dalla fase di innesco a quella di propagazione - pervenendo in tal modo a diversi scenari di pericolosità.

I risultati ottenuti sono stati impiegati per la stima delle conseguenze attese in termini di perdita di vita umana con riferimento sia all'individuo maggiormente esposto all'interno di ciascun edificio impattato dal flusso (a cui compete la più alta probabilità spaziale e temporale) e sia all'individuo mediamente esposto al rischio in spazi aperti (il cui comportamento è mediamente rappresentativo di un insieme di persone).

La procedura di stima quantitativa del rischio ha consentito, infine, di classificare le porzioni di territorio urbanizzato a rischio e, di conseguenza, di individuare le aree che necessitano prioritariamente di interventi strutturali di mitigazione del rischio.

ABSTRACT

In recent years, the disasters caused by landslides tragically increased due to the demographic growth and the indiscriminate use of land. Among the different types of landslides, flow-like phenomena - often simultaneously affecting large areas - are associated with the most catastrophic consequences in terms of loss of human life and economic damage.

Understanding, forecasting and controlling the risk posed by flow-like phenomena are now recognised to be a priority for the safety of human life. As a result, a growing interest of both technical and scientific Communities, in performing risk analyses aimed at estimating the risk in a quantitative way has been recorded (Corominas et al., 2013).

This PhD Thesis focus on the use of the quantitative risk analysis (QRA) procedures, specifically aimed at estimating the risk to life posed by flow-like phenomena.

The use of QRA can allow the overcoming of some limits inherent to qualitative risk analyses in addressing practical problems (i.e. the prioritisation of management and mitigation actions as well as the allocation of associated resources). However, mainly theoretical contributions are provided on the topic at the international level. This can be due to the complexity of the procedures to be adopted for QRA purposes as well as to the significant amount of required input data (of both technical and socio-economic nature). The main goal of this research is to fill this gap by applying, improving and optimising the use of the QRA as a formal and structured tool for professionals involved in the management of the risk posed by flow-like phenomena.

In this regard, the research activities focus on the quantitative estimation of the risk for loss of life, at medium and site-specific scale, posed by the occurrence of hyperconcentrated flows.

The Thesis preliminarily provides a description of the main features of the flow-like phenomena, with an emphasis to those dealing with debris flows and hyperconcentrated flows. Then, the basic concepts and methodological approaches (with their limits and potentialities) of both qualitative and quantitative risk analysis and zoning are discussed. An

overview of the current risk zoning in Italy, performed via qualitative risk analyses, is thus presented.

On the basis of the above premises, the relevant benefits that, at regional and at site-specific scales, can be achieved passing from a qualitative to a quantitative risk analysis are highlighted.

At medium scale, the analysis of historical records of landslide events in the Campania region (southern Italy) allows the identification and the characterisation of the different flow-like phenomena that may occur. In particular, these latter are individuated within a homogeneous geological context where carbonate slopes are covered by pyroclastic soils systematically affected by rainfall-induced slope instabilities later propagating as – often catastrophic in terms of life and properties losses – debris flows or hyperconcentrated flows.

The thorough studies and researches carried out as well as the original results achieved allow to make relevant considerations – from both technical and scientific points of view – concerning both their spatial and temporal distribution (in terms of frequency) and the initial and boundary conditions which influence their occurrence.

At detailed scale, the research activity focus on the quantitative estimate of the risk to life loss with reference to residents at the toe of Monte Albino (located in the Municipality of Nocera Inferiore (SA), Campania region), posed by the occurrence hyperconcentrated flows.

The novelty of the proposed procedure consists in conjugating the fundamentals of the risk theory with the geotechnical approach, providing a deeper understanding of the mechanisms that leads to the different and complex stages of movement. To this aim, a thorough in-situ investigations (with the purpose of framing the geological and geomorphological characteristics and to identify the 'hillslope' proneness to different slope instabilities, to characterise the spatial distribution of soil pyroclastic covers and their litho-stratigraphic structure) and laboratory tests (in order to have a complete physical and mechanical characterisation of the involved soils) are carried out. This study represents the indispensable prerequisite for the correct engineering modelling of phenomena at detailed scale - from the triggering stage to the propagation stage - obtaining in this way the definition of different hazard scenarios.

The obtained results are used to estimate the expected consequences in terms of loss of human life with reference both to the most exposed persons within each of the impacted houses (to which corresponds the

highest temporal-spatial probability) and to the average exposed person in open space (representing the average behaviour of a group of people). Finally, the procedure of quantitative risk estimate has allow to rank the portions of the urbanised territory at risk and, consequently, to provide a prioritisation of the areas needing structural mitigation measures.

ACKNOWLEDGEMENTS

The extraordinary experience of the PhD course has been characterised by an infinite variety of positive emotions and great satisfaction. It would not have been possible without the involvement of many people to whom I want to express my deepest and most sincere gratitude.

Above all, I would like to say a special thanks to my tutor Prof. Leonardo Cascini for making possible the attainment of this long path of cultural and human growth and for his trust in me, for which I will always be indebted. I am very grateful for his continuous encouragement and guidance throughout this exciting challenge.

Words can never be enough to thank my co-tutor Prof. Settimio Ferlisi that can be defined as my "*SHADOW*". He was always available in good and bad times, with the right solution and smart approach for every situation. Thanks for going through every word of this thesis and making the right comments.

Special thanks go to Doct. Fabio Matano for his availability and for the interesting discussion about the geologic aspects that allowed me to improve this work.

A heartfelt thanks to Prof. Sorbino who with his critical spirit has given me valuable suggestions and support for the development of the thesis. I am sure that in heaven He can appreciate and He will be proud of the obtained results.

A dutiful thanks go to the whole Teachers's College of the PhD Course of Civil and Environmental Engineering for the helpful suggestions provided.

I cannot miss in this list all colleagues and all people that animate the geotechnical laboratory "Giuseppe Sorbino" and that, in one way or another, have contributed to my scientific work giving me friendship and moral support.

A big thanks goes to my parents and my family who have supported and encouraged me during these years of study keeping me always harmonious.

I would like to thank Tommaso, the special person with whom I shared joys, concerns and satisfactions...Thanks for always being there for me!

The work carried out in this PhD Thesis was partially founded by POR CAMPANIA Rete di Eccellenza FSE. Progetto "*Tecnologie e monitoraggio ambientale per la sostenibilità delle Aree Vaste*" (TEMASAV), cod Ufficio 4-17-11, cod. CUP B25B09000090009.

ABOUT THE AUTHOR

Giovanna De Chiara si laurea nel Settembre 2010 in Ingegneria per l'Ambiente ed il Territorio - Difesa del Suolo - presso l'Università degli Studi di Salerno con votazione 110/110 e lode. Nel Febbraio 2011 supera l'esame di ammissione al Dottorato di Ricerca in Ingegneria Civile per l'Ambiente ed il Territorio (XII ciclo Nuova Serie) presso l'Università degli Studi di Salerno. Durante il Corso di Dottorato si dedica a tematiche di ricerca inerenti la stima del rischio, per il singolo individuo e per la società, connesso all'accadimento di fenomeni franosi di flusso rapido. Allo scopo di approfondire tali tematiche segue numerosi seminari e corsi nell'ambito di Scuole di Alta Formazione, svolgendo parte dell'attività di studio e ricerca presso la facoltà di Geo-Information Science and Earth Observation dell'Università di Twente in Enschede, Olanda.

Giovanna De Chiara graduated in September 2010 in Environmental Engineering at the University of Salerno with 110/110 cum laude. In February 2011 she passed the admission exam for the PhD course in Civil and Environmental Engineering (XII cycle- New Series) at the University of Salerno. During the PhD course she developed research topics on individual and societal risk estimation, related to the occurrence of fast moving flow-like landslides. To deepen these themes, she has taken several seminars and courses within PhD International Schools, undertaking part of her study and research activities at the Faculty of Geo-Information Science and Earth Observation of the University of Twente in Enschede, Netherlands.

1 INTRODUCTION

In recent years, due to a significant increase of human pressure and the consequent aggressive and indiscriminate use of land, landslides have become a major problem with regard to the safety of the population and damage to residential areas, infrastructures, service networks and to the environmental heritage. Specifically, the most serious consequences in terms of loss of life and damage to the economic goods are, generally, associated with flow-type slope movements, widespread all over the World and involving different geological contexts. The catastrophic characters of these phenomena are essentially related to the little or no warning signs, long travel distances and high velocities during the propagation stage. The relevance of societal consequences require the setting up of proper protection strategies aimed at avoiding or mitigating their effects. To this aim, the landslide risk analysis surely represents a fundamental issue as it provide, for a given area, the estimation of the level of risk to which the people or properties are exposed. It can be based on different conceptual assumptions, techniques and tools and it can be used at different scales of analysis in relation to the available dataset and to the purposes to be achieved.

The studies and research carried out in the present Thesis are focused on the use of the quantitative risk analysis (QRA) to life loss posed by flow-like phenomena in a complex geological context, in which the slopes are covered by pyroclastic soils. The main goal of this research is to apply, improve and optimise the use of the QRA as a formal and structured tool for scientists and engineers involved in the management of the risk in order to provide an helpful decisional support for the proper identification and design of the most appropriate structural mitigation measures.

Particularly, Chapter 2 provides an overview of the main features of flow-like phenomena, on the basis of the scientific classifications. Within the wider category of this phenomena, particular attention is given on two types: debris flows and hyperconcentrated flows.

The Chapter 3 focuses on the methodological approach, shared by the international scientific Community, of landslide risk management and summarises the current risk analysis state of practice.

Chapter 4 concerns with the different approaches, methods, levels, types and purposes of landslide risk zoning. In particular, it describes the current zoning in Italy, stressing on its potentialities and limits.

In the chapter 5 the main results of an historical analysis of past flow-like events occurring in the Campania Region, aimed at the quantification of societal landslide risk, are discussed. In particular, studies are mainly directed to the recognition of the frequency occurrence of different types of flow-like events, namely debris flows and hyperconcentrated flows, belonging to the wide category of flow-like phenomena. The achieved results lead to important implications in terms of classification of the areas at very high risk that urgently need the implementation of non-structural risk mitigation measures.

Chapter 6 focuses on the selected Monte Albino hillslope test site, located in the Municipality of Nocera Inferiore (Campania region) on which the Quantitative Risk Analysis (QRA) procedures will be tested. In particular, the performed investigation activities (historical analyses, field surveys and in-situ tests) and the main results achieved during this fundamental stage of the work are discussed.

Chapter 7 is aimed at understanding, at detailed scale, of the geomorphological factors and geomorphological processes contributing to the definition of the actual litho-structural and morphologic settings of the test site. The derived information are of relevant importance for the identification of the "hillslopes" proneness to slope instabilities, including the associated triggering mechanism.

Chapter 8 discusses the results of a thorough susceptibility and hazard analysis of the hyperconcentrated flow triggering with reference to Monte Albino hillslope, for which an accurate catalogue of historical data, as well as geological and geomorphological features, litho-stratigraphic information and geotechnical characteristics of the soils are available. These studies are based on the use of detailed numerical analysis, through physically based engineering models, for the simulation and modelling of the triggering and propagation stage of hyperconcentrated flows. The achieved results represent the cognitive basis to perform quantitative risk analyses at detailed scale.

Chapter 9 shows the results of a quantitative estimation of the risk (QRA) of fatality to residents at the toe of Monte Albino posed by

hyperconcentrated flows. The estimated risk for life loss is calculated at both the individual level (risk to the average and most exposed person) and societal level. The obtained results are represented in risk maps and used to rank the portions of the urbanised territory at hyperconcentrated flow risk, in order to clearly identify the areas needing structural mitigation measures.

Finally, the chapter 10 presents the discussion of the achieved results of quantitative estimate of risk posed by hyperconcentrated flow both at regional and site-specific scale, highlighting the extraordinary perspective and repercussion in the technical and political fields.

2 THE FLOW-LIKE PHENOMENA

Landslides are an extremely widespread natural event resulting in one of the main causes of risk for social and economic structure. On a World scale, among natural disasters that have caused human life losses, landslide phenomena are set in the seventh place after windstorms, floods, droughts, earthquakes, volcanoes and extreme temperature (EM-dat, 2007). Moreover, it is important to observe that landslides interact with many other natural phenomena (such as earthquakes, storms, floods) so that they are considered the second most significant natural hazard among those identified by the United Nation Development Programme (UNEP, 1997).

The spatial distribution of landslides and their consequences are different in each Country, as testified by the global statistics on major events that have occurred during the past century. According to OFDA/CRED database (Table 2.1) Asia was impacted by 286 landslides events - the most of any region of the World - but America has suffered the most deaths while Europe registered an average economic loss of about \$ 67 million per landslide.

The increasing number of disasters (Figure 2.1), accentuated during the last two decades, and the consequent growth of damage can be mostly attributed to the new reality of more extreme weather conditions combined with overexploitation of natural resources and deforestation, increased urbanisation and uncontrolled use of land (Nadim et al., 2006).

Among all the types of landslides, flow-type movements surely represent a global issue that in many cases affect large areas at the same time, with catastrophic consequences on the exposed elements. Significant examples, in this sense, are provided by the phenomena systematically occurring in Southern Italy (1954,1998), in many States of the western USA (1997), in Japan (1998), in Venezuela (1999), in China (1999), El Salvador (2001), and in New Zealand (2002, 2004).

In the following, an overview of the main features of flow-type phenomena is provided, with particular attention to two types of phenomena involving granular soil: debris flows and hyperconcentrated flows.

Table 2.1 Global landslides statistics between 1900-2011 (source EM-DAT www.emdat.be).

Region of the World	Event	N° of Events	Killed	Total Affected	Damage (000 US\$)
Africa	Landslide	31	1,197	58,124	0
	Average per event		38.6	1,875	0
Americas	Landslide	157	19,373	5,509,275	2,521,727
	Average per event		123.4	35,091	16,062
Asia	Landslide	286	19,136	8,010,607	2,766,916
	Average per event		66.9	28,009	9,675
Europe	Landslide	35	15,342	25379	2,334,000
	Average per event		438.3	725	66,686
Oceania	Landslide	18	546	20,315	2,466
	Average per event		30.3	1,129	137

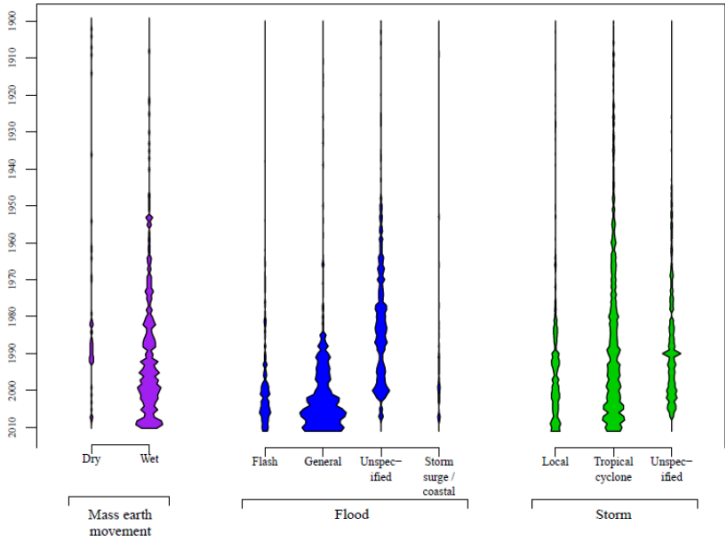


Figure 2.1 Number of natural disasters between 1900 - 2011 (source EM-DAT www.emdat.be).

2.1 CLASSIFICATION AND GENERAL FEATURES

Flow-like phenomena are characterised by very complex features and various attempts have been proposed in scientific literature to establish a unique and systematic classification (Hungre et al., 2001; Hutchinson 2003). Moreover, also the terminology commonly used is quite confusing and not exhaustive to describe the high variability of the physical and mechanical behaviour.

The flow type phenomena are composed of mixtures of air, steam, water and solid fractions of different nature: such as fractured rocks, sands, silts including loess and volcanic ashes, sensitive and stiff fissured clays and organic soils (Hungre et al., 2001).

In order to frame the fundamental characteristics of flow-like movements, in the following the main scientific classifications are described.

The Varnes (1978) classification is certainly the widely used and it is also the starting point of the other classifications proposed in the scientific literature. The Author classifies landslides on the basis of two fundamental characteristics through which to assign the appropriate name of the recognised phenomenon: the typology of movement and the type of involved material before the initiation of the movement (Table 2.2). With reference to the type of involved material the Author distinguishes between: rock (a hard or firm mass that was intact and in its natural place before the initiation of movement) and soil (aggregate of solid particles that either was transported or was formed by the weathering of rock in situ). Soil is divided into earth and debris: earth describes material in which 80% or more of the particles are smaller than 2 mm; debris contains a significant proportion of coarse material that is from 20% to 80 % of the particles are larger than 2 mm and the remainder are less than 2 mm. Movements are divided into five types: falls, topples, slides, spread and flows. The Author defines the flow as a spatially continuous movement in which surfaces of shear are short-lived and usually not preserved. The instability does not occur as a movement on one or more sliding surfaces, but rather, the involved material, not being able to resist the tangential stress variation produced by distortional deformations, flows as a viscous fluid.

Table 2.2 Abbreviated classification of Slope Movements (Cruden, 1978).

TYPE OF MOVEMENT		TYPE OF MATERIAL		
		BEDROCK	ENGINEERING SOILS	
			Predominantly coarse	Predominantly fine
<i>FALLS</i>		Rock fall	Debris fall	Earth fall
<i>TOPPLES</i>		Rock topple	Debris topple	Earth topple
<i>SLIDES</i>	<i>ROTATIONAL</i>	Rock slide	Debris slide	Earth slide
	<i>TRASLATTIONAL</i>			
<i>LATERAL SPREAD</i>		Rock spread	Debris spread	Earth spread
<i>FLOWS</i>		Rock flow	Debris flow	Earth flow
		(deep creep)	(soil creep)	
<i>COMPLEX</i>		Combination of two or more principal types of mevement		

This classification is then revised and completed by Cruden and Varnes (1996) through the addition of the third component: the velocity reached by the landslide body in the paroxysmal stage of the motion (Table 2.3).

Table 2.3 Landslides velocity scale (Cruden and Varnes, 1996).

Velocity class	Description	Velocity [mm/s]	Typical Velocity
7	Extremely Rapid	5-10 ³	5 m/s
6	Very Rapid		
5	Rapid	5-10 ¹	3 m/min
4	Moderate	5-10 ⁻¹	1.8 m/hr
3	Slow	5-10 ⁻³	13 m/month
2	Very Slow	5-10 ⁻⁵	1.6 m/year
1	Extremely Slow	5-10 ⁻⁷	16 mm/year

A first classification of these phenomena based on the morphology, mechanism, material and rate of movement is performed by Hutchinson (1988). Within the framework of flow-like phenomena the Author distinguishes five types of movement (Figure 2.2), in which the shear failure and flow processes are contemporarily present although in different measure from each case:

- Mudslides (non-periglacial);
- Periglacial mudslides;
- Flow slides;
- Debris flows;
- Sturzstroms.

In Mudslides phenomena the shear failure process prevails over flow process; in flow slides and debris flow phenomena the two processes coexist while in sturzstroms the flow processes exclusively occur.

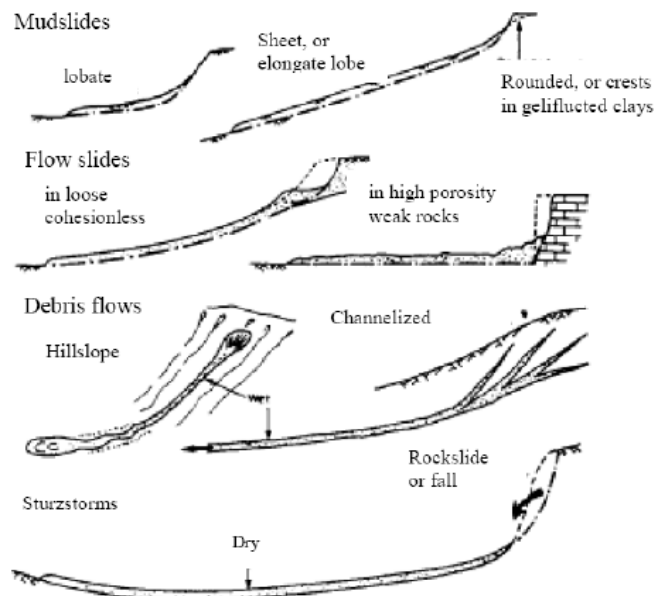


Figure 2.2 Main type of flow-like phenomena (Hutchinson, 1988).

It should be noted that the Author distinguishes, within the large spectrum of the flow-like phenomena, the mass transport phenomena and mass movement phenomena.

This distinction is based on water content value and unit weight of the mixture (Figure 2.3). In particular, debris flows are characterised by sediment concentration by weight of more than 80% and unit weight higher than 2 t/m³. Smaller values are characteristic of the mass transport phenomena such as hyperconcentrated flows and streamflow.

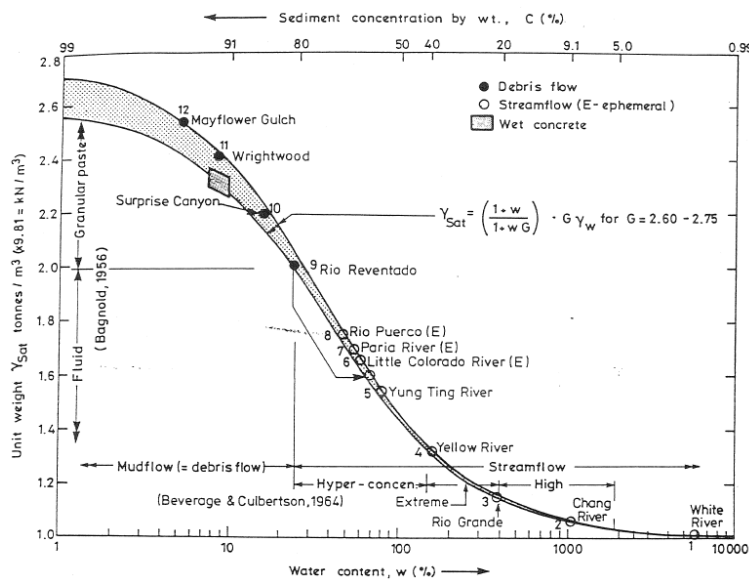


Figure 2.3 Continuous spectrum of sediment concentration. (Hutchinson, 1988).

The classification of flow-like phenomena from a rheologic, geomorphic and sedimentologic point of view, must be attributed to Costa (1988). In particular, the Author compares three different types of flows (Table 2.4):

- Water Flood
- Hyperconcentrated Flows
- Debris Flows

Coussot and Meunier (1996) propose a revision of the flow-like phenomena classification on the basis of their physical characteristics and mechanical behaviour (Figure 2.4). Within debris flows the relative velocity of water and solid is small so it can be considered as a (one-phase) viscous fluid; in water flood or hyperconcentrated flows the mean velocity of the coarsest solid particles, which are on the bed (bed-load), significantly differ from that of the water-solid suspension which flows around it, so they are constituted by a two-phase flow.

Table 2.4 General Rheologic Classification of Water and Sediment Flows in Channels (Costa, 1988).

Flow	Sediment concentration	Bulk Density [g/cm ³]	Shear Strength [dyne/cm ²]	Fluid Type
Water flood	1– 40 % by wt. 0.4–20 % by vol.	1.01 – 1.33	0 - 100	Newtonian
Hyperconcentrated flow	40 – 70 % by wt. 20 – 47 % by vol.	1.33 – 1.80	100 - 400	Non-Newtonian (?)
Debris flow	70 – 90 % by wt. 47 – 77 % by vol.	1.80 – 2.30	>400	Viscoplastic (?)

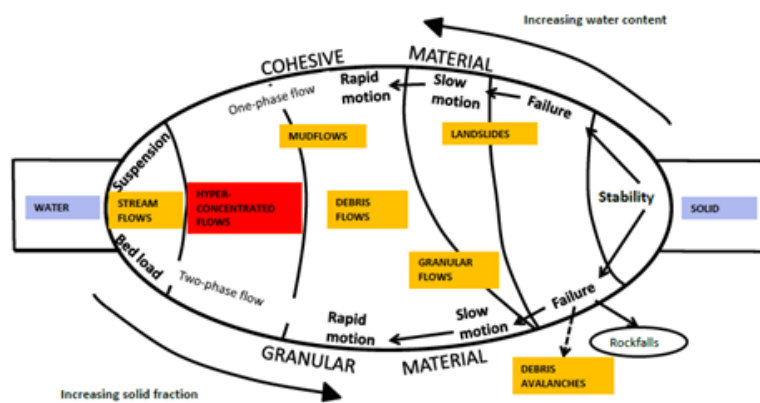


Figure 2.4 Classification of flow-like phenomena as a function of solid fraction and material type (Coussot and Meunier, 1996).

In order to simplify the characterisation and the definition of different flow-like phenomena additional classifications have been proposed

In this regard, Hutchinson (2003), starting from its previous geomorphological classification, identifies four types of flow-type landslides grouped into two different categories depending on the involved material: flow-type landslides in granular materials (debris flows, flow slide and rock avalanche) and flow-type landslides in cohesive material (mudslides). Hungr et al. (2001 and 2012) propose a very detailed and comprehensive classification based on four basic elements: material, water content, special conditions and velocity (Table 2.5).

All the classifications provide a useful conceptual framework mainly with reference to propagation stages, taking into account morphology, type of movement, state of activity, velocity (Hungr et al., 2001). In the following, according to the analysed classifications (Varnes 1978; Hutchinson, 1988; Costa, 1988; Coussot & Meunier, 1996; Cruden & Varnes, 1996; Hungr et al., 2001; Hutchinson, 2003; Hungr et al., 2012), the main feature of flow-like phenomena will be illustrated.

Flow-type phenomena are caused by several factors such as: rainfall, earthquakes, weathering, human activities or a combination of them. Among these factors, rainfall is surely the most common.

In order to describe the main phenomenological features of flow-type slope movements, the characterisation of all the different zones and stages involved in the phenomena is needed. From the geomorphological point of view, Hungr et al. (2001) recognise three main zones: the source area (which refers to a triggering zone of the landslide), the transport zone (it may or not coincide with a pre-existing valley incision along which the material in place can be eroded, further increasing the volume of the flowing mass) and the depositional area. In such areas the triggering, the propagation and the deposition stages of the phenomenon are respectively associated.

Table 2.5 Classification of flow-like phenomena (Hungri et al., 2001).

Material	Water Content ¹	Special Condition	Velocity	Name
Silt, Sand, Gravel, Debris (talus)	dry, moist or saturated	- no excess pore pressure - limited volume	various	Non-liquified sand (silt, gravel, debris) flow
Silt, Sand, Debris, Weak rock ²	saturated at rupture surface content	- liquefied material ³ - constant water	Ex. Rapid	Sand (silt, debris, rock) flow slide
Sensitive clay	at or above liquid limit	- liquefaction in situ ³ - constant water content ⁴	Ex. Rapid	Clay flow slide
Peat	saturated	- excess pore-pressure	Slow to very rapid	Peat flow
Clay or Earth	near plastic limit	- slow movement - plug flow (sliding)	<Rapid	Earth flow
Debris	saturated	- established channel ⁵ - increased water content ⁴	Ex. Rapid	Debris flow
Mud	at or above liquid limit	- fine grained debris flow	>Very Rapid	Mud flow
Debris	free water present	- flood ⁶	Ex. Rapid	Debris flood
Debris	partly or fully saturated	- no established channel ⁵ - relatively shallow, steep source	Ex. Rapid	Debris avalanche
Fragmented Rock	Various, mainly dry	- intact rock at source - large volume ⁷	Ex. Rapid	Rock avalanche

¹ Water content of material in the vicinity of the rupture surface of failure.

² Highly porous, weak rock (example weak Chalk, weathered tuff, pumice).

³ The presence of full or partial in situ liquefaction of the source material of the flow slide may be observed.

⁴ Relative to in situ source material

⁵ Presence or absence of a defined channel over a large part of path, and an established deposition landform (fan). Debris flow is a recurrent phenomenon within its path, while debris avalanche is not.

⁶ Peak discharge of the same order as that of major flood or an accidental flood. Significant tractive forces of free flowing water. Presence of floating debris.

⁷ Volume greater 10,000 m³ approximately. Mass flow, contrastino with fragmental rock fall.

Triggering is assumed to be the process leading a soil mass as a result of irreversible deformation. It depends on many factors – not always independent of each other – that are substantially attributable to two processes: i) erosion and undermining of debris-mass; ii) break slope with subsequent transformation of the unstable mass in flow.

Propagation stage refers to the rapid movement of unstable masses from the source area downslope to the depositional area wherein, due to slope angle decrease and pore-water pressure dissipation, the mass comes to rest (Major et al., 1997). During the propagation stage, additional soil masses lying along the path of the flowing mass may be entrained by erosive processes and incorporated in the original triggered mass (Iverson, 2005).

The phenomenological and kinematic characteristics are clearly related to the failure and post-failure mechanisms (Leroueil et al., 1996) affected by several factors such as morphology, boundary condition, characteristics of the involved material, initial state of stress, etc. After the triggering stage, the flow-type phenomena propagate with characteristics similar to those of a viscous fluid reaching, in the paroxysmal phase, very high values of velocity (up to tens m/sec); furthermore, the flowing mass is able to attain long travel distances (up to tens of kilometres) by adapting to the morphology of the area (following natural and/or human tracks or spreading laterally over flat slopes).

2.2 DEBRIS FLOWS

Debris flows are very rapid to extremely rapid surging flows of saturated non-plastic debris (plasticity index < 5% in sand and finer fractions) in a steep channel with a strong entrainment of material and water from the flow path. It is distinct from other types of landslides since it occurs periodically on established paths, usually gullies and first or second order drainage channels. (Hungri et al., 2012).

Debris flow events usually occur during a period of heavy rainfall or melting snow, with peak discharge up to 40 times greater than those of extreme floods (Hungri et al., 2001). The high discharge is responsible for greater flow depth, higher velocity, higher impact loads and the ability to move large boulders. The measured velocities range between 3 and 12 m/sec and, exceptionally, velocities of about 30 m/sec and even more

have been measured (Hutchinson, 1988) with travel distances up to several kilometres. The thickness of the material in motion ranges from few meters to a maximum of twenty meters.

The materials involved in debris flows can be defined as loose unsorted materials ranging from clay to boulders of several meters in diameter, produced by mass wasting processes (colluvium), weathering (residual soils), glacier transport, or unsorted anthropogenic waste (Hungar et al., 2001). They may also contain a significant portion of organic material such as trees and timber (Swanston, 1974).

The flow may be initiated by a slide, debris avalanche or rock fall from a steep bank, or by spontaneous instability of the steep stream bed, carrying heavy water flow. Once soil material begins to move in a steep channel, the flowing masses start to incorporate the material lying along the slope (Sassa, 1985), hence greatly increasing of the solid fraction concentration that approximately reaches 80% by volume. It is important to note that the bulk of the material involved in a debris flow event usually originates from entrainment along the path, while the triggering volume is insignificant.

During the propagation stage, solid particles and water move at the same velocity as a single visco-plastic body (one-phase flow) in a laminar flow, undergoing large homogeneous deformations without significant changes to its mechanical properties (Coussot and Meunier, 1996).

Among the many rheological models proposed in scientific literature, field observation (Johnson, 1970; Coussot, 1992; Whipple and Dunne, 1992) and rheometric studies (O'Brien and Julien, 1988; Phillips and Davies, 1991; Major and Pierson, 1992; Wang et al., 1994; Coussot and Piau, 1995; Martino, 2003; Martino and Papa, 2008), lead the conclusion that in debris flows the resistance to flow (or deformation) results from shear strength originating from cohesion, internal friction and viscosity (Costa, 1988). Therefore, the debris flows exhibit a behaviour well described by a visco-plastic rheological models such as the Bingham model (Bingham and Green, 1919) or the Herschel-Bulkley model (Herschel and Bulkley, 1926).

Since debris flow materials have a high density and they are very viscous, strongly sheared and mixed during the flow, the sedimentary structures – including stratification – in debris flows deposits are not existent; however, along the longitudinal profile they show an inverse sorting that generate a particular depositional process. As the flow reaches the apex

of the depositional fan, coarser debris are expelled to the sides forming ridges or levees while the front may be by-passed by the finer liquefied debris travelling behind it and coming to rest (Hung et al., 2001; Takahashi, 1991).

2.3 HYPERCONCENTRATED FLOWS

Hyperconcentrated flows are mass transport phenomena characterised by very rapid flow of water, heavily charged with debris, in a steep channel (Hung et al., 2012). Hyperconcentrated flows are also called non cohesive mudflows (Kurdin, 1973), turbulent mudflows (Gagoshidze, 1969), intermediate flows (Bull, 1964), type III and IV sediment flows (Lawson, 1982), mud floods (Committee on Methodologies for Predicting Mudflow Areas, 1982) and debris floods (Hung et al., 2001). They occur as a result of erosion phenomenon performed by the volumes of water in motion or when debris flows lose coarse sediment through dilution and selective deposition.

Documented triggering mechanisms include: hillslope and channel erosion during intense rainstorms (Beverage and Culbertson, 1964; Major et al., 1996; Pierson et al., 1996), lake-breakout floods (Rodolfo et al., 1991; O' Connor et al., 2002), glacier-outburst floods (Maizels, 1989), dilution and/or selective deposition at the heads and tail of debris flows (Pierson, 1986; Pierson and Scott, 1985; Cronin et al., 2000), and inputs of large sediment volumes to water floods by landslides (Kostaschuk et al., 2003). Therefore, they commonly occur in semiarid and arid regions, particularly where the basins are steep, hillslopes are eroded, channel banks are fragile, and channel beds are unreinforced and erodible (Gerson, 1977; Laronne et al., 1994). It is important to note that hyperconcentrated flows are common in pyroclastic soils recently impacted by explosive eruption. In this geological context, in fact, the well documented hyperconcentrated flow events (Table 2.6) have been observed (Pierson, 2005), consisting in a rapid releases of water able to erode and to incorporate exceptionally large volumes of cohesionless deposits on hillslope and in channels. The transported material can result from: *i*) erosion along the riverbed, *ii*) erosion along the lateral banks of the riverbed, *iii*) instability phenomena along the river banks that are triggered by the above-mentioned erosion phenomena.

According to Costa (1988), hyperconcentrated flows are characterised by a solid concentration by volume ranging from 20% to about 47%; the sediment may be transported in the form of massive surges, leaving sheets of poorly sorted debris ranging from sand to cobbles or small boulders.

Table 2.6 Observed or measured characteristics of hyperconcentrated flows to approximate times of peak sediment (Pierson, 2005)

	19-20 March 1982: Toutle River, Mount St Helen, USA	26 September 1993: Sacobia River, Mount Pinatubo, Philippines	29 September 1995: Whangaehu River, New Zealand
Trigger	<i>Eruption</i>	<i>Rainfall</i>	<i>Eruption</i>
Observation location	<i>73 km downstream from source</i>	<i>20-25 km downstream from source</i>	<i>42 km downstream from source</i>
Flow discharge (m³/s)	<i>450</i>	<i>10 (estimated)</i>	<i>42 (peak, measured 14 km farther downstream)</i>
Flow depth (m)	<i>2.1 (mean estimated)</i>	<i>0.5-0.7</i>	<i>2.3 (estimated)</i>
Flow velocity (m/s)	<i>3.5-4 (estimated)</i>	<i>2.6-3.1</i>	<i>2.7-3.0 (estimated)</i>
Concentration peak lag behind flow peak (min)	<i>38</i>	<i>Not measured</i>	<i>50</i>
Suspended sediment concentration (vol%)	<i>43</i>	<i>30</i>	<i>52</i>
Silt+clay (fraction of total suspended sediment)	<i>0.22</i>	<i>0.34</i>	<i>0.19</i>
Maximum clast size in suspension	<i>30-40 mm observed</i>	<i>16-32 mm</i>	<i>Up to 40 mm</i>
Bedload movement	<i>Boulder movement</i>	<i>Pebbles</i>	<i>Boulders</i>

They are often generated by rainfall events of high intensity and short duration that determine the development of sudden river flooding, with peak discharge comparable to that of a water flood. In particular, the phenomenon is mostly concentrated in the autumn months, during which there are the highest soil suction values that lead to the occurrence

of erosion phenomena or localised small-size slope instabilities, typically turning into hyperconcentrated flows (Cascini et al., 2013 a).

The hyperconcentrated flows may be generalised as a turbulent, solid–liquid two-phase flow, gravity-driven flows of water and sediment in which the mean velocity of the coarsest solid particles, which are pushed and rolled on the bed (bed-load), significantly differ from that of the water-solid suspension which flows around it (Coussot and Meunier, 1996).

Rheological and fluid characteristics are greatly controlled by the amount of fine-grained material (silt and clay) in the transported mass: flows with low concentration of sediment, high percentages of fine material and low strain rates follow a Newtonian behaviour (Costa, 1988); with the increasing of the sediment concentrations the flow mechanism begins to change: viscosity, shear strength and particle collisions increase so flows exhibit a behaviour well described by a viscous-plastic rheological models such as the Bingham model (Bingham and Green, 1919), the Herschel-Bulkley model (Herschel and Bulkley, 1926) or collisional-viscous-plastic rheological model like the quadratic shear stress model (O'Brien and Julien, 1985).

Hyperconcentrated flow deposits are massive to crudely stratified; the sorting is intermediate between that of debris flow and most water flood deposits. In particular, they have a coarse, sandy texture with distinctly less fines than debris flow deposits and are more poorly sorted than water flood deposits of similar medium size (Costa, 1988).

It is important to note that, unlike a debris flows, hyperconcentrated flows usually do not develop high impact forces and, consequently, they are responsible for economic damage to structures and properties (resulting from flooding and burying of the objects impacted by the flow) but the risk for life loss is limited. However, this depends on the size of the drainage where they are originated. While debris flows are limited to steep drainages of less a few square kilometres, hyperconcentrated flows can occur in much larger river catchments, with greater hydrologic flood discharges which are magnified by heavy sediment loads. An important example is given by the catastrophic flood and landslide disaster of the Serrana Region of Brazil, in January 2010 (Hungri et al., 2012).

Moreover, hyperconcentrated flows are ubiquitous and often transitional to debris flows (Figure 2.5) with an obvious dramatic increase in

potential damage (Svendsen et al., 2003). It might happen, in fact, that the flow of water and sediment possess a high energy able to incorporate, within the moving mass, high solid fractions and very large boulders, in this case the event turns into a debris flow (this is the case of the event that affected the city of Salerno, Italy in October 1954). On the other hand, a debris flow surge can dilute itself to a hyperconcentrated flow by entraining water from the channel and discarding the coarsest sediments to the side of the channel (Pierson, 2005).

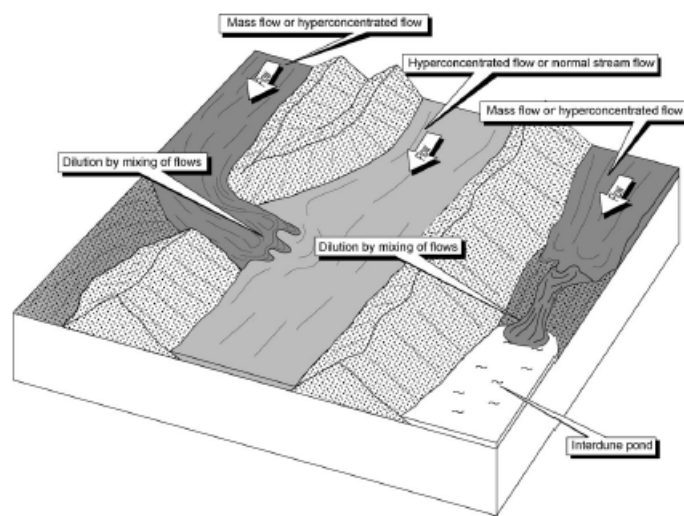


Figure 2.5 Processes causing dilution of mass and hyperconcentrated flows (Svendsen et al., 2003).

3 RISK ANALYSIS

The increasing trend in spatial and temporal occurrence of landslides and the awareness of the caused catastrophic consequences, in terms of victims and social-economic impacts, have greatly contributed to the development of issues related to the landslide risk and, in particular, those pertaining to the risk analysis and zoning as well as its mitigation. Several Authors have proposed definitions, not always fully shared, of the terms that concur to the generation of risk (Varnes, 1984; Einstein, 1988; Fell, 1994; Leroi, 1997; Fell e Hartford, 1997; Ho et al., 2000; Cascini, 2005 b; Fell et al., 2005; Fell et al., 2008). In this Thesis the definitions provided by The International Society of Soil Mechanics and Geotechnical Engineering (ISSMGE) Technical Committee on Risk Assessment and Management (TC32, 2004) are considered (<http://www.engmath.dal.ca/tc32/publications.html>), namely:

- *Risk (R)*: A measure of the probability and severity of an adverse effect to health, property or the environment. Risk is often estimated by the product of probability of a phenomenon of a given magnitude times the consequences.
- *Hazard (H)*: A condition with the potential for causing an undesirable consequence. The description of landslide hazard should include the location, volume (or area), classification and velocity of the potential landslides and any resultant detached material, and the probability of their occurrence within a given period of time.
- *Vulnerability (V)*: The degree of loss to a given element or set of elements within the area affected by the landslide. It is expressed on a scale of 0 (no loss) to 1 (total loss). For property, the loss will be the value of the damage relative to the value of the property; for persons, it will be the probability that a particular life (the element at risk) will be lost, given the person(s) is (are) affected by the landslide.

- *Element at Risk (E)*: Population, buildings and engineering works, infrastructure, environmental features and economic activities in the area affected by a hazard.

The prediction of the currently or potentially level of risk, in a specific area affected by a given landslide phenomenon, requires the combination of information derived from the knowledge of the landslide hazard and from the analysis of the expected consequences posed by its occurrence. In the most general form, the risk estimation can be expressed through the widely accepted formula of Varnes (1984):

$$R = H \cdot E \cdot V \quad (3.1)$$

Hazard analysis involves the characterisation of the landslide process and the corresponding frequency (i.e. annual probability) of occurrence. Consequence analysis, generally represented as the product of E times V, is the outcome of hazard and it includes the identification and the quantification of the elements at risk (property, persons) as well as the evaluation of their temporal and spatial probability and vulnerability.

Risk analysis represent the first step of the whole risk management process as it allows the estimation of landslide risk on the basis of the risk theory concepts applied to natural systems and it plays a leading role in the general landslide risk management by supporting decisions of owners, regulators and governments about protection options to be set.

In the following, after a description of the theoretical background of landslide risk management, the different stage characterising the risk analysis phase are analysed. Special attention is given to the description of different methods for the hazard and consequence analyses, highlighting their potentialities and limits.

3.1 GENERAL FRAMEWORK OF THE RISK MANAGEMENT PROCESS

Understanding, forecasting and controlling the risks posed by landslide phenomena are recognised to be a priority in achieving an acceptable quality of life. Due to the importance of the topic, there has been a growing interest in the technical and scientific Community towards the adoption of a rigorous approach aimed at prevention, mitigation and control of landslide risk (Fell et al., 2005) in effectively and efficiently way. To this aim, Fell et al. (2005) suggested a logical framework for landslide risk management, received within the guide line of JTC-1 (Joint Technical Committee on Landslides and Engineered Slopes) (Fell et al., 2008), that includes three phases (Figure 3.1):

- Risk Analysis
- Risk Assessment
- Risk Management

In this framework, the risk analysis represents the basic level of risk management process. Risk analysis is essentially aimed at the estimation Risk assessment takes the output from risk analysis and it assess the estimated risk against reference values – established on the basis of political judgements or acceptance criteria – in order to decide if the level of risk is low enough to be accepted or tolerated from the community.

Finally, risk management takes the output from risk assessment and considers the use, where the risk level cannot be tolerated, of appropriate mitigation options. Mitigation options are the treatments and priorities that are set in order to reduce risk within the context of social and economic needs and realities. Such measures can be essentially grouped in two categories: active and passive. The active measures are generally devoted to the implementation of engineering works designed to directly control the phenomena, while the passive measures refer to strategies such as avoidance, tolerance and warning/monitoring of landslide hazards.

Obviously, as can be understood, the whole process of the risk management involves a large number of stakeholders including owners, inhabitants, appointed authorities of the territory government, geotechnical engineers, geologists as well as risk analysts.

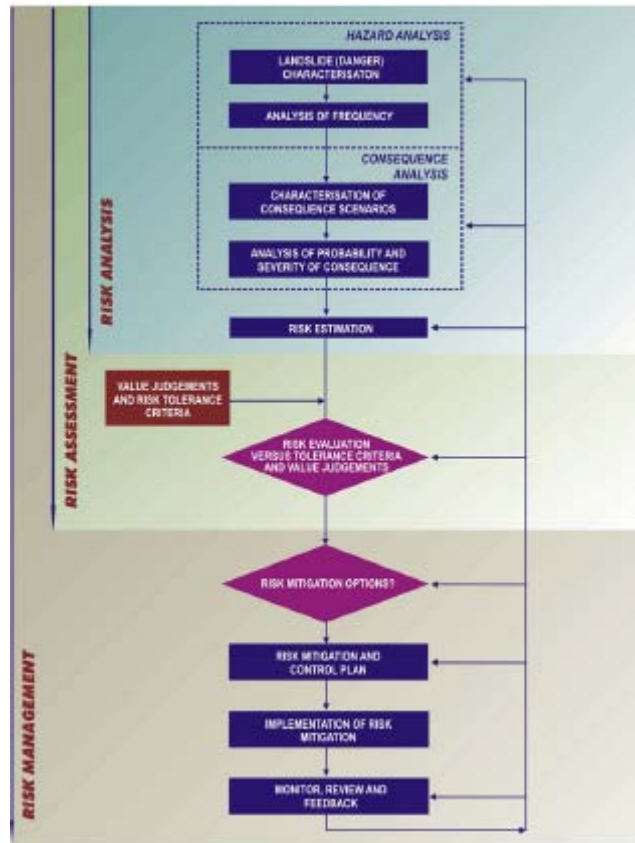


Figure 3.1 Framework for landslide risk management (Fell et. al, 2008).

As reported in Landslide risk management concepts and guidelines of Australian Geomechanics Society (AGS) (2000), this process can be achieved by providing the proper answers to the following main questions:

- What might happen?
- How likely is it?
- What damage or injury may result?
- How important is it?
- What can be done about it?

Risk analysis, certainly, plays a leading role in the general risk management framework by providing support to the planning of active mitigation measures, to the effective design of passive strategies and, above all, to the development of land utilisation regulations aimed at minimise the loss of life and to reduce the damage costs.

3.2 RISK ANALYSIS

Landslide risk analysis is based on the general concepts of the risk theory that has been extensively used for practical problems associated with industrial, human, environmental and natural systems. According to this theory, the risk is defined by the intersection of two main components: hazard and consequence (Varnes, 1984). The risk analysis can be carried out at different scales (from small to detailed scale) depending on the scope of the work, the extension of the study area, the amount and quality of available information as well as the financial and/or time constraints (Bell and Glade, 2004; Fell et al., 2008).

This section introduces a brief overview of each step of the risk analysis process consisting in: scope definition, hazard analysis and consequence analysis.

3.2.1 Scope definition

The importance of defining a scope of the risk analysis ensures that the relevant issues are being addressed, the needs of professionals implicated in the complex process of risk management are being satisfied, and it avoids misunderstandings between parties (Fell et al. 2005). Scope definition allows to define the geographical limits of the study area and level of detail, elements at risk of concern, the methodology best suited for the risk analysis, the required resources, the units in which to measure the outcome of analysis, and what will the analysis (and in turn, the assessment) be used for (Fell et al., 2005; Crozier and Glade, 2005). It should be also defined the nature of the end product of the risk analysis - report, maps, and how these will be communicated to the interested parties.

Obviously, all these factors that characterise the purpose of the risk analysis and assessment are dictated by technical, social, economic and political interests.

3.2.2 Hazard analysis

Hazard is the most complex factor to be determined for the estimation of the landslide risk. In particular, hazard analysis contemplates the identification and the characterisation of the potential landslides together with evaluation of their corresponding frequency of occurrence (Fell et al., 2005).

The identification phase involves the definition of landslide processes that may occur in the study area. This phase can be supported by the landslide susceptibility analysis that takes into account geomorphologic, geological, hydro-geological features of the study area as well as the analysis and the identification of past landslide phenomena (through the interpretation of aerial photographs and evaluation of historical information). In particular, according to JTC-1 (Fell et al., 2008) the landslide susceptibility analysis by using the landslide inventory map, which includes the description of past landslides, allows the classification and the identification of spatial distribution of existing and potential landslides in the study area, their state of activity, their triggering mechanism and their travel distance.

In order to define the hazard scenario, once the landslide phenomenon is identified, it is necessary to characterise its corresponding frequency of occurrence. Hazard analysis, unlike susceptibility analysis, requires the estimation of the spatial-temporal and magnitude probabilities of potential landslides (Guzzetti et al., 1999; Glade and Crozier, 2005; Fell et al., 2008; Van Asch et al., 2007; Corominas and Moya, 2008; van Westen et al., 2008).

In scientific literature there are several applications of assessment of the future occurrence of landsliding (Mostyn and Fell, 1997; Baynes and Lee, 1998; Aleotti and Chowdhury, 1999; Picarelli et al., 2005; van Westen et al., 2006; Corominas and Moya, 2008), which can be synthetically grouped into heuristic, statistical and deterministic methods.

The choice of the most suitable approach, obviously, depends on: the scale of work, the availability of the data and the aim of the landslide risk analysis (see Section 4.1).

In operational practice, for the assessment of the landslide frequency occurrence IUGS (1997) recommends the use of more than one method among those proposed:

- Historic data within the area of study, or areas with similar characteristics, e.g. geology, geomorphology.
- Empirical methods based on correlations in accordance with slope instability ranking systems.
- Use of geomorphological evidence (coupled with historical data), or based on expert judgment.
- Relationship to the frequency and intensity of the triggering event, e.g. rainfall, earthquake.
- Direct assessment based on expert judgment, which may be undertaken with reference to a conceptual model, e.g. use of a fault three methodology.
- Modelling the primary variable, e.g. piezometric pressures versus the triggering event, coupled with varying levels of knowledge of geometry and shear strength.
- Application of probabilistic methods, taking into account the uncertainty in slope geometry, shear strength, failure mechanism, and piezometric pressures. This may be done either in a reliability framework, or taking into account the frequency of failure (for example by considering pore pressures on a frequency basis).
- Combinations of the above methods.

It is worth observing that, in general, is better to estimate the frequency quantitatively as it enables an uniformity of results allowing to compare, in a simple way, the hazard arising from the occurrence of different types of landslides. To this aim, Corominas and Moya (2008) suggest the use of the frequency descriptors in absolute or in relative terms. The first category (absolute descriptors) is appropriate in the case of repetitive occurrence of first-time slope failures, or reactivation events of dormant landslides, or acceleration episodes (surges) of active landslides, generally involving a single slope; the associate descriptor can be expressed in terms of annual probability of occurrence or reactivation (e.g. failure/year, reactivation/year). The second category (relative descriptors) contemplates groups of landslides involving multiple slope (regional scale); therefore, it is necessary to normalise the data per unit

area or length (e.g. landslides/unit area/year, landslides/unit length/year) when descriptors are dealing with.

The results of the hazard analysis are usually represented in a landslide hazard map showing the areas that are stable and the areas that are and/or may be affected by landslides, including those where landslides may travel onto them (Corominas and Moya, 2008).

In order to properly assess the effect and the behaviour of the exposed elements (structures or persons), the landslide hazard maps should also provide information on the landslides intensity (Varnes, 1984). According to Hungr (1997) intensity can be defined as a set of quantitative or qualitative spatially distributed parameters, which determine the potential of a given landslide phenomenon to cause damage. Its definition is strictly related to, besides the extent of analysis (a site-specific or a regional analysis), the typology of the landslide (slow movement or fast movement) as well as to the characteristic of the exposed element. With reference to a given landslide it is possible to use as intensity parameter: the velocity, the volume, the total or differential displacement, the depth of the moving mass or the depth of the deposit. With regards to the interaction of the landslide phenomenon with the exposed element at risk, depending on its nature, derived parameters may be considered such as the peak discharge per unit width, kinetic energy per unit area, maximum thrust or impact pressure. On the other hand, it must be observed that different intensity values could pertain to a given landslide along its path for instance, the kinetic energy of a rock fall continuously changes along its trajectory (Fell et. al., 2008).

3.2.3 Consequence analysis

The consequence analysis allows to define the spatial and the temporal probability of the landslide impact on the exposed element at risk and to establish, at the same time, the potential damage W defined as the product of the vulnerability and the element exposed at risk.

This analysis can be implemented using different approaches that may include the use of historical information, expert judgment and analytical modelling of the landslide phenomenon.

The analyses of historical information may allow the definition of the empirical relationships able to identify the size of the potential damage posed by the occurrence of a given landslide. This method can be used

only when very accurate and detailed information are available and the landslides are appropriately classified (Corominas, 1996).

Expert judgment, based on the competence of the specialist, gives subjective evaluation criteria of consequence scenario. It is usually adopted where the scenario components are too complicated to consider systematically and where past experience allows sensible judgments (Wong et al., 1997).

Analytical methods allow to describe the physical phenomenon with the aid of mathematical laws. Through the use of numerical modelling is possible, therefore, to define the intensity of the phenomenon in terms of velocity and mobilised volumes of soil and to identify the flooding area.

Specifically, the consequences analysis consists in the following steps (Fell et al., 2005):

- Identifying and quantifying the elements at risk including property and persons;
- Assessing temporal and spatial probability for the elements at risk;
- Assessing vulnerability of the elements at risk, in terms of property damage and loss of life/injury .

Elements at risk refer to the population, buildings, civil engineering works, infrastructure, economic activities, public services, vehicles, environmental features, which are in the area affected by the hazard (Fell et al., 2005). The elements at risk, therefore, are located within the body of the landslide or in the area onto which the phenomenon could be propagated or laid down.

Each element at risk can be associated with special characteristics, in function of its peculiar nature: spatial (concerning their location in relation to the hazard), temporal (in function of the temporal dynamics of the element in a well-defined space) or thematic characteristics (i.e. buildings material or the gender distribution of the population) (van Westen et al., 2006).

The census and the characterisation of the elements at risk can be carried out at different levels, depending on the aim of the analysis. It is worth noting that, often, the information regarding the characteristics of the elements at risk can result from different sources that refer to discordant

territorial limits: grid cell (in the case of interpretation of satellite images, inspections, submitted questionnaires) or different administrative units - countries, provinces, municipalities, neighbourhoods, census tracts - (in the case of existing cadastral databases, existing census date). For this reason, it is necessary to relate all the information to homogeneous units - with similar characteristics in terms of type and density of elements at risk - in order to achieve results that well represent the scale of analysis (van Westen et al., 2008).

In order to identify the expected damage as a result of the occurrence of a given hazard it is necessary to define the value of the element at risk (E). In particular for the element at risk “population” the number of exposed persons is used while for the “property” its economic value is used. In this regard, scientific literature proposed several methods and procedures based on economic considerations which results are highly dependent on the economic conditions of the reference Country. Among them there are:

- the calculation of the specific value for individual element (DRM, 1990);
- the use of utility functions (Crosta et al., 2001);
- the use of empirical formulas (Del Prete et al., 1992);
- qualitative assessment of the global value in a specific area (Bonnard et al., 2004).

Due to difficulties involved in the quantification of non-tangible effects (i.e. social and psychological effects on the community, the environmental degradation, etc) most of these procedures adopt as the value of the element at risk the number of buildings or persons affected by the hazard or the tangible costs of physical damage.

Since the exposed element at risk can be characterised by a spatial and temporal variability, it is necessary to define the temporal spatial probability ($P_{S,T}$), namely the conditional probability that the element at risk is in the area affected by the hazard at the time of its occurrence (Fell et al., 2005). This term assumes unit value for structures located on or in the path of the landslide. For persons in a building, it strictly depends on social variables such as age, gender, employment, health, and, certainly, on their location since people that live near the triggering area are less likely to run away from the slide than those who are below the landsliding area. Furthermore, the ($P_{S,T}$) is linked to the nature of the

phenomenon (i.e. intensity, mobilised volume, velocity, presence of warning signs, existence of monitoring system and of evacuation system). Moreover, these aspects are contemplated in the evaluation of $P_{(T,L)}$ that is the conditional probability of landslide reaching the element at risk. It depends on the relative location of the element at risk and the landslide source, together with the path the landslide is likely to travel below the source (Fell et al., 2005). The $P_{(T,L)}$ term assumes unit value for structures located on the source of the landslide.

The consequences analysis, finally, involves the assessment of the vulnerability. According to Fell et al. (2005), vulnerability is the degree of loss (or damage) to a given elements, within the area affected by the hazard. It is a conditional probability, given the landslide occurs and the element at risk is on or in the path of landslide.

Depending on the considered element at risk and on the type of the damage, it is possible to distinguish: physical, social, environmental and economic vulnerability. According to Amatruda et al. (2004), for each of these components the following definitions can be given:

- Physical vulnerability: defined as the damage, in terms of structural failure, caused by the impact of the instable mass on the building, structure, infrastructure, network and other object. It depends on the phenomenon intensity, on the type and function of the structure, on the quality of the materials used, as well as its state of maintenance and capacity for deformation.
- Social vulnerability: is the rate of impact due to a landslide on the exposed population, in terms of the loss of life, injury, problems on mental health and living conditions (loss of home, evacuation). It depends on the phenomenon intensity (which is in relation to the warning factor), on the population sensitivity (depending on its age and capacity to anticipate a landslide) and on the capacity of understanding the phenomenon and to move away from the exposed zone.
- Environmental vulnerability: is defined with respect to the direct impact on natural environment (forests, animals, plants, water). The damage of these natural components cannot be evaluated in monetary terms, especially as far as forests (which now have nearly no commercial value), wild animals and rare plants are concerned. The main criteria for determining the value of environmental vulnerability is to consider the intensity of the

phenomenon in relation to its disrupting effect on nature, to evaluate the function of the forest or of the endangered animal and plant species and to consider the rarity of these species.

- Economic vulnerability: is defined with reference to an indirect economic impact of the phenomenon on human activities (due to obstructed traffic, reduced touristic demand, longer travel distance for industrial goods, loss of value of adjacent plots of land, etc). The main criteria to be considered in the assessment of the economic vulnerability is to consider the types of services implied, the types of economic activities affected, the traffic and the cost of blocking a route, the possibilities of alternative routes.

From a mathematical point of view, the vulnerability V_L can be expressed as (Einstein, 1998):

$$V_L = P[D_L \geq 0 \mid L], \quad (0 \leq D_L \leq 1) \quad (3.2)$$

where D_L is the assessed or expected damage to an element at risk given the occurrence of a landslide (L).

Vulnerability of element at risk can be expressed in relative terms using word such as “no damage”, “some damage”, “major damage” and “total loss”, or adopting a numerical scale (Amatruda et al., 2004). In particular, for property the numerical scale ranging between 0 (no damage) to 1 (total loss) while for persons it is usually expresses as the probability (between 0 and 1) that given person located along the path of landslide may lose his/her life (Fell et al., 2005).

In order to estimate the vulnerability many approaches can be used which can be grouped in: direct approach, event tree approach and consequence model (Wong et al., 1997).

The direct approach allows the evaluation of the effects of a potential slope failure based on experience and expert judgment without reference to scenario components (Table 3.1). It is most suitable for the qualitative risk assessment and where past experiences allow sensible judgments; in this regard the assessment is subjective and not explicit. Table 3.1 provides an example of the range of vulnerability values for person in open space detected by the use of historical information.

Table 3.1 Example of assessment by a direct approach of Vulnerability for person in open space (extracted from Finlay et al., 1997).

<i>VULNERABILITY OF PERSON IN OPEN SPACE</i>			
<i>CASE</i>	<i>Rang in Data</i>	<i>Recommended Value</i>	<i>Comments</i>
1. If struck by a rockfall	0.1-0.7	0.5 ⁽¹⁾	May be injured but unlikely to cause death
2. If buried by debris	0.8-1.0	1.0	Death by asphyxia
3. If not buried	0.1-0.5	0.1	High chance to survival
Note: (1) Better considered in more detail, i.e. the proximity of person to the part of the building affected by sliding.			

In the event tree approach, the expected consequences of a given hazard are assessed through the progression of the various combined scenario components, using logic tree technique and inductive reasoning to translate the different scenario components into a range of possible outcomes. It is most suitable for the quantitative risk assessment at site-specific scale and it is very useful for very complex landslide where important facilities are at stake.

The consequence model involves the use of a rational framework based on the consideration of key factors affecting the consequence of failure, such as the travel distance of debris, type and proximity of facilities affected, spatial and temporal distribution of population at risk.

In this regard, the vulnerability curves can be used (Figure 3.2). The vulnerability curves represent an enhanced consequence model developed for the landslide quantitative risk analysis (QRA), which incorporated consideration of the hazard type, run-out mechanism, run-out path, debris mobility and vulnerability formulation (Wong et al., 2005). In particular, they express the estimation of the possible degree of damage as a function of an intensity parameter, via damage relations derived from historical inventories or from detailed structural modelling or through empirical relations.

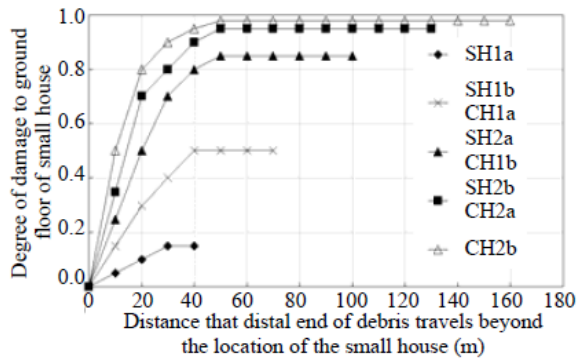


Figure 3.2 Vulnerability curves adopted in the QRA process by the Engineering Control Office in Hong Kong (Wong et al., 2005).

3.2.4 Risk estimation

The risk analysis phase concludes with the definition of the level of risk that can compete to a single element or a plurality of elements through a qualitative, quantitative, or semi-quantitative approach. The choice of a method rather than one depends on the nature of the problem and therefore on the purpose of the risk analysis, the desired accuracy of the result and it should be compatible with the quality and the amount of available data and from the experience of the specialist. Generally, for large area, where the quality and quantity of the data are too poor, the qualitative analysis is preferred while for a site-specific slopes a quantitative risk estimation is preferred (Dai et al., 2002 a).

3.2.1 Qualitative or Quantitative risk estimation

The qualitative risk estimation methods are widely used in landslide risk management on a small scale. They allow a quick comparison of the risks pertaining to various sites allowing to identify the main level of criticality in the area and to promulgate, at the same time, suitable measures of the territory government. These methods are based on the attribution of scores or indicators to each factors that contribute to the risk definition (Eq. 3.1). The final risk output consists in nominal, descriptive or numerical scales. One of the preferred approaches is to combine, through the use of risk matrices, the qualitative scores resulting from the consequence analysis with those derived from the scoring of the hazard

analysis. In this context, each cell of the matrix can be labelled by the qualitative (high, medium, low) or quantitative indicators in order to indicate the level of expected risk. In this regard, Table 3.2 gives an example of qualitative risk estimation for property used by AGS (2000).

Table 3.2 Example of a method for qualitative risk estimation to property (Extracted from AGS, 2000).

QUALITATIVE RISK ANALYSIS MATRIX - LEVEL OF RISK TO PROPERTY						
LIKELIHOOD		CONSEQUENCES TO PROPERTY				
	Indicative Value of Approximate Annual Probability	1: CATASTROPHIC	2: MAJOR	3: MEDIUM	4: MINOR	5: INSIGNIFICANT
<i>A - ALMOST CERTAIN</i>	10-1	VH	VH	VH	H	M or L
<i>B - LIKELY</i>	10-2	VH	VH	H	M	L
<i>C - POSSIBLE</i>	10-3	VH	H	M	M	VL
<i>D - UNLIKELY</i>	10-4	H	M	L	L	VL
<i>E - RARE</i>	10-5	M	L	L	VL	VL
<i>F - BARELY CREDIBLE</i>	10-6	L	VL	VL	VL	VL

RISK LEVEL IMPLICATION		
RISK LEVEL		Example Implication
VH	VERY HIGH RISK	Unacceptable without treatment. Extensive detailed investigation and research, planning and implementation of treatment options essential to reduce risk to Low; may be too expensive and not practical. Work likely to cost more than value of the property.
H	HIGH RISK	Unacceptable without treatment. Detailed investigation, planning and implementation of treatment options required to reduce risk to Low. Work would cost a substantial sum in relation to the value of the property.
M	MODERATE RISK	May be tolerated in certain circumstances (subject to regulator's approval) but requires investigation, planning and implementation of treatment options to reduce the risk to Low. Treatment options to reduce to Low risk should be implemented as soon as practicable.
L	LOW RISK	Usually acceptable to regulators. Where treatment has been required to reduce the risk to this level, ongoing maintenance is required.
VL	VERY LOW RISK	Acceptable. Manage by normal slope maintenance procedures

Although easy to use, fast and cheap, the results of qualitative risk analyses are not very reliable and the outputs represent an oversimplification of the reality as well as being highly subjective. For this reason, this risk estimate must be undertaken in a critical manner and with the support of experts in the field.

It should be noted, moreover, that the use of subjective scales to rank the risk involves problems of perception and comprehension of the expected level of risk. This contributes to difficulties in communication and complications to determination whether the identified risk levels are acceptable or not. However, the limitations of qualitative analysis and the increasing tendency of society to communicate and make decisions based on quantified risks, induces the adoption of quantitative risk analysis (QRA) (Lee and Jones, 2004).

The quantitative risk estimate, compared with the qualitative one, requires a huge amount of data with different nature, thus an interdisciplinary collaboration and a considerable computational effort are usually necessary; but, on the other hand, it is a reliable criterion which results are easily repeatable and allow - in a simple and consistent way - to define the extent of the expected damage posed by the occurrence of given landslide phenomenon.

The use of the Quantitative Risk analysis (QRA) in geotechnical engineering started in the 90s, particularly in the mining industry, dam management and slope safety (i.e. Fell & Hartford 1997, Wong et al. 1997, Ho et al. 2000). Only in recent years this tool has found use in the landslide risk field and details on the methods that can be used for quantification of each step of the risk analysis are provided in scientific literature (Fell & Hartford, 1997; IUGS, 1997; Ho et al., 2000; Wong et al., 1997; Bell & Glade 2004; Lee and Jones, 2004; Crozier and Glade; 2005, AGS, 2007; Corominas et al., 2013).

The growing interest of the geotechnical Community towards these issues is linked to (Ho et al., 2000):

- the desire of the clients to know their exposure to risk and assign priorities;
- regulatory requirements by governments;
- the concern expressed by public bodies about adequacy of safety systems or measures, especially after a landslide disaster.

According to Corominas et al. (2013), the potentiality of the QRA lies in the possibility to quantify, in an objective and reproducible manner, the probability of a given level of loss posed by the occurrence of a given landslide phenomenon. Therefore, it allows to achieve an uniformity of the results making possible, in a simple way, the comparison of the risk level pertaining to one location (site, region, etc) to another or to different type of landslide phenomena and the implementation of cost–benefit analysis; in this way it provides the basis for the ranking of management and mitigation actions and the associated allocation of financial resources. Moreover, for society, it helps to increase the awareness of existing risk levels and the appreciation of the efficacy of the actions undertaken.

The QRA allows the identification of the probability of the expected level of risk related to a single element, to a group of elements or to a community through a combination of the quantitative measures of likelihood and the consequences.

The risk can be presented in different ways (Fell et al., 2005):

- *Annual risk*: in which the probability of occurrence of the danger is combined with their consequences and summed over all hazard. It is expressed as expected economic damage per annum or potential loss of lives per annum.
- *Frequency - consequence pairs (f-N)*: where the annual probability of certain magnitudes of loss are plotted (the probability of 1 life, 5 lives or 100 lives being lost).
- *Cumulative frequency-consequence plots (F-N plots)*, where the probability of a consequence magnitude or higher is plotted (the annual probability of N or more lives being lost).

In order to calculate the annual risk - with reference to property or to persons- the general expression of the risk (Eq. 3.1) proposed by Varnes (1984) can be detailed as follow:

$$R_{[PROP]} = \sum P_{[L]} \times P_{[T:L]} \times P_{[S:T]} \times V_{[E]} \times E \quad (3.3)$$

$$P_{[LOL]} = \sum P_{[L]} \times P_{[T:L]} \times P_{[S:T]} \times V_{[E]} \quad (3.4)$$

In particular, Eq. 3.3 expresses the annual loss of property value $R_{[PROP]}$ while Eq. 3.4 refers to the annual probability $P_{[LOL]}$ that a particular person may lose his/her life. The $P_{[L]}$ term represents the frequency of the landsliding, $P_{[T:L]}$ is the probability of the landslide reaching the element at risk, $P_{[S:T]}$ is the temporal spatial probability of element at risk, $V_{[E]}$ is the vulnerability of the element at risk, and E is the economic value of the element at risk (in the case of buildings, infrastructures, economic activities) or the number of people exposed (when estimating risk to life). To obtain the total value of risk, summation is required over all hazards and for all exposed population.

Focusing on persons as exposed elements, the risk can be expressed in different ways :

- *Individual Risk*: The likelihood of fatality or injury to any identifiable (named) individual who lives within the zone impacted by the landslide; or who follows a particular pattern of life that might subject him or her to the consequences of the landslide (AGS, 2007).
- *Societal Risk*: The risk of multiple fatalities or injuries in society as a whole due to a specified event or a particular category of events. It is usually defined as the product of the frequency of occurrence of a specified hazard and the number of people in a given population suffering from a specified level of harm, and is normally restricted to events potentially capable of causing large-scale loss of life, injury etc. (AGS, 2007; Lee and Jones, 2004).
- *Group Risk*: is the risk faced by particular groups within society, based on activity, occupation or other relevant divisions. (Lee and Jones, 2004).

4 RISK ZONING

Landslide zoning is the division of land into homogeneous areas or domains and their ranking according to degrees of actual or potential landslide susceptibility, hazard or risk (ISSMGE-TC 32). It is the tangible instrument through which the Governmental Authority is able to plan and develop prediction tools, land-use planning and risk prevention and mitigation measurements. Given its extraordinary importance in the technical sphere, during the last decades significant developments of landslide zoning was recorded (AGS, 2000; AGS, 2007) particularly regarding the scale of work (Cascini et al., 2005) and attainable goals, the methods (Fell et al., 2008), the approaches adopted from site-specific (Wong, 2005) to global scale (Nadim et al. 2006; Nadim and Kjekstad, 2009; Hong et al. 2007).

This Chapter introduces the basic concepts of risk zoning and it analyses the different zoning methods and achievable goals. Therefore, the main developments in the technical field are presented with reference to the Italian case study wherein, starting from the end of the nineties, the landslide risk zoning showed a significant progress making it a leading European nation in terms of landslide risk zoning. Indeed, Italy is among the few European Countries for which the risk zoning maps, performed via qualitative methods, are available all over the Country. Obviously, further progress can be implemented through the employment of landslide risk zoning based on quantitative risk estimation procedures. To this aim, hereinafter the relevant benefits that, at regional and site-specific scale, can be achieved passing from a qualitative to a quantitative risk analysis will be highlighted.

4.1 GENERAL TOOLS

The landslide risk zoning may be developed by preparing different maps that, according to the type of zoning (Corominas et al., 2013), can be distinguished among:

- landslide inventory map;
- landslide susceptibility zoning map;
- landslide hazard zoning map;
- landslide risk zoning map.

Within the framework of landslide risk management (Figure 3.1) the landslide zoning maps may pursue different purposes among those conventionally defined as (Fell et al., 2008): information, advisory, statutory, design. Considering the number of stakeholders involved in the landslide risk management – owners, occupiers, affected public, regulatory authorities, geotechnical professionals and risk analyst (Fell et al., 2005) – as well as the different extension of the areas to be zoned, the landslide zoning maps must be prepared, via the use of suitable methods, at an appropriate scale to get the information needed at that scale (Table 4.1).

The scientific literature suggests a large number of methods for landslide inventory mapping as well as for landslide susceptibility and hazard zoning (Atkinson and Massari, 1998; Evans and King, 1998; Baeza and Corominas 2001; Dai and Lee, 2002 b; Donati and Turrini 2002; Cascini et al., 2005; Cascini, 2008). On the contrary, only few examples are furnished with reference to the activities to be carried out for the identification/quantification of the elements at risk (van Westen, 2004; van Westen et al., 2008) and the analysis/zoning of the consequences (Amatruda et al., 2004; Remondo et al. 2005; Kaynia et al., 2008; Pisciotta, 2008). Independently from the proposed approach, all the available methods can be essentially placed in well defined categories that can be defined as knowledge-driven/heuristic, empirical/data-driven or deterministic/probabilistic (Soeters and van Westen, 1996; Fell et al., 2008).

In knowledge-driven or heuristic methods the landslide zoning is carried out on the basis of the so-called “expert opinion”. These methods are subjective, as they largely depend on the experience and time involvement of the expert. However, these methods have been

extensively used for landslide susceptibility and hazard zoning in many Countries (Cascini et al, 2005) and, depending on the expertise of the person (geologist or geotechnical engineer) carrying out the zoning, may lead to accurate results. Generally, knowledge driven/heuristic methods are of direct type, as the expert interprets a given topic (e.g. the landslide susceptibility) directly in the field based on the observed phenomena and the geological/geomorphological setting, and can also be supported with other methods (e.g. data-driven). Knowledge-driven/heuristic methods can also be applied indirectly using a GIS, by combining a number of factor maps that are considered to be important for landslide occurrence. In this regard, several techniques can be used such as Boolean overlay, Fuzzy logic, multi-class overlay and Spatial Multi-Criteria Evaluation.

Empirical methods are based on field observations (dealing with the landslide phenomena and/or the elements at risk) whose data can be used to obtain relationships – in some cases statistically-based – useful for the analysis purposes (e.g. the run-out distance estimate, the consequence prediction, etc.). Empirical methods are based on simplified assumptions and, consequently, they might not always have an evident interpretation (Hungri et al., 2005). In data-driven methods the combinations of factors that have led to landslides in the past are statistically evaluated and quantitative predictions are made for current landslide free areas with similar conditions. Three main data-driven approaches are mainly used, namely: bivariate statistical analysis, multivariate methods, and Artificial Neural Network analysis.

Deterministic/probabilistic (or analytical) methods apply classical theory and principles such as limit equilibrium, limit analysis and finite/boundary/distinct element or finite difference techniques. These methods, including the so-called physically-based models such as SHALSTAB (Montgomery and Dietrich, 1994) and TRIGRS (Baum et al., 2008) are useful for landslide susceptibility analyses over large areas, require high-quality input data for both landslide phenomena (such as soil thickness, soil strength, groundwater regime, slope geometry, etc.) and the elements at risk. Uncertainties in input data can be introduced in probabilistic methods such as FORM, FOSM and Monte-Carlo simulations (Nadim et al., 2005).

Independently from the adopted method, hazard and risk assessment can be intrinsically considered quantitative only when a single landslide and element at risk, or homogeneous aggregates of one or both of them are introduced in the analysis. This is essentially related to the inapplicability

of the risk formula when each term cannot be properly quantified on the basis of a physical meaning.

The current practice in Europe (Corominas and Mavrouli, 2010) shows that the scale of the landslide zoning maps – required by State or local Authorities – varies significantly from Country to Country depending on the coverage, input data and methods that are used and the information provided (qualitative or quantitative). In particular, it is possible to distinguish: Small, Medium, Large and Detailed scale to each of which corresponds a suggested types/methods of zoning (Table 4.1) and pursued purposes (Table 4.2).

At the small scale or national zoning map scale ($< 1:100,000$) knowledge-driven/heuristic methods are suggested for landslide inventory mapping and susceptibility zoning (Malet et al., 2009) even though hazard and risk zoning has been proposed at this scale (Castellanos Abella and van Westen, 2007). According to Soeters and van Westen (1996) this zoning scale is intended to give a general inventory of problem areas for an entire Country that can be used to inform national policy makers and the general public; furthermore, it may be also profitably used to individuate and plan warning systems in the charge of central Authorities. The areas to be investigated are larger than tens of thousands of square kilometres.

At the medium scale or regional zoning map scale ($1:100,000$ to $1:25,000$) the best methods for susceptibility and hazard zoning (risk zoning can be developed once the necessary input data are available) are represented by the knowledge-driven/heuristic ones; data-driven methods are recommended only when appropriate input data are available (Fell et al., 2008). The zoning map developed at the regional scale may be used for information and advisory purposes. Indeed, as quoted by Soeters and van Westen (1996), the regional scale is meant for planners in the early phases of regional development project or for engineers evaluating possible constraints due to instability in the development of large engineering project and regional development plans; furthermore, they may be also adopted to individuate and plan warning systems and urban emergency plans at regional level. Typical areas to be investigated are larger than $1,000 \text{ km}^2$ up to tens of thousands of square kilometres.

At the large scale or local zoning map scale ($1:25,000$ to $1:5,000$) the empirical/data-driven methods for hazard and risk zoning are the preferred ones even though knowledge-driven/heuristic may be also used in combination with other methods; deterministic/probabilistic

methods can be applied once the high quality of all the necessary input data is guaranteed. The local scale is usually used for statutory purposes and it is the reference scale to plan and implement urban developments, warning systems and emergency plans at local level. Moreover, this scale is absolutely relevant to rank the most at risk areas and, then, to prioritise those needing mitigation measures aimed at reducing the risk to persons. Areas of zoning usually range from 10 to 1,000 km².

At the detailed scale or site-specific zoning map scale (>1:5,000) deterministic/probabilistic methods must be necessarily adopted to develop landslide hazard and risk zoning maps; knowledge-driven/heuristic method may be used in combination with other methods just as the preliminary stage of zoning. This scale may be used for statutory purposes while is the only one that can be adopted at the level of the site investigation before the design phase of control works (Soeters and van Westen, 1996). The size of study areas may range up to tens of square kilometres.

Table 4.1 Methods, levels, and types of zoning at different scales (Cascini, 2008 mod.).

Scale description	Indicative range of scales	Zoning methods			Zoning levels			Type of zoning	Purpose
		Basic	Intermediate	Advanced	Preliminary	Intermediate	Advanced	Susceptibility	
Small	< 1:100,000	*			*			*	Regional zoning - Information
Medium	1:100,000 to 1:25,000	*	(*)		*	(*)		*	Regional zoning - Information - Advisory
Large	1:25,000 to 1:5,000	*	*	*	*	*	*	*	Local zoning - Information - Advisory - Statutory
Detailed	> 1:5,000	[*]	(*)	*	[*]	(*)	*	[*]	Site specific zoning - Information - Advisory - Statutory - Design

The landslide inventory mapping and the identification/quantification of the elements at risk are the basis for all the zoning; indeed, it is important that these activities are done thoroughly independently from the pursued purposes and the scale of zoning. With this aim, the landslide inventory and the elements at risk should be mapped at a larger scale than the other zoning maps. Anyway, even though this principle is properly taken into account, some constraints can arise due to the scale of zoning. Particularly, at national and regional scales, only aggregates of landslides and elements at risk can be placed, or are better to place, in the maps; depending on the scale and purposes of zoning, the aggregates may include homogeneous (this is the case of quantitative approaches) or not homogeneous data as it concern the types of landslide and elements at risk. On the contrary, at local and site scales the single landslide and element at risk must be analysed and depicted in the maps.

Table 4.2 Landslide zoning mapping scales and their application (Fell et al., 2008 mod.).

<i>Scale Description</i>	<i>Indicative Range of Scales</i>	<i>Examples of Zoning Application</i>	<i>Typical Area of Zoning</i>
Small	< 1:100,000	Landslide inventory and susceptibility to inform policy makers and the general public	>10,000 square kilometres
Medium	1:100,000 to 1:25,000	Landslide inventory and susceptibility zoning for regional development; or very large scale engineering projects. Preliminary level hazard mapping for local areas	1000 – 10,000 square kilometres
Large	1:25,000 to 1:5,000	Landslide inventory, susceptibility and hazard zoning for local areas Intermediate to advanced level hazard zoning for regional development. Preliminary to intermediate level risk zoning for local areas and the advanced stages of planning for large engineering structures, roads and railways	10-1000 square kilometres
Detailed	> 5,000	Intermediate and advanced level hazard and risk zoning for local and site specific areas and for the design phase of large engineering structures, roads and railways	Several hectares to tens of square kilometres

Notwithstanding the absence of a standardised procedure for landslide risk zoning, several hazard and risk maps have been developed in order to promote political actions aimed at forecasting and preventing the landslide risk. Focusing on Europe, some Countries (France, Italy, Norway and Switzerland) developed, on official bases, landslide hazard and risk zoning maps – at medium and large scales – where hazard and risk posed by both existing and potential landslides are ranked according to established criteria. Although the procedures adopted for hazard and risk analysis and zoning are different among the Countries, they are commonly based on qualitative methodological approaches.

In the following, the Italian case study will be presented. In particular, the adopted method for hazard and risk zoning, which was developed - at large scale and over all Country - to confront the urgent need requested by the Central Authorities, will be discussed.

4.2 THE ITALIAN CASE STUDY

Landslides are extremely widespread throughout the Italian territory; in the period spanning from the 1116 to December 2007 were surveyed more than 482,000 landslide events involving an area of 20,573 km², equal to 6.8% of the Country (Figure 4.1) (<http://www.isprambiente.gov.it/it>).

The analysis of the census data revealed that 5,708 Italian municipality out of a total of 8,101 (70,5% of the territorial extent) are affected by landslides.

The exposed population to landslide risk, estimated by the using of the IFFI Inventory and the census data ISTAT 2001, amounts to 992,403 inhabitants.

The severity of the problem is highlighted even more by considering the consequences to exposed elements recorded in recent years. In the Twentieth century, in fact, with reference to damages to persons, the landslides in Italy caused 5,831 deaths, 108 missing and 1,860 injured, with an average deaths of 59.4 per year, value that sets Italy to the fourth place in the world behind the Andean countries, China and Japan (Guzzetti, 2000). In this regard, northern Italy has suffered more death due to rock falls, rock-slides, rock avalanches and debris-flows while in south Italy the number of victims were mainly related to the occurrence

of flow-type phenomena involved granular soils (e.g. Salerno 1954; Sarno, Siano, Bracigliano, Quindici 1998; Cervinara, 1999; Soverato 2000; Messina 2009; Casamicciola 2009; Maierato, 2010; Atrani 2010; Messina 2011).

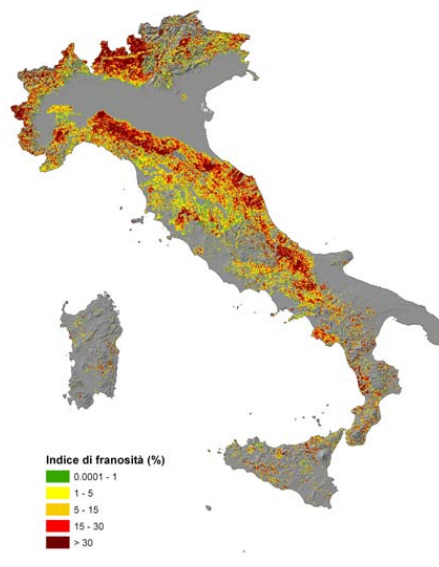


Figure 4.1 Landslide Index (%). Calculated on a mesh size of 1 km expresses the landslides incidence on the regional territory potentially affected by landsliding phenomena (www.isprambiente.gov.it).

Due to the particularly serious consequences of past landslide events, the Italian Government has charged the technical Community to make use of legislative tools aimed at the prevision and prevention of landslide risk.

Nevertheless, the most recent disasters that affected north and south Italy seem to confirm a continued worsening of the level of risk to which the population is exposed. This is likely to be related to the intense anthropogenic and disorderly urbanisation that began in the '50s, to the widespread deforestation and abandonment of the countryside together with the intrinsic fragility of the territory with a very young geological and morphology structure and a climate characterised by heavy and short-time concentrated rain.

Therefore, so that common and frequent landslides do not become natural catastrophes, it is necessary to pursue an interventionist action that makes use of structural and non-structural mitigation measures ranging from engineering control works - for the consolidation of unstable slopes and make safe the urbanised towns - to the relocation and instrumental monitoring networks which allow the activation of warning systems.

4.3 RISK ZONING IN ITALY

In Italy at the beginning of the 20th century the so-called “hydrogeological hazards” (including floods and landslides) were indirectly accounted for several national regulations that generally imposed legal bindings and land-use limitations to specific areas or activities. After the severe flooding of Florence occurred in 1966, in order to prevent the occurrence of further disaster, there was the need to adopt a land-use planning at basin-scale. This led to the enactment of Law 183/1989 defining the “Hydrographic Basin” as the reference terrain unit within which to concentrate the planning actions. The Basin Authorities were, therefore, tasked to oversee such units; to them were assigned the duty to prepare the "Basin Plan" containing information regarding the physiographic outlines and the land-use planning. The Basin Authorities began an intense study that soon pointed out all the difficulties inherent legislative requirements, with reference to landslides zoning, due to the significant diffusion of landslides in the national territory, their inherent complexity and a lack of a well-established scientific culture in the field of landslide risk. Therefore, the work remained unfinished until 1998 when, due to the catastrophic events of flow-like fast-moving landslides in Campania region (Southern Italy), there was a growing awareness from both public administrations and scientific Community to undertake a correct policy of territorial management through a deep understanding of the natural processes. This interest led to the acquisition of a greater knowledge of landslide mechanisms and the definition of the useful instruments to manage and forecast landslides triggering. In this regard, the scientific Community started a highly advanced cognitive process for understanding the triggering mechanisms of these phenomena, the evaluation of the

residual risk inside the towns threatened by past landslide events and the identification of other sites affected by an analogous risk in the Campania region (Cascini, 2004; Cascini, 2005 a, b). The important answer given by the scientific Community gave impetus to a strong legislative process. In particular, the Central Government promulgated the Law 267/1998 requiring the Basin Authorities to adopt the Hydrogeological Setting Plans in order to provide the identification and analysis of all areas at risk with reference to landslides (PsAI-Rf) and flooding (PsAI-Ri).

The difficulties inherent the preparation of such plans implied the enactment of additional legislation that imposed the immediate adoption of the "Extraordinary Plan" (Law 226/1999) aimed to remove the higher risk situations R4. The legislative process restarted after the Soverato events (Law 365/2000) with the adoption of the Hydrogeological Setting Plans, on the whole national territory. Within the so-called "Hydrogeological Setting Plans" hazard and risk zoning was updated according to criteria given by the Central Government (D.P.C.M. 29/09/98) that distinguished, according to the expected consequences to landslides, four risk classes:

- Very high (R4), where human life loss and destruction of buildings, infrastructures and the environment as well as the interruption of economic activities are expected;
- High (R3), where victims, functional damage to buildings and infrastructures, as well as partial interruption of economic activities are possible;
- Medium (R2), where limited damage to buildings, infrastructure and the environment may occur;
- Low (R1), where social, economic and environmental damage are of marginal relevance.

Through so in-depth work, which has been produced in the 2-3 years following the disaster of 1998, Italy today can be considered a leading European nation in terms of landslide risk zoning.

The analysis of the contents of PsAI-Rf has highlighted that approximately 4.5% of the country has a very high level of risk R4 (www.apat.gov.it). In the areas classified as R4 or R3 legislation states that it is possible to realise only not-delocalised engineering works by Public Bodies. Private parties may, conversely, intervene only in the areas

with a lower level of risk (R2-R1). At the regulatory level the various River Basin Authority have, therefore, adopted specific rules that regulate land use in the different classes of risk (R1-R4).

Taking into account that hazard and risk zoning will be probably updated in the next future, since the Basin Authorities will be reorganised in 8 District Authorities covering the whole national territory (Legislative Decree 152/2006, according to the E.U. 2000/60 Directive about water resources management), the main goals pursued through current landslide hazard assessment practices will be discussed, focusing the attention on the methodological integration to be undertaken in order to make the process as smooth as possible.

4.4 FROM QUALITATIVE TO QUANTITATIVE RISK ANALISYS AND ZONING

The assessment of landslide risk all over Italy was implemented by the various Basin Authorities (6 National Basin Authorities and 11 Interregional Basin Authorities) following general instructions (D.P.C.M. 29/09/1998). In particular, the analysis of Hydrogeological Setting Plans, conducted under the PRIN 2007 project - *Susceptibility and hazard analysis and zoning of landslides triggered by extreme events (rainfall and earthquake)* (Cascini, 2012) - highlighted that PsAI-Rf can be considered at a preliminary level of zoning (Fell et. al, 2008) since they were realised with basic methods based on heuristic procedures and, therefore, they can be used for the pursuit of well-defined purposes intimately linked to the input data, to adopted methods and topographic scale that, in most cases, coincides with 1:25,000 scale.

However, it worth noting that no European Nation has a preliminary level of landslide risk zoning throughout the Country.

Nevertheless, some critical points must necessarily be observed that require further efforts.

The first critical issues is strictly related to the different methodologies used by the Basin Authorities which give rise to a non-uniform hazard and risk zoning. This circumstance requires the identification of a common methodology, which hypothesis have already been advanced (Cascini et al., 2012), in order to transform the current plans in a truly unique document for completeness and preparation.

With reference to the general framework of the risk management (Figure 3.1), the current risk zoning can be considered as the cartographic representation of the risk analysis phase to which persons or economic goods are exposed, through a qualitative approach that makes use of descriptive indicators of the expected consequences (R1, R2, R3, R4). The risk zoning map, just exactly how it was conceived, is useful for land-use planning purposes - as it allows to identify the most critical situation in the area - and, consequently, it allows the implementation of appropriate strategies for the safety of human life through the use of early warning systems. Conversely, due to the limitation of available knowledge and to the used topographic scale for the analysis, it appears inadequate for the achievement of purposes related to the implementation of mitigation control works.

In this regard, the use of quantitative risk estimation methods may allow, on the one hand, to increase the level of knowledge within the zones recognised - on the basis of qualitative studies - at very high risk, and secondly, to compare - in a simple way - the critical situations concerning different areas thanks to the possibility to express the risk in terms of annual probability of loss of life or economic damage. It is important to note that this methodology can also set up a prioritisation of areas requiring urgent protective measures favouring, efficiently and effectively, the proper allocation of available financial resource.

On the basis of the above premises, hereinafter, an original methodology aimed at quantify the risk posed by flow-like phenomena are presented, highlighting the considerable benefits that can be achieved passing from a qualitative to a quantitative risk analysis.

5 QUANTITATIVE RISK ANALYSIS AT MEDIUM SCALE: THE CAMPANIA REGION CASE STUDY

The quantitative analysis of landslide risk to life is generally aimed at estimating the so-called individual and societal risk to life.

Individual risk to life is defined as “*the risk of fatality or injury to any identifiable (named) individual who lives within the zone impacted by the landslide or who follows a particular pattern of life that might subject him or her to the consequences of the landslide*” (Australian Geomechanics Society, 2007). It is usually expressed as the annual probability that the person most at risk will lose her/his life due to the occurrence of a landslide of a given intensity.

On the other hand, the concept of societal risk is based on society’s aversion to high-fatality incidents; society, in fact, is more inclined to tolerate frequent events that cause few casualties rather rare events with high loss of human life (Ho et al., 2000). It is defined as “*the risk of multiple fatalities or injuries in society as a whole: one where society would have to carry the burden of a landslide causing a number of deaths, injuries, financial, environmental and other losses*” (Australian Geomechanics Society, 2007).

At large (1:25,000 to 1:5,000) and detailed ($> 1:5,000$) scales, societal risk is generally expressed by F-N or f-N curves, that represent in a bi-logarithmic plane a cumulative annual probability F - or the annual probability f - that N or more lives will be lost based on fatal event scenarios (Ho et al., 2000; Leroi et al., 2005).

When landslide risk analyses are carried out at either a small ($< 1:100,000$) or medium (1:100,000 to 1:25,000) scale, it is feasible to derive the societal risk starting from historical incident data, namely by correlating the cumulative annual frequency F of landslides causing N or more fatalities versus the number N of fatalities. In such a case, it is possible to quantify the societal risk under the following hypotheses (Düzgün and Lacasse, 2005):

- the location of past and present landslides are the source of future landslides;

- future landslides have the same conditions as the past and present landslides;
- only the considered factors determine the distribution of past and present landslides.

Hence, the obtained F-N curve reveals the rates of fatal landslides and related consequences that society has implicitly found acceptable; in other words, it represents what society lives with now (Christian, 2004).

According to Fell and Hartford (1997), Guzzetti (2000), Düzgün and Lacasse (2005) and Cascini et al. (2008 b). The F-N curves generated from historical incident data can be derived for various geographical units (State, Country, Region, Province, etc.) in order to compare the societal risk due to several hazards (landslides, earthquakes, dams, airplane crashes, etc.) or to compare the societal risk situation in different geographical unit for a given hazard, since they can be used for developing acceptability and tolerability risk criteria.

If the historical records are selected on the basis of simple criteria (i.e. soils involved in past fatal landslides, geological-structural setting of the geological context in which they occurred, typology of landslides, etc.) the corresponding F-N curves could be used by Public Authorities to establish, within a given area, a rank of the most at risk sub-areas that need the application of QRA procedures (Cascini et al., 2008 b). This is the case of the Campania region for which, through a careful analysis of a comprehensive catalogue of incident data dealing with flow-like phenomena that have caused casualties, it was possible to identify the F-N curves for different geological contexts (Cascini et al., 2008 b; Vitolo 2009).

In the following, after a brief presentation of the documentary sources used for collecting historical data and the description of the geological contexts of the Campania region, the main results of the societal risk analysis related to fatal (undistinguished) landslides (Cascini et al., 2008 b) are exposed. Further issues are then devoted to the analysis of spatial and temporal distribution of two main types of flow-like phenomena, namely debris flows and hyperconcentrated flows.

5.1 THE CAMPANIA REGION

The Campania region (southern Italy) covers a territory of 13,590 km² and includes 551 municipalities (Figure 5.1 a). Within the region it is possible to distinguish three main geological contexts (Figure 5.1 b) which are quite different from each other owing to geological, hydrogeological and geomorphological features as well as age and type of pyroclastic deposits (Cascini et al., 2008 b).

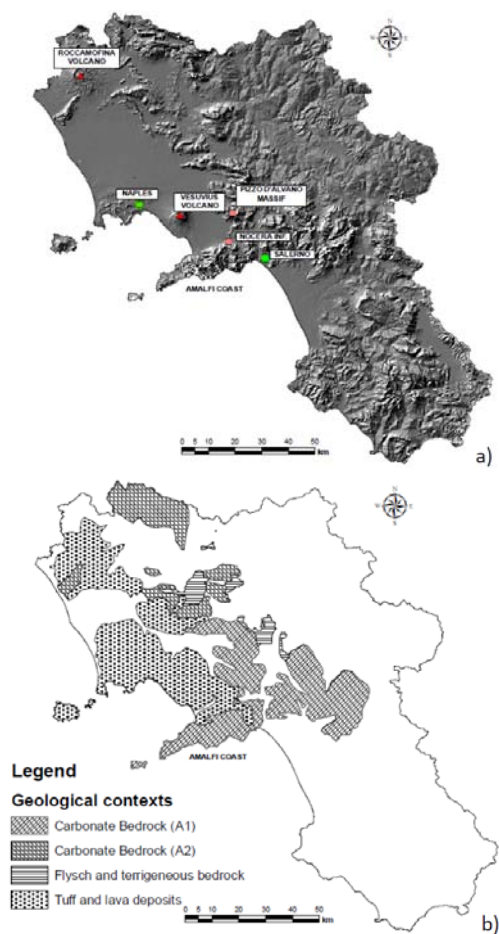


Figure 5.1 a) The territory of the Campania region (southern Italy); b) Map of the areas of the Campania region where pyroclastic soils cover different bedrocks (modified from Vitolo, 2009).

According to Cascini et al. (2008 b) the geological context (A) coincides with large sectors of the Campanian Apennine chain, constituted by Mesozoic carbonate rocks where the presence of pyroclastic covers can be recognised. This context, in turn, can be distinguished into two different sub-contexts (A1 and A2). The first one (A1) corresponds to areas of the Campania region where loose cohesionless pyroclastic soils mainly deriving from the plinian phases of the Somma-Vesuvius volcanic activity cover the slopes as primary air-fall and re-worked deposits (Rolandi, 1997). The second sub-context (A2) is located in the northern part of the region, where the presence of weakly cemented pyroclastic deposits can be essentially related to the Roccamonfina volcanic activity which presumably ended about 50,000 years ago.

The context (B) corresponds to the Phlegraean district, including the city of Naples as well as the islands of Ischia and Procida and it is characterised by a bedrock of Late Pleistocene volcanic tuffs and lavas overlaid by pyroclastic deposits which can reach a thickness of several metres (Calcaterra et al. 2004).

Finally, the third main context (C), essentially located in the north-west of Sarno and Picentini Mounts, includes thin pyroclastic deposits mantling flysch and terrigenous bedrock.

5.2 THE HISTORICAL DATABASE

Historical research on the landslides in Campania region started at the University of Salerno since 1997 (Migale, 1998; Operative Unit 2.38, 1998) through a systematic investigation of different documentary sources (Cascini et al., 2008 b; Vitolo, 2009).

In particular, with reference to landslide events occurred before the 19th century, the information are mostly collected from literary works (Camera, 1999) as well as from documents preserved in the parish archives.

For the 19th century the main documentary sources are those of the “Intendenza del Regno delle Due Sicilie (Sezione Opere Pubbliche)”, founded by the Bourbons in 1806, and housed in the State Archive of Salerno. Additional contributions are provided by documents kept in the archives of the ‘Genio Civile’ (dating back to 1816) and ‘Prefettura di Gabinetto’ (i.e. the Province Administration, founded in 1861 and

instituted prior to the Unification of Italy in 1861) as well as other documents labelled ‘Protocolli Notarili’.

In relation to the 20th century, the most important contemporary source of information is mostly constituted by the historical literature (Mansi, 1912; Amarotta 1994). Further information can be obtained from many essays written following the events of May 1998 (Migale and Milone, 1998; Buono and Milone 2000; Mazza and Amendola 1999; State Archive of Salerno, 2000; Celentano, 2001), from a book describing the hydrogeological events that involved the Italian territory after the end of the Second World War up to 1990 (Catenacci, 1992) as well as from local and national newspapers kept in the Provincial Library of Salerno. The recovered data were systematically integrated with those of the Italian National Research Council’s AVI Special Project archive (http://sici.irpi.cnr.it/danni_persone.htm), created after the analysis of newspaper articles, scientific and technical papers as well as reports and interviews with landslide experts (Guzzetti, 2000; Guzzetti et al. 2005).

5.3 F-N CURVES FOR THE CAMPANIA REGION

In order to provide a quantitative estimation of the landslide risk in Campania Region, Cascini et al. (2008 b) analysed the information gathered from the documentary sources described in Sect. 5.2 with reference to 311 fatal landslide events occurred from 1640 up to 2008.

Leaving out the aspects related the completeness of the historical catalogue as well as the associated uncertainties, widely discussed in Cascini et al. (2008 b), the Authors plotted in a bi-logarithmic plane the F-N points obtained from the above analysis and then interpolated them with the following mathematical expression:

$$\log F = a - b \log N \quad (5.1)$$

It is worth noting that the relationship (5.1) between the annual cumulative frequency F and the number of fatalities N follows a power-law similar to the one established by Gutenberg and Richter (1956) for earthquakes (Eq. 5.2):

$$F = c N^b \quad (5.2)$$

where: $c \ni a = \log c$

The parameter a depends on the time period for which the historical records are available as well as on the areal extension of the territory under study. On the contrary, the parameter b which identifies the curve slope is independent of the time period.

The comparison of F-N curves related to the Campania region with that of the Italian territory (Guzzetti, 2000) (Figure 5.2) highlights that Campania is one of Italian regions with the highest societal risk due to landslides, since its F-N curve is very close to that of Italy.

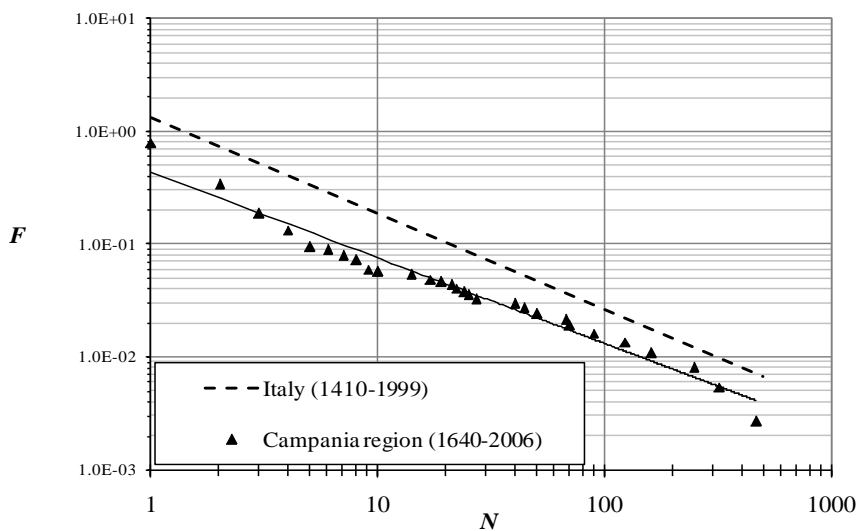


Figure 5.2 F-N curves related to fatal landslides in the territory of Campania region and Italy (Cascini et al., 2008 b, modified).

Further interesting considerations can be done comparing the $F-N$ curves for fatal landslides occurred in the three geological contexts in which pyroclastic covers are present (Figure 5.3). They, in fact, allow to detect the portions of the Campania region where the biggest and most catastrophic events are most likely to occur.

In particular, Figure 5.3 shows that people living within context A1 are the most exposed to the landslide risk essentially related to the occurrence of fast flow-like phenomena.

The obtained results are helpful for the Authorities in charge of landslide risk management. Indeed, they allow the identification – within the large

area including 212 municipalities whose urban areas are indiscriminately classified at very high risk from the PsAI-Rf – of the most critical situations; or, in other words, the prioritisation of the Municipalities needing structural or non-structural (i.e., emergency plans and warning systems) measures aimed at mitigating the landslide risk to life (Table 5.1).

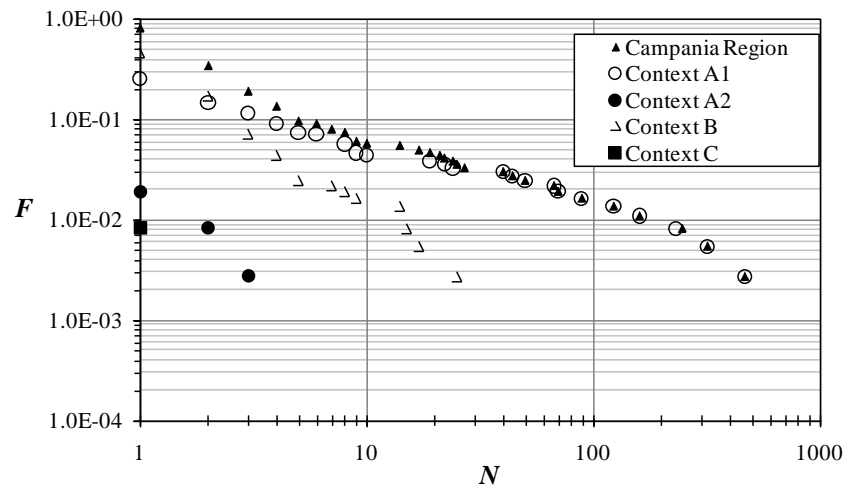


Figure 5.3 F-N curves related to fatal landslides in the Campania region and in different geo-environmental contexts. All curves refer to a 366-year period between 1640 and 2006 (Cascini et al., 2008 b).

Table 5.1 Classification of area at risk with reference to flow-like phenomena.

<i>Geological context</i>	<i>Number of Municipalities</i>	<i>Number of Municipalities threatened by fatal landslides</i>	<i>Recorded number of deaths</i>
A1	121	57	1790
A2	70	7	11
B	157	39	301
C	66	3	3

5.4 FEATURES OF DIFFERENT FLOW-LIKE PHENOMENA

The studies carried out by Cascini et al. (2008 b), on the basis of a comprehensive catalogue of historical data concerning fatal events, showed that pyroclastic soils resting on a carbonate bedrock belonging to the Campania region are systematically affected by slope instabilities, later propagating as flow-like phenomena characterised by a high destructiveness in terms of fatalities as well property and economic losses. However, when frequency estimations and/or design of non-structural mitigation measures at regional scale are dealing with, the historical analyses cannot be limited only to fatal events; indeed, all incident data must be considered for the achievement of the above purposes.

This issue was specifically addressed in this Thesis with the further aim to separate the historical events accompanied by the occurrence of rainfall-induced slope instabilities later propagating as debris flows from those originating hyperconcentrated flows. As highlighted in Chapter 2, these two kind of flow-like phenomena are characterised by own: (in the source areas) triggering factors, involved materials, mobilised volumes; (in the propagation/deposition areas) rheology as well as geometrical and kinematical characteristics of the flowing water-sediment mixtures, and, therefore, different expected consequences.

In order to achieve the abovementioned goal, all incident data (1,230) coming from the comprehensive catalogue of slope instabilities – occurred in Campania Region from the 16th century up to 2010 and triggered by rains, earthquakes or man-made actions – were re-examined in order to firstly select only the events associated to rainfall-induced slope instabilities that later propagated as flow-like phenomena. In this regard, 185 rock-involved landslides were recognised and removed from the database as well as 53 events dealing with landslides triggered by earthquakes and anthropic factors. The remaining 992 data – dealing with rainfall-induced flow-like phenomena – were then considered for further analyses.

In particular, the corresponding cumulative curve (Figure 5.4 a) shows a sharp increase in its slope starting from the 19th century when more circumstantiated records (in terms of typology of the occurred flow-like phenomena, related consequences, etc.) are available; the cumulative curve is steepest starting from the mid-20th century, in which the number

of incident data related to flow-like phenomena resulting in minor consequences and with limited areal extent significantly increases.

A similar trend is shown by the cumulative curve referring to flow-like phenomena occurred in the geological context A1 (Figure 5.4 b) that exhibits a constant slope for the period spanning from the 1500 to 1812, after which it presents a marked change of the slope similarly to the cumulative curve of the totally events recovered for the Campania region. Therefore, in relation to the geological context A1, in agreement with the previous studies (Cascini et al., 2008 b), the historical catalogue can be considered as sufficiently complete for the last three centuries.

As for the remaining geological contexts few incident data were recovered (Figure 5.4) starting from the 20th century.

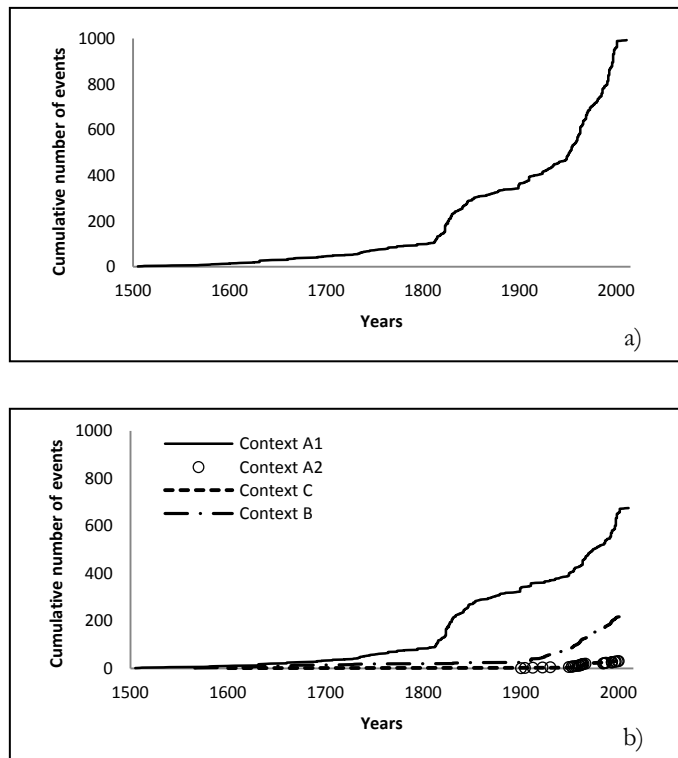


Figure 5.4 Cumulative curve of flow-like phenomena occurred a) in the territory of Campania region and b) in the geological contexts (A1, A2, B, C) from the 16th century to 2011.

With reference to the flow-like phenomena occurred in the geological context A1, thanks to a detailed analysis of the information provided by the historical documents (in terms of rainfall characteristics, run-out distances, magnitude of the recorded consequences, etc.), it was possible to disaggregate the different types of flow-like phenomena occurred in the study area in two main classes: hyperconcentrated flows and debris flows. It is important to note that data about 46 hyperconcentrated flows events have been recovered in the time period spanning from the 1631 to 2010 while 185 debris flows events have been identified from 1588 to 2001.

On the basis of the performed disaggregation, relevant considerations about the temporal distribution over the year as well as the main features of both boundary and initial conditions leading to slope instabilities later propagating as hyperconcentrated flows and debris flows can be done.

With reference to the temporal distribution, the knowledge of the date of occurrence of the censored events – total for hyperconcentrated flows and partial for debris flows (171/185 events) – allowed the individuation of the period of year in which the phenomena are likely to occur. In particular, focusing on debris flows affecting the context A1 (Figure 5.5 a) the obtained results show that their monthly distribution follows a bimodal distribution with an absolute maximum value in the October month, a relative maximum value in the month of May and a minimum value during the summer months. It is worth noting that, according to Cascini et al. (2008 b), the most catastrophic events - in terms of loss of life - are concentrated over the months of October and November (i.e. at the beginning of the rainy season).

On the other hand, referring to hyperconcentrated flows (Figure 5.5 b) the monthly distribution is essentially concentrated over two autumnal months (October and November).

Obviously, the monthly distribution of events is closely linked to rainfall pattern as well as to the initial conditions existing in the study area that spatially drastically change during the year, particularly at regional scale. Therefore, in order to individuate the critical conditions for the triggering of both debris flows and hyperconcentrated flows it is necessary to pay due attention on the relationship between the rainfall pattern and the current soil suction levels with the trigger mechanism accompanying the occurrence of a well defined flow-like phenomenon.

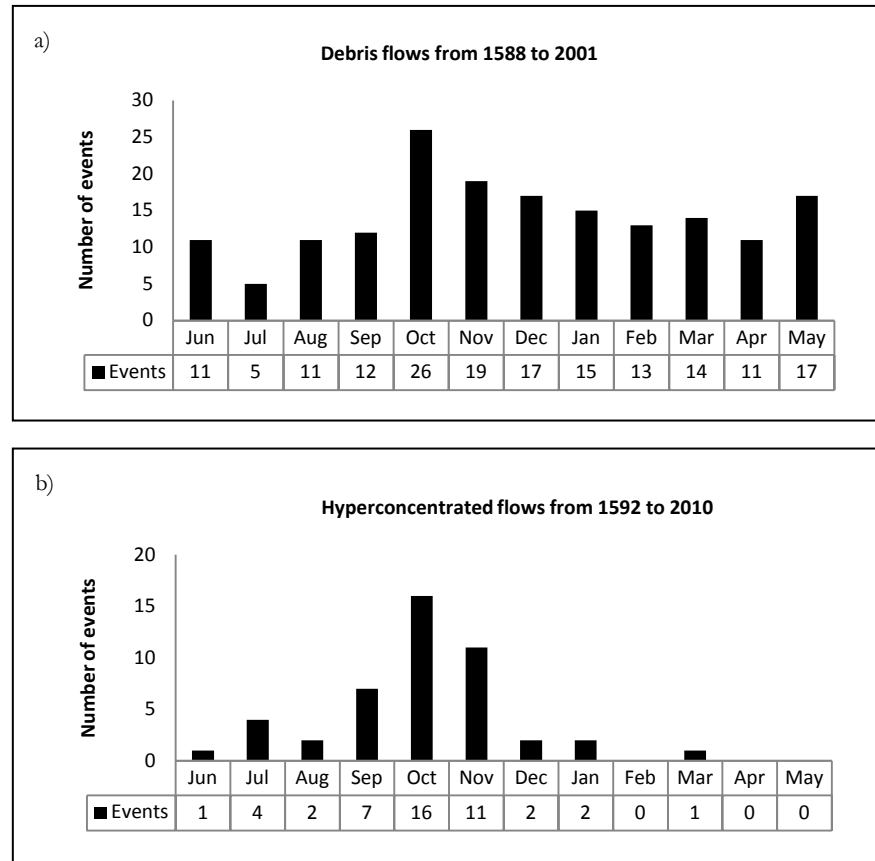


Figure 5.5 Montly distribution of a) debris flows and b) hyperconcentrated flows in the geo-environmental context A1 of the Campania region.

As far as the boundary conditions – in terms of triggering rainfall – are concerned, it must be preliminary observed that in the Mediterranean three different meteorological processes are prevailing (De Luca et al., 2010; De Luca, 2013), namely:

- *Frontal or cyclonic phenomena* affecting large areas ($10^3 - 10^4 \text{ km}^2$) and generated by the movement of large masses of warm moist air that meet cold air masses. They have a typical stratiform structure, characterised by rainfall of moderate intensity (1-10 mm/h), in which it is often possible to identify cells – or clusters

of cells – with high intensity. The duration extends from several hours to several days.

- *Isolated convective cells* having a spatial extent of about 10–50 km², i.e. the same order of size of small hydrographic catchments. They are associated with the convective movement of warm moist air masses towards the cold layers of the overlying atmosphere. The resulting spatial distribution is heterogeneous with instantaneous and average intensity spanning a wide range of typically 10–100 mm/h in a few minutes. Each cell usually lasts less than an hour (typical summer storms) and it may take several hours for all of the active cells to dissipate.
- Hurricane - like rainfall, i.e. convective events having their origin in the sea, under particular thermophysical conditions, and able to generate “extreme” rainfall events involving, in less than 24 hours, areas whose extent is of the order of 10²-10³ km². They generally affects specific areas near/along the sea coast, depending on the presence of a suitable topography and specific physical conditions. Typically, they are observed from the end of August to November (Reale and Atlas, 2001).

Then, thanks to the availability of hydrological records (collected in the annals of the Italian Hydrographic and Mareographic Service) dealing with periods of the last century when flow-like phenomena occurred in the Campania region, it was possible to associate a given type of flow-like phenomenon (i.e. debris flow or hyperconcentrated flow) with the meteorological process accompanying the related triggering rainfall. In particular, the analysis of the spatial distribution and the peculiar characteristics of rainfalls, in terms of duration and intensity, revealed that debris flows are mostly associated with frontal storms (Figure 5.6), typical of the rainy period. They are generally characterised by a continuous sequence of rainy days with final peak values of more than 100 mm of cumulated rain (Figure 5.7), in turn leading to a progressive decrease of the soil suction values and to the consequential occurrence of first-time shallow slides (i.e. flowslides or debris avalanche) at source areas later propagating as debris flows (Cascini et al., 2013 a).

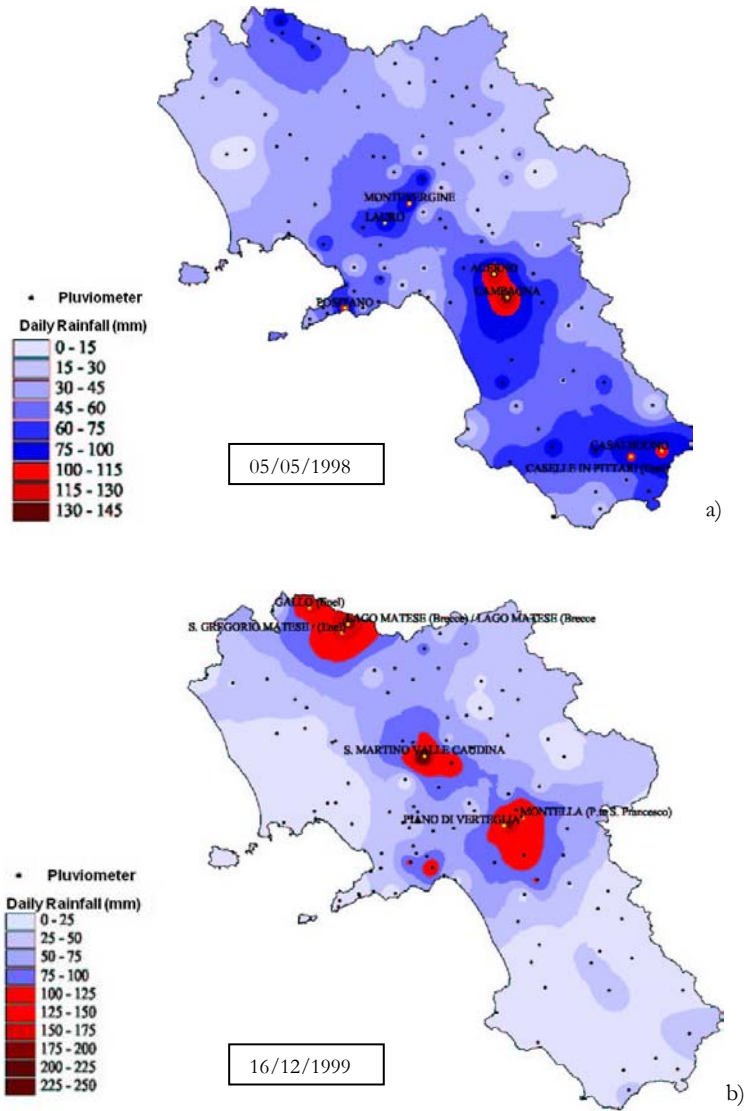


Figure 5.6 Example of frontal rainfall events triggering debris flows (reconstruction obtained by CERIU, 2003).

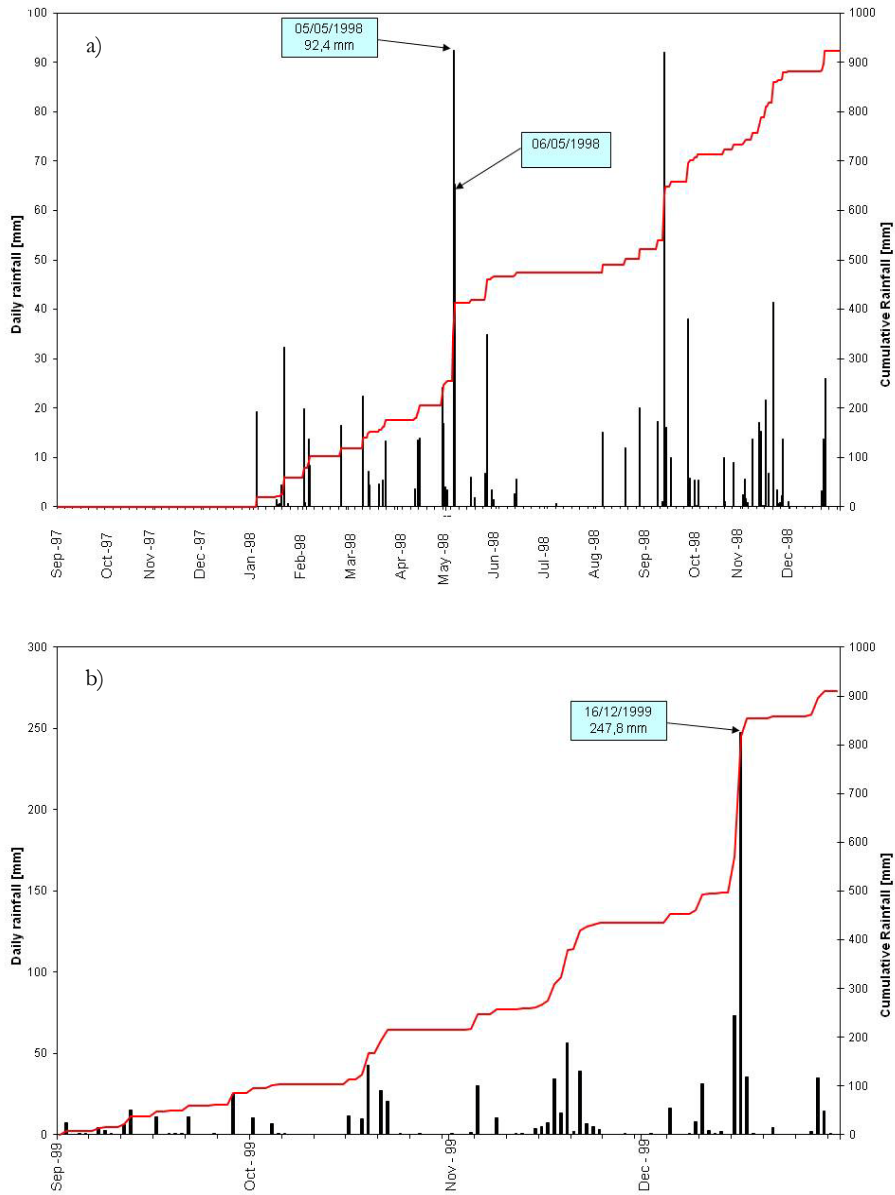


Figure 5.7 Rain events monitored at a) Lauro Town for the debris flows occurred in May 1998 and at b) S. Martino Valle Caudina Town for the debris flows occurred in December 1999 (reconstruction obtained by CERIU, 2003).

On the other hand, the occurrence of hyperconcentrated flows is related to isolated convective cells (Figure 5.8 a) or hurricane-like rainfall (Figure 5.8 b). These meteorological processes are associated to rainfalls of high intensity and short duration, not preceded by long-lasting rains (Figure 5.9). Hyperconcentrated flows are frequent in the summer season or at the beginning of the rainy period, when superficial soils experience high levels of the matrix suction and, therefore, low permeabilities. This condition inhibits the water infiltration into the soil and runoff prevails; these, in turn, lead to the occurrence of erosion phenomena or localised small-size slope instabilities, typically turning into hyperconcentrated flows (Cascini et al., 2013 a).

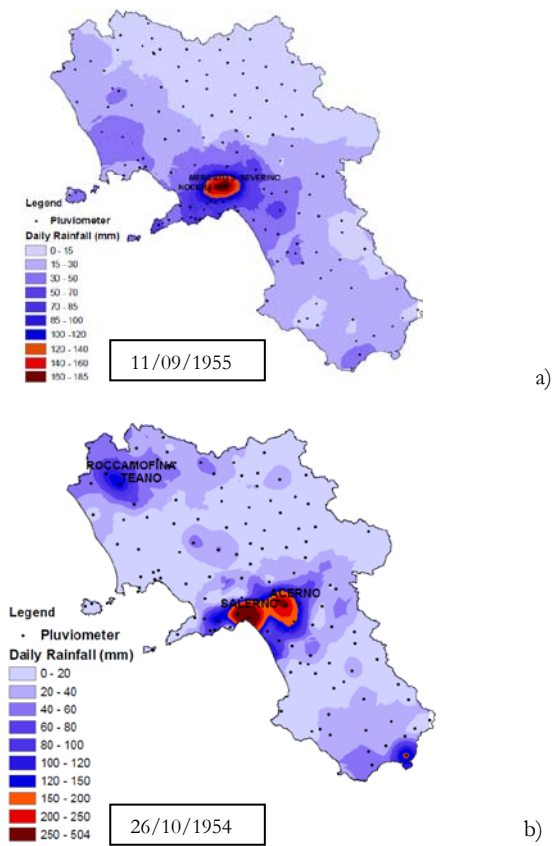


Figure 5.8 Example of meteorological structures attributable to the occurrence of hyperconcentrated flows: a) Isolated convective cells; b) Hurricane - like rainfall.

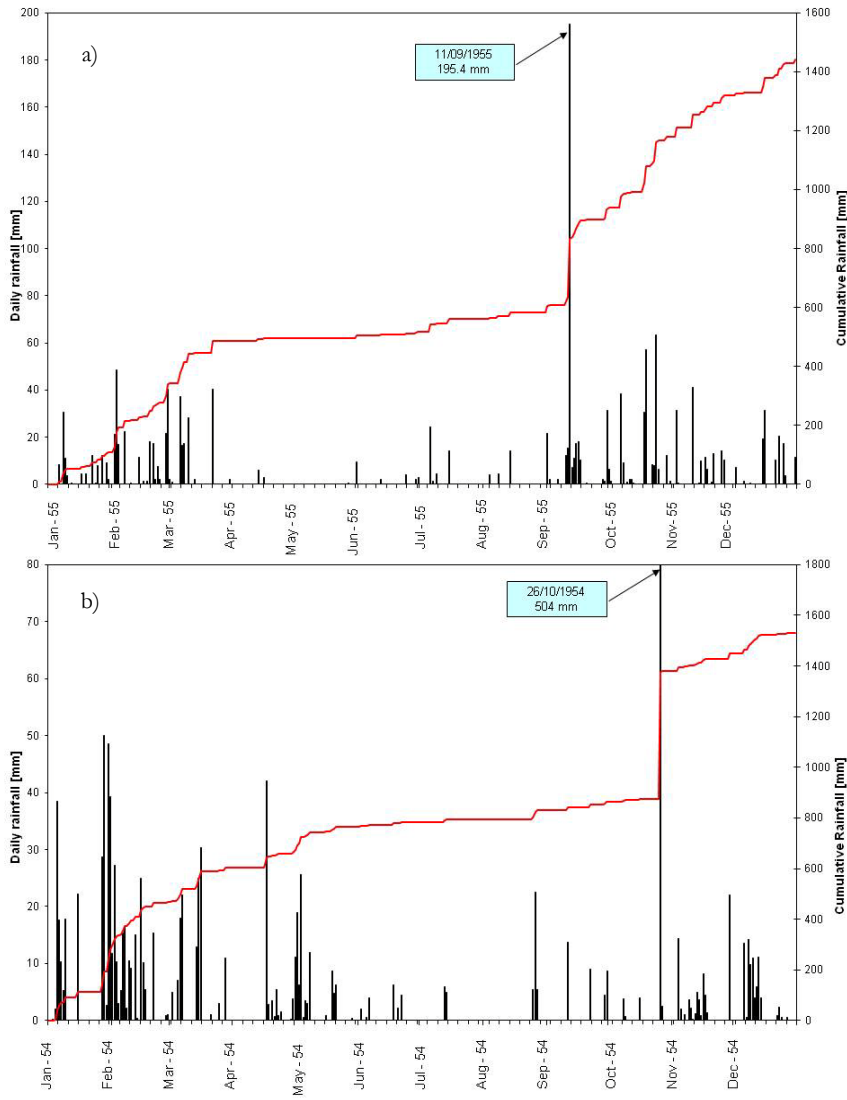


Figure 5.9 Rain events monitored at a) Nocera Inferiore Town for the hyperconcentrated flows occurred in September 1955 and at b) Salerno Town for the hyperconcentrated flows occurred in October 1954.

The above considerations allow the identification of the areas of the Campania region systematically affected by the flow-like phenomena at hand (this datum is relevant when hazard and risk might be assessed) and provide useful suggestions about their genesis.

In particular, the hyperconcentrated flows occur mostly in areas close to the coastline (Figure 5.10), involving 25 out of a total of 121 Municipalities belonging to the geological context A1. This can be due to the peculiar morphology of the affected areas. Indeed, the presence of orographic barriers (Lattari Mounts and Sarno Mounts) influences the rainfall intensity that amplifies at upwind hillslope and later reduces at downwind hillslope (Tropeano et al., 2005). Obviously, the spatial distribution of areas affected by hyperconcentrated flow can be also related to the relevant thickness (up to 5 m) of the pyroclastic soil deposits in turn including continuous ashy and pumice soil layers (Cascini et al., 2013 a).

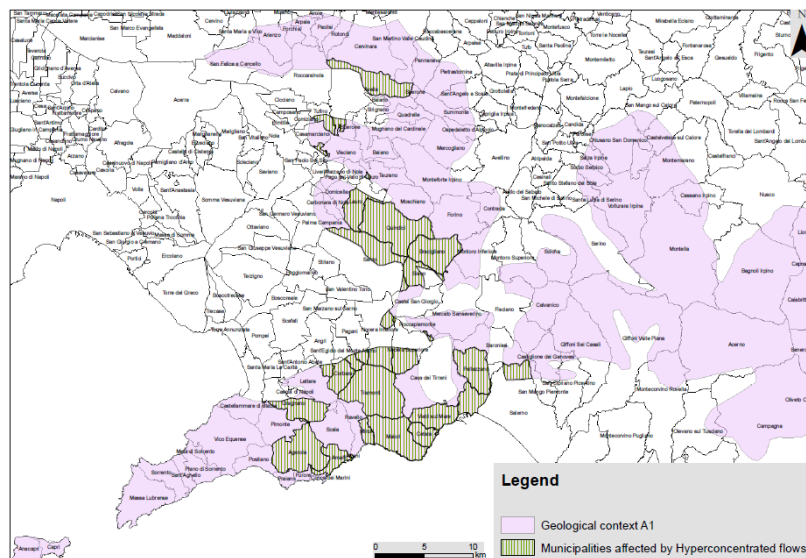


Figure 5.10 Spatial distribution in the geological context A1 of municipal territories historically affected by hyperconcentrated flows.

With reference to debris flows events it is possible to note that they affect, in comparison with hyperconcentrated flows, a larger portion of the geological context A1 including 59 over a total of 121 Municipalities (Figure 5.11). This effect is mainly due to the different meteorological

processes associated with them as well as to the different triggering mechanisms (Cascini et al., 2008 a; Cascini et al, 2013 a); moreover, the important role played by anthropogenic (i.e. track-ways and cut slopes) and hydrogeological factors (i.e. springs) in triggering a number of first-time shallow slides occurred in Campania region cannot be neglected (Cascini et al., 2005; Cascini et al., 2008 a).

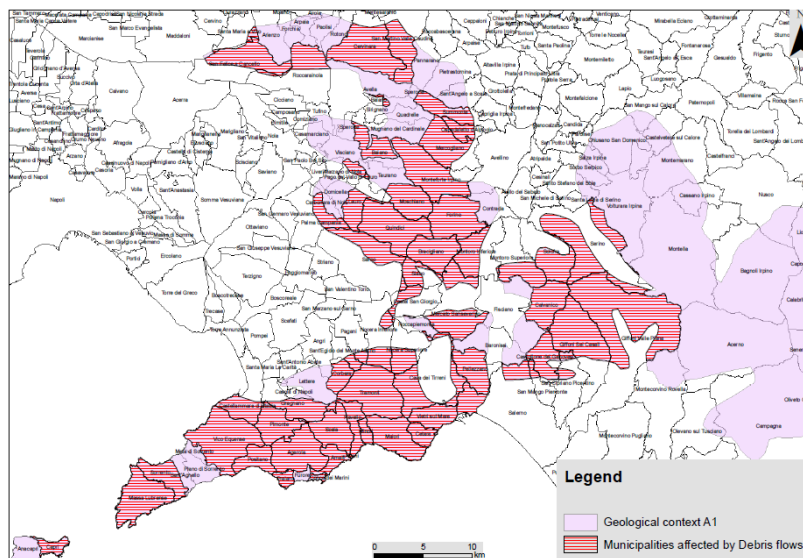


Figure 5.11 Spatial distribution in the geological context A1 of municipal territories historically affected by debris flows.

5.5 FREQUENCY ANALYSIS AT REGIONAL SCALE OF THE TWO CONSIDERED CLASSES OF FLOW-LIKE PHENOMENA

The different issues addressed in the previous sections highlight the relevant extent and complexity of the problems related to the detection of areas potentially affected by debris flows or hyperconcentrated flows; furthermore, they underline the urgent need to plan adequate prediction and prevention actions for the several sites exposed to the occurrence of above flow-like phenomena. In order to define the most appropriate risk mitigation strategies at regional scale, frequency-magnitude relationships must be assessed.

To this aim, in the present thesis the frequency was estimated from the analysis of incident data dealing with past events, in the hypothesis that they are recurrent and occur randomly and independently, while the associated magnitude was expressed in terms of numeric or areal indexes in turn related to the number of municipalities or to the portion of areal extent of municipal territories of Campania region historically affected by flow-like phenomena. In this regard, it is firstly necessary to categorise the occurred events in two main classes respectively including the so-called “local” and “extensive” events (Cascini and Ferlisi, 2003). Local events are those affecting a single municipality in a given day, whereas events involving more than one municipality are referred to extensive ones. Whereby, the numerical index I_n (Eq. 5.3) represents the ratio between the number of municipalities (N_m) affected by a well-defined type of flow-like phenomena (hyperconcentrated flows or debris flows) in a given day and the total number of municipalities N_{tot} affected by the considered flow-like phenomena in the different years of observation:

$$I_n = \frac{N_m}{N_{tot}} \quad (5.3)$$

On the other hand, the areal index I_a (Eq. 5.4) is defined as the ratio between the area of Municipalities A_m affected by a well-defined type of flow-like phenomena in a given day and the total area A_{tot} of all Municipalities affected by the considered flow-like phenomena in the different year of observation:

$$I_a = \frac{A_m}{A_{tot}} \quad (5.4)$$

With reference to the relationship between the annual cumulative frequency per unit area (i.e. normalised by the total slope area of all Municipalities historically affected by a given type of flow-like phenomena) and the numerical index I_n for the two classes of considered phenomena Figure 5.12 shows that, at a parity of I_n value, hyperconcentrated flows exhibit a frequency greater than that of the debris flows.

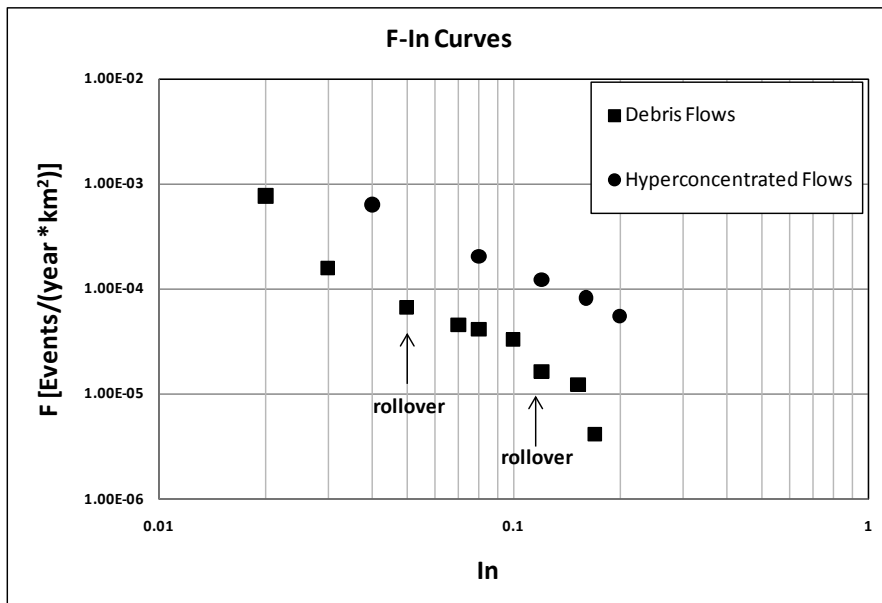


Figure 5.12. $F-I_n$ curves for hyperconcentrated flows and debris flows.

Furthermore, the $F-I_n$ curve concerning hyperconcentrated flows exhibits a linear trend (in the bi-logarithmic plane) while debris flows present two rollover points in correspondence of extensive events affecting at least three or six Municipalities. According to Cascini et al. (2008 b), the relatively high slope values characterising the first part of the $F-I_n$ curve (i.e. at the left of the first roll-over point) can be due to a lack of historical information related to the most ancient events; on the other hand, $F-I_n$ points at the right of the second rollover points refer to the events of largest magnitude triggered by extreme rainfalls.

As for the relationship between the annual cumulative frequency per unit area (i.e. normalised by the total slope area of all Municipalities historically affected by a given type of flow-like phenomenon) and the areal index I_a , Figure 5.13 highlights that, for events affecting small-size areas, the frequency of hyperconcentrated flows is equal to that of debris flows; on the other hand, with the increasing of the extent of affected areas, hyperconcentrated flows exhibit a normalised frequency higher than that of debris flows.

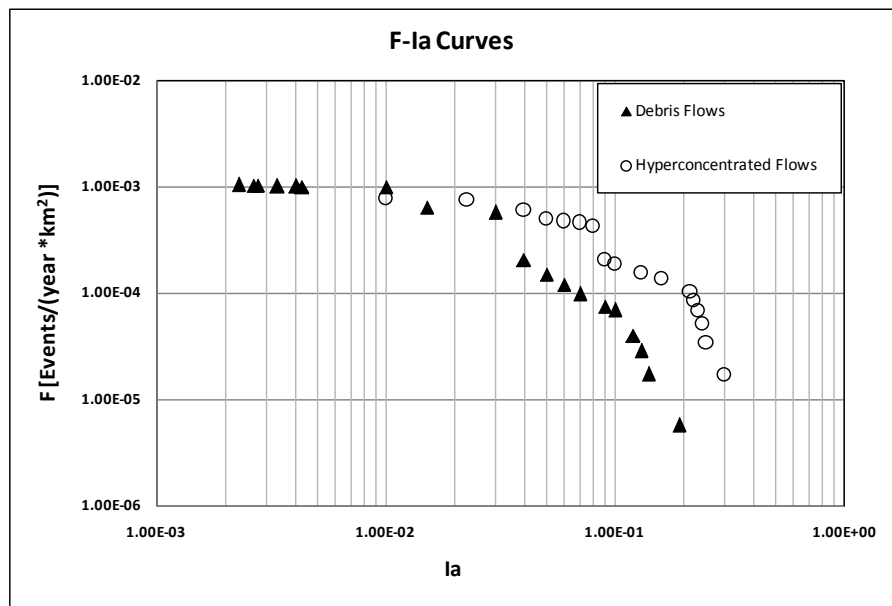


Figure 5.13 F- I_a curves for hyperconcentrated flows and debris flows.

The obtained $F-I_n$ and $F-I_a$ curves represent useful tools for Authorities in charge of the safeguard of human life via emergency plans at provincial and regional levels. Indeed, they allow the prediction of the magnitude (in numerical or areal terms) associated to the occurrence of well-defined flow-like phenomena of given frequency and, consequently, the conceivment of the most appropriate risk reduction strategies.

Focusing on the hyperconcentrated flows, further interesting considerations can derive from the distinction of the $F-I_n$ relationship related to different periods: the period spanning from 1631 to 1850 in which there was an intense strombolian activity of the Somma-Vesuvius

volcanic complex, and the post-eruptive period extending from 1851 up to now (Figure 5.14).

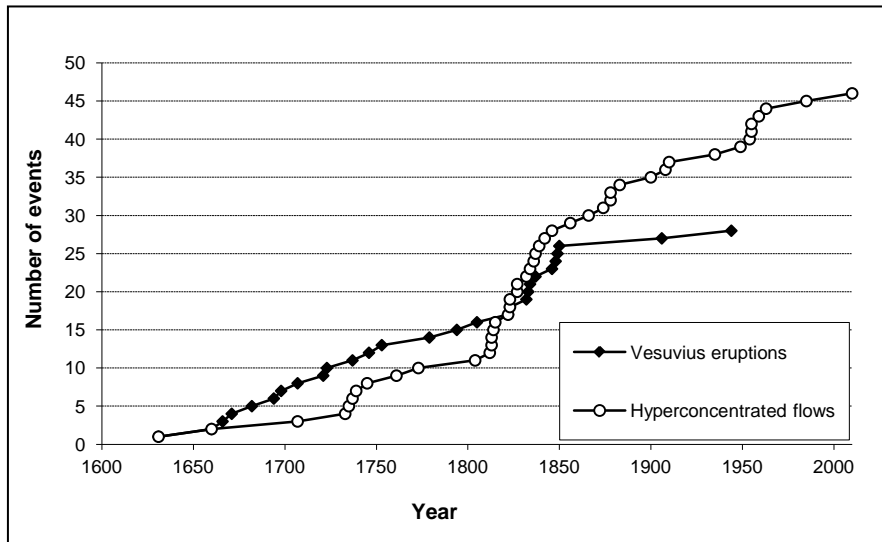


Figure 5.14 Cumulative curves of hyperconcentrated flows events and Vesuvius eruptions interesting the geological context A1.

With reference to these different periods it can be observed that $F-I_n$ points referring to the whole period of observation (from 1631 up to now) are practically overlapped to $F-I_n$ points dealing with events occurred in the period 1631-1850; on the contrary, $F-I_n$ points associated to events occurred after 1851 progressively diverge from those referring to the whole period of observation (Figure 5.15). This is likely due to either a climate inhomogeneity or different initiation processes. Indeed, in the period 1631-1850, as a result of the availability of loose and cohesionless pyroclastic deposits, the triggering of hyperconcentrated flows was related to the washing of soil particles operated by rainfall; as a matter of fact, a marked correlation exists between the cumulative curve of incident data dealing with the flow-like phenomena at hand and that of eruptions whose pyroclastic products interested the slopes located in the geological context A1 (Figure 5.14).

Conversely, in the recent period, the hyperconcentrated flows were generated by erosion due to rainfall of high intensity and short duration.

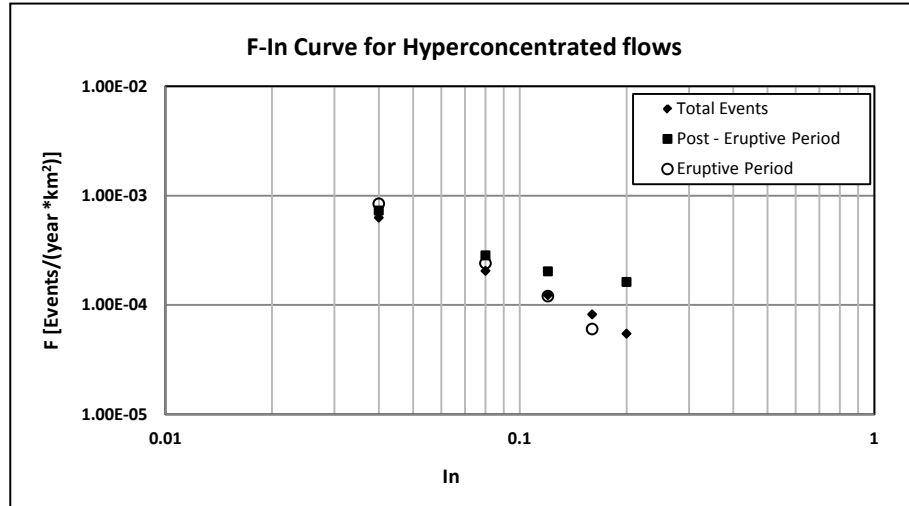


Figure 5.15 F-I_n curves for hyperconcentrated flows with reference to different time periods.

It is worth noting that, in Figure 5.15, F-I_n points dealing with the highest values of I_n are associated, in the period spanning from 1851 up to now, to events that in the last century caused the most severe consequences in terms of loss of human life (Table 5.2; Figure 5.16). Finally, the most destructive recent hyperconcentrated flows are characterised by an annual frequency per unit area higher than the fatal debris flows events (Figure 5.17). This result testifies the need to pay the greatest attention to these flow-like phenomena when the design of non-structural mitigation measures at provincial/regional scale is pursued.

Table 5.2. Fatal events of hyperconcentrated flows recovered in the 20th century.

<i>Hyperconcentrated flows events</i>	<i>Affected Municipalities</i>	<i>Number of deaths</i>
24/10/1910	Vietri sul mare, Maiori, Cetara, Amalfi	221
20/08/1935	Gragnano	8
02/10/1949	Lauro, Maiori, Quindici, Minori, Nocera Inf	10
26/10/1954	Vietri sul mare, Maiori, Tramonti, Minori, Salerno	319

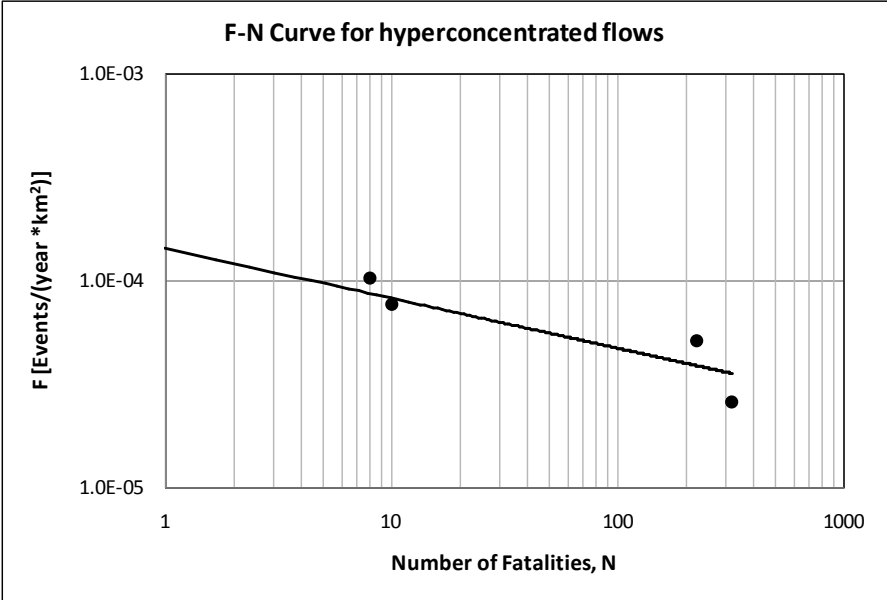


Figure 5.16 F-N curve for hyperconcentrated flows with reference to the 20th century.

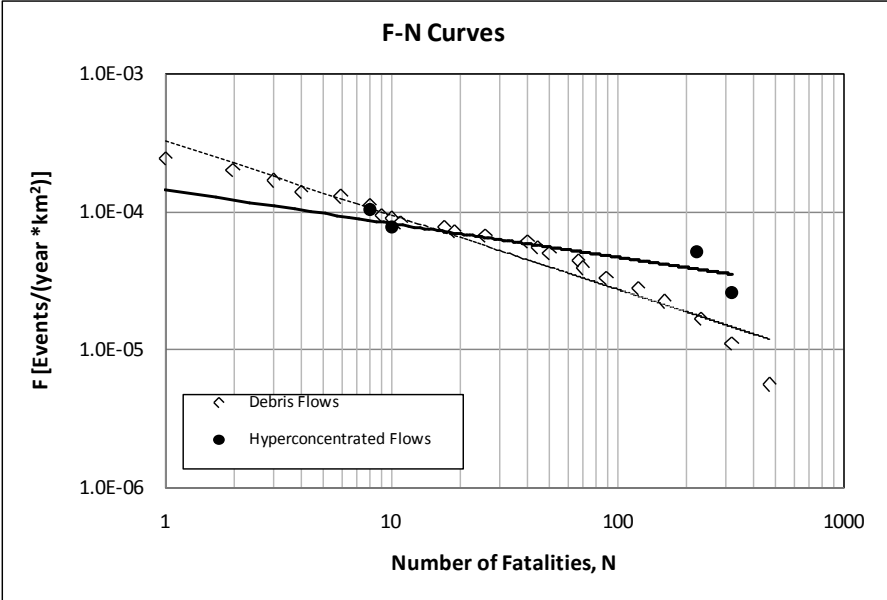


Figure 5.17 F-N curves for hyperconcentrated flows and debris flows.

The results of the quantitative risk estimation at a regional scale, that specifically identify the Municipalities systematically affected by given flow-like phenomena (debris flows or hyperconcentrated flows), give rise to the need to identify, within a given Municipality, the areas that urgently require the implementation of the most suitable risk-mitigation measures, which is able to respect economic and technical requirements (type, location and dimensions). To this aim, it is necessary to carry out estimates of the risk of loss of life at detailed scale.

In the following a first application of QRA for hyperconcentrated flows is provided, with reference to Monte Albino hillslope located in Nocera Inferiore (SA), belonging to the 25 municipalities of the Campania region systematically affected by the considered phenomena.

6 INVESTIGATION AT SITE-SPECIFIC SCALE FOR QRA

The quantitative risk analysis procedures requires a huge amount and accurate input data of different nature (i.e. geological, geomorphological, geotechnical, historical) and a high-quality DEM to evaluate a range of possible risk scenarios, to characterise the design events and their return periods, and to modelling the mechanical behaviour of the considered phenomenon (Corominas et al., 2013).

For the achievement of QRA purposes it is necessary to use data coming from interdisciplinary investigations which are often able to optimise economic resources and enhance individual professional contributions.

To this aim, the Monte Albino hillslope and its piedmont area (Figure 6.1) – located in the municipality of Nocera Inferiore, Campania Region – was selected as test site.

The criterion applied to choose this area was based on: well-recognised existence of a very high risk to life posed by flow-like phenomena; well documented incident data of flow-like phenomena; accessibility for fieldwork; information availability from other sources and institution (technical reports, etc.); good quality and quantity of the data (e.g. DEM, maps, images).

In the following the investigation programme in the selected study area and the results of in-situ/laboratory tests will be illustrated, highlighting the usefulness of the interdisciplinary approach in the achievement of the purposes related to both the characterisation of the geo-environmental context and the understanding of the related issues.

6.1 THE TEST SITE

The Monte Albino massif belongs to the Lattari mountain chain and extends over a total area of about 400 ha (from 90 m a.s.l. to 890 m a.s.l.), with a prevalent exposure to north.

The piedmont area, extending until the A3 Naples-Salerno highway with elevation values lower than 200 m a.s.l., is characterised by the presence of several buildings - mainly consisting of reinforced concrete structures for residential use or masonry storehouse - as well as of an articulated road system.

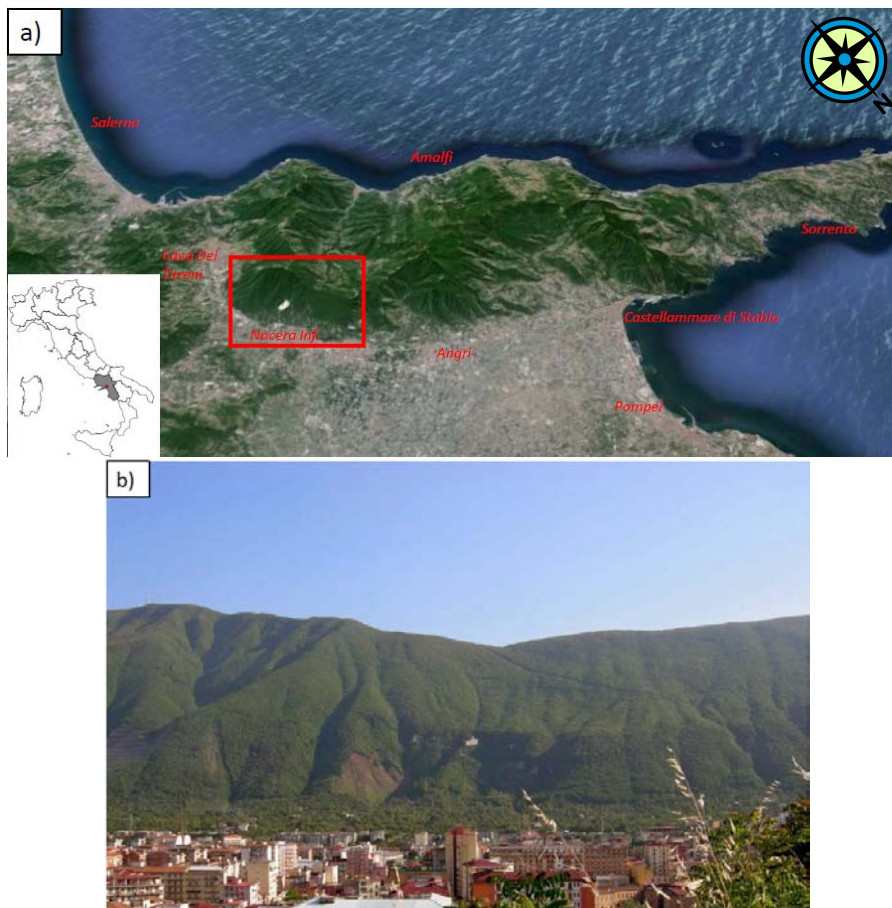


Figure 6.1 a) Geographical setting of the test site of Monte Albino (Google Earth image); b) General overview of Monte Albino slope (photo dated 2011).

In order to define the geological and geomorphological setting as well as to deepen the knowledge of the different types of phenomena which can occur on the slope, field survey and investigations as well as laboratory tests were carried out following a multidisciplinary approach (involving competences on geology, morphology, hydrogeology, geotechnics, historical data treatment, geomatics, geostatistics, etc.). The main results achieved during this preliminary step of the work are herein presented.

6.2 GEOLOGICAL AND HYDROGEOLOGICAL SETTINGS

The Monte Albino massif is located at the northern side of the Lattari Mts. ridge, with a WSW-ENE elongated horst consisting in Mesozoic carbonate rocks covered by pyroclastic deposits of the late Pleistocene-Holocene, coming from air-fall deposition related to the explosive volcanic activity of Somma-Vesuvius and Campi Flegrei eruptive centres. The Monte Albino northern slope bedrock is formed by three dolomitic limestone units and it exhibits a morpho-structural setting characterised - at large scale - by steps related to an extensional fault system (Figure 6.2). The slope, in particular, is formed by a series of sub-vertical, E-W oriented and northward declined normal faults, going from the Monte Chiunzi-Monte S. Angelo ridge to the plain of Pagani-Nocera. The main fault of this system is named “Monti Lattari nord” fault; it has a length of 23 km and it presents a vertical slip rate of 1-2 mm/yr belonging to the Middle Pleistocene – Late Pleistocene/Holocene age (Galadini et al., 2000) which reduces at > 0.5 mm/yr during Holocene age (Cinque et al., 2000).

These tectonic elements intersect, in the central and western sectors of the slope, the NW-SE and NE-SW oriented normal fault systems.

The pyroclastic deposits that cover the carbonate bedrock, belonging to the “Recent Pyroclastic Complex” (De Vita et al., 2012), reach up to 8 m thick and they are mainly formed by the Mount Somma-Vesuvius explosive activity products. In particular, they are mostly attributable to the Vesuvius eruptions products dated 79 AD, the only recent ones having the dispersion axis directed towards the south (Rolandi et al., 2007).

The pyroclastic deposits are generally cohesionless soils. They are mainly composed by both reworked and in-situ ash and pumice soils, which are

mixed - in minor part - with limestone debris, landslide deposits, stream and hyperconcentrated flows deposits and colluvial deposits.

On the slope sector mainly fine-grained, reworked pyroclastic soils are widespread with local accumulations of colluvial deposits, filling the hollows, and slope debris, locally laying on pumice and ash discontinuous horizons in primary position with paleosols at the top.

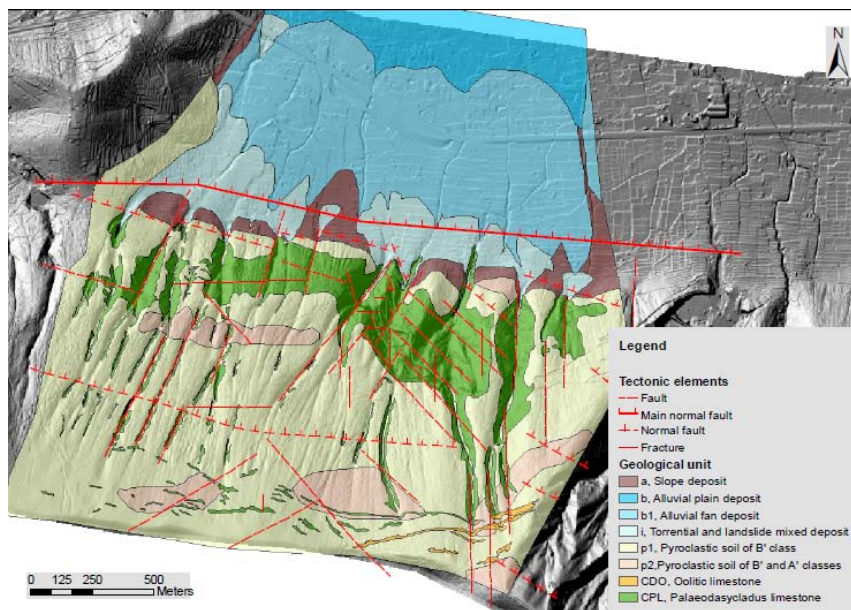


Figure 6.2 Geological map of Monte Albino.

In piedmont area, instead, various types of deposits are recognised:

- Slope deposit, formed - in the proximal sector - by incoherent and heterometric calcareous debris with reworked pyroclastic matrix and - in the distal sector - by sandy - silty and reworked pyroclastic deposits. These materials are produced by the washing out of the pyroclastic soils along the slopes and by the calcareous debris stream transport.
- Torrential and landslide mixed deposit, which forms a strip of coalescing debris - alluvial fans that develops at the base of the slope. The deposits consist of reworked, sandy-silty-clayey texture, pyroclastic material, which is usually cohesionless or weakly cohesive; the deposits has also calcareous and pumice

clasts and blocks and cross-stratified, coarse debris-alluvial level sand chaotic debris-pyroclastic levels deposited by landslide processes.

- Alluvial fan deposit, which forms the wide alluvial fan bodies that develop between 100 and 70 m a.s.l.; it consists of clayey silts and silty sands of pyroclastic and calcareous nature with calcareous gravel sand pumice levels.
- Alluvial plain deposit, that is found in the urbanised plain sector of the bottom of valley. It is formed by mainly pyroclastic, silty-clayey and sandy-silty sequences deposited by river processes with lenses of limestone gravel sand pumice levels. The thickness is several tens of meters; at its base is placed at the horizon of the Ignimbrite Campanian Auct.

From hydrogeological point of view (Figure 6.3), it is important to note that the study area corresponds to the northern portion of the hydrogeological unit of Lattari Mounts (Celico et al., 2003), characterised by a deep basal groundwater. The local water circulation is affected by the main tectonic elements that give rise to springs in the upper portion of the slope. In this sector, in fact, it is possible to recognise the presence of the ephemeral springs related to the temporary suspended water tables as well as the presence of sinkholes related to the strong karstic action. The main water sources at the base of the slope, instead, are represented by fountains.

On the slope, four main hydrogeological complexes are recognised (pyroclastic complex, debris-pyroclastic complex, alluvial-pyroclastic complex and carbonate complex).

The piezometric measures data along the slope and in the piedmont area are lacking, while in the alluvial area the aquifer should be tested at a depth between 20 and 30 m a.s.l..

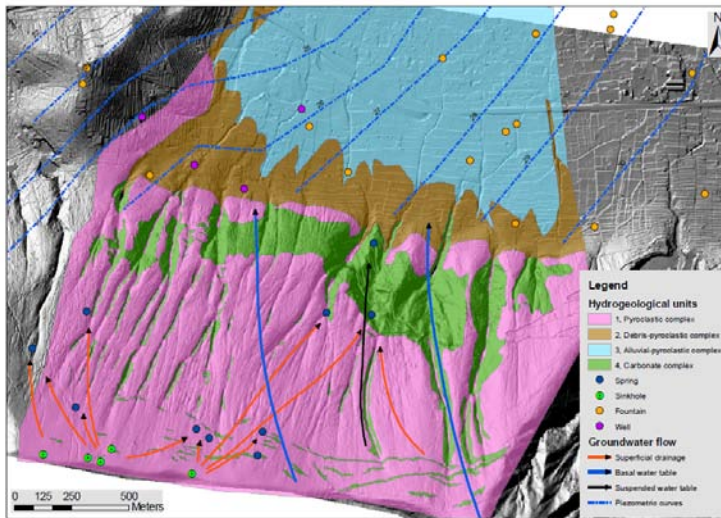


Figure 6.3 Hydrogeological map of Monte Albino.

6.3 GEOMORPHOLOGICAL SETTING

The Lattari Mts. are constituted by a recent tectonic uplift and block faulting, where remnants of gentle erosional Pliocene to Early Pleistocene landscapes are suspended above Middle – Late Pleistocene features, formed by steep fault scarps and steep V-shaped valleys. The mature landscapes are characterised by sub-horizontal surfaces alternating with slope angles lower than $26\text{--}28^\circ$, while the Middle – Late Pleistocene fault scarps and valley side slopes are characterised by higher gradient and composite transverse profiles (alternating sub-vertical scarps and slope inclined at $30\text{--}35^\circ$) (Cinque and Robustelli, 2009). According to Aucelli et al. (1996) most of the present tectonic structures of Lattari Mts. ridge could be the result of exhumation processes, due to the intense erosion, during Quaternary, of Late Miocene - Pliocene tectonic elements.

The Monte Albino slope morphology is strongly controlled by tectonic setting. In particular it is possible to identify:

- A lowered sector, filled by pyroclastic and debris-alluvial deposits (alluvial plain), going down to 30 m a.s.l.;

- an intermediate sector (piedmont area), which is attested around an average of 200 m a.s.l., where the lower border of the open slopes, the debris-alluvial fans and of the outlets of the mountain valley are located;
- an up-lifted sector (fault slope), consisting of carbonate bedrock with debris-pyroclastic covers, where slopes mainly evolved by recession processes of the main fault planes.

The fault slope presents a polycyclic profile, characterised by a well developed concave profile in the upper part of the slope, a sharp break in slope incline in the medium sector (about 300 m a.s.l.), and a straight profile in the lower steeper part of the slope.

The slope was characterised by two main morpho-tectonic evolutionary stages. The first phase refers to the differential tectonic uplift of the slope sector during Early-Middle Pleistocene.

The upper part of the slope completely evolved, probably during Quaternary cold stages, after the cliff recession model (Lehman, 1933; Bakker and Le Heux, 1952) with the intermediate plain representing the ancient erosion base level.

The lower part of the slope is related to the partial linear erosion of the fault slope (Brancaccio et al. 1978, 1979) probably reactivated during Middle-Late Pleistocene, producing a set of triangular facets, delimited by V-shaped valleys steep slopes.

The geomorphological evolution produced a considerable amount of calcareous debris and reworked pyroclastics, which gradually accumulated in the piedmont areas in the form of detrital talus and detrital-alluvial fans. The drainage network development completes the areal shaping and the linear erosion of the carbonate bedrock along the slope. The most recent morphogenetic cycles were characterised by the alternation of depositional phases of pyroclastic soils, deriving from the explosive activity of the Vesuvius and of Campi Flegrei, and denudation stages, as result of erosion and instability phenomena.

6.4 IN SITU TESTS

The quantitative landslide risk estimation requires, first of all, the acquisition of the accurate data assets of both geotechnical and geological nature. To this aim, in-situ (over the whole Monte Albino hillslope) and laboratory tests were carried out in order to gather relevant information about the soil cover thickness and the stratigraphic settings, the soil suction regime, the physical and mechanical properties of the pyroclastic soils.

The above activities were carried out as part of the consultancy assignment stipulated on 5 November 2010 with the Fondazione Universitaria dell'Università di Salerno and the Representative Government Commissariat for Hydrological Interventions in the Campania Region (ex O.P.C.M. n. 3849 del 19.02.2010).

The location of the field investigation was derived from a careful planning (Figure 6.4) obtained on the basis of the most critical evidences (potential triggering zones and propagation zones) identified from the analysis of bibliographic data of regional nature as well as preliminary geological and geomorphological investigations. In particular, the in-situ tests were carried out from November to December and they consisted of:

- n. 40 dynamic penetration tests (DL030);
- n. 70 man-made pits;
- n. 20 sampling;
- n. 1,082 iron-rod drillings;
- n. 54 suction measurements
- n. 68 seismic field test.

The dynamic penetration tests - DL030 - (Figure 6.5 f) consisted in the penetration of a metallic rod into the ground by blows from a slide hammer with a weight of 30 kg falling through a distance of 200 mm. The rod, with a conical tip, was driven 10 cm into the ground and then the number of blows needed for the tip to penetrate each 10 cm up to a depth of 140 cm was recorded. These tests helped to identify the pyroclastic deposits thickness, with different penetration strength, and to reconstruct their litho-stratigraphy settings.

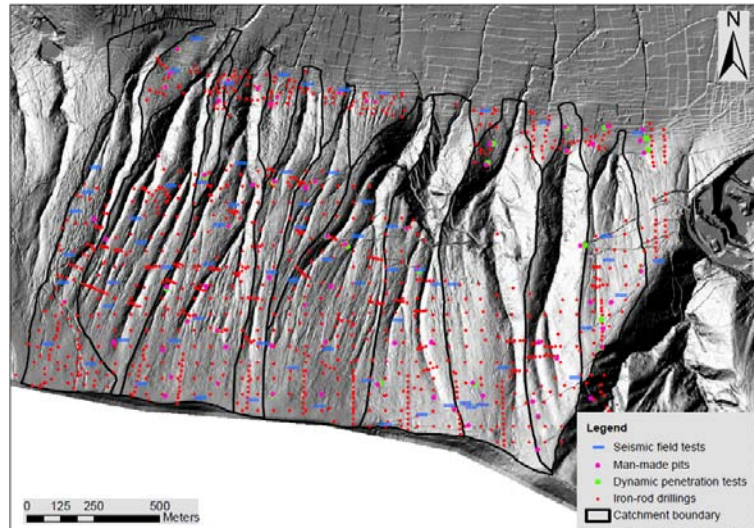


Figure 6.4 DTM obtained on the basis of the data achieved via a LIDAR survey technique (Avioriprese s.r.l., edition of 2005, 1:1,000 scale), with indication of the sites where the in-situ tests were carried out.

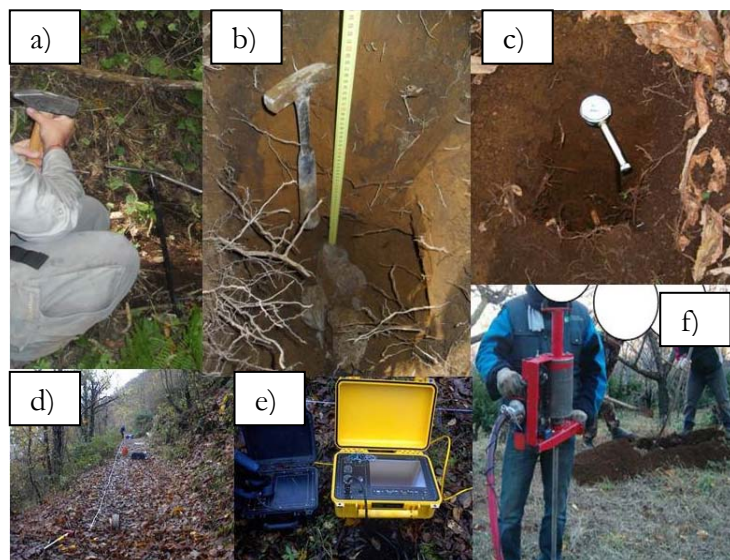


Figure 6.5 In-situ tests: a) Iron-rod drilling; b) Man-made pit; c) Suction measurement; d) Seismic field test; e) Seismograph; d) Dynamic Penetration test.

On the basis of the data achieved through man-made pits, the stratigraphy of the superficial covering deposits was further objectified and integrated. Indeed, the man-made pits (Figure 6.5 b), with a maximum depth of 2 meters, were realised closeness to the verticals interested by the penetration tests.

The reconstructed litho-stratigraphic arrangement was integrated with data resulting from iron-rod drillings (Figure 6.5 a) performed through the use of steel rods of circular cross section, with a reduced diameter (<18 mm) and length of 306 cm. The metal rods, driven into the ground by hand or with the aid of a hammer, allowed the definition of the pyroclastic thicknesses with a low resistance and, where possible, the depth of the lithological contact pyroclastic cover / bedrock or debris substrate.

For the use of advanced models aimed at analysing the landslide triggering stage, soil suction measures are needed (Figure 6.5 c). In this regard, tests were conducted in the autumn months, within the survey-holes at different depths (20 cm, 40 cm, 60 cm, 80 cm, 100 cm and 120 cm) via a “Quick Draw” tensiometer.

The geophysical survey (Figure 6.5 d, e), based on the use of seismic refraction, was performed in order to seismically characterise the different surface deposits in the area and to obtain, at the same time, information about the geometry and thicknesses of the different layers forming the subsoil. Every seismic profile was performed using 24 geophones disposed on the ground surface along a straight line of 60 meters, at a variable distance between 3 and 5 meters. The seismic profiles refer to 3 bursts (direct, reverse and intermediate). The acquired data were processed using the commercial software INTERSISM (Geo & Soft International - www.geoandsoft.com).

Finally, in order to perform laboratory tests, twenty soil samples representative of different lithologies and grain sizes were taken within the exploratory wells at varying depths (from 0.2 m to 2.0 m from the ground surface), through the beat insertion of a Shelby cylindrical sampler (0.1 m wide and 0.3 m long).

6.5 LABORATORY TEST RESULTS

Laboratory tests were aimed at defining both physical and mechanical properties of the pyroclastic soils (ashy and pumice) covering the carbonate bedrock. The adopted experimental procedures are well-explained in Bilotta et al. (2005) and they were specifically devoted to assess the grain size distribution, the index properties, the Atterberg limits and the shear strength parameters of undisturbed soil specimens.

As for grain size distribution, Figure 6.6 shows a high variability of the grading curves obtained with reference to n. 16 soil specimens (including n. 1 of pumices). Following a suggestion provided by Bilotta et al. (2005) on ashy soil samples collected over the Pizzo d'Alvano massif (about 10 km far from Monte Albino), the ashy soils investigated in the present work can be roughly categorised in two main classes called A' and B'. In particular, class A' includes ashy soils with a finer grain size distribution (Figure 6.6), higher porosity values and lower specific weight of solid fraction values than those belonging to class B' (Table 6.1).

The mechanical characterisation was performed through direct shear tests on specimens at constant (natural) water content. The average values of the obtained shear strength parameters (cohesion c' and friction angle φ') are reported in Table 6.2 for ashy soils of both A' and B' classes.

Table 6.1 Range of main physical properties of A' and B' ashy soils.

Soil class	γ_s (kN/m ³)		γ (kN/m ³)		γ_d (kN/m ³)		e	
	min	max	min	max	min	max	min	max
A'	25.1	26.3	10.1	15.7	6.8	10.8	1.42	2.84
B'	25.5	27.3	11.8	13.4	7.5	9.7	1.67	2.44

Note: γ_s = specific weight of the solid fraction; γ_d = dry unit weight; γ = unit weight at natural water content; e = porosity index. Laboratory tests were performed on n. 15 specimens (n. 6 of class A' and n. 9 of class B').

Table 6.2 Average values of shear strength parameters of A' and B' ashy soils.

Soil class	c' (kPa)	φ' (°)
A'	6.1	30.7
B'	4.1	37.3

Note: Direct shear tests were performed on specimens obtained from n. 8 undisturbed soil samples (n. 4 of class A' and n. 4 of class B').

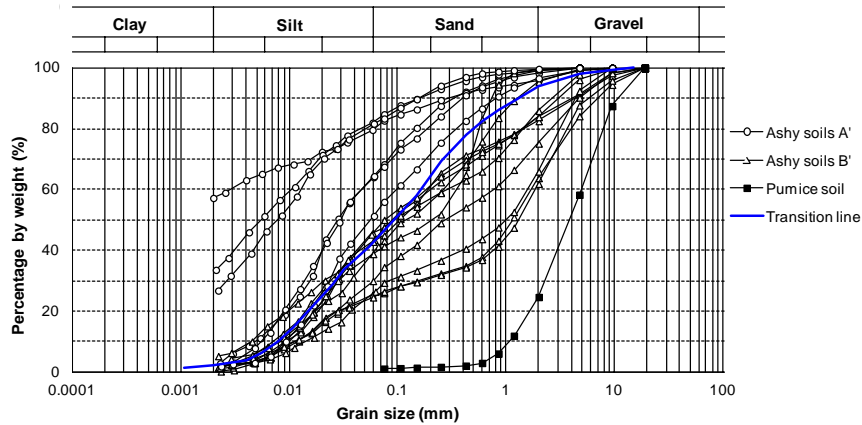


Figure 6.6 Grain size distribution of the investigated pyroclastic soil specimens.

6.6 IN SITU TEST RESULTS

6.6.1 Spatial distribution of the pyroclastic soils and their thickness

The assessment of the thickness of the pyroclastic soil covers together with their litho-stratigraphic settings are considered among the most important information for susceptibility analysis purposes as well as for the use of engineering models aimed at defining the volumes of material potentially mobilised during the occurrence of a given slope instability. In this regard, data achieved via two types of in-situ tests (see Section 6.4) namely iron-rod drillings and dynamic penetration tests, integrated with field observations deriving from the man-made pits, were used. Anyway, it must be observed that iron-rod drillings, carried out at relative distances ranging from 5 to 50 meters, as a simple and inexpensive test for detecting the soil thickness, presents strong limitations that may generate significant inaccuracies. These limitations are related to: the level of the force set by the operator for the insertion of the rod; the presence of a hinder root system or stone blocks; the reduced length of the metal rods. Therefore, the thickness value derived

from iron-rod drilling data must be referred to soil strata having a low strength placed above a more resistant substrate.

The dynamic penetrometer data were used to assess the pyroclastic soil thickness up to a maximum depth of 14 meters resulting therefore, in addition to the results of the geophysical surveys, as complementary of data achieved via iron-rod drillings. It also made it possible to provide information about the stratigraphy of the investigated soil layer. The limits of its use are due to the higher cost compared to those of the iron-rod drilling as well as to transport difficulties in not easily accessible areas.

In order to derive a high-detailed map of the pyroclastic soil thickness the results of the in-situ tests were managed in a GIS environment. Through the analysis and comparison of the in-situ test results, data with errors were identified and deleted (as not in agreement with the results of the different investigations and geological observations made in the surrounding areas, or not intercepting the lithological contact). With reference to not investigated portions of the slope, being characterised by slope angles that actually make them inaccessible or presenting pyroclastic soil cover of negligible thicknesses, orthophotos observation was made in order to define the areal extent of the outcropping rock. The geostatistical interpolation of data using the kriging technique allowed the generation of the pyroclastic soil thickness map at 1:1,000 scale (Figure 6.7). It is worth noting that the results of this activity allowed a significant improvement of an available soil thickness map at 1:25,000 scale (Cascini et al., 2013 b).

The spatial distribution of the pyroclastic soil thickness is significantly controlled by the morphology of the carbonate bedrock. Indeed, where slope angles attain the lowest values and the hills are more conservative (ridges and paleo-slope) most of the maximum thickness of the pyroclastic deposits was preserved; on the contrary, the bared areas correspond to steep morpho-structural slopes and to eroded valley-channels. In particular, the soil thickness values range between 3 m and 4 m along the catchment B1 as well as in the ridge zone (where slope angles are of few degrees in value); here, the presence of morphological concavities – namely “Zero Order Basins” (Cascini et al., 2008 a) – filled by pyroclastic soils can be recognised. There is a very large portion in which the thickness values do not exceed 1.5-2 m even though, locally, pyroclastic soils of 3.5 m thick can be found. Where the slope angles reach high values, soil thickness values are generally negligible (lower

than 0.5 m, in the lateral sectors of the gullies) while, in the valley zone they reach the highest values (locally larger than 5 m).

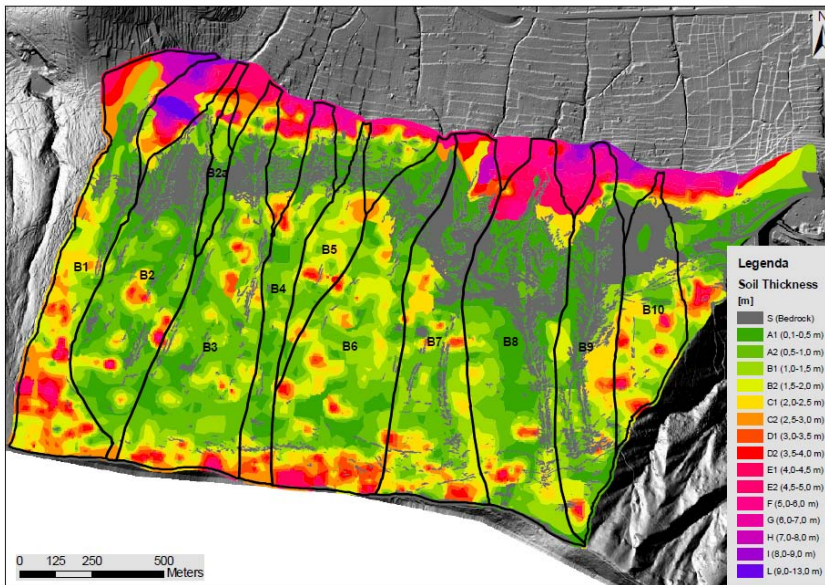


Figure 6.7 Soil cover thickness map.

The integrated analysis of data achieved via dynamic penetration tests and of the stratigraphic descriptions of the lithological units recognised through the man-made pits, also allowed the reconstruction of the litho-stratigraphic structure of the pyroclastic deposits. To this aim, the numbers of hits recorded during the dynamic penetration tests were correlated with the corresponding values of the dynamic resistance to the tip Rpd [kg/cm^2] through the formula (Eq. 6.1) (Sanglerat et al., 1980):

$$Rpd = \frac{M^2 \cdot H}{[A \cdot e \cdot (M + P)]} \quad (6.1)$$

being:

M, the weight of the trip hammer;

H, the fall height;

A, the penetrometer tip section;

e, the average insertion of the rod in relation to each blow;

P , the total weight of the rods and of the beating system;
 N , the number of the recorded blows for each considered interval.

Then, $R_{p,d}$ data were plotted as a function of the associated depth z (m) (Figure 6.8), bearing in mind that information on both magnitude and trend with depth of $R_{p,d}$ may concur to the identification of type and thickness of pyroclastic soils.

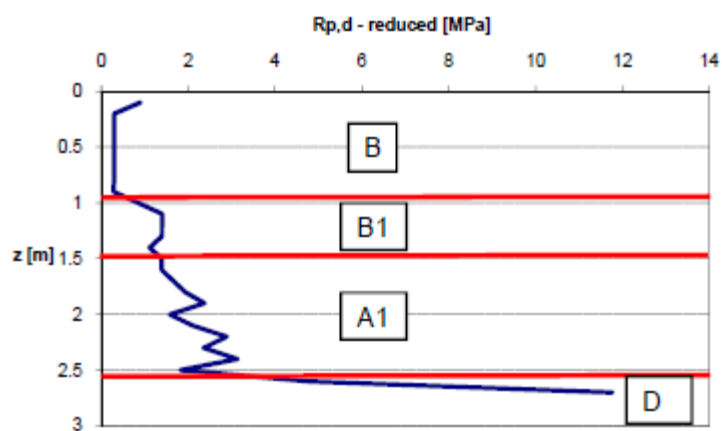


Figure 6.8 Typical trend of vertical stratigraphic intervals.

At the end of the analysis carried out, six classes of litho-stratigraphic units were identified namely:

- Class A1: Silts with sandy clay
- Class A: Silts with clayey sands
- Class B: Sands with weakly gravelly silts (low presence of millimetric pumice)
- Class B1: Silty-gravelly sands (presence of abundant of heterometric pumice)
- Class C: Sandy gravels (heterometric pumice with low presence of pyroclastic matrix)
- Class D: Blocks (dolomitic limestone surrounded by sandy-silt matrix).

From the spatial distribution of the reconstructed stratigraphic profiles (Figure 6.9) it can be observed that coarse-grained soils (type B' from laboratory tests) are generally overlaid on fine-grained soils (type A' from laboratory tests). In the eastern (steep) part of the slope, coarse-grained soils over carbonate bedrock are prevailing while, in the central part, coarse-grained materials lying over the fine-grained ones are mostly detected.

It is worth noting that the knowledge of the spatial distribution of the stratigraphic settings dealing with the two main classes of the recorded lithotypes (A' and B') as well as their relative thickness values (respectively shown in Figure 6.10 and Figure 6.11) is a fundamental information for carrying out advanced analyses aimed at identifying and characterising the triggering mechanism of any slope instability.

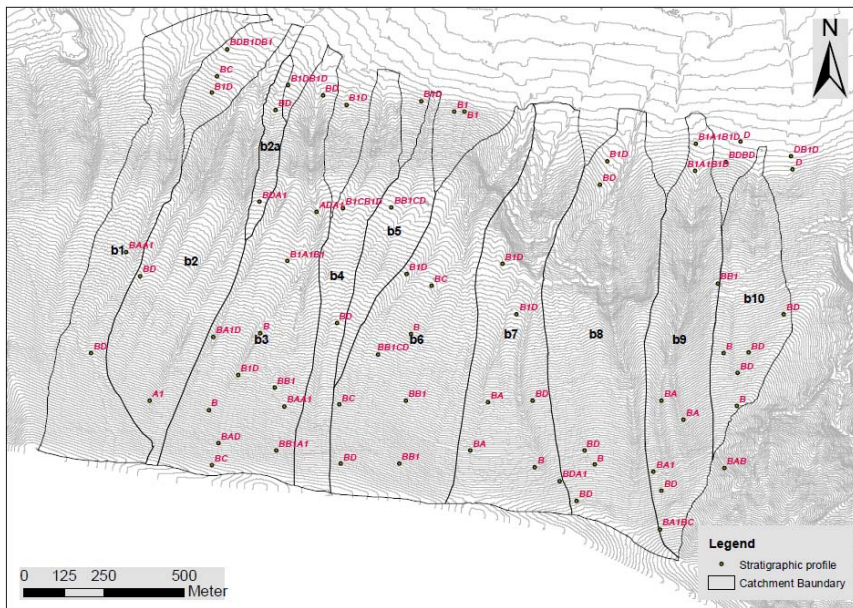


Figure 6.9 Areal distribution of vertical stratigraphic trend.

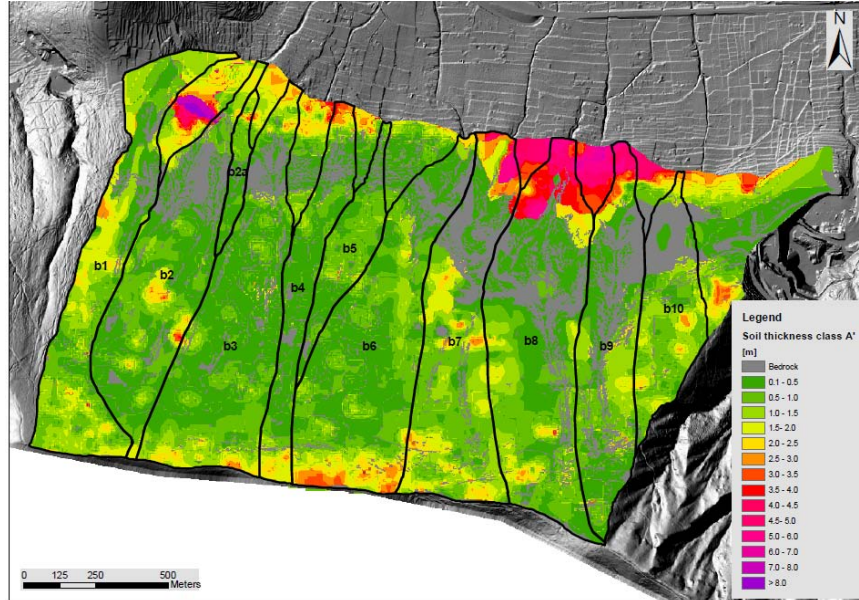


Figure 6.10 Areal distribution of the class A' lithotype.

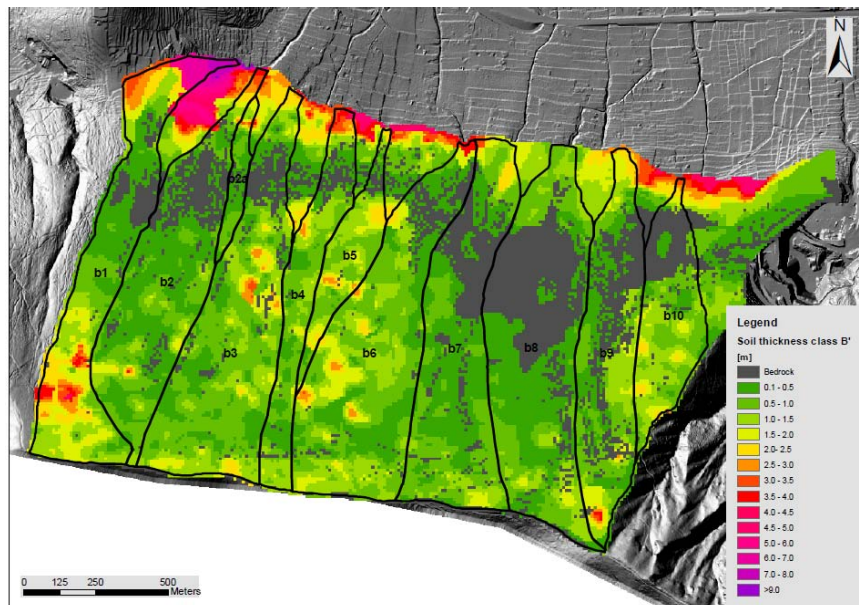


Figure 6.11 Areal distribution of the class B' lithotype.

6.6.1 Soil suction regime

In order to have a detailed description of the mechanical behaviour of pyroclastic soils under saturated and unsaturated conditions, in-situ tests aimed at obtaining the spatial and temporal distribution of soil suction values all over the Monte Albino hillslope were carried out. The suction measurements – achieved via portable tensiometer (“Quick-Draw”) – lasted about two months (November and December 2010). These measurements were collected at different depths from the ground surface; the maximum depths reached – considering the poor technology (shovel and pick) employed for the execution – equals 1.20 m.

The diagrams (Figure 6.12) showing the trend of suction values with time highlight that suction values do not exceed 10 kPa, independently from the considered depth of measure. This result could be justified considering that the measurements were achieved in a rainy period. In this regard, only in the month of November there were 21 days of rain with a maximum cumulative height of rainfall in 24 hours of 52.8 mm recorded on 17/11/2010.

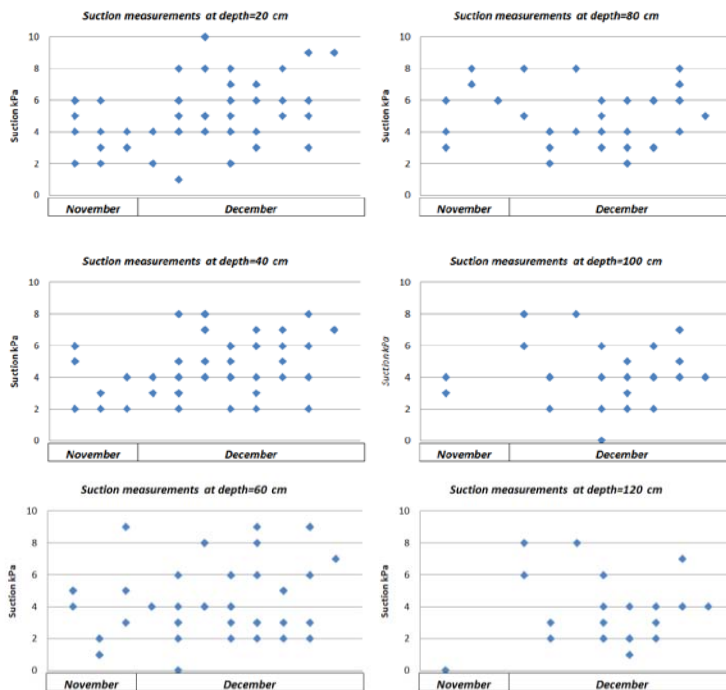


Figure 6.12 Soil suction measurements.

Furthermore, it must be observed that the abovementioned soil suction measurements confirm the preceding in-situ suction values and the time trend (Figure 6.13) provided by Cascini and Sorbino (2002) with reference to Quindici hillslopes (in the Pizzo d'Alvano massif, about 20 km far from Monte Albino) which are quite similar to Monte Albino hillslopes in both stratigraphy and slope aspect (north-exposed).

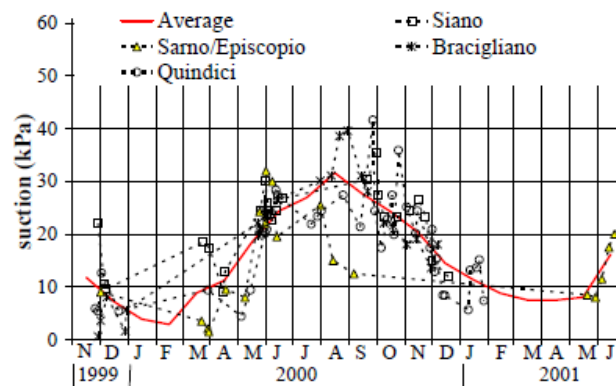


Figure 6.13 Suction value for Pizzo d'Alvano massif (Cascini and Sorbino, 2002).

6.7 ANALYSIS OF HISTORICAL INCIDENT DATA

The collection of historical information related the occurrence of flow-like phenomena provides a significant improvement of the knowledge deriving from the standard geological-geomorphological analyses together with a better definition of different aspects dealing with the risk analysis. In particular, a comprehensive catalogue of incident data enables not only to recover information about past events whose traces on the slope surface are no more visible, but also to: individuate the type of prevailing slope instabilities; estimate their frequency; identify the main triggering factors (adverse climatic conditions, earthquakes, etc.); evaluate the run-out distances on the basis of the location of the hit areas; provide detailed information on the direct and/or indirect effects on the territory.

Starting from these considerations, with reference to the study area, an historical analysis - developed on the basis of the documentary sources

and hereafter described - was carried out in order to accomplish some of the abovementioned goals.

6.7.1 Results of the historical analysis

In the study area a comprehensive catalogue of incident data, spanning from 1600 up to now, was implemented on the basis of different documents (see Section. 5.2).

It is worth noting that, although the different nature of the documentary sources, the gathered information is mostly related to the description of the affected areas and to recorded consequences (in terms of economic damage and life loss) while information pertaining to the main geometrical and kinematic characteristics of the occurred flow-like phenomena are lacking.

The analysis of the contents of the recovered historical documents revealed that most of events occurred in 18th and 19th centuries corresponds to hyperconcentrated flows (Costa, 1988). On the other hand, the incident data referring to the 20th century confirm the recurrence of hyperconcentrated flows but also highlight the occurrence of first-time landslides on open slopes (including the event dated March 2005).

Focusing on the hyperconcentrated flows, information provided by the documentary sources on the earliest events (Table 6.3) essentially concentrates on the consequences recorded on the exposed facilities.

In particular, as far as the events occurred in the 18th century are concerned, the described consequences essentially refer to buildings located in urbanised portions of Nocera de' Pagani (this is the name of the Municipality at that time) and/or in the district called "Vescovado" (Figure 6.14); furthermore, these consequence seem to had been more severe, in terms of damage, than those occurred in the 19th century. In fact, the consequences caused by the hyperconcentrated flows occurred in the 19th century essentially consisted of troubles in accessing some sections of the consular road (Figure 6.14), near the built-up areas. These marked differences are mainly caused by the relevant presence of cohesionless pyroclastic deposits on the slope as well as by the construction of the hydraulic control works in the piedmont area undertaken by King Ferdinand IV (Marciani, 1930; Beguinot, 1957). Thanks to these mitigation measures, in the later time, the consequences

related to the hyperconcentrated flow phenomena were limited to troubles in accessing some sections of the consular road. Finally, it is worth noting that some documents also furnish interesting information about the cost (in ducats) required for the removal of the sediments transported over the corridors.

Table 6.3 Recorded incident data of hyperconcentrated flows occurred from 1707 to 1846, with indication of the affected areas.

ID	Day	Month	Year	Affected area
1	21	10	1707	The town ^(*)
2	11	11	1733	The town and the consular road
3	24	10	1739	The town and the “Vescovado” district
4	02	12	1745	The town and the “Vescovado” district
5	11	11	1773	The town and the “Vescovado” district
6		1	1804	The consular road
7	24	1	1823	The consular road
8	30	11	1832	The consular road
9	02	10	1846	The consular road

^(*) The term “town” indicated the built-up area at the time when the phenomena occurred.

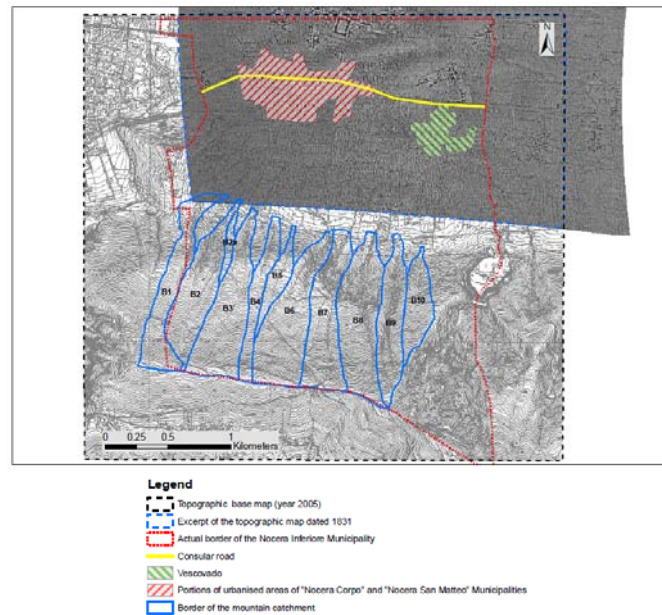


Figure 6.14 Urbanised areas affected by hyperconcentrated flows occurred during the 18th and the 19th centuries.

As far as the 20th century is concerned, the analysis of information gathered from the recovered documents – mainly the newspapers “Roma” and “Il Mattino” - reveal the occurrence of three hyperconcentrated flows - dated 2 October 1949, 12 September 1955, 26 September 1963.

Regarding the event dated 2 October 1949 the historical sources testify the overflowing of several mountain creeks with consequent transport and building invasion of alluvial material, boulders and trees. The newspaper “Roma” dated 7 October 1949 reports that:

"The Under-Secretary of State for the Agriculture, Hon. Colombo, led to Nocera Inferiore where [...], personally ascertained the extensive damage to agriculture caused by the overflowing of the Cavaiola stream and of its affluent [...]. The Under-Secretary was particularly interested in the really alarming conditions prevailing in the Vescovado district, where the road was interrupted by the huge quantity of alluvial material, coming from the above mountain [...]".

Focusing on the event dated 12 September 1955 the documentary sources deal with a violent storm that caused widespread flooding - of mud and debris coming from the Lattari Mount - of the village. This latter statement seems to be confirmed by the exam of historic air photograph highlighting the occurrence of slope instabilities, in some portions of the Monte Albino hillslopes, later propagating as flow-like phenomena.

The newspapers “Roma” dated 12 September 1955 report that: *"In Nocera the torrential water coming from Monte Albino hillslope, crossing the national road 18, in the access routes of Capo Casale, Casale del Pozzo, via delle Prigioni, via Origliano has entered and finally along the Corso Vittorio Emanuele has spill out, causing flooding in the ground floors of shops and courtyards. In the Largo S. Biagio town there have been flooding; in particular, the water has reached the height of over one meter in Astatì road, in Casolla district, in S. Chiara locality and in Railroad Square and. In the afternoon a wave of mud has reached 50 cm in the residential area.. Here there has been a temporary interruption of traffic, following the fall of the airline between Nocera Inferiore and Cava dei Tirreni"*.

The rain fell during the 26 September 1963 swelled the mountain streams of mud, stones and tree branches finding an outlet in the urbanised area. This implied the flooding of entire districts with huge economic damage.

All the available data furnish the cumulative curve of past hyperconcentrated flow events shown in Figure 6.15 that is characterised by a stepped shape during the time period spanning from 1707 to 1846.

Figure 6.15 also shows that the occurrence of some of these events may be correlated with the explosive eruptions of the Vesuvius volcano; in particular, between the 1811 and 1848, during a period of intensive strombolian activity of the volcano (Scandone et al., 2008), n. 3 hyperconcentrated flow events were recorded (Table 6.3). In this regard, these phenomena could be ascribed to: *i*) the availability of pyroclastic soils over the hillslope, transported by the winds that - in the autumn-winter period - blowing toward the eastern sectors (Rolandi et al., 2007); *ii*) the washing operated by rainfall of short duration and high intensity. On the other hand, for the latest events occurred after the last Vesuvius eruption dated 1944 it is reasonable to consider that the genesis of hyperconcentrated flows changed being strictly related to rainfall-induced erosion processes.

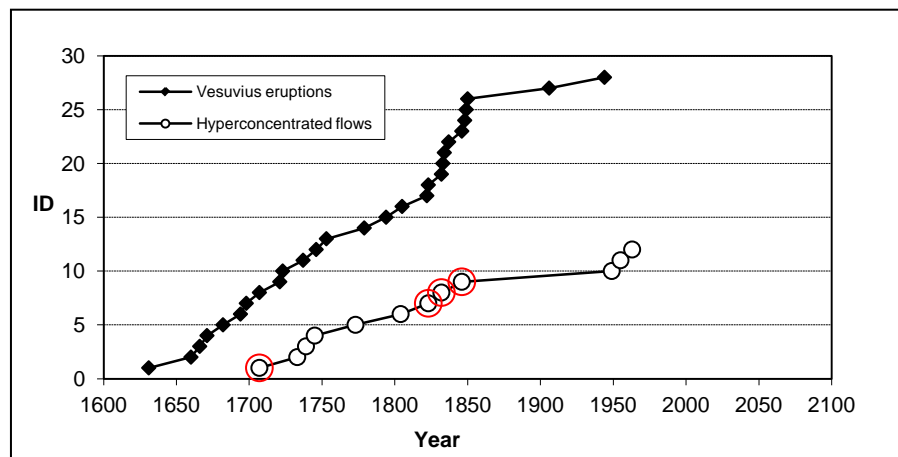


Figure 6.15 Cumulative distributions of: i) Vesuvius explosive eruptions occurred from 1631 up to now; ii) hyperconcentrated flow incident data (events occurred after the Vesuvius eruptions are circled in red).

With reference to the seasonal distribution of the past events, Figure 6.16 shows that the recorded incident data concentrate between September and January, with a maximum in November. This confirms that the initiation processes of occurred phenomena can be associated to the washing action operated by autumnal storms (rainfall with short duration and high intensity). It is worth noting that the latest events occurred in September/October months, i.e. a period of the year in which soil suction values are high enough to prevent the initiation of any

first-time shallow slides while erosion phenomena can be triggered by high-intensity rains (Cascini et al. 2013 b).

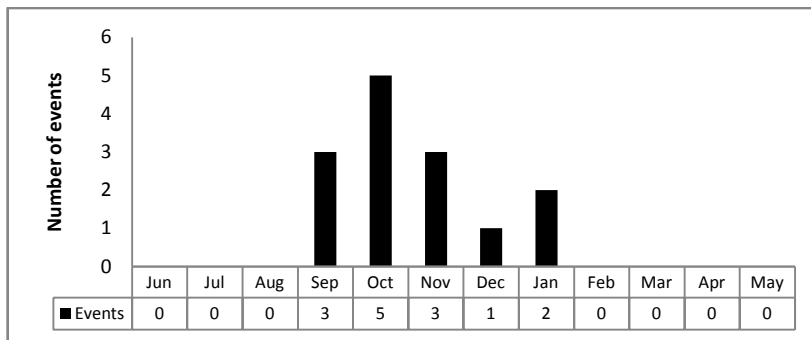


Figure 6.16. Monthly distribution of the hyperconcentrated flows which, in the past, interested the Monte Albino hillslope.

Finally, with reference to the first-failure landslides on open slopes it can be observed, on the basis of the available data (Table 6.4), that starting from 1935 up to now four events were detected.

Table 6.4. Recorded incident data of landslides on open slopes occurred from 1935 to 2005, with indication of the consequences to the exposed persons and properties.

ID	Day	Month	Year	Fatalities/Endangered sites
1	-	-	1935	-
2	24	10	1954	-
3	-	-	1958	-
4	4	3	2005	3 fatalities/some houses destroyed

7 SLOPE EVOLUTION MODEL OF MONTE ALBINO MASSIF

The overall results achieved with field investigations significantly contributed to increase the knowledge, in order to promote the acquisition of indispensable elements for the development of the geomorphological slope evolution models and of the engineering models aimed at the identification of the triggering mechanisms of flow-like phenomena within reworked and in-situ pyroclastic deposits mantling the Monte Albino hillslope.

Bearing in mind the contribution that these information can provide in the prediction and prevention of landslide risk, in the following sections the acquired geological and geotechnical data are illustrated.

7.1 ANALYSIS OF GEOMORPHOLOGICAL PROCESSES

The geomorphological analysis was performed by using topographic-maps at different scale (IGM 1:25,000 scale - editions of 1909, 1936, 1941, 1955, 1980, 1987; Campania Region CTR, 1:5,000 scale- editions of 2000, 2004; Topographic map derived from a DEM from LIDAR flights of 2010, 1:1,000 scale), orthophotos (dated 2005, 2006, 2007 by GoogleMap™), historical aerial photographs (flight of the Campania Region dated 1954-55) and field surveys results.

In particular, this analysis allowed to identify the geomorphological elements, named *morphotypes* (Figure 7.1), that significantly influence the triggering and propagation stage of landslide phenomena. Morphotypes are linear or areal homogeneous elements in terms of morphological and lithological characteristics.

The geomorphological elements has been verified and validate through the results of field surveys; moreover, the availability of numerous stratigraphic data, derived from excavations and drillings, allowed to obtain a detailed check of the identified forms. In this way, it has been

possible to associate at the different geomorphological forms their dominant processes and state of activity.

Along Monte Albino hillslope different morphotypes were distinguished (Figure 7.1): *a*) zero Order Basin; *b*) morphological hollows with relevant thickness of pyroclastic and detrital deposits shaped by the water surface drainage; *c*) structural limestone scarps, generally related to the presence of fault planes (e.g. the road to the St. Mary sanctuary of Monte Albino) or of headings of carbonatic strata (e.g. heads of the valleys); *d*) erosion channel (gully) characterised by linear erosion processes within detrital-pyroclastic deposits that, however, presents significant thicknesses; *e*) erosion scarp along the gullies, which is mainly linked to linear erosion processes that have incised the pyroclastic covers and sometimes also the carbonate bedrock, often in correspondence of buried tectonic elements; *f*) depositional areas related to gravity erosion processes; *g*) depositional areas related to the torrential waters action (debris-alluvial fans); *h*) detachment and deposits areas of past landslides.

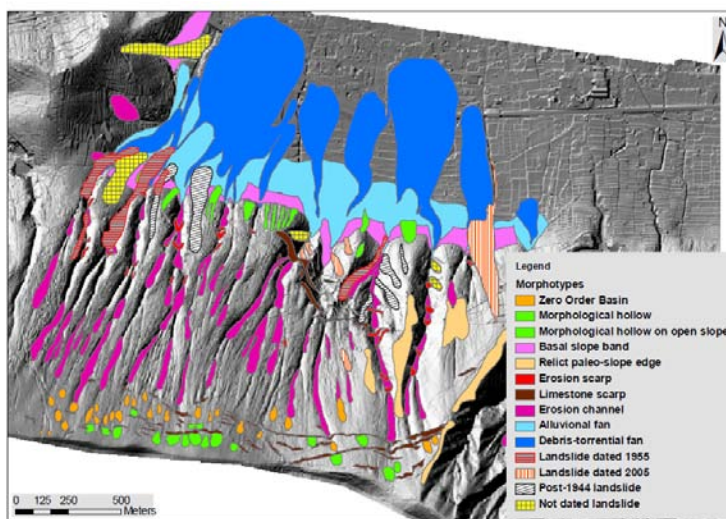


Figure 7.1 Morphotypes map.

The filling and subsequent emptying dynamic of morphological hollows is characterised by the continuous contributions of material from the upper zones and the progressive transfer in the lower sector or in the first order channels of the drainage network.

In the western sector of the slope, immediately downstream of the ZOBs, the incisions are positioned. These are characterised by linear erosion processes within the debris-pyroclastic soil that still presents significant thicknesses. In the eastern sector instead, just downstream of the ZOBs, generally torrential channels deeply incised in the carbonate bedrock are present.

In the lateral areas of channels, in the watershed areas and along the open slopes, morphological elements presumably related to landslide processes are detected.

7.2 CHARACTERISATION OF MORPHOLOGICAL UNITS

In the test site, two main morphological sectors are recognised: the mountain-slope sector and piedmont sector with the overlooking plain.

At large-scale, the morphological structure is strongly controlled by tectonic setting, characterised by a lowered sector, filled by pyroclastic and detrital-alluvial deposits (alluvial plain), and by an up-lifted sector, consisting of very thick carbonate sequences with thin debris-pyroclastic covers, which has evolved by recession processes of fault planes located in the mountain-slope sector. The normal faults system is masked, in the piedmont sector, by copious debris accumulations.

Owing the influence that the tectonic structures have on the morphology, slope angle and exposure characters of the slope were examined, in order to define the geomorphological zoning.

The distribution of the slope angle values in different classes (Figure 7.2), defined through the use - in GIS environment - of a detailed DTM (1m x 1m), detects the slope distribution pattern. In particular, the valley portion (north of the highway) is characterised by slope angles generally lower than 5°; the piedmont sector, instead, presents slope angle values generally ranging between 5° and 25°. The basal strip of the slope is characterised, for all its extension, by high gradients, generally ranging between 30° and 60°. The middle and upper sectors of the slope show a strong asymmetry between the western area and the eastern area. The western side is characterised by an intermediate morphological plain in which slope angles are rather moderate (10° to 25°); it is connected upwards with the top portion of the slope with gradients generally comprised between 25° and 60°. In the eastern side slope angles are

distributed in an irregular manner from 30° to 60° in correspondence of the head of the torrential channels.

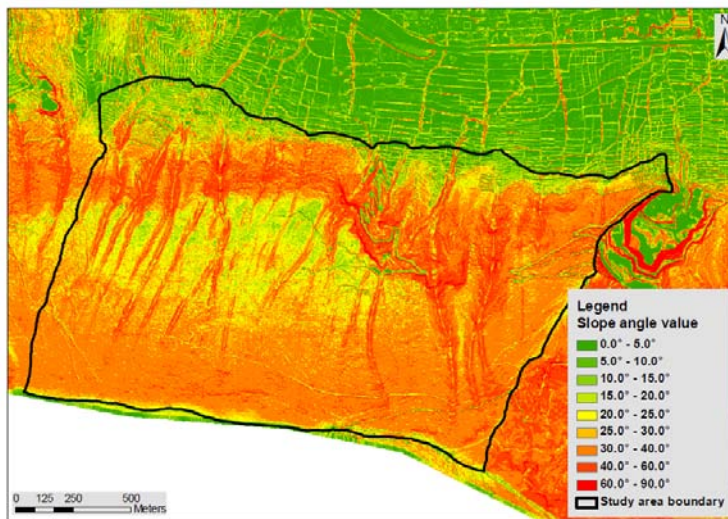


Figure 7.2 Slope angle map.

The analysis of exposure values, grouped into eight classes with opening angle of 22.5° according to the orientation N, NE, E, SE, S, SW, W, NW (Figure 7.3), shows a prevalent exposure of the whole slope toward north. In the western portion, areas with equally distributed exposure to N and NE are detected, while in the eastern sector regions with N and NW exposure are prevalent. It is interesting to note that, while in the western sector areas with homogeneous exposure appear to continue throughout the longitudinal development of the slope, in the eastern sector the exposures distribution is more uneven as a result of the presence of tectonic elements and deep incisions of the hydrographic network.

The integrated analysis of morpho-structural and clinometric forms as well as exposure and slope angles characters has allowed to carry out a morphological zoning of the Monte Albino slope aimed at analysing erosion and landslide processes.

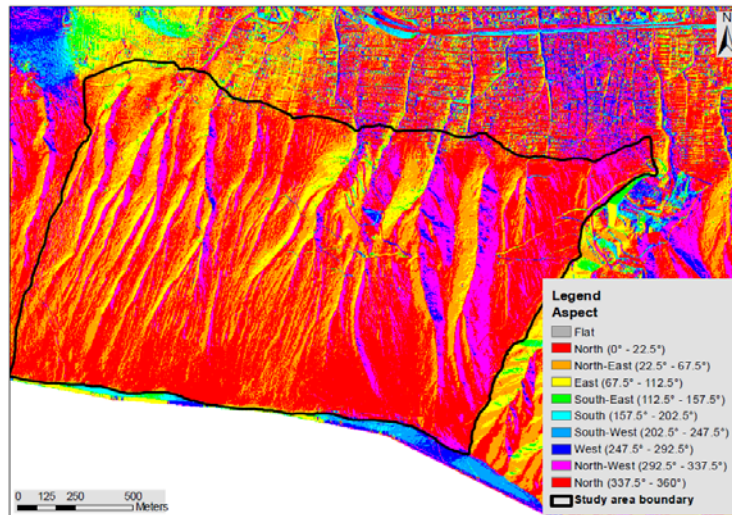


Figure 7.3 Exposure map.

On the basis of this morphological evidences seven morphological ambits (or “zones”) can be detected (Figure 7.4).

In this regard, moving from the highest elevations to the lowest ones, the *ridge zone* is detected. It develops in a continuous way between Chiunzi Mount (855 m a.s.l.), the Chiancolelle pass (731 m a.s.l.) and St. Angelo Mount (1,130 m a.s.l.), along the watershed with the Regina Major hydrographic catchment. The ridge has a width that reaches 50 m, with a prevalent E-W exposure in the western part and NW-SE exposure in the eastern section. The ridge zone is characterised by a well-evolved mature morphology, without evidences of erosive processes, and thick soil cover deposits (larger than 3 m on average).

In the *upstream zone* the presence of ephemeral watersheds and hollows affected by colluvial processes can be generally observed; moreover, in the eastern part of this zone, rills originated by erosive processes are widespread while they are lacking in the western side.

The *incision zone* is characterised by longitudinal gullies developing up to from 500 m a.s.l. to 630 m a.s.l.; in the eastern sector a close and deepened hydrographic network is detected, that documents the development of intense linear erosion processes. The *flat zone* is a transition sector between the incision zone and the erosion zone and mainly interests the mountain catchments labelled from B1 to B7, with slope angle ranging from 20° to 30° and a constant depth of the gullies.

In the *erosion zone*, slope angle values progressively increase giving rise to local morphological scarps. At lowest elevations it is possible to recognise the presence of the *valley zone*, characterised by a marked decrease of the slope angle values as well as the presence of ten *open slopes* (triangular facets).

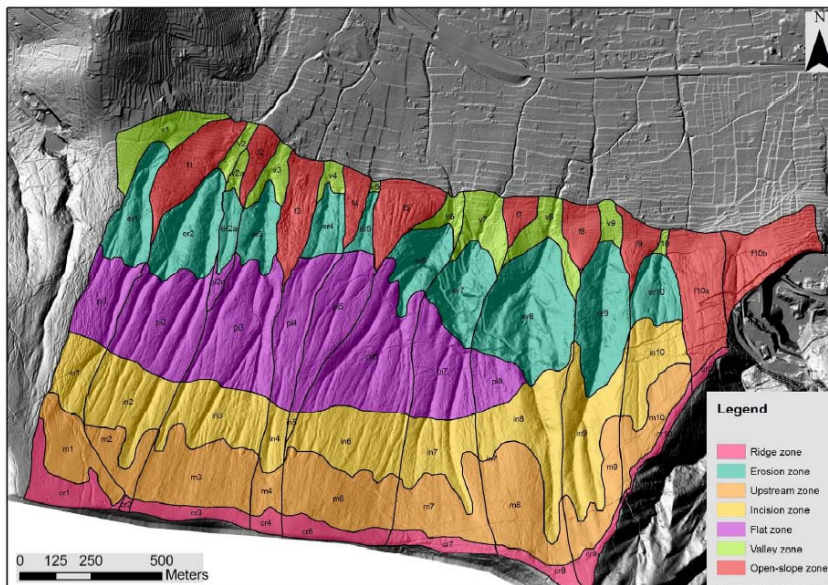


Figure 7.4 Morphological zoning map.

7.3 CHARACTERISATION OF MOUNTAIN CATCHMENTS

The Monte Albino hillslope can be divided into eleven mountain catchments (Figure 7.5) whose main characteristics are summarised in Table 7.1.

The analysis of morphometric data of the mountain catchments (Table 7.1) brings out that average slope angles are very high (with a maximum value of 37° in the mountain catchment B9) and, in particular, they greatly increase passing from the western to the eastern section of the slope.

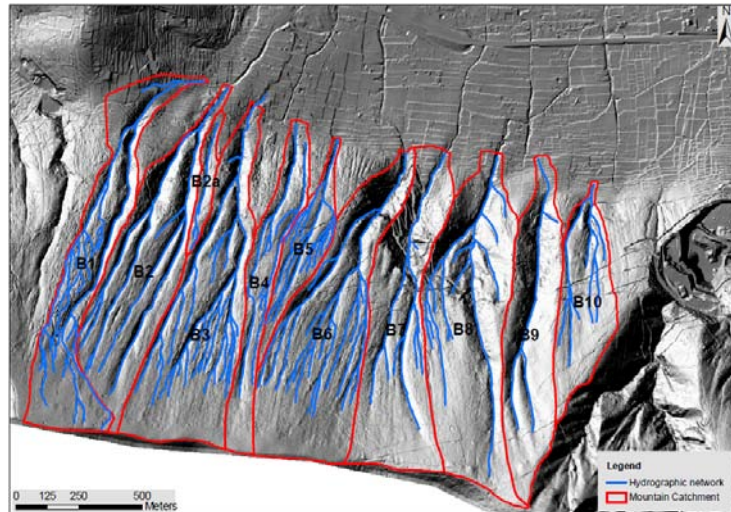


Figure 7.5 Mountain catchments along the Monte Albino hillslopes superimposed to a DTM derived from 1-m resolution data achieved via a LiDAR survey.

Table 7.1 Morphometric characteristics of the mountain catchments.

<i>Catchment</i>	<i>Area</i>	<i>Max elevation</i>	<i>Min elevation</i>	<i>Average slope</i>
-	[ha]	[m a.s.l.]	[m a.s.l.]	[°]
B1	25.9	855.0	119.0	29.0
B2	27.8	820.0	114.0	32.0
B2a	3.0	402.0	135.0	27.0
B3	33.9	818.0	113.0	32.0
B4	13.8	791.0	104.0	29.0
B5	82.5	581.0	103.0	25.0
B6	36.1	790.0	95.0	31.0
B7	29.8	787.0	99.0	31.0
B8	36.7	887.0	94.0	35.0
B9	22.3	887.0	99.0	37.0
B10	14.3	707.0	112.0	34.0

The analysis of the hydrographic network characteristics was deepened through the study of different elevation profiles - 20 elevation profiles along longitudinal sections and 250 elevations profiles along cross section – built in 1:2,000 scale on the bases of the available DEM (Figure 7.6).

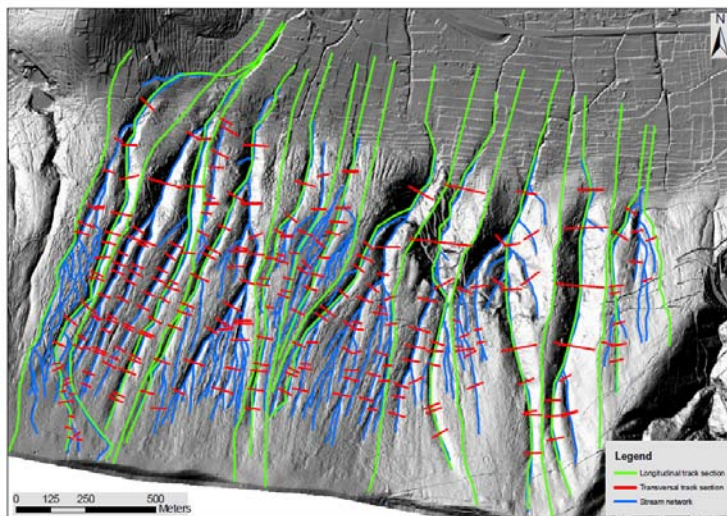


Figure 7.6 Longitudinal and transversal track section.

The analysis of the elevation profiles along longitudinal sections, plotted in correspondence of the gullies and watershed zones, allows to produce important considerations about the understanding of morphological factors that control the triggering and evolution stages of flow-like phenomena. The elevation trend of the analysed longitudinal sections further confirms the morphological setting above discussed. In this sense, in fact three main types of longitudinal altitude profiles are recognised, namely LP1 - LP2 - LP3 (Figure 7.7), each featuring a well-defined portion of the slope.

The eastern sector (B8, B9, B10) is characterised by a longitudinal profile rather regular or devoid of abrupt changes of slope angle (LP1), a dense and deepened hydrographic network with an angled pattern that documents the development of intense erosion phenomena (area of intense linear erosion). These elements show a high degree of morphological maturity of the eastern sector.

The mountain catchment B7, however, represents a morphological transition zone between the eastern and the western zone of the Monte Albino hillslope; in fact, it shows a very similar trend to that of the eastern portion up to an altitude of 300 m a.s.l. then it exhibits a morphological jump of about 80 meters with an average slope angle of 60°.

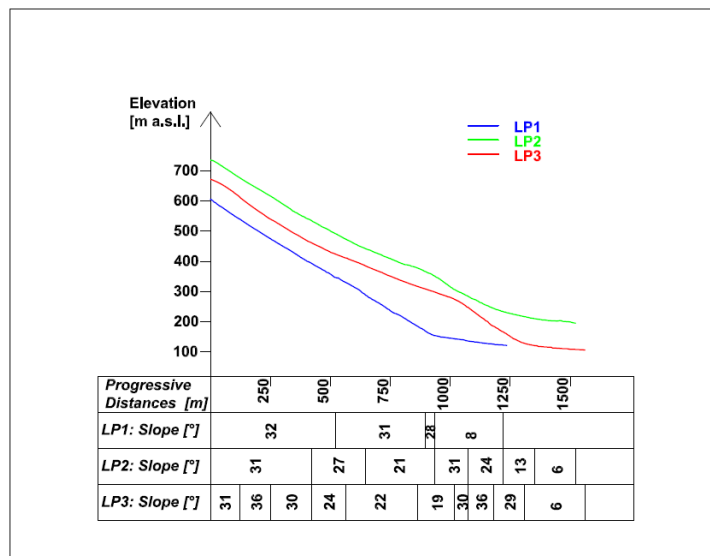


Figure 7.7 Typical longitudinal profile.

The mountain catchments located in the central portion of the slope (B3, B4, B5, B6) are joined by a non-regular longitudinal profile (LP3), showing different slope angle discontinuities and relevant pyroclastic thicknesses variously distributed. The presence of such discontinuities allows the delimitation of three homogeneous longitudinal sectors, dissected from a linear-parallel hydrographic network. In particular, in the middle portion - between 300 and 480 m a.s.l. - a morphology plain is recognises, with inclinations less than 20-25°, passing upward to a relict recession slope with slope angles between 25-40°, which presents up to 650 m a.s.l. a development of linear incisions.

The western section of the slope (B1, B2), morphologically less evolved than the other portions, have a longitudinal profile partially regular (LP2) as such the slope angles trend is very graduated and are also present significant pyroclastic thicknesses.

The analyses of 250 transversal profiles along the hydrographic channels showed the existence of five prevalent profiles types of cross sections (Figure 7.8 and Figure 7.9). The profile TP1 is mainly detected in the medium-high portion of the mountain catchment B1. It is characterised by a rather regular elevation trend moderate slope angle (on the order of 5° to 10°), an average width of 15 meters and relevant presence of pyroclastic thicknesses. From a morphological point of view, the presence of TP1 suggests a recent genesis of the slope.

The profile TP2, widely distributed in the central area of the slope, exhibits a very gentle trend in which the torrential incision is barely visible. The width of the channel does not overcome 40 meters, the average slope angles is attested at about 15° , the thickness of the whole pyroclastic cover range from 1 m to 3 m while the pyroclastic soil thickness related only to the lithotype A' (see Section 6.5) does not exceed 1 meter.

The profile TP3 is found, for the greatest part, in the middle-portion of the slope and it is characterised by low gradients of slope angle. It is distinguished for a marked evidence of channels tract that assumes the typical "U" shape with a width that does not overcome 40 meters. Along the profile TP3 significant thicknesses of pyroclastic soils are present, homogeneously divided among the lithotype B' and A'.

The TP4 profile, widely extended in the middle-low zones of the eastern portion of the slope, is connoted by the presence of incised channels that assume a gentle form thanks to the existence of the redeposited pyroclastic soils. It is worth noting that the width of the gullies is larger than the previous ones (about 60 meters) and the slope angles are attested at about 35° .

The profile TP5 differs from the previous ones due to the poor presence of pyroclastic soils that are mostly present along the lateral sides. Particularly, it exhibits a typical "V" shape, essentially linked to the erosion action practiced by water which, over time, has contributed to modelling the channel beds. The width of the channel bed is attested around 60 meters while the slope angles of the lateral banks may reach 50° .

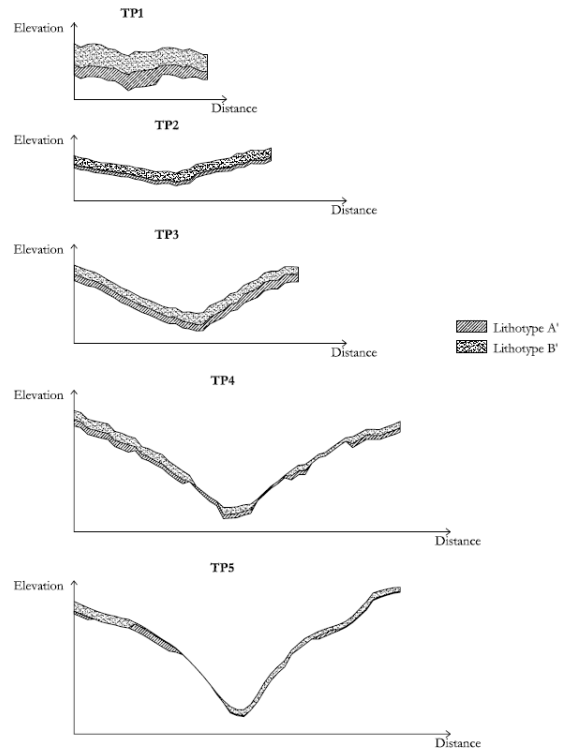


Figure 7.8 Typical transversal profile.

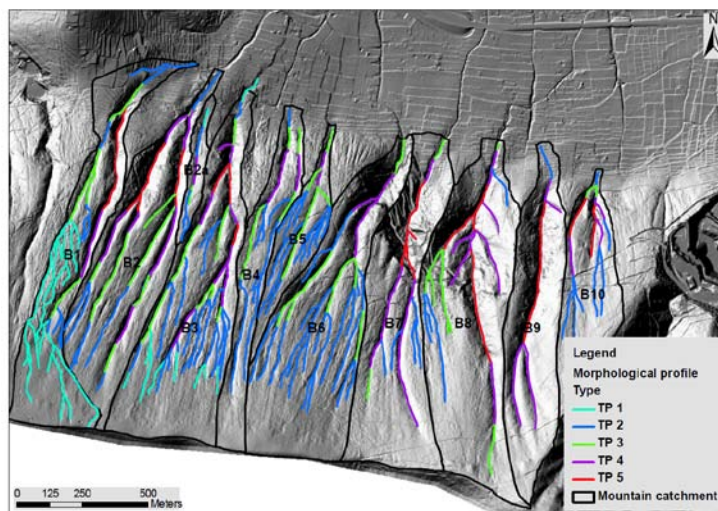


Figure 7.9 Transversal profile type distribution.

7.4 CHARACTERISATION AND CLASSIFICATION OF ALLUVIAL FANS

Within the piedmont area, an articulated system of alluvial fans of different generations was recognised (Figure 7.10), and further analyses were performed in order to define the state of activity and the hierarchical organisation.

The geomorphological analysis allowed to recognise a system of ancient re-incised debris-alluvial fans and a system of recent/active debris-alluvial fans (Figure 7.10). The available stratigraphic data on debris-alluvial deposits in the valley area were obtained by drilling stratigraphy of the ISPRA archive (Institute for Environmental Protection and Research) and by surveys results (seismic field tests and dynamic penetrometric tests) (Figure 7.11) commissioned by the Nocera Inferiore Municipality for the revision of the Urban Municipality Planning (P.U.C.). These data allowed to perform a preliminary classification of alluvial fans.

The first fan system may be classified as an ancient re-incised debris-alluvial fans, placed at the base of the slope, with average slope values ranging from 5° to 10° (Figure 7.10). Then, it is possible to recognise five ancient debris-alluvial fans with average slope values ranging from 2° and 5° . The age of alluvial fans can be dated beginning from 39,000 years ago, as their base lays down on a horizon of *Ignimbite Campana* deposits.

Re-incised ancient talus develops from an altitude of 135 m a.s.l. to about 70 m a.s.l. with a maximum length - in the western sector of the slope - of over 600 meters (at the base of the hydrographic catchment B1), while in the eastern sector their length is about 200-300 meters with altitude ranges from 130 m a.s.l. to 85 m a.s.l..

Ancient fans have a maximum linear extension of about 600 meters and develop from altitudes between 85 and 50 m a.s.l., crossing the highway A3 track. They are present in the “Capo Casale” zone (western sector) - where in the past the urbanised area of the town was located - and in the “Vescovado” zone (eastern sector).

A second system of debris-alluvial fans - with a most recent genesis and a more restricted size - overlaps the ancient fan system. This system is formed by active debris-alluvial fans and torrent-alluvial fans, linked to different depositional processes. The active debris-alluvial fans are distributed in the portion closest to the base of the slope with the apexes

coincident with the outlet of the valleys; the shape is more elongated in the western sector (with a maximum length of approximately 600 meters) while it shows wider in the eastern sector (with a maximum width of about 110 meters). These alluvial fans are generally incised from channel-road and they represent depositional zones linked both to the normal torrential accumulation processes and to hyperconcentrated flows and, in the proximal portion, to mass transport.

The torrential-alluvial fans are more extensive than debris-alluvial fans. They have a length ranging between 400 and 800 meters and a width between 30 and 100 meters. They develop, from the incised channels-road, in the debris-alluvial fans and reach the underlying plain for some hundred meters beyond the highway. They are depositional forms related to the normal torrential accumulation processes and, in the proximal portion, to the contribution of hyperconcentrated flows.

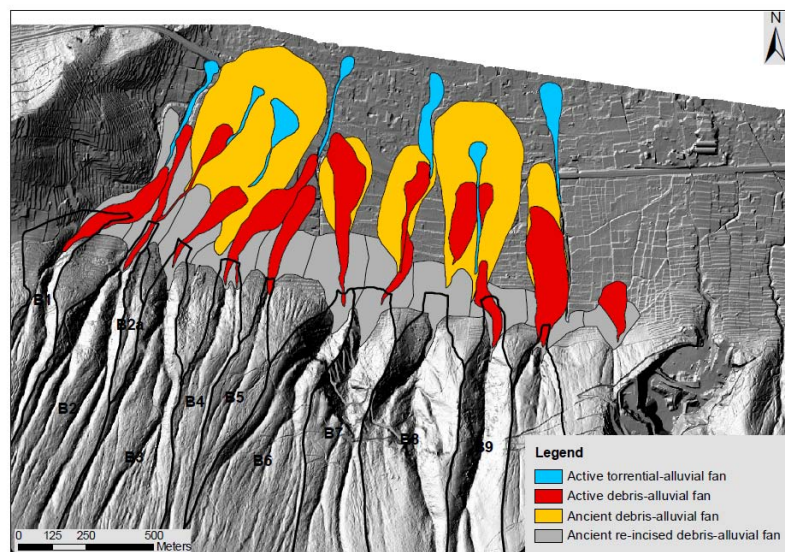


Figure 7.10 Alluvial fan distribution.

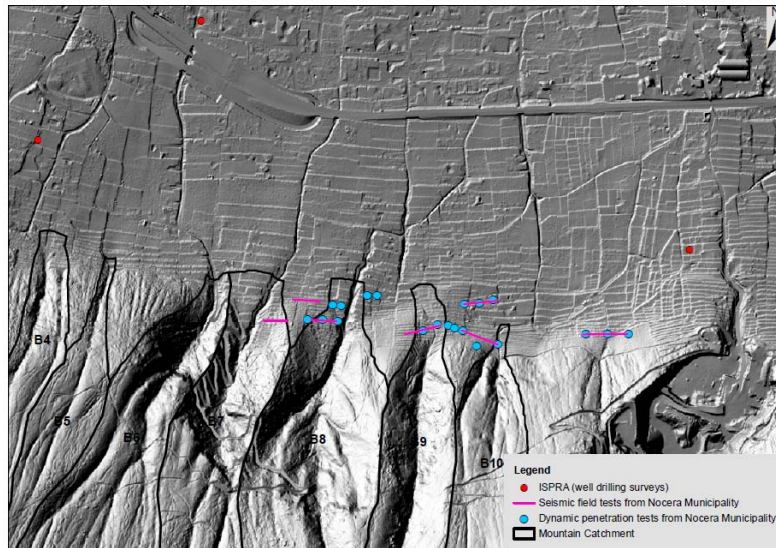


Figure 7.11 Field surveys deriving from ISPRA and Nocera Inferiore Municipality.

In order to evaluate the average and maximum thickness of the active debris-alluvial fan deposits and, consequently, to estimate their volumes, available surveys data was used or, where lacking, was alternatively derived by an empirical procedure. In this last case, the difference in elevation of the lateral boundaries of the alluvial fans was considered, assuming that this could represent the minimum value of the soil deposit thickness along the cross section of the alluvial fans. The preliminary estimate of the volume of pyroclastic deposits within each active alluvial fan (Table 7.2) was obtained by multiplying its areal extent for the estimate soil thickness along different cross-section. It is worth noting that the obtained results do not take into account the possible presence of buried valleys and concave shapes or morphological steps in the carbonate or cemented slope debris bedrock, which could highly increase the amount of soil deposits.

Table 7.2 Active alluvial fan volume.

<i>Basin</i>	<i>Volume (mc)</i>
B1	82,850
B2	37,793
B2A	
B3	44,741
B4	99,402
B5	41,719
B6	98,208
B7	27,075
B8	42,144
B9	44,695
B10	184,703

7.5 EMPIRICAL ANALYSIS OF FIELD SURVEYS RESULTS

In order to identify the areas of the Monte Albino hillslope that have mostly contributed to increase the development of the piedmont alluvial fan systems, an empirical analysis of the cover thickness was performed. This analysis focused on the definition of a conceptual model of the air-fall pyroclastic deposits distribution on the test site after the Ignimbrite Campania eruption (39 ka BP), highlighting the effect of the denudation processes which have contributed to the achievement of the present equilibrium state. The study, although was conducted at a preliminary level, may constitute a reference point for further studies aimed at analyse the landslide susceptibility.

Data related to the pyroclastic thickness covers above the carbonate bedrock, resulting from field surveys (see Section 6.4) were compared with the different morphometric characters of the slope (elevation, slope, aspect, curvature, plan curvature, profile curvature).

The analyses of iron-rod drillings data revealed a complete absence of possible correlations with the different morphometric characteristics (Figure 7.12).

The analyses of the penetration tests data are few significant if they are contextualised in relation to the different morphological units, due to the

restricted number of the available surveys as well as the sporadic areal distribution. The different combinations of the penetration tests results with different morphometric characteristics of the slope (Figure 7.13) reveal that pyroclastic thickness decreases with increasing of altitude and slope angle and that in the eastern part of the slope (mainly exposed to north-west) soil thickness values are more reduced.

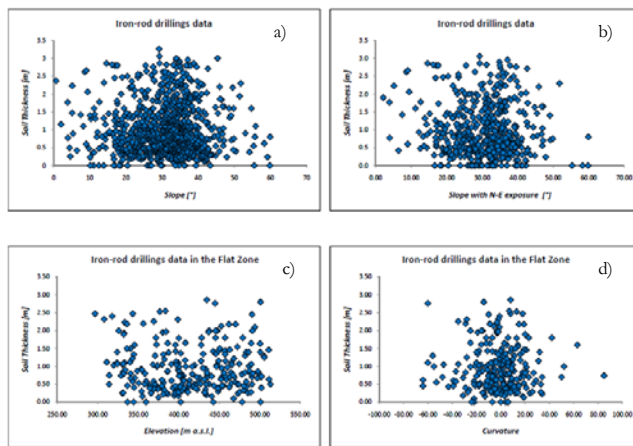


Figure 7.12 Iron-rod drillings data correlation with a) slope angle, b) slope angle with N-E exposure, c) elevation and d) curvature.

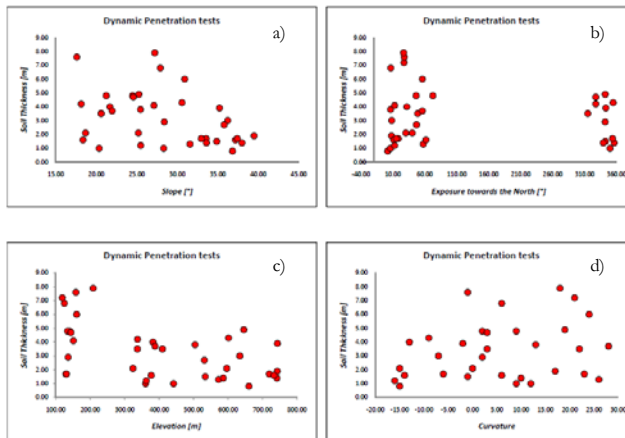


Figure 7.13 Dynamic penetration tests correlation with a) slope angle, b) exposure towards the North, c) elevation and d) curvature.

According to De Vita et al. (2006; 2012) pyroclastic soil deposits, resulting from the explosive activity of the Vesuvius volcano, cover the slope through a planar stratification parallel to the slope angle. The deposition process is well described by an empirical law (Eq. 7.1) in which the maximum theoretical thickness, measured orthogonally to the plane of the slope (St) is a function of the slope angle (α) and of real thickness (S)(soil thickness currently present in the test site):

$$St = S \cos \alpha \quad (7.1)$$

Through a second order regression of the data regarding the relationship between slope angle and soil thickness (resulting from the analysis of penetration tests data) is noticed that $S = 4.3$ (Figure 7.14), so the general formulation for the Monte Albino is expressed in the following form (Eqs. 7.2 and 7.3):

$$St = 4.3 \cos \alpha \quad \text{for } \alpha \leq 41^\circ \quad (7.2)$$

$$St = 0.1 \quad \text{for } \alpha \geq 41^\circ \quad (7.3)$$

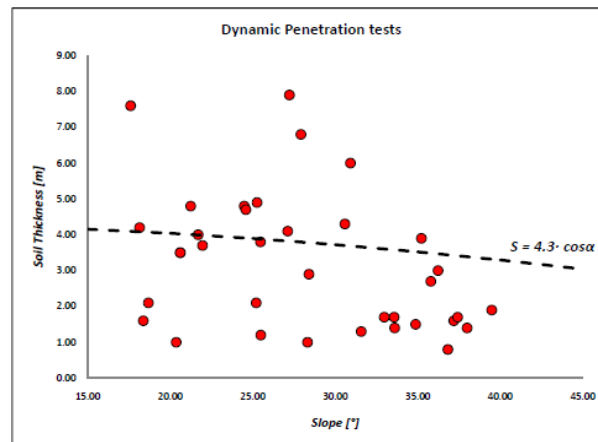


Figure 7.14 Correlation between the real thickness of the pyroclastic soils and the slope angle.

Albeit in a roughly way, such conceptual model has allowed, therefore, to define a theoretical pyroclastic thicknesses distribution map in a 1:5,000 scale (Figure 7.15).

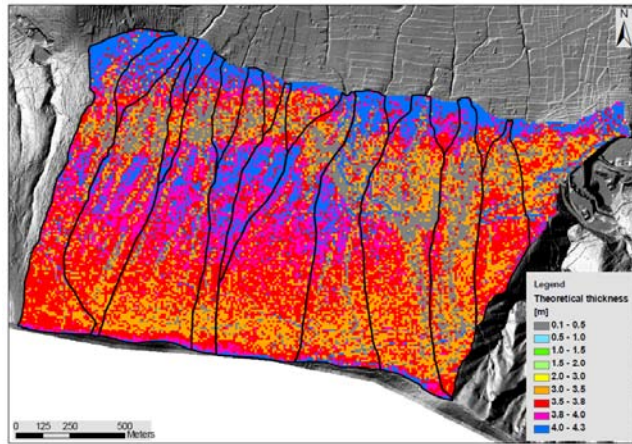


Figure 7.15 Map of theoretical thickness of the pyroclastic soils.

The validity of this formulation is strengthened by the fact that in the morphological units with a conservative character (in which the of accumulation or denudation processes are negligible), generally located in the ridge zone, pyroclastic thicknesses layer are comparable with that of the maximum theoretical thickness. The statistical analysis of slope angles, in correspondence of outcropping limestone, has also allowed to identify a threshold limit (equal to 41°) above which the depositional processes can be considered negligible.

7.6 GEOMORPHOLOGICAL SLOPE EVOLUTION

The estimation of the maximum theoretical pyroclastic soil thickness and of the currently pyroclastic soil thickness on the Monte Albino hillslope allow to draw important considerations, albeit at a preliminary level and in relative terms, about the geomorphological evolution stage of the different mountain catchments and to objectify their volumetric contribution to the piedmont alluvial fans systems.

Since the oldest pyroclastic soil deposits in the test site are related to Ignimbrite Campana eruption (39 ka BP), all the above considerations should be reported to the chronological interval between 39 ka BP and the present.

The analysis of the theoretical pyroclastic soil volumes in each mountain catchment allowed to identify the portion of the slope with a greater

availability of pyroclastic soil deposit for the onset and development of erosive processes. To this aim, the *Evolutionary stage of the mountain catchment Index* $E_{s,bi}$ was introduced (Eq. 7.4). This index, defined as the ratio between the theoretical cumulative volumes of pyroclastic soil for each mountain catchment ($V_{mt,i}$) and the relative area of the catchment ($A_{b,i}$), indicates the amount of pyroclastic soil deposits per unit area, after the Ignimbrite Campana eruption, in each mountain catchment.

$$E_{s,bi} = \frac{V_{mt,i}}{A_{b,i}} \quad (7.4)$$

The analysis of $E_{s,bi}$ index distribution for each mountain catchment (Table 7.3 and Figure 7.16) clearly shows lower values (between 2.61 - 3.18 m^3/m^2) in the eastern portion of the slope and in the mountain catchments B2, while the highest values (between 3.32 - 3.67 m^3/m^2) are detected in the western portion of the slope. Lower values of $E_{s,bi}$ index should be related to the presence of higher slope angle classes at the time of deposition processes, indicating that channels had already suffered intense erosion processes in the carbonate bedrock before the Ignimbrite Campana eruption. Therefore, the eastern portion of the slope is characterised by a morphological evolution stronger than the remaining portion.

Table 7.3 $E_{s,bi}$ index value for each mountain catchment of Monte Albino hillslope.

ID	$E_{s,bi}$ <i>mc/mq</i>	Ranking
-	-	-
B1	3.43	3
B2	3.18	7
B2A	3.61	2
B3	3.32	6
B4	3.37	5
B5	3.67	1
B6	3.39	4
B7	3.13	9
B8	2.90	10
B9	2.61	11
B10	3.14	8

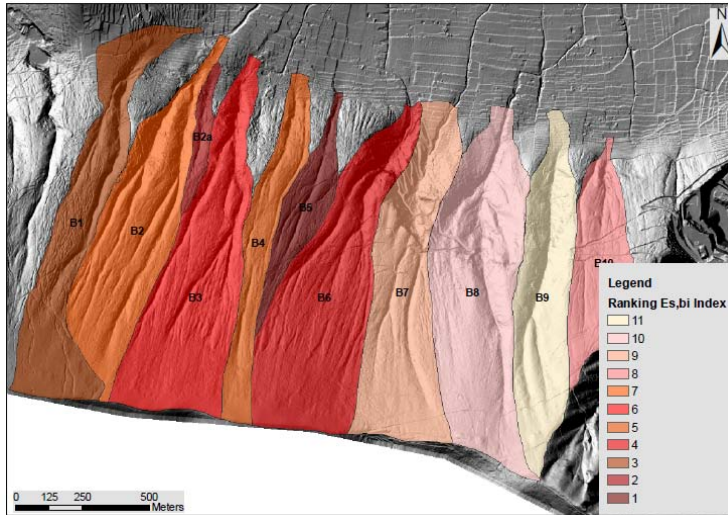


Figure 7.16 Ranking of $E_{s,bi}$ index.

The intensity of erosive processes in pyroclastic deposits, in each mountain catchment, can be well described through the use of the *Evolutionary Maturity level of the mountain catchment* $E_{m,bi}$ (Eq. 7.5):

$$E_{m,bi} = \frac{V_{m,i}}{A_{b,i}} \quad (7.5)$$

in which $V_{m,i}$ represents the average eroded volumes after the Ignimbrite Campana as it is defined as the difference between the volume of theoretical pyroclastic soils and the volume of pyroclastic soils actually available in the whole catchment while $A_{b,i}$ is the area of each mountain catchment.

The distribution of the $E_{m,bi}$ index values is shown in Table 7.4 and in Figure 7.17. Obviously, a high value of $E_{m,bi}$ index indicates a high intensity of erosive processes in the pyroclastic deposits. In this regard, the highest values are detected in the western-central sector of the slope, intermediate values in the eastern sector while the lowest value, indicating not very widespread erosion processes in the pyroclastic soil covers, is detected in the mountain catchment B1 located in the western portion of the slope.

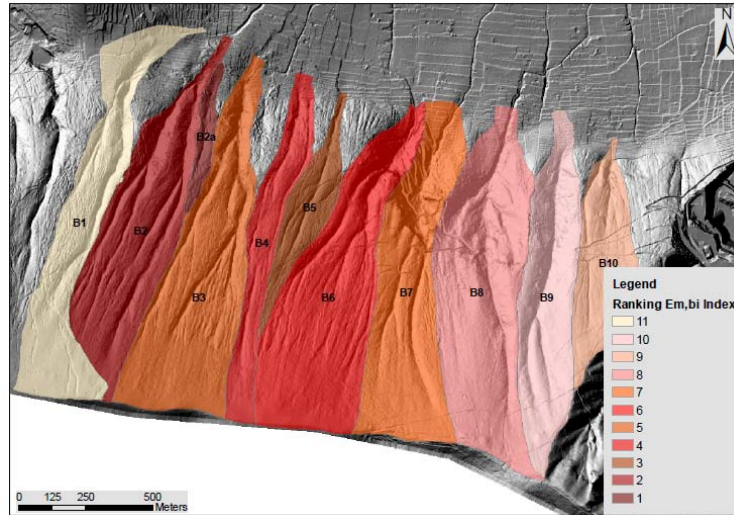


Figure 7.17 Ranking of $E_{m,bi}$ index.

Table 7.4 $E_{m,bi}$ index value for each mountain catchment of Monte Albino hillslope.

ID	$E_{m,bi}$ <i>mc/mq</i>	Ranking
-	-	-
<i>B1</i>	1.32	11.00
<i>B2</i>	2.23	2.00
<i>B2A</i>	2.41	1.00
<i>B3</i>	2.04	5.00
<i>B4</i>	2.06	4.00
<i>B5</i>	2.07	3.00
<i>B6</i>	1.92	6.00
<i>B7</i>	1.81	7.00
<i>B8</i>	1.81	8.00
<i>B9</i>	1.53	10.00
<i>B10</i>	1.71	9.00

With reference to the morphological units, the intensity of the erosion processes in the pyroclastic soil covers can be evaluated through the use of the *Evolutionary Maturity level of the morphological unit* $E_{m,u}$ (Eq. 7.6):

$$E_{m,u_i} = \frac{V_{m,u_i}}{A_{u,i}} \quad (7.6)$$

in which V_{m,u_i} represents the average eroded volume for each morphological unit and $A_{u,i}$ is the relative areal extension.

Looking at the distribution of the $E_{m,u}$ index through five homogeneous class intervals with respect to the different morphological units (Figure 7.18), it is noticed that in the conservative morphological unit (ridge zone) the intensity of erosive processes is very low while in the flat zone and in the incision zone these processes are very intense.

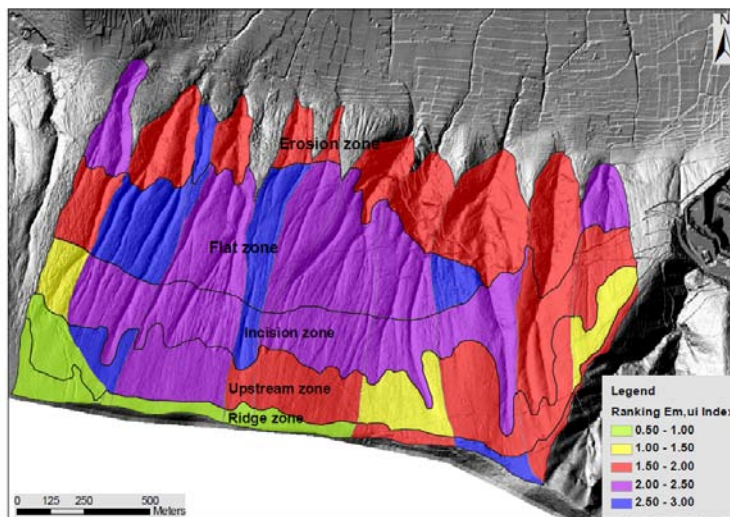


Figure 7.18 Ranking of $E_{m,ui}$ index.

A quantitative indication of the future evolution of erosion processes along the slopes can be derived from the analysis of the volumes of pyroclastic soils currently present in the test site. To this end, for each mountain catchment the volume of the lithotype B' - being the surface cover layer and more susceptible to the detachment phenomena - normalised to the areal extension of the mountain catchment was considered (E_e). The analysis of the spatial distribution of pyroclastic soil volume currently available in the test site (Table 7.5) shows that the mountain catchment B1 has a greater propensity for the development of future erosion processes.

Table 7.5 Residual pyroclastic soil volumes per unit area.

Catchment	E_r [m ³ /m ²]	Ranking
<i>B1</i>	<i>1.45</i>	<i>1</i>
<i>B2</i>	<i>0.51</i>	<i>9</i>
<i>B2A</i>	<i>0.60</i>	<i>8</i>
<i>B3</i>	<i>0.79</i>	<i>6</i>
<i>B4</i>	<i>0.88</i>	<i>3</i>
<i>B5</i>	<i>1.12</i>	<i>2</i>
<i>B6</i>	<i>0.82</i>	<i>4</i>
<i>B7</i>	<i>0.48</i>	<i>10</i>
<i>B8</i>	<i>0.36</i>	<i>11</i>
<i>B9</i>	<i>0.62</i>	<i>7</i>
<i>B10</i>	<i>0.79</i>	<i>5</i>

The analysis of the geomorphological evolution of the Monte Albino hillslope can be objectified by comparing the volumes of pyroclastic soil deposited in the active alluvial fan systems (Table 7.2) and the eroded volumes of pyroclastic soils in the mountain catchments. In this regard, the V_m Index (Eq. 7.7), given by the ratio between the volume of active alluvial fans pertaining to the examined mountain catchment V_{af} and the volume of eroded pyroclastic soil in each mountain catchment after the Ignimbrite Campana eruption $V_{m,i}$, was introduced.

$$V_m = \frac{V_{af}}{V_{m,i}} * 100 \quad (7.7)$$

The analysis of the V_m Index distribution along Monte Albino hillslope (Table 7.6) shows that only the 15% of the eroded pyroclastic soils are stored in the active debris-alluvial fans; probably a substantial rate could be deposited in ancient alluvial fans of the upper-middle Pleistocene, for which it is not available a reliable estimate of the volume. In addition, the eroded volumes not stored in the active alluvial fans of the Holocene period may have been partly re-eroded by the water runoff and transported in the floodplain. Moreover, it is worth noting that the B1 catchment, although has high values of pyroclastic soils thicknesses

inclined to future detachment phenomena, presents - together with the catchments B4, B5 and B10 - high values of V_m that indicate a recent activities of the erosive processes within the pyroclastic covers. Conversely, a lower percentage of V_m denotes an oldest activation of erosive processes (Middle-Upper Pleistocene) whose products have fuelled the ancient alluvial fans systems.

Table 7.6 V_m Index value.

Bacino	V_m %
<i>B1</i>	<i>24.2</i>
<i>B2 - B2A</i>	<i>5.5</i>
<i>B3</i>	<i>6.5</i>
<i>B4</i>	<i>35.0</i>
<i>B5</i>	<i>24.4</i>
<i>B6</i>	<i>14.1</i>
<i>B7</i>	<i>5.0</i>
<i>B8</i>	<i>6.3</i>
<i>B9</i>	<i>13.1</i>
<i>B10</i>	<i>76.0</i>
<i>Total</i>	<i>15.0</i>

The analysis and the comparison of the above mentioned morphological indices allows to draw important considerations about the evolution character of the Monte Albino hillslope (Table 7.7).

The mountain catchment B1 was characterised by a low erosion processes both in the limestone substrate ($E_s = 3.43 \text{ m}^3/\text{m}^2$) than in pyroclastic deposits ($E_m = 1.32 \text{ m}^3/\text{m}^2$); it has a high availability of pyroclastic deposit that predispose the triggering of future erosion processes, which seem to be already quite active ($V_m=24.2 \%$).

Conversely, the mountain catchments B2 and B2A were affected by intense erosion processes both in the carbonate bedrock ($E_s = 3.18 \div 3.61 \text{ m}^3/\text{m}^2$) than in pyroclastic deposits ($E_m = 2.23 \div 2.41 \text{ m}^3/\text{m}^2$) resulting in poor availability of pyroclastic deposit to future erosion processes, which therefore were mainly developed in the past ($V_m = 5.5 \%$).

The mountain catchment B3 basin was characterised by low erosive processes in the limestone substrate ($E_s = 3.23 \text{ m}^3/\text{m}^2$) and intense erosive processes in pyroclastic deposits ($E_m = 2.04 \text{ m}^3/\text{m}^2$) resulting in a non-high availability of pyroclastic deposit to future erosion processes, which therefore were mainly developed in the past ($V_m = 6.5 \%$).

Table 7.7 Comparison of morphological indices at the mountain catchment scale.

Mountain Catchment	Area	E_s	E_m	E_r	V_m
<i>ID</i>	<i>m²</i>	<i>m³/m²</i>	<i>m³/m²</i>	<i>m³/m²</i>	<i>%</i>
<i>B1</i>	<i>259.207</i>	<i>3.43</i>	<i>1.32</i>	<i>1.45</i>	<i>24.2</i>
<i>B2</i>	<i>278.112</i>	<i>3.18</i>	<i>2.23</i>	<i>0.51</i>	<i>5.5</i>
<i>B2A</i>	<i>29.965</i>	<i>3.61</i>	<i>2.41</i>	<i>0.60</i>	
<i>B3</i>	<i>339.142</i>	<i>3.32</i>	<i>2.04</i>	<i>0.79</i>	<i>6.5</i>
<i>B4</i>	<i>137.662</i>	<i>3.37</i>	<i>2.06</i>	<i>0.88</i>	<i>35.0</i>
<i>B5</i>	<i>82.527</i>	<i>3.67</i>	<i>2.07</i>	<i>1.12</i>	<i>24.4</i>
<i>B6</i>	<i>360.897</i>	<i>3.39</i>	<i>1.92</i>	<i>0.82</i>	<i>14.1</i>
<i>B7</i>	<i>297.797</i>	<i>3.13</i>	<i>1.81</i>	<i>0.48</i>	<i>5.0</i>
<i>B8</i>	<i>367.441</i>	<i>2.90</i>	<i>1.81</i>	<i>0.36</i>	<i>6.3</i>
<i>B9</i>	<i>223.644</i>	<i>2.61</i>	<i>1.53</i>	<i>0.62</i>	<i>13.1</i>
<i>B10</i>	<i>142.562</i>	<i>3.14</i>	<i>1.71</i>	<i>0.79</i>	<i>76.0</i>
<i>Tot.</i>	<i>2.518.956</i>	<i>3.19</i>	<i>1.85</i>	<i>0.73</i>	<i>15.0</i>

The mountain catchments B4, B5 and B6 have similar characteristics to B2 with reference to erosion processes ($E_s = 3.37 \div 3.67 \text{ m}^3/\text{m}^2$, $E_m = 1.92 \div 2.07 \text{ m}^3/\text{m}^2$), even if they differ in a greater amount of pyroclastic soil covers (in particular the catchment B5) and in high values of V_m (varying between 14% and 35%) indicating a recent increase activity of erosion processes in pyroclastic covers. Lastly, the mountain catchments

B7, B8, B9 and B10 were characterised by intense erosion processes in the carbonate bedrock ($E_s=2.61 \div 3.14\text{m}^3/\text{m}^2$) that become smaller in pyroclastic deposits ($E_m=1.53 \div 1.81\text{m}^3/\text{m}^2$), resulting in a moderate availability of pyroclastic deposits to future erosion processes, which therefore were mainly developed in the past ($V_m=5.0 \div 13.1\%$) except for the catchment B10, where there is a high availability of pyroclastic soil and a high value of V_m ($> 75\%$), indicating a very recent erosive activity on the slope.

7.7 GENERAL FEATURES OF THE PREVAILING SLOPE INSTABILITIES

The results of both in situ surveys, historical and geomorphological analyses show that Monte Albino hillslope can be affected by several types of instability phenomena that differ in triggering mechanism, mobility (in terms of maximum travel distances) and intensity.

Before discussing about them, it must be observed that also flooding phenomena, associated to rainfall not involving soil in place, can be happen. However, it is worth to note that, due to the intense anthropic and agricultural use of the land as well as the scarcity of the channel-cleaning, the triggering rainfall is not always to be tied to an exceptional event; therefore, the frequency of flooding occurrence is very high. The associated consequences mainly consist of troubles for people living in the exposed areas; the level of risk associated with these phenomena, based on the current regulations (D.P.C.M. - Presidential Decree of the Councils of Ministers - of 29/09/1998), can be considered equal to R1-low - R2 or - moderate.

Whereas the volumes of water in motion are able to erode the solid material along their path, or to sustain material present along the longitudinal development of the river basins, hyperconcentrated flows (Coussot and Meunier, 1996) can occur.

In the case study at hand, the transported material can result from: *i*) erosion along the gullies, *ii*) erosion along the lateral banks of the gullies, *iii*) instability phenomena along the channel's sides that are triggered by the above-mentioned erosion phenomena. They are often generated by rainfall events of high intensity and short duration; in particular, as already evidenced, the occurrence of this kind of flow-like phenomenon

mainly concentrates in the autumn months, when the high values of soil suction predispose the superficial soils to erosion processes and, locally, to shallow first-time landslides (Cascini et al., 2013 a).

As for the expected consequences in the urban area of Nocera Inferiore, it can be observed that these phenomena usually involve high-risk situations for properties and low risk for the safety of people so that at risk areas can be classified, on the basis of the current regulations (D.P.C.M. 29.09.1998), as R3 (high risk) or R4 (very high risk).

Another type of potential flow-like phenomena is represented by the debris flows that differ from previous hyperconcentrated flows for the features of the initiation processes as well as for higher volumetric concentration of sediment (Coussot and Meunier, 1996).

These phenomena could be triggered in morphological zones over the Monte Albino hillslope through two main mechanisms labelled as M1 and M5 (Cascini et al., 2008 a). In detail, the trigger mechanism M1 (Cascini et al., 2008 a) can happen in colluvial hollows associated to Zero Order Basins (ZOB) affected by convergent sub-superficial groundwater circulation inside the pyroclastic deposits and by temporary springs from the bedrock. The mechanism M5 (Cascini et al., 2008 a) is typical of convex longitudinal profiles and it can be related to the presence of deep natural or anthropogenic gullies inside the pyroclastic deposits; these source areas are characterised by rectilinear planforms with a concave transversal profile and located along the maximum slope directions.

The debris flows, generated by high values of cumulative rainfall over the whole event, can mobilise large volumes of materials in a very short time frame. The expected huge consequences define a very high (R4) level of risk for both people and properties (D.P.C.M. 29/09/1998) as well as sadly highlighted by the routinely events that occur in the Campania Region.

Finally, landslides that may involve the lateral banks of the watersheds or that can be triggered on the open slopes can be mentioned.

The first ones can be essentially associated to the availability of solid material along the longitudinal development of the basins, so increasing the probability of occurrence hyperconcentrated flows; in particular conditions they could led to “dam break” phenomena, that consist on the obstruction of the river basin resulting in water accumulation and subsequent evolution of the flow toward downstream.

The first-time landslides on open slopes are, compared to previous ones, more dangerous for different reasons among which the involvement of

relevant volumes of soil, the possibility of propagation as debris avalanche (Cascini et al., 2013 a) and the presence, in a short distance from the foot of the slopes, of buildings for civil use (R4 - very high risk-D.P.CM. 29/09/1998). They are usually generated by rainfall with a long duration and low intensity, typically observed in the winter period, and develop - according to the triggering mechanism M2 (Cascini et al., 2008 a) - on open steep slopes ($> 30^\circ$) characterised by the presence of anthropogenic/natural discontinuities in pyroclastic soils (i.e. presence of trails/roads or outcrops of the bedrock). During the triggering phase, the first-time failures occur up to these discontinuities due to the effects of rainwater, so involving small volumes of soil; thereafter, the unstable masses are spread down at high velocity and, due to the impact and/or removal of additional debris effect, they can markedly increase their volume along the path. The described phenomena assume the typical pseudo-triangular shape with the apex pointing upwards. A typical example of this landslide is represented by the event happened on the Monte Albino in March 2005 when three people died (Figure 7.19).



Figure 7.19 Frontal view of the landslide occurred on March 2005.

8 GEOTECHNICAL MODEL AND HAZARD ANALYSIS AT SITE-SPECIFIC SCALE

The characterisation of the geological context where flow-like phenomena are likely to occur certainly represents the first fundamental step to carry out analyses aimed at quantifying - at site-specific scale - the risk to life posed by them.

As far the case study at hand is concerned, the performed geological analyses and geotechnical in-situ/laboratory tests allow the identification of the relevant (predisposing) factors (i.e., lithology, thickness of pyroclastic soil and their spatial distribution, physical and mechanical properties of soils) to be considered as input data in modelling - via advanced procedures - the hyperconcentrated flows originating over Monte Albino hillslope.

In this chapter, the main results of the hazard analysis of hyperconcentrated flows at site-specific scale are described. The performed analysis includes the description of the extent of the triggering areas and their mechanisms, the analysis of the frequency occurrence and the modelling of the propagation stage.

8.1 SUSCEPTIBILITY ANALYSIS

The analysis of the hyperconcentrated flow susceptibility can be considered the initial step towards a hazard and risk analysis, at site-specific scale, since it may be aimed at orienting and supporting the numerical modelling of the triggering stage. Indeed, the susceptibility analysis identifies the location of the potential triggering areas of hyperconcentrated flows (based on a combination of geological, topographical and soil-cover distribution) and their spatial extension. Considering that the occurrence of future hyperconcentrated flows can be caused by erosion of the streambed and/or instabilities of the channel's sides along the gullies, the susceptibility analysis was performed through the use of an heuristic procedure (basic method) that allowed a

classification of the stream channels taking into account of the combined role played by two predisposing factors, namely the slope angle (in degrees) of the channel's sides along the maximum slope line and the thickness (in meters) of the soil cover belonging to the B' lithotype (see Section 6.5). To this aim, four classes of slope angle and soil thickness (which is added the class of no soil cover) were introduced, on the basis of their quartiles distribution in the area delimited by the watershed of each channel. The combination of these factors (Table 8.1) allowed, therefore, the estimation of the susceptibility to erosion phenomena and to local instability of the channel's sides on the basis of four classes (VL = very low, L = low, M = medium, H = high).

Table 8.1 Susceptibility matrix for the triggering of hyperconcentrated flows.

SUSCEPTIBILITY		COVER THICKNESS ALONG STREAMBED				
		0 m	0,1-0,5 m	0,5-1,5 m	1,5-2,5 m	> 2,5 m
SLOPE ANGLE OF CHANNEL'S SIDE	< 25°	VL	VL	L	M	M
	25° - 30°	VL	L	L	M	M
	30° - 35°	VL	M	M	H	H
	> 35°	VL	M	M	H	H

The results of the analysis were reported in a susceptibility zoning map (Figure 8.1); the portions of the slope with the highest level of susceptibility were located in the western part which appears morphologically less developed with a typical trend of the cross section of the channel shaped like a "U" (see Section 7.3). It is worth noting that the obtained susceptibility levels do not have an absolute meaning, but rather should be understood as relative terms.

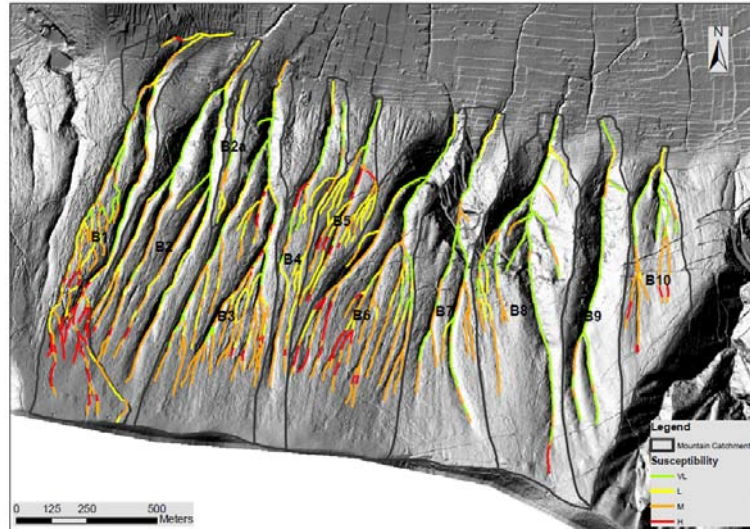


Figure 8.1 Susceptibility map of triggering area of hyperconcentrated flows.

8.2 THE FREQUENCY ANALYSIS

The temporal occurrence of hyperconcentrated flows can be expressed in terms of frequency that is a measure of likelihood expressed as the number of occurrences of an event in a given time (Fell et al., 2008). It can be evaluated through the analysis of incident data dealing with past events; in such a case, hyperconcentrated flows can be considered as recurrent events that occur randomly and independently (Corominas et al., 2013).

When complete catalogues of incident data covering a long time span are available, two probability distributions can be used to assess the annual probability of occurrence: the binomial distribution and the Poisson distribution (Corominas and Moya, 2008). In particular, the binomial distribution can be applied considering discrete time intervals and only one observation for interval (usually a year). Accordingly, the annual probability of a landslide event of a given magnitude which occurs on average one time each T years is:

$$P_{(N=1;t=1)} = \frac{1}{T} = P_{(HF)} \quad (8.1)$$

where T is the return period of the event and $P_{(HF)}$ the expected frequency for future occurrences.

In the case study at hand, the results of the historical analysis (see Section 6.7.1) lead to some considerations about the return period of the hyperconcentrated flows (Figure 8.2). In particular, with reference to the time period $\Delta T1$ spanning from 1707 to 1846 ($\Delta T1 = 140$ years), the average return period $T1$ of the censored events – mainly related to washing processes – equals 16.6 years (140 years/9 events). If the $\Delta T2$ time period (from 1846 up to now) is considered, owing to the reduced recurrence of strombolian eruptions of the Vesuvius volcano, the average return period $T2$ of the hyperconcentrated flows is greater than $T1$.

Moreover, since their occurrence is related to erosion rather than washing, $T2$ could equal the return period $T3$ of the triggering rainfall events.

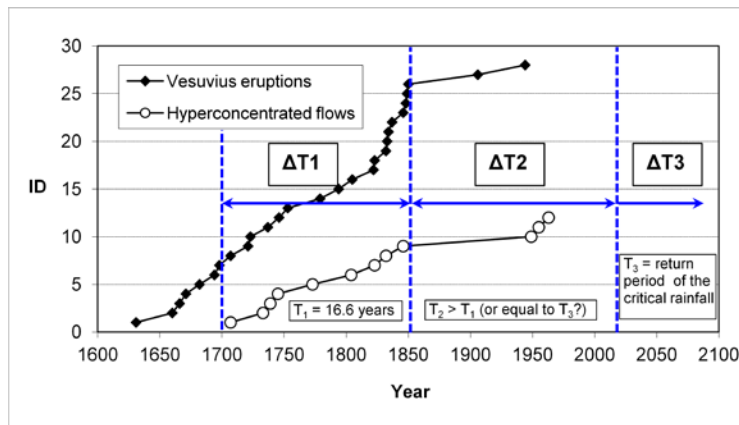


Figure 8.2 Cumulative distributions of hyperconcentrated flow events and Vesuvius explosive eruptions.

Taking into account the low annual probability that, according to De Natale et al. (2006) can be associated with the occurrence of air-fall pyroclastic deposits, future hyperconcentrated flows will be characterised by an average return period equal to $T3$, being their occurrence mainly related to huge erosive processes and localised instabilities along the gullies.

In order to determine T_3 , the results of the hydrologic analysis carried out by De Luca (2013) with reference to critical rainfalls that triggered hyperconcentrated flows in the Campania region on 20th century were considered. In particular, on the basis of the probabilistic coefficient of growth for a given return period K_T – defined as the ratio between the maximum annual value of the daily rainfall in the i -th stations for the j -th year ($MP_{gg,i,j}$) and the sampling average value rainfall of annual maximum daily rainfall in the i -th station ($mMP_{gg,i}$) (De Luca, 2013) – the Author provides the return periods T of the above critical rainfalls. In Table 8.2, relevant data on critical rainfalls associated to the triggering of hyperconcentrated flows over Monte Albino hillslope are summarised.

Table 8.2 Main data on the critical rainfalls that triggered hyperconcentrated flows over Monte Albino hillslope.

<i>Hyperconcentrated flows events (date of occurrence)</i>	<i>Duration [h]</i>	<i>Return Period [years]</i>
02/10/1949	12	50
12/09/1955	24	200
26/09/1963	12	100

8.3 MODELLING THE TRIGGERING MECHANISMS

The hazard analysis of the triggering of hyperconcentrated flows was carried out by considering, separately, the contribution of the mobilised soil volumes provided by both surface erosion and instability of the channel's sides. To this aim, three different return periods T (50, 100 and 200 years) of rainfall as triggering causes were considered according to the results of the hydrological analysis discussed in Section 8.2 (see also Table 8.2).

In order to determine the intensity (I) and the duration (d) of the rainfall to be associated to each of the three considered return periods, the pluviometric probabilities curves for Monte Albino test site were generated on the basis of the regionalisation criterion provided by Rossi and Villani (1995). The obtained curves are synthetically plotted in the bi-logarithmic plane shown in Figure 8.3.

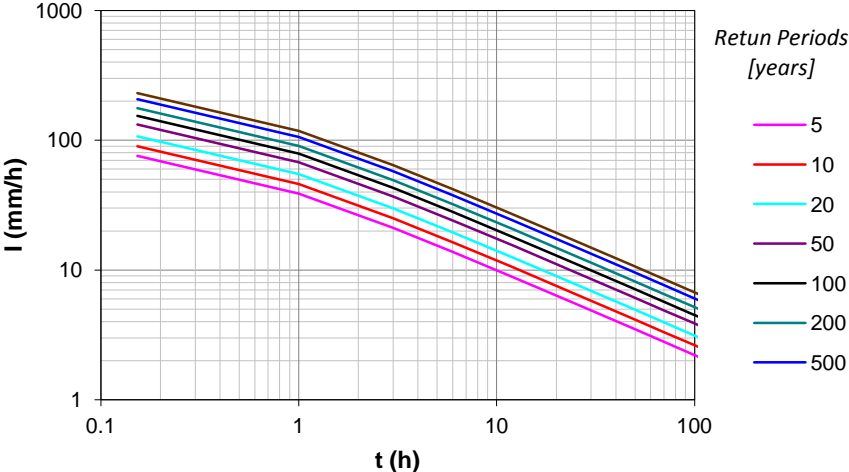


Figure 8.3 Pluviometric probabilistic curves for the Monte Albino test site.

Assuming that the rainfall duration equals 12 hours, according to the information dealing with the critical rainfalls recorded in the 20th century (Table 8.2), it was possible to derive the maximum cumulative height of rain corresponding to each of the considered return period (Table 8.3).

Table 8.3 Rainfall characteristics for Monte Albino test site.

<i>Return Period</i> <i>[years]</i>	<i>Duration</i> <i>[h]</i>	<i>Cumulative</i> <i>Rainfall</i> <i>[mm]</i>
50	12	186.14
200	12	216.40
100	12	248.50

8.3.1 Modelling of surface erosion phenomena: The LISEM MODEL

Soil erosion is defined as a progress of detachment and transportation of soil particles caused by an erosive agent (Ellison, 1947). In humid temperate climates erosion due to rain is the most common. The erosion process is activated by shear stress exercised, on the surface of the soil, from the raindrops impact and from the flowing generated by water runoff. The basic natural factors, which create the soil erosion by water, are rainfall, the type of soil, the geomorphology of area (Park et al., 1982), vegetation cover and use of land.

Water erosion can be considered the main physical process able to generate the triggering of hyperconcentrated flows.

The erosive processes are differentiated in relation to the spatial context in which they occur (Bagarello and Ferro, 2006). The erosion that occurs in the portions of the surface occupied by the grooves, takes the name of rill erosion. The areas between the grooves are called interrill areas and the erosion that occurs in them takes the name of interrill erosion. Altogether rill and interrill areas define the portion of the surface affected by overland flow and diffused or areal erosion. Within interrill areas, the detachment processes take place exclusively due to the impact of raindrops; transport is operated by overland flow. In the rills, however, the detachment and transport processes are only attributable to the runoff that moves in the form of a channelled flow.

In the portion of the surface area occupied by channels and, therefore, affected by linear erosion, it is usual to distinguish between gully erosion and channel erosion (Bagarello and Ferro, 2006).

The whole shallow erosion process involves, from a physical point of view, different stages of evolution. The first stage of the erosion process is constituted by the splash erosion. It occurs when raindrops hit bare soil. The detachment of soil particles by raindrop impact and their removal downslope by overland water flowing as a sheet represents the sheet erosion. A more or less uniform layer of fine particles is removed from the entire surface of an area, sometimes resulting in an extensive loss of rich topsoil. When sheet flows begin to concentrate on the land surface, rill erosion occurs. This type of erosion occurs when the duration or intensity of rain increases and runoff volumes accelerate. As detachment continues or flow increases, rills will become wider and deeper. Rill erosion evolves into gully erosion when the duration or the

intensity of rain continues to increase and runoff volumes continue to accelerate. Stream bed erosion occurs when the flow bares the toe of the channel, making it deeper. Stream bed erosion occurs as flows cut into the bottom of the channel, making it deeper. As the stream bed erodes, and the channel deepens, the sides of the channel become unstable and slough off; resulting in stream bank erosion.

In the areas affected by erosion phenomena it is necessary, in order to identify the possible management strategies required by the planning agencies and policy makers, to have quantitative information about soil erosion rates. At the basin scale, due to the extreme spatial and temporal variability as well as the considerable complexity of erosion processes, it is necessary to have a physical model able to describe the individual sub-processes that control, for a given rainfall input, the drainage basin response in terms of volume or sediment weight that crosses the outlet of the drainage catchment. In this regard, there are several catchment scale erosion models that simulated both the hydrology and soil erosion processes: CREAMS (Knisel, 1980), ANSWERS (Beasley et al., 1980), AGNPS (Young et al., 1989), KINEROS (Smith, 1981; Woolhiser et al., 1990), EUROSEM (Morgan et al., 1992; Morgan, 1994), WEPP (Lane et al., 1992), EROSION3D (Schmidt et al., 1999), LISEM (De Roo et al., 1996 a). In all models, different approximations to reality are made. No model is completely comprehensive.

In this Thesis, the evaluation of the eroded material volume after a rainfall event, within each of the ten drainage catchment belonging to the Monte Albino test site, was carried out by the use of the Limburg Soil Erosion Model (LISEM) (De Roo et al., 1996 a, b). It is a physically-based hydrologic and soil erosion model operating at the catchment scale, completely integrated into a GIS, in which all spatial input and output data are in the form of raster maps. The model - receiving as input the pluviogram as well as information relating to topography, use of land, physical and mechanical properties of erodible soils - gives both the weight of eroded/deposited material and the flood hydrograph at the outlet section of the mountain catchment with the relative volume concentrations of solid material transported by the flow. The model incorporates the process of interception, surface storage in micro depressions, infiltration, vertical movement of water in the soil, overland flow, channel flow, detachment by rainfall and throughfall, detachment by overland flow and channel flow, and deposition on overland flow planes and in channels (De Roo and Jetten, 1999). Also, the influence of

tractor wheels and small paved roads on the hydrological and soil erosion processes is taken into account. The infiltration and vertical movement of water in the soil can be simulated in several ways: *i*) SWATRE model (Belmans et al., 1983); *ii*) Green- Ampt infiltration equation (Green and Ampt, 1911; Li, 1979); *iii*) Holtan infiltration equation (Holtan, 1961; Overton, 1965). Surface storage depression processes are simulated by a set of equations developed by Onstad (1984) and Linden et al. (1988), using the concept of random roughness as a measure of micro topography. Overland flow and channel flow are routed independently using four-point finite-difference solution of the kinematic wave together with Manning's equation (Chow et al., 1988; Moore and Foster, 1990). A flowchart of LISEM is presented in Figure 8.4.

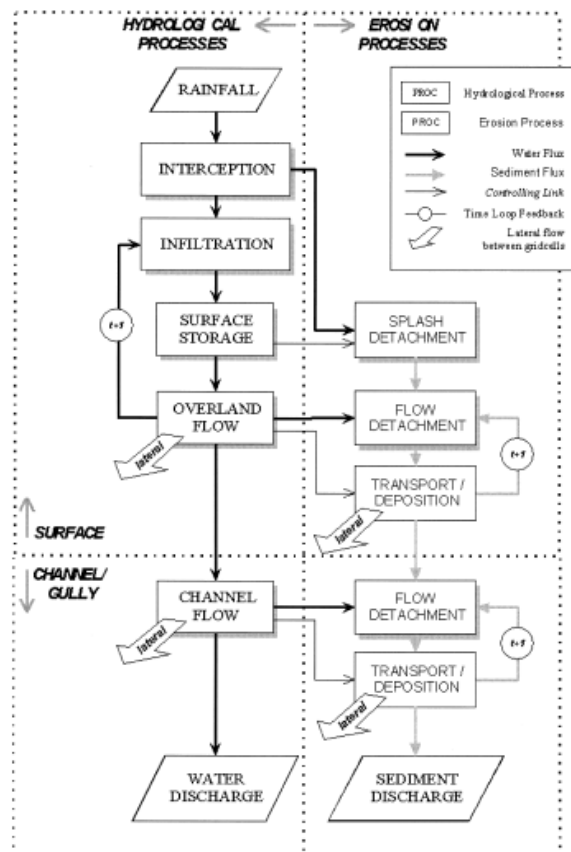


Figure 8.4 Flowchart of the LISEM model (from De Roo and Jetten, 1999).

Many of the sediment and erosion equations in LISEM are derived from the EUROSEM model (Morgan et al., 1992; Morgan, 1994) in which it is assumed that the transport capacity concentration of the runoff reflects a balance between the continuous counteracting processes of erosion and deposition (Jetten, 2002). Erosion is sum of splash detachment by rain drops (D_s), and flow detachment by runoff (D_f). The amount of sediment in suspension (e) is then calculated as the following formula (Eq. 8.2):

$$e = D_s + D_f - D_p \quad (8.2)$$

Splash detachment D_s is simulated as a function of soil aggregate stability, rainfall kinetic energy and the depth of the surface water layer. This sub-model is calibrated by field experiments. The kinetic energy can arise from both direct through-fall and drainage from leaves. Using splash tests the following general equation (Eq. 8.3) has been derived (De Roo et al., 1996 a):

$$D_s = \left[\frac{2.82}{A_s} \cdot K_e \cdot \exp^{-1.48 \cdot h} + 2.96 \right] \cdot (P - I) \cdot \frac{dx^2}{dt} \quad (8.3)$$

in which D_s is the splash detachment (g/s), A_s is the soil aggregate stability (median number of drops to decrease the aggregate by 50%), K_e is the rainfall kinetic energy (J/m²), h is the depth of the surface water layer (mm), P is the rainfall (mm), I is the interception (mm), dx is the size of an element (m) and dt is the time increment.

The ability of flowing water to erode its bed is assumed only as function of the energy expended by the flow. The total energy of flow available for the triggering of erosion phenomena is shared between the detachment and transport processes. This distribution is closely related to the value assumed by the transport capacity of overland flow (Govers, 1990), that is modelled as a function of unit stream power (Eq. 8.4):

$$Tc = C \cdot l \cdot [S \cdot V - 0.4]^{Dl} \quad (8.4)$$

where Tc is equal to the volumetric transport capacity (cm³/cm³); S is the slope gradient (m/m); V is the mean flow velocity (cm/s); C , D and l are empirically derived coefficients that depend on the $D50$ of the upper soil

layers (Govers, 1990). For fixed value of slope angle and flow velocity, the weight of the material that can be transported, in the time unit and per width unit of the flow, is reduced with the increase of the size of transported particles.

If the amount of the transported sediments is equal to the transport capacity, the detachment is void because the totality of the available energy of the flow is employed in the transport processes.

In other words, when the flow has a solid load different from zero but less than the transport capacity, the detachment operated by the flow is equal to the difference between the transport capacity and the effective instantaneous load. Whenever the flow has an effective solid load greater to the transport capacity, deposit phenomena occur.

The equation for soil detachment by flow and deposition during flow, expressed in terms of settling velocity and transport capacity (Eq. 8.5), then becomes (De Roo et al., 1996 a; Jetten 2002):

$$D = Y \cdot (Tc - C) \cdot V_s \cdot w \cdot dx \quad (8.5)$$

in which D (kg/s) is the detachment rate, Tc is the transport capacity of the flow (kg/m^3), C is the sediment concentration in the flow (kg/m^3), V_s is the settling velocity of the particles (m/s), w is the width of the flow (m) and Y is a dimensionless efficiency factor. The latter takes into account that the detachment will be limited by the cohesion of the soil material. The pick-up rate for cohesive soil therefore needs to be reduced by a coefficient whenever C is less than Tc . By definition, for Y equal to 1 deposition takes place, i.e. when C is larger than Tc , and when erosion takes place it is calculated as (Eq. 8.6) (Rauws and Govers, 1988):

$$Y = \frac{u_{min}}{u_c} = \frac{1}{0.89 + 0.56 \cdot Coh} \quad (8.6)$$

in which u_{min} is the minimum value required for critical grain shear velocity (cm/s); u_c is the critical grain shear velocity for rill initiation (cm/s); and Coh is the cohesion of the soil at saturation (kPa).

8.3.2 Modelling of surface erosion phenomena: The input parameters

The use of the LISEM model to Monte Albino hillslope allowed the achievement of two main goals: first, the definition of design rainfall event on which to focus all the analysis aimed at quantifying the risk of loss of life posed by hyperconcentrated flows and, secondly, the characterisation of erosion phenomena.

With reference to the rainfall event, once both the duration and intensity of the rainfall associated to a given return period are fixed (Table 8.3), different pluviometric distribution scenarios – having a constant value of the cumulative rainfall – were hypothesised (Figure 8.5).

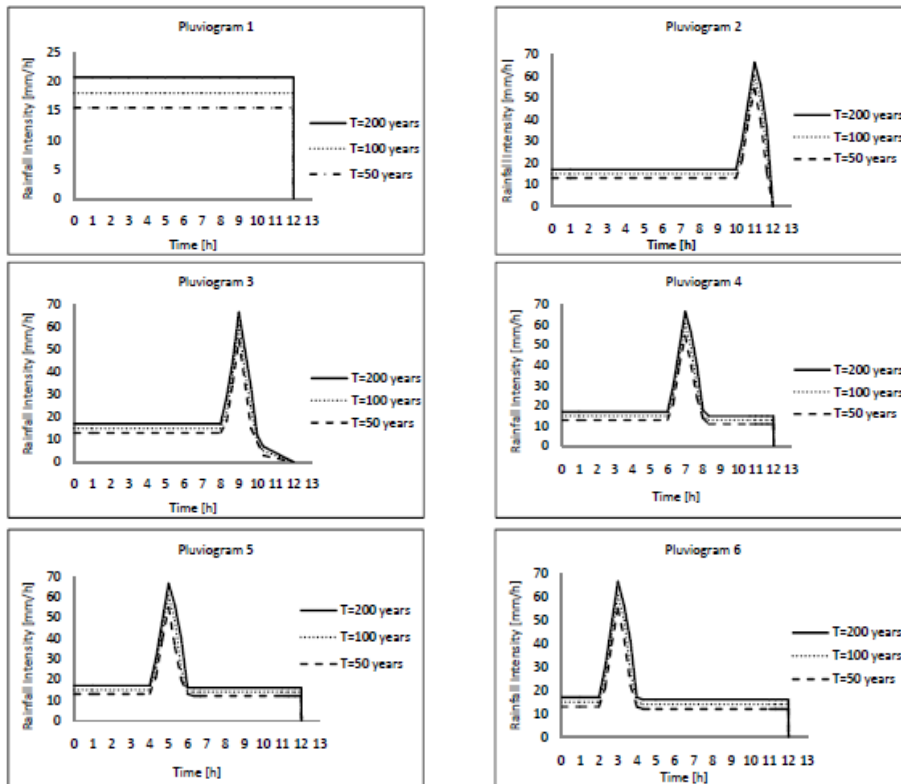


Figure 8.5 Different scenarios of rainfall event.

The design pluviograms, for each return period, were generated considering either a constant rainfall intensity for the whole event (fixed to 12 hours) or a surge of rain lasting two hours - typical duration of rain causing the triggering of hyperconcentrated flows - according with that observed by Bovolin (2012) in a geological context similar to that of Nocera Inferiore. The design pluviograms were considered homogeneous over the Monte Albino hillslope.

For the test site at the hand, information related to topography, physical and mechanical properties of the pyroclastic soils and use of land data were available. In particular, topographical information (local drain direction, slope gradient, location of permanent channels, catchment boundaries) were derived from the available digital elevation model (DEM) at 1:1,000 scale. Information related to the soil distribution on the slope were derived from the corresponding distribution map of pyroclastic soil thickness (see Section 6.6.1). The slope was assumed as homogeneous with respect to the soil lithotype distribution; the implemented analysis, in fact, focused on the layer of pyroclastic soil belonging to the class B' since, due own physical and mechanical properties, it has the highest proneness to erosion. The land use data were achieved from the Agricultural Use of Soils in Campania region (CUAS-2009) at 1:50,000 scale (sit.regione.campania.it). Along the Monte albino slope 4 land units were identified: *i*) orchards and small fruit unit (11.7 %); *ii*) Broad-leaved forest units (87 %); *iii*) sclerophyllous vegetation units (0.03 %); *iiii*) urbanised units (0.1 %). The soil surface and the land use-related variables such as Manning's *n*-values (*n*), Leaf area index (*LAI*), Random Roughness (*RR*), were estimated using tables available in literature (Chow, 1959; Napolitano et al., 2006; Renard et al., 1997); while the fraction of soil covered by vegetation (*PER*) and vegetation height (*CH*) were deduced from field observations in combination with the guidelines of the LISEM manual (Jetten, 2002).

Among different infiltration models available in the LISEM, the Green and Ampt model (Green and Ampt, 1911) was adopted in this study. It requires – as input – the saturated hydraulic conductivity (K_{sat}), initial and saturated volumetric water contents and the initial suction at wetting front, for each defined land unit. Since pyroclastic soil covers of the Monte Albino slope were assumed as belonging to the class B' only, one set of hydrological variables were considered for the analysis purposes. In particular, the initial soil suction was posed equal to 10 kPa, in

agreement with the suction values in-situ detected in the autumn months. The initial (θ_i) and the saturated (θ_s) volumetric water contents (Figure 8.6) were derived from the characteristics curves of pyroclastic soils having the same physical and mechanical characteristics of those investigated (Sorbino and Foresta, 2002; Bilotta et al., 2005) and belonging to the geological context A1 (see Section 5.1).

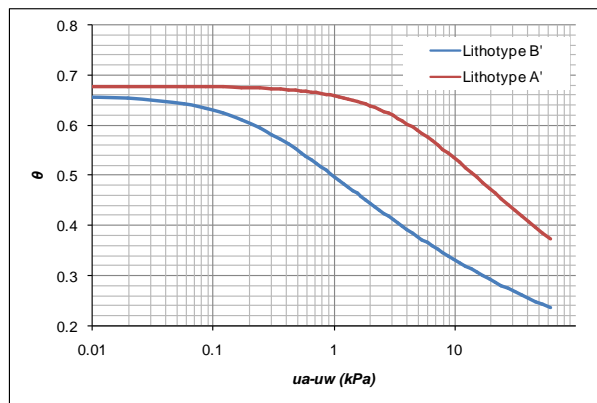


Figure 8.6 The adopted soil-water retention relationships (adapted from Bilotta et al., 2005).

In order to take into account, within the simplified Green and Ampt model, the hydraulic behaviour of the “real” pyroclastic soil cover constituted by two layer of soils (classes A’ and B’), a calibration analysis of k_{sat} value was carried out. To this aim, the k_{sat} values of pyroclastic soils having the same size distribution and mechanical properties of those of Monte Albino were firstly fixed on the basis of information gathered from results of tests carried out in the Laboratory of Geotechnics of University of Salerno (Sorbino and Foresta, 2012); in particular, these k_{sat} values equal $1 \cdot 10^{-7}$ m/s for B’ lithotype and $7 \cdot 10^{-8}$ m/s for A’ lithotype.

In order to assess the equivalent value of k_{sat} of the lithotype B’, representing the hydraulic response of a pyroclastic soil layer constituted by two lithotypes A’ and B’, a numerical analysis of infiltration rate was performed. To this aim, two computational slope sections were built: the first one is constituted of pyroclastic soils belonging to class B’; the second one includes both lithotypes (A’ and B’) (Figure 8.7). The numerical integration of the Richard's equation (Richards, 1931), via the use of the numerical code SEEP/W (GeoSlope, 2005) implementing a

finite element method, allowed the estimation of unit discharge of water (q_i , $i = D, E$ or D', E') through the unsaturated soil (Richards, 1931; Childs and Collins-George, 1950) in two control sections. In particular, these results refer to the end of a rainfall of fixed intensity and duration, wherein the initial conditions – in terms of soil suction values – are posed equal to 10 kPa.

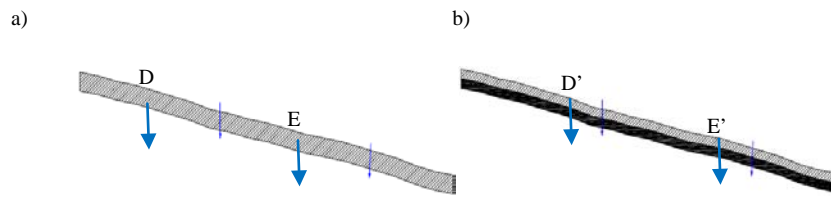


Figure 8.7 Computational slope section constituted of a) pyroclastic soils belonging to class B' and b) pyroclastic soils belonging both lithotypes (A' and B').

By varying the k_{sat} value for the section constituted by lithotype B' only (Figure 8.7 a), the condition for which $q_D = q_{D'}$ and $q_E = q_{E'}$ defines the pursued value of k_{sat} ; in particular, $k_{sat} = 5 \cdot 10^{-7}$ m/s.

Once the spatial input data - consisting in raster maps with topography information, land use- related variables, soil surface-related variables, soil hydrological-related variables - are defined (as briefly summarised in Table 8.4), it was possible to quantify the cumulative infiltration at the end of the rainfall event, the runoff fraction, the total erosion (sum of splash and flow detachment) and the total deposition. Non-spatial output consists of the total water and sediment discharge at the outlet of each catchment of the Monte Albino hillslope.

Table 8.4 Input parameter values of LISEM for the different types of use of land.

<i>Land unit</i>	<i>ksat</i> [m/s]	<i>Suction</i> [kPa]	<i>θi</i> [-]	<i>θs</i> [-]	<i>RR</i> [cm]	<i>n</i> [-]	<i>PER</i> [-]	<i>CH</i> [m]	<i>LAI</i> [-]
<i>Orchards and small fruit</i>	$5 \cdot 10^{-7}$	10	0.33	0.66	0.60	0.04	0.70	3	2.05
<i>Broad-leaved forest</i>	$5 \cdot 10^{-7}$	10	0.33	0.66	0.60	0.04	0.90	10	2.05
<i>Sclerophyllous vegetation</i>	$5 \cdot 10^{-7}$	10	0.33	0.66	0.60	0.04	0.90	10	2.05
<i>Urbanised unit</i>	$5 \cdot 10^{-7}$	10	0.33	0.66	0.60	0.02	0.0	0.0	2.05

The performed erosion analysis, with reference to the different considered scenarios of rainfall events (Figure 8.5), revealed that – independently from the chosen return period T of the triggering rainfall – the highest values of soil loss volume (after deducting deposition rate) was recorded for the pluviogram 2 (Figure 8.8). Moreover, this pluviogram, which exhibits a surge lasts two hours at the end of the rainfall event, maximises the total water discharge that flows at the outlet of each mountain catchment.

Therefore, in order to estimate the expected consequences - in terms of loss of life - as a result of the occurrence of hyperconcentrated flows it is reasonable to perform the QRA with reference to the most destructive scenario (namely, that corresponding to the pluviogram 2).

The estimation of the erosion rate, through the use of the physically-based model LISEM with reference to the design rainfall event, allows to highlight that erosion phenomena are able to generate hyperconcentrated flows because, for each of the considered return periods in all mountain catchments - with the exception of the B7- the achieved volumetric concentrations of sediment (Table 8.5) are equal or are very close to those characterising hyperconcentrated flows, i.e. $C_v = 20 \div 47$ % (Costa, 1988).

Table 8.5 Sediment concentration by volume and soil loss volume at the outlet of mountain catchments for different return period T .

	<i>T=200 years</i>	<i>T=100 years</i>	<i>T=50 years</i>	<i>T=200 years</i>	<i>T=100 years</i>	<i>T=50 years</i>
	<i>C_{v,max} [%]</i>	<i>C_{v,max} [%]</i>	<i>C_{v,max} [%]</i>	<i>V_{soil loss} [m³]</i>	<i>V_{soil loss} [m³]</i>	<i>V_{soil loss} [m³]</i>
B1	23	22	22	8304	6274	4550
B2	20	20	20	9222	7132	5216
B2a	22	22	21	944	713	517
B3	24	24	24	15058	11783	8754
B4	19	19	18	3311	2479	1787
B5	19	19	18	2033	1534	1113
B6	21	21	20	9598	7147	5128
B7	14	13	13	2080	2944	4042
B8	24	24	24	16517	12907	9570
B9	19	19	19	6932	5311	3795
B10	24	25	27	6750	5330	4019

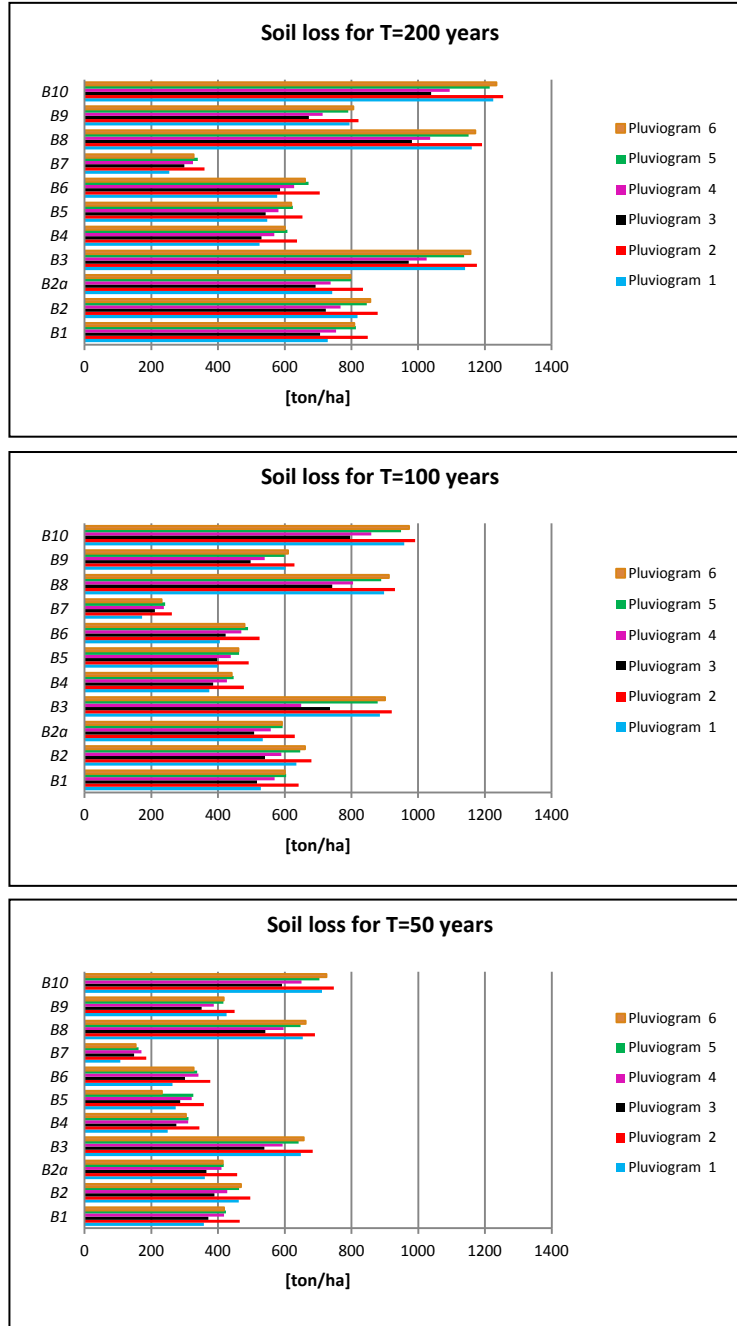


Figure 8.8 Soil loss volume value per unit area for different rainfall scenario.

Obviously, the definition of the mixture (water + sediment) hydrographs at the outlet of catchments together with the relative volumetric concentrations of solid material in the flowing mixture (an example is shown in Figure 8.9), was an essential prerequisite for a proper definition of the hazard scenarios.

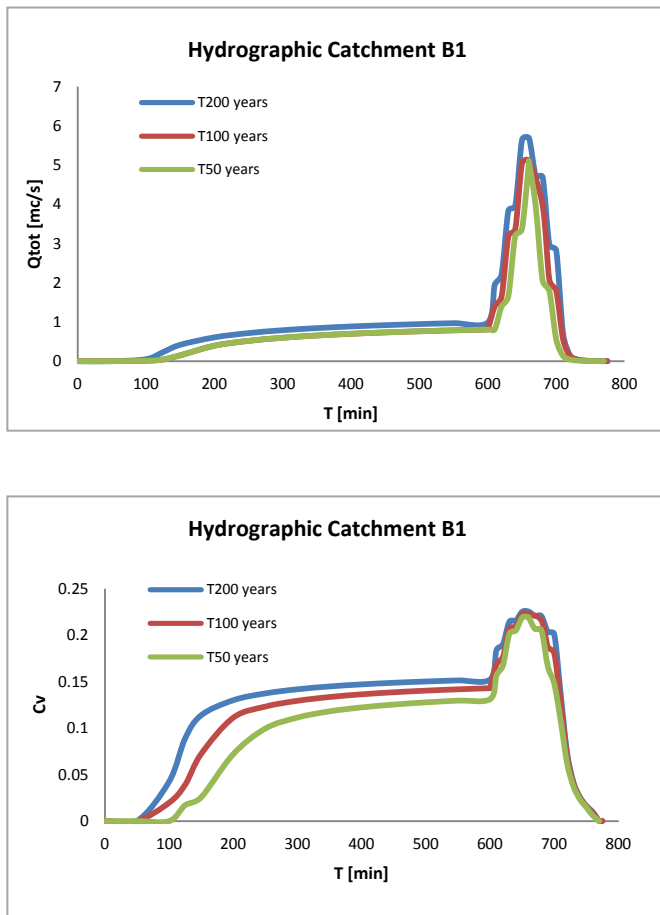


Figure 8.9 Mixture hydrograph and relative volumetric concentrations at the outlet of mountain catchment B1 for different return period T .

8.3.3 Modelling of the channel's sides instability

Additional contribution to the volume of solid material carried by hyperconcentrated flows may result from local instabilities, in turn caused by erosion processes at the toe of the channel's sides along the gullies.

The analysis of these phenomena was carried out for the same return periods considered in the study of the surface erosion with reference to the pluviogram 2 (Section 8.3.2), coupling the groundwater modelling with the Limit Equilibrium Method, through the assumption of rigid, perfectly plastic behaviour of soils. The groundwater modelling was devoted to the estimation of pore water pressure regime under unsaturated soil conditions; then, the resulting pressure values were used to compute the Safety Factor via the Limit Equilibrium Method. In particular, starting from the stratigraphic reconstruction of 145 cross-sections in correspondence of channels of the hydrographic network (Figure 8.10), the pore water pressure regime, that established at the end of a rainfall event, was examined by assuming an initial condition of constant (i.e. depth-independent) soil suction level equal to 10 kPa. The analysis was carried out through the numerical integration of the bi-dimensional Richard's equation (Richards, 1931), by using a finite element analysis performed with the numerical code SEEP/W (GeoSlope, 2005).

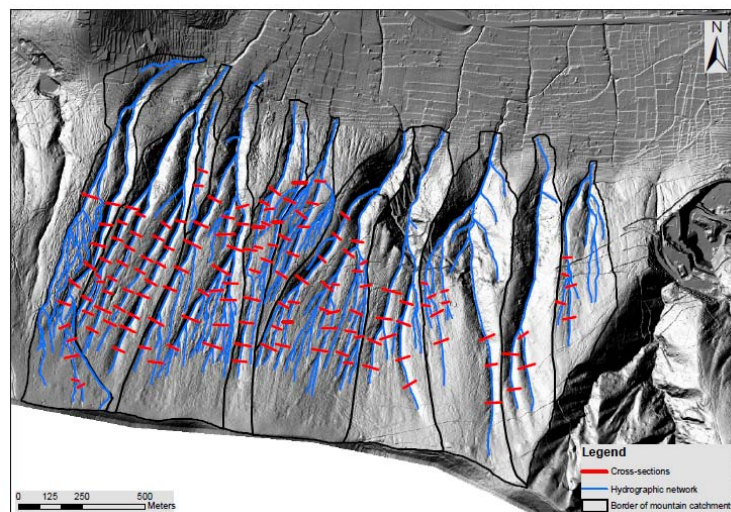


Figure 8.10 Examined cross-section tracks.

With reference to a generic section with defined local Cartesian coordinate system (Figure 8.11) the Richards' equation, that governs unsteady variable saturated Darcian flow of groundwater in response to a rainfall event, can be written as:

$$\frac{\partial}{\partial x} \left[k_x(\psi) \left(\frac{\partial \psi}{\partial x} \right) \right] + \frac{\partial}{\partial y} \left[k_y(\psi) \left(\frac{\partial \psi}{\partial y} \right) \right] + Q = \frac{\partial \theta}{\partial t} \quad (8.7)$$

in which ψ is groundwater pressure head, θ is the volumetric water content, t is the time, k_x and k_y are the hydraulic conductivity, respectively, in the x-direction and y-direction, Q is the applied boundary flux. In unsaturated condition of slope, both water content and conductivity are strictly related to the pore water pressures by means of non-linear relationships (Richards, 1931).

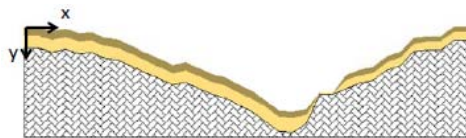


Figure 8.11 Local coordinate system.

The obtained results were then used as input data in subsequent slope stability analysis performed with the Morgenstern and Price's limit equilibrium method (Morgenstern and Price, 1965) implemented in the numerical code SLOPE/W (GeoSlope, 2005). The analysis of the critical surface of each examined cross-section at the end of the rainfall event – for which the safety factor FS (Eq. 8.8) is less than one – allowed the estimation of the unstable volume of soil.

Conventionally, the factor of safety (FS) is expressed by a single number defined as follows:

$$FS = \frac{\tau_f}{\tau} \quad (8.8)$$

where, τ_f is the average shear strength of the soil along the potential failure surface, whereas τ the average the shear stress on the same surface.

The obtained locally results, in terms of mobilised volume for each considered section, were exported in a GIS environment and integrated

with those derived from stability analysis conducted on a large area with the physically based model called *The transient rainfall infiltration and grid-Based regional Slope-Stability Model* (or TRIGRS-unsaturated) (Savage et al., 2004) in order to extend the solutions to the portion of channels localised between two examined sections.

TRIGRS-unsaturated is an analytical model that couples the Infinite Slope model (Taylor, 1948) with a solution of Richards' equation in transient conditions of pore water pressure regime and different conditions of soil saturation (Baum et al., 2008) and it operates in a GIS environment. It models rainfall infiltration, resulting from storms having durations ranging from hours to a few days, using analytical solutions for partial differential equations that represent one-dimensional, vertical flow in isotropic, homogeneous materials for unsaturated conditions (Baum et al., 2008); then, it uses a simple infinite-slope model to compute factor of safety on a cell-by-cell basis.

A complete description of all the formulas adopted by the code can be found in Savage et al. (2004) and Baum et al. (2008).

It is important to underline that stability analyses performed both with the limit equilibrium methods and the numerical code TRIGRS-unsaturated have shown that the critical slip surface is generally located at the interface between the lithotype A' and B'. Moreover, this last model, although more conservative than conventional limit equilibrium methods, shows an agreement for 85% of cases with the results of the software SLOPE/W.

The obtained results, deriving from the combination of two stability analysis models, allowed the definition of the overall unstable areas at different return periods (T=50 years, T=100 years, T=200 years) and the average unstable volumes (Figure 8.12). In particular, the integrated analysis of unstable areas with in situ-recognised geomorphological forms allowed the definition of the instability nature: ZOB instability (located on the Zero Order Basins) or Bank instability (located on the channel's side).

It is worth noting that the contribution to the solid material transported by hyperconcentrated flows resulting from local instability of the banks is negligible because the volumetric concentrations of the solid material do not exceed 5% (Table 8.6).

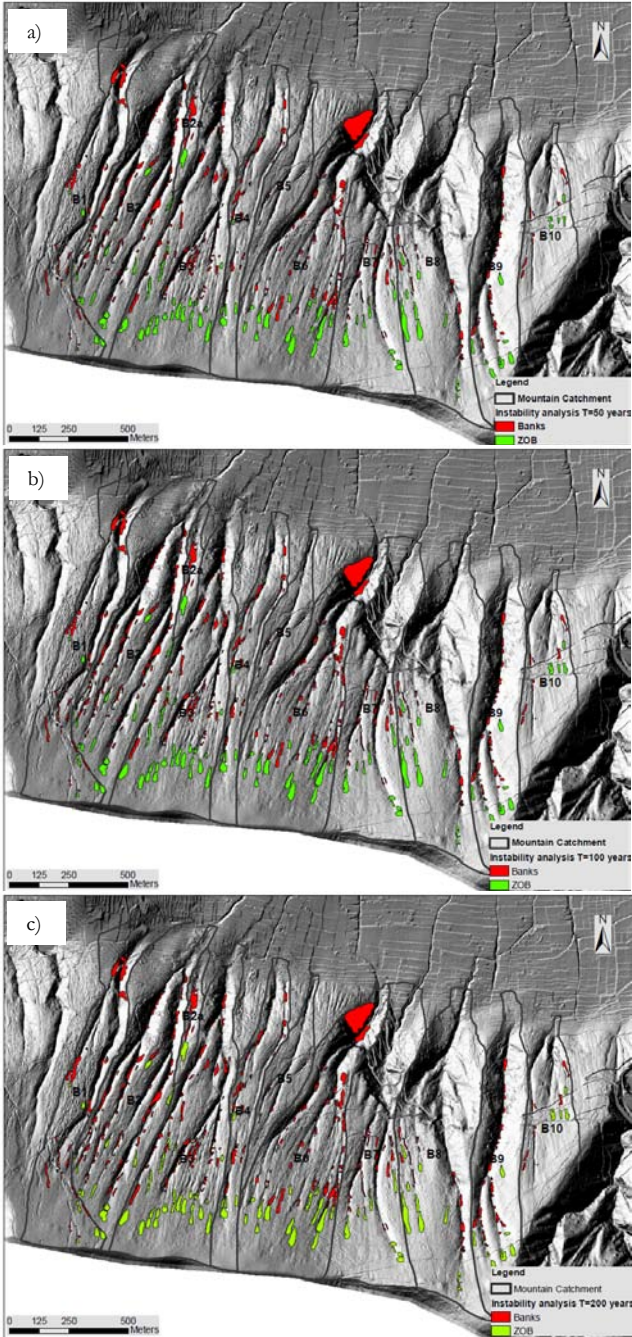


Figure 8.12 Instability analysis for a) T=50 years, b) T=100 years, c) T=200 years.

Table 8.6 Instability channel's sides volumes and volumetric concentration of sediments.

	<i>T=50 years</i>		<i>T=100 years</i>		<i>T=200 years</i>	
	<i>Volume m³</i>	<i>C_v %</i>	<i>Volume m³</i>	<i>C_v %</i>	<i>Volume m³</i>	<i>C_v %</i>
<i>B1</i>	3707	5	3762	4	4028	3
<i>B2</i>	1619	2	1850	2	2118	2
<i>B2A</i>	599	6	638	5	675	4
<i>B3</i>	2537	3	2755	2	2845	2
<i>B4</i>	962	2	1105	2	1232	2
<i>B5</i>	79	0	98	0	108	0
<i>B6</i>	3830	4	4175	3	4476	2
<i>B7</i>	460	1	535	0	580	0
<i>B8</i>	498	0	535	0	536	0
<i>B9</i>	578	1	678	1	719	1
<i>B10</i>	694	2	848	1	865	1

8.4 HAZARD ANALYSIS

The quantitative hazard analysis can be defined as a combination of hyperconcentrated flow frequency of occurrence (herein computed as the reciprocal of return period) and its intensity.

The frequency of hyperconcentrated flows is strictly related to the occurrence of critical rainfall event of a given return period ($T = 50$ years, $T = 100$ years, $T = 200$ years) and can be related to the total volume (or magnitude) of material that can be mobilised at the source areas as a result of erosion processes and local instabilities of channel's sides. These relations may be expressed with the frequency–magnitude (F-M) curves.

For the test site, the F-M curves were generated for each mountain catchment of Monte Albino hillslope (Figure 8.13). To this aim, the frequency was normalised with respect to the extension of the individual mountain catchment. The relative magnitude was estimated through the

assessment of the total volume of material involved in hyperconcentrated flows at source areas.

From Figure 8.13 it is possible to note that, for each mountain catchment, as the volume of involved material increases the frequency of occurrence decreases.

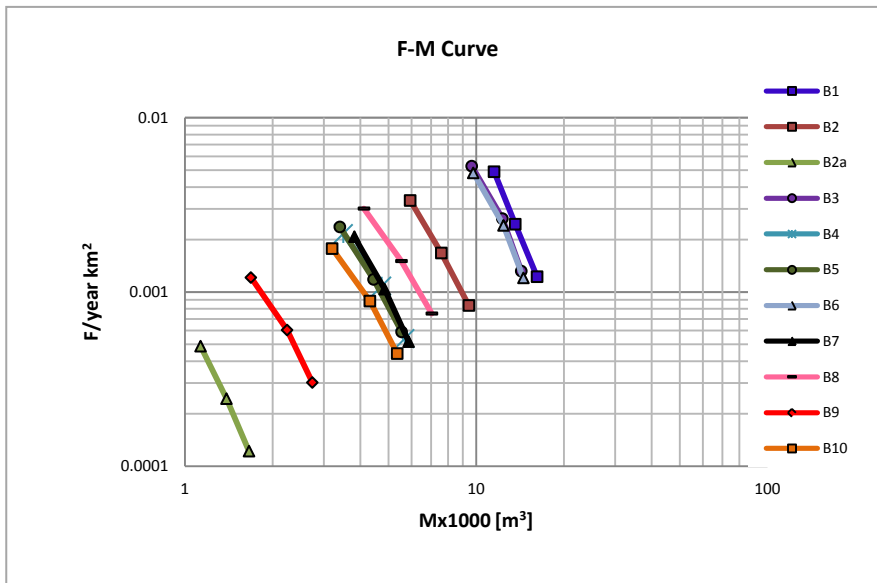


Figure 8.13 F-M curves for Monte Albino slope.

In this regard it should be noted that areas threatened by potential flow-like events of catastrophic consequences might be ranked as a low hazard if the probability of occurrence is very low (Lateltin, 1997; 2002); on the other hand, frequent events of low magnitude may determine that an area could be classified as moderate or high hazard (Corominas and Moya, 2008). Moreover, for an equal value of frequency per unit area, the catchments namely B1, B3, B6 involve a higher volume of materials. Once the frequency-magnitude curves are produced, the triggering hazard can be represented on topographic maps of suitable scale. To this aim, the volume of material involved in hyperconcentrated flows was normalised to the length of the channel's longitudinal section in which the same susceptibility level has been recognised (see Section 8.1). The magnitude values were grouped into four classes (Table 8.7). Combining, therefore, the relative magnitude in each channel's longitudinal section

with the return period of the triggering rainfall, the classification of the hazard level into four classes was performed (VL = very low, L = low, M = moderate, H = high).

Table 8.7 Hazard matrix for the triggering of hyperconcentrated flows.

HAZARD		T = 50 years	T = 100 years	T = 200 years
Magnitude [m ³ /m]	> 3	H	H	M
	3 - 2	M	M	L
	2 - 1	L	L	VL
	< 1	VL	VL	VL

The obtained results were finally represented in three distinct hazard maps of triggering of hyperconcentrated flows, one for each of the return period considered (Figure 8.14). The use of colour shadings facilitates the identification of ranges of hazard along the gullies. The hazard maps show that the maximum value of hazard level lies in the different channel sections, with reference to rainfall event having a return period equal to T=50 years. This result is very useful for the design of active control works.

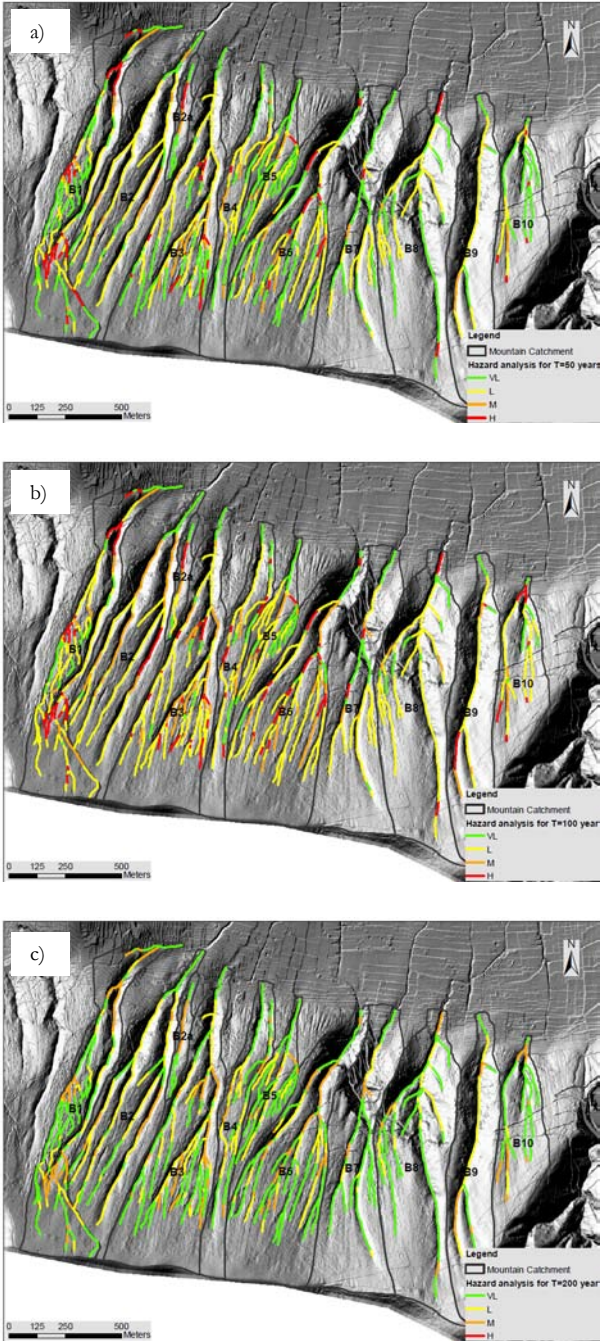


Figure 8.14 Hazard maps of hyperconcentrated flows: a) T= 50 years, b) T=100 years and c) T=200 years.

It is also noted that the normalised volumes of mobilised soil in the different considered hazard scenarios are, on average, two orders of magnitude lower than the maximum normalised mobilised volumes deriving from the susceptibility analysis (Figure 8.15).

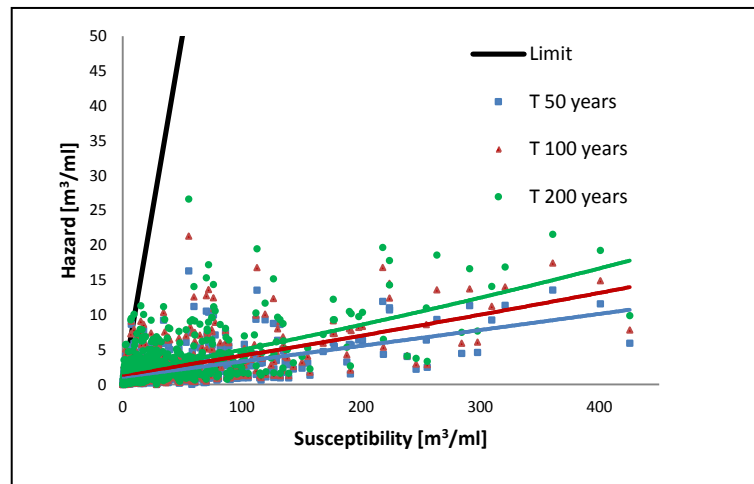


Figure 8.15 Relationship between hazard and susceptibility in terms of mobilised normalised volumes.

Passing from source to run-out areas, the hazard analysis implies the use of models able to simulate the propagation stage. The obtained results, represented in hazard zoning maps, can be adopted to determine the type and scale of structural mitigation measures as well as to plan the use of land and provide restrictions for the urban development (Jakob, 2005).

8.5 RUN-OUT ANALYSIS

Run-out prediction is important for defining affected areas and intensity parameters of hyperconcentrated flow, which are essential elements for the definition of the expected consequence scenarios.

The main factors that determine the run-out of flow-like phenomena are the released volume of water and sediment, the rheology of the moving mass and the topographical characteristics of the path.

In order to analyse the behaviour of the flowing mixtures as well as their geometric/kinematical characteristics, multiple run-out methods have been developed. These methods can be divided into: empirical methods and dynamic methods; the latter can be further divided in analytical and numerical methods (Dai et al., 2002 a; Rickenmann, 2005).

Empirical methods (e.g. Corominas, 1996; Rickenmann, 1999) are usually based on extensive amounts of field observations and on the analysis of the relationships between the run-out distance and different landslide mechanisms, their morphometric parameters, the volume of the landslide mass and the physical and mechanical characteristics of soils (Quan Luna, 2012). They are based on simplified assumptions, are often easy to use and they should only be applied to conditions similar to those on which they are based. They do not explicitly account for the mechanics of the movement process and only a preliminary prediction of the travel distance is possible.

Analytical methods (e.g. Hutchinson, 1986; Takahashi, 1991; Hungr et al., 1992; Sassa and Wang, 2000) include different formulations based on lumped mass approaches and continuum mechanics models in which the mass is assumed as a single point. They are unable to determine complex patterns of failure and internal deformation of the sliding mass, to account for the lateral confinement and spreading of the flow, to identify basal elevation function pattern and downhill condition (such as obstacles), to simulate the motion of the flow front or the momentum changes (Chen and Lee 2004; Dai et al., 2002 a).

Numerical methods for determining the run-out behaviour (e.g. O' Brien et al., 1993; D'Ambrosio et al., 2003; Crosta et al., 2003; Pitman and Le, 2005; Kelfoun and Druitt, 2005; Kwan and Sun, 2006; Poisel and Preh, 2007; Chen and Lee, 2007; Pirulli and Mangeney, 2008; Medina et al., 2008; Begueria et al., 2009; Pastor et al., 2009; Hungr and McDougall, 2009; Christen et al., 2010) are physically based models and they have been developed either for distinct element or for continuum based

models, which also simulated the deformation of the moving mass along the flow path. The distinct element model can be defined as the numerical technique that studies the mechanical behaviour of granular assemblages of materials subjected to gross motion. The equations of motion between these blocks are solved by the detection and treatment of contacts between these blocks (van Asch et al., 2007).

Continuum fluid mechanics models, the most common approach, are based on the mass, momentum and energy conservation equations that describe the dynamic motion of flow (Quan Luna, 2012). By solving a set of governing equations, with a selected rheological model describing the flow properties, the velocity, acceleration, depth and run-out distances can be predicted (Chen and Lee, 2000). A major difficulty in developing numerical models is the choice of appropriate rheological law of the flow.

Dynamic run-out models that have a numerical methodology as a background can be classified in the following types (Quan Luna, 2012):

- Models based on the solution dimension in 1D or 2D: 1D models analyse the movement considering the topography as a cross-section of a single predefined width while 2D models make the analysis considering the topography in plan and cross-section;
- Models based on the solution reference frame: the equation of motion can be formulated in two difference frames of reference: Eulerian or Lagrangian. An Eulerian reference frame is fixed in space, analogous to an observer standing still as a landslide passes, and require the solution of a governing equation using a dense, fixed computational grid. A Lagrangian reference frame moves with the local velocity, analogous to an observer riding on top of landslide;
- Models based on the basal rheology: the rheology of the flow is expressed as the resistance forces that interact inside the flow and at the interface between the flow and the bed path. The most common rheological laws used in the dynamic models are: *i*) "*Frictional*" (or "*Coulomb*") resistance (Hung and McDougall, 2009); *ii*) the frictional-turbulent "*Voellmy*" resistance (Voellmy, 1955); *iii*) the visco-plastic "*Bingham*" (or "*Herschel-Bulkey*") resistance (Coussot, 1997; Malet et al., 2004); *iiii*) the "*Quadratic*" resistance (O' Brien et al., 1993).

According to Quan Luna (2012), one of the advantage of the numerical methods is that they have the ability of computing the flow path over irregular topographic slope; since the computed outputs of the models give directly the intensity parameters of the flow, they can be coupled directly to vulnerability - with reference to persons or to structures - for a quantitative risk assessment.

To this aim, among several 2D dynamic numerical run-out models developed (Table 8.8), in this research the FLO-2D model has been used for which, among other things, interesting examples of application for flow-like phenomena in the scientific literature are available (e.g. Pirulli and Sorbino, 2008; Papa et al., 2011; Quan Luna, 2012; Jakob et al., 2013 a).

Table 8.8 An overview of several 2D dynamic numerical run-out models (from Quan Luna, 2012)

Model	Rheology	Solution approach	Reference frame	Variation of rheology
MADFLOW (Chen and Lee, 2007)	Frictional, Voellmy and Bingham	Continuum Integrated	Lagrangian with mesh	No
TOCHNOG (Crosta et al., 2003)	Frictional (elastoplastic model)	Continuum Integrated	Differential (adaptive mesh)	Yes
RAMMS (Christen et al., 2010)	Voellmy	Continuum Integrated	Eulerian	Yes
DAN3D (Hungar & McDougall, 2009)	Frictional, Voellmy and Bingham	Continuum Integrated	Lagrangian	Yes
FLATMODEL (Medina et al., 2008)	Frictional and Voellmy	Continuum Integrated	Eulerian	No
SCIDDICA S3-hex (D'Ambrosio et al., 2003)	Energy based	Cellular Automata	Eulerian	No
3dDMM (Kwan and Sun, 2006)	Frictional and Voellmy	Continuum Integrated	Eulerian	Yes
SPH (Pastor et al., 2009)	Frictional, Voellmy and Bingham	Continuum Integrated	Lagrangian meshless	Yes
MassMov2D (Begueria et al., 2009)	Voellmy and Bingham	Continuum Integrated	Eulerian	Yes
RASH 3D (Pirulli and Mangeney, 2008)	Frictional, Voellmy, Quadratic	Continuum Integrated	Eulerian	No
FLO-2D (O'Brien et al., 2003)	Quadratic	Continuum Integrated	Eulerian	No
TITAN2D (Pitman and Le, 2005)	Frictional	Continuum Integrated	Lagrangian with mesh	No
PFC (Poisel and Preh, 2007)	Inter-particle and particle wall interaction	Solution of motion of particles	Distinct element method	No
VolcFlow (Kelfoun and Druitt, 2005)	Frictional and Voellmy	Continuum Integrated	Eulerian	No

FLO-2D is an Eulerian two-dimensional finite difference physical process model that simulates homogeneous and isotropic non-Newtonian flows, over unconfined flow surfaces or in channels, taking into account the possible presence of obstacles. The numerical code predicts the flooding area, the maximum velocity and depth of the flow in different time in each cell constituting the topography. As far as this aspect is concerned, it needs the definition of the position, on a digital elevation model (DEM), of the source area of the flow-like phenomena. In FLO2D, the topographic surface is overlaid with a square finite difference grid system and the flow is routed in eight possible flow directions (the four compass directions and the four diagonal directions). The inflow condition is defined in one or more upstream grid elements with a hydrograph (water discharge vs. time) and values of C_v (volumetric sediment concentration) for each point in the hydrograph; the outflow condition is specified in one or more downstream grid elements (O' Brien et al., 1993).

Flow in two dimensions is accomplished through a numerical integration of the continuity equation of fluid volume (Eq. 8.9) and the dynamic wave momentum equation (Eqs. 8.10 and 8.11) expressed in a depth-averaged way as follows:

$$\frac{\partial h}{\partial t} + \frac{\partial(h\bar{v}_x)}{\partial x} + \frac{\partial(h\bar{v}_y)}{\partial y} = i \quad (8.9)$$

$$S_{fx} = S_{ox} - \frac{\partial h}{\partial x} - \frac{\bar{v}_x}{g} \frac{\partial \bar{v}_x}{\partial x} - \frac{\bar{v}_y}{g} \frac{\partial \bar{v}_x}{\partial y} - \frac{1}{g} \frac{\partial \bar{v}_x}{\partial t} \quad (8.10)$$

$$S_{fy} = S_{oy} - \frac{\partial h}{\partial y} - \frac{\bar{v}_y}{g} \frac{\partial \bar{v}_y}{\partial y} - \frac{\bar{v}_x}{g} \frac{\partial \bar{v}_y}{\partial x} - \frac{1}{g} \frac{\partial \bar{v}_y}{\partial t} \quad (8.11)$$

where V_x and V_y denotes the depth-averaged flow velocity, h is the flow depth, i is the rainfall intensity on the flow surface and g is the gravity constant. The friction slope components S_{fx} and S_{fy} are written as functions of the bed slope S_{ox} and S_{oy} , the pressure gradient and the convective and local acceleration terms.

As far as the rheological characteristics of the flowing mass are concerned, FLO-2D adopts the quadratic rheological approach proposed

by Julien and Lan (1991), in which the total shear stress τ in hyperconcentrated sediment flows is a combination of five shear stress components: the cohesive yield stress τ_c , the Mohr-Coulomb shear τ_{mc} , the viscous shear stress τ_v , the turbulent shear stress τ_t , and the dispersive shear stress τ_d (FLO-2D Users Manual, 2009). The proposed constitutive equation has the following form (Eq. 8.12) (O'Brien and Julien, 1985):

$$\tau = \tau_y + \mu \left(\frac{dv}{dy} \right) + C \left(\frac{dv}{dy} \right)^2 \quad (8.12)$$

being τ_y the Bingham's yield stress, μ the Bingham's viscosity, C a coefficient able to take into account the effects of both collisions between particles and turbulent stresses, du/dy the strain rate. Both Bingham's yield stress and viscosity depends on the sediment concentration by volume (C_v) according the following relationships (Eqs. 8.13 and 8.14) (FLO-2D Users Manual, 2009):

$$\tau_y = \alpha_2 e^{\beta_2 C_v} \quad (8.13)$$

$$\mu = \alpha_1 e^{\beta_1 C_v} \quad (8.14)$$

where α_i and β_i are empirical coefficients to be estimated via rheometric tests.

In this regard, on the basis of the results achieved by Martino (2003) on the pyroclastic soils involved in the debris flows triggered over Pizzo d'Alvano massif on May 1998, Papa et al. (2011) showed that the above empirical coefficients are equal to: $\alpha_1 = 0.0145 \text{ Pa}\cdot\text{s}$; $\beta_1 = 8.3$; $\alpha_2 = 0.0134 \text{ Pa}$; $\beta_2 = 14.1$.

The validity of this assumption was checked by simulating – with the aid of the numerical code FLO-2D, on a 10-m resolution grid – the propagation stage of the hyperconcentrated flows occurred on 12 September 1955. To this aim, the availability of information related to the cumulative rainfall values over 24 hours (195.4 mm), recorded by the rain gauge located in Nocera Inferiore, a constant pluviogram was taken into account. Assuming an initial condition of uniform soil suction over the Monte Albino slope equal to 10 kPa, the flood hydrograph - for each mountain catchment - was obtained thanks to the use of the hydrologic and soil erosion model LISEM. The achieved propagation results (Figure

8.16), considering a digital elevation model deriving from a historical topographic map, match the description - on the basis of historical information - of the past event. In fact, the run-out distances of simulated hyperconcentrated flows are able to reach the areas hit by the past event, with maximum flow depth of about 0,5 m (see Section 6.7.1), giving validity to the choice of the rheological parameters.

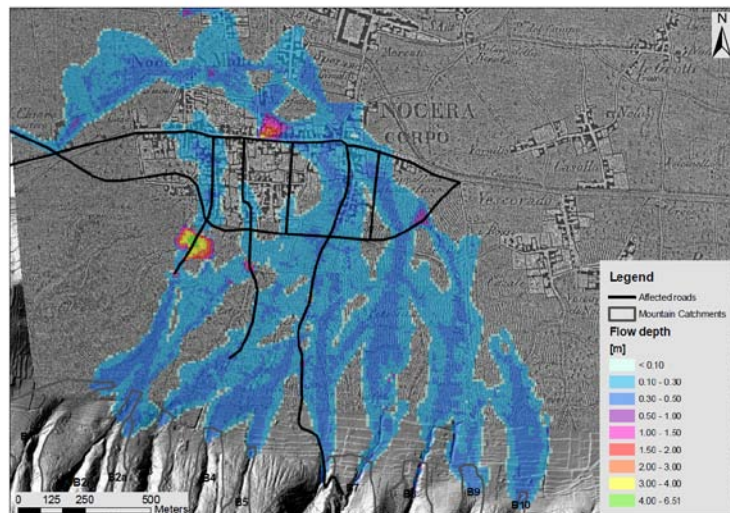


Figure 8.16 Map of the run-out simulation, via the use of FLO-2D numerical code, of hyperconcentrated flows occurred on 12 September 1955.

Once the rheological parameters of the flowing masses were validated, the FLO-2D numerical code was applied for the three considered hazard scenarios ($T = 50$ years, $T = 100$ years, $T = 200$ years) on a topographic surface overlaid with a computational grid cells of 5 m x 5 m width. As far as the input parameters, the hydrographs of water and the relative C_v values obtained from the LISEM model (Table 8.5) and incremented by the rate deriving from slope instability modelling (Table 8.6) in the time frame wherein LISEM model provides the triggering of hyperconcentrated flows ($C_v > 20\%$), were positioned at the outlet of each mountain catchment. The obtained results are synthesised in Figure 8.17 and Figure 8.18, respectively, in terms of maximum depth (d) and velocity (v) reached by the flowing mixtures in each of the computational grid cells; these spatially distributed parameters are considered in the following as a measure of the hyperconcentrated flow intensity.

Run-out analyses shows that flooding area and flow depth increase with the increasing of the return period T while velocity decrease with increasing of the return period. This is due to the significant increase of the solid fraction in the fluid mixture. Generally, the maximum flow depths do not exceed 0.5 m in the piedmont area while they attain the highest values (generally, less than a meter) near the lay-out of the highway. It is important to note that in the western part of the piedmont area, the maximum flow depth exceeds 4 meters, due to the presence of a topographic discontinuity (depression). As for the maximum flow velocities, they reach the maximum values (of about 2.5 m/s) along the main roads.

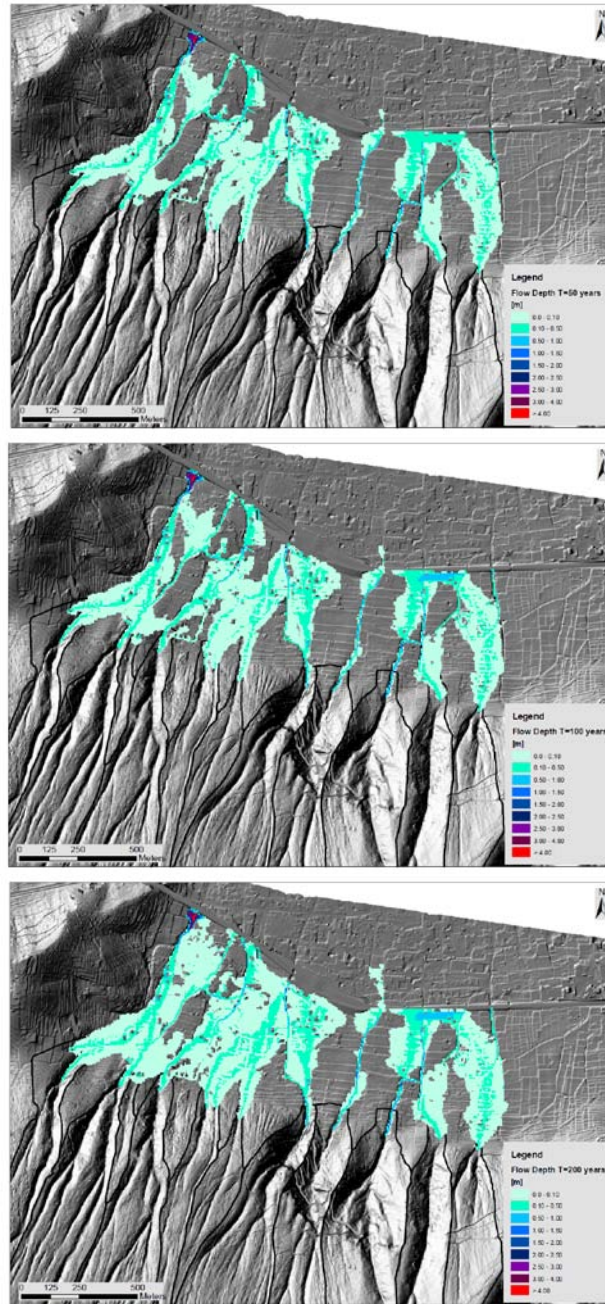


Figure 8.17 Maps of the maximum flow depth (d) reached by the FLO-2D simulated flowing mixtures in each of the computational grid cells for the three considered hazard scenarios (T = 50, 100 and 200 years).

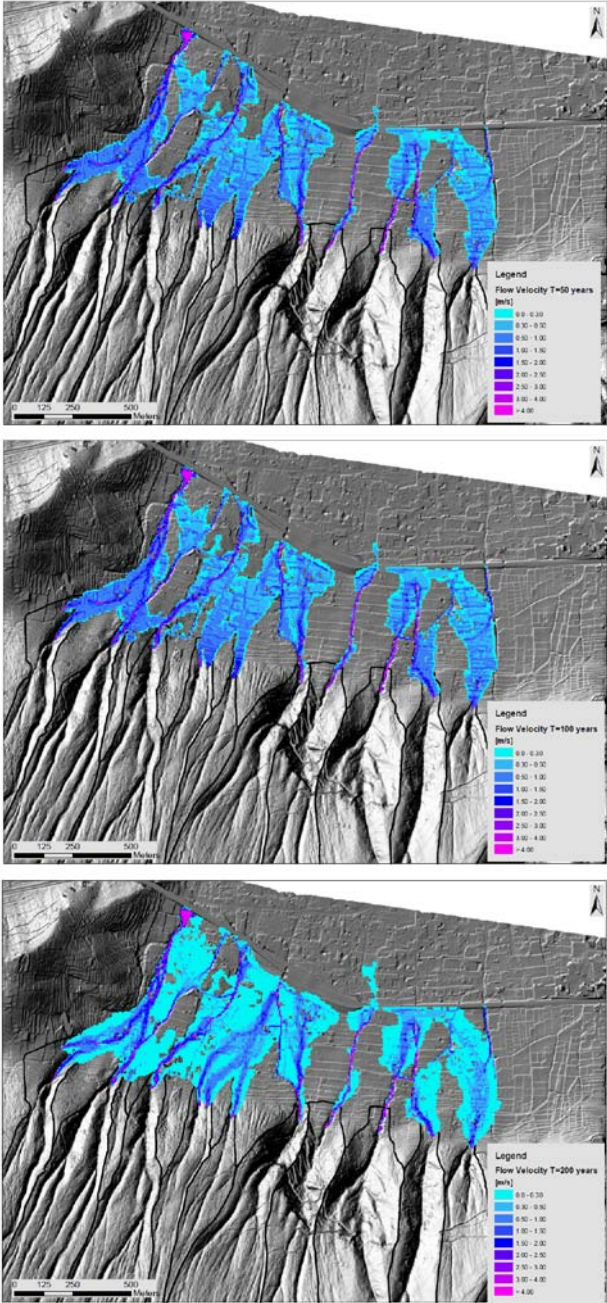


Figure 8.18 Maps of the maximum flow velocity (v) reached by the FLO-2D simulated flowing mixtures in each of the computational grid cells for the three considered hazard scenarios ($T = 50, 100$ and 200 years).

9 QUANTITATIVE ESTIMATION OF THE RISK FOR LIFE LOSS AT THE SITE-SPECIFIC SCALE

In order to assess the risk to life loss posed by hyperconcentrated flow, it is necessary to determine in which way the investigated hazard situations may affect the elements at risk in a dangerous area. To this aim, at site-specific scale, it is essential to rely on the availability on the propagation stage modelling that allows the prediction of the run-out distance, run-out width, velocity, pressures, depth of the moving mass and depth of deposits. Once the hazard scenario have been identified it is possible to evaluate the consequence scenario on the exposed elements at risk.

In the present chapter the adopted procedures and the achieved results of a quantitative estimation of the expected consequences posed by the occurrence of hyperconcentrated flows and, consequently, of the risk of fatality to residents at the toe of Monte Albino slope are presented. In particular, the estimated risk for life loss is calculated at both the individual level (risk to the average and most exposed person) and the societal level.

9.1 THE ADOPTED PROCEDURE

The main purpose of the QRA analyses consists of the estimation of the risk to life loss posed by the hyperconcentrated flows that could originate over the Monte Albino hillslope to (average or most exposed) persons living in the piedmont area. In order to pursue this goal, the methodological approach provided by Fell et al. (2005) was adopted. Accordingly, the annual probability that a “particular person” (e.g. the most exposed one to the hyperconcentrated flow risk) may lose his/her life $P_{(LOL)}$ was calculated through the following formula (Eq. 9.1):

$$P_{(LOL)} = P_{(HF)} \times P_{(I:HF)} \times P_{(S:T)} \times V_{(D:T)} \quad (9.1)$$

where $P_{(H:HF)}$ is the frequency of the hyperconcentrated flows; $P_{(T:HF)}$ is the probability of the hyperconcentrated flow reaching the exposed person; $P_{(S:T)}$ is the temporal spatial probability of the exposed person whose vulnerability equals $V_{(D:T)}$.

If the element at risk is exposed to a number of different sizes (e.g. volumes of water-sediment mixtures) of hyperconcentrated flows – such as in the problem at hand – the corresponding risks have to be summed in order to obtain the total risk, provided that the hazards are independent of each other (Fell et al. 2005). In such a case, the expression can be rewritten as (Eq. 9.2):

$$P_{(LOL)} = \sum_{i=1}^n (P_{(L)} \times P_{(T:L)} \times P_{(S:T)} \times V_{(D:T)}) \quad (9.2)$$

n being the number of hazards.

9.2 CONSEQUENCES ANALYSIS

The consequence analysis involves the identification and quantification of the elements at risk as well as the estimation of both their temporal-spatial probability and vulnerability (Fell et al. 2005).

9.2.1 Element at risk and their temporal-spatial probability

Referring to the case study at hand, the modelling of the propagation stage of hyperconcentrated flows allowed the detection of the affected urbanised areas for each of the three considered scenarios; within these areas, elements at risk (i.e., having a $P_{(T:HF)} = 1$) can be easily identified.

Focusing the attention only on the exposed people, the estimation of the temporal spatial probability $P_{(S:T)}$ of a given person (average or most exposed) generally call for the analysis of demographic, economic and social aspects; moreover, the evaluation of factors related to the risk perception as well as to the existence of alarm systems and related preparedness should be also taken into account (Roberds, 2005).

In the present work, temporal spatial probability values dealing with the average exposed person in open space were estimated by adapting to the problem at hand a semi-quantitative procedure conceived in the SafeLand Project for societal vulnerability – in terms of coping capacity

– purposes (SafeLand Deliverable D2.6, 2011). This procedure is applicable in risk areas corresponding to census tracts (Figure 9.1) provided that newly collected census data as well as information achievable via interviews to a representative sample of residents are available.

On the basis of this data and information, the procedure contemplates the use of indicators characterizing the demographic, social and economic setting as well as indicators representing the degree of preparedness, the effectiveness of the response and the capacity to recover. Each indicator is weighted, based on its overall degree of influence, and ranked using a semi-quantitative scale with five levels whose related scores p_i range from 1 ($p_{i,min}$) to 5 ($p_{i,max}$).

Referring to SafeLand Deliverable D2.6 (2011) for further details, in the present thesis it must be noticed that the following indicators were considered:

- demographic (age distribution, rural population, population density);
- economic (occupation level);
- social (education level);
- preparedness (hazard evaluation, regulation control, emergency response, early warning system).

Furthermore, the value pertaining to the global indicator (GI_k) associated to a given “k” census tract was computed as (Eq. 9.3):

$$GI_k = \frac{\sum_{i=1}^n (I_i \cdot p_i)}{\sum_{i=1}^n I_i} \quad (9.3)$$

being $n = 8$ the total number of the considered indicators. The obtained results are synthesised in the Table 9.1.

Finally, in order to obtain the $P_{(S:T),k}$ value to be assigned to the average exposed person within each census tract (Table 9.1), the following expression was adopted (Eq. 9.4):

$$P_{(S,T),k} = \frac{GI_k - 1}{p_{i,\max} - p_{i,\min}} \quad (9.4)$$

In the case study at hand, information useful for analysis purposes was gained on the basis of both the available census data (Italian National Institute of Statistics—ISTAT 2001 census) and the results of a questionnaire survey to 373 persons living in the municipal territory of Nocera Inferiore (SafeLand Deliverable D5.7, 2011).

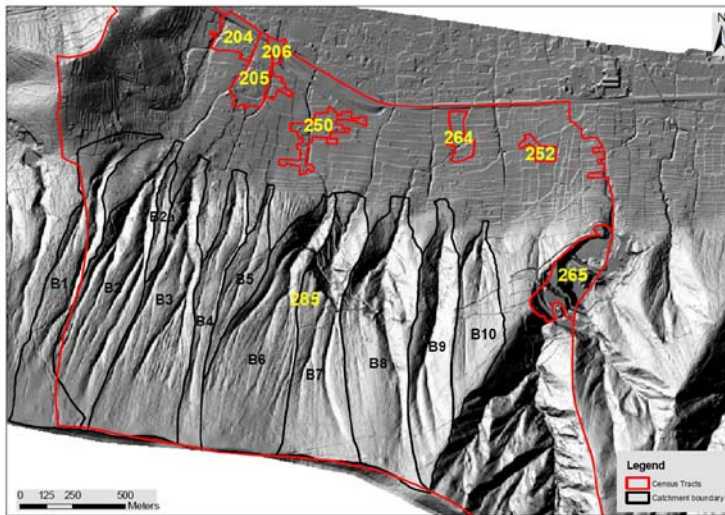


Figure 9.1 Map of the census tracts (data from the Italian National Institute of Statistics-ISTAT 2001 census).

Table 9.1 Global indicator values (GI_k) associated to the different census tracts and the corresponding temporal-spatial probabilities pertaining to the average persons at risk living within.

<i>ID of census tract</i>	<i>No. of residents</i>	GI_k	$P_{(S,T),k}$
204	61	2.37	0.34
205	8	3.00	0.50
206	33	2.11	0.28
250	97	2.42	0.36
252	18	3.00	0.50
264	65	2.58	0.39
265	3	2.11	0.28
285	426	2.74	0.43

As far as the most exposed persons (living within each of the impacted houses), the $P_{(S:T)}$ terms (Table 9.2) were assessed on the basis of the age of the inhabitants (Uzielli et al. 2008; Jakob et al., 2013, b) disregarding the existence of the warning system for hyperconcentrated flows. The necessary data were furnished by the Civil Protection Unit of the Nocera Inferiore municipality during the SafeLand Project activities. In the few cases in which information about people living in the impacted houses were lacking, a $P_{(S:T)}$ value equal to 0.75 was assumed.

Table 9.2 Temporal-spatial probability value adopted on the basis of the age of the inhabitants for most exposed persons.

<i>Age (years)</i>	<i>P(S:T)</i>
<i>0 ÷ 5</i>	<i>1</i>
<i>6 ÷ 18</i>	<i>0.75</i>
<i>19 ÷ 65</i>	<i>0.5</i>
<i>66 ÷ 75</i>	<i>0.75</i>
<i>> 75</i>	<i>1</i>

9.2.1 Vulnerability of the elements at risk

In order to estimate the vulnerability $V_{(D:T),AVE}$ of the average exposed person in open space, the product $v^2 \cdot d$ of the FLO-2D outputs (Figure 8.17 and Figure 8.18) – for each of the 5 m x 5 m computational grid cells – was considered as spatially-distributed intensity parameter. Then, similarly to Jonkman et al. (2008), who conceived a method aimed at assessing the loss of life caused by the flooding of low-lying areas protected by flood defences, a $V_{(D:T),AVE}$ not exceeding 0.02 in value was considered for $v^2 \cdot d$ values less than (or at least equal to) $4 \text{ m}^3/\text{s}^2$ (Table 9.3). Indeed, in such cases, the intensity level of the flowing mixture offers to exposed people the possibility to find shelter.

Beyond the above threshold the most serious consequences in terms of loss of human life are to be expected and, therefore, a $V_{(D:T),AVE}$ value equal to 1 can be conveniently assumed (Table 9.3).

Table 9.3 $V_{(D:T)}$ values adopted with reference to the vulnerability of the average person in open space exposed at the hyperconcentrated flow risk.

$v^2 \cdot d$ [m^3/s^2]	<i>Estimated range of $V_{(D:T)}$ values</i>	<i>Adopted $V_{(D:T)}$ values</i>
≤ 4	0 - 0.02	$0.005 v^2 \cdot d$
> 4	1	1

The vulnerability $V_{(D:T)}$ of persons most at risk living within the potentially impacted buildings (i.e. having $P_{(T:HF)} \neq 0$) was assessed by using the values reported in Table 9.4 as a function of the output data (v and d) of the FLO-2D numerical code. Bearing in mind that this data – for each computational cell – does not necessarily refer to the same time and takes into account the inherent uncertainties associated to the numerical modelling (Jakob et al., 2013 b), maximum values of both peak flow depths and velocities dealing with the cells located around each facility were cautiously considered for the consequence analysis purposes.

The $V_{(D:T)}$ limit value of 0.01 (to be considered when $v^2 \cdot d = 25 m^3/s^2$) was fixed according to the criteria adopted by Jakob et al. (2013 b); it is worth observing that this datum is consistent with the consequences recorded to the exposed people during the hyperconcentrated flow event which occurred in Atrani (Salerno Province) on September 2010 (Bovolin, 2012).

Table 9.4 $V_{(D:T)}$ values adopted with reference to the vulnerability of the person most exposed at the hyperconcentrated flow risk.

$v^2 \cdot d$ [m^3/s^2]	<i>Estimated range of $V_{(D:T)}$ values</i>	<i>Adopted $V_{(D:T)}$ values</i>
≤ 25	0 - 0.03	$0.0004 \cdot v^2 \cdot d$
> 25	0.8 - 0.1	1

9.3 QUANTITATIVE ESTIMATION OF THE RISK FOR LIFE LOSS

On the basis of the results of the above described hazard and consequence analyses, the risk to both average (in open space) and most (within impacted buildings) exposed persons was quantified according to the Equation (9.1) in terms of annual probability of loss of life.

In particular, as far as the average exposed persons in open space are concerned, the total risk ($P_{(AVE)}$) values were computed for each of the computational cell by summing the risk for $T=50$, $T=100$ and $T=200$ years hyperconcentrated flow scenarios. The obtained results are summarised in the map shown in Figure 9.2. From this Figure, it can be argued that the highest risk value ($P_{(AVE)} > 10^{-5}$ / annum) mainly took place in correspondence of some relevant roads corresponding to viable escape routes in the existing Municipal Emergency Plan on Hydrogeological Risks.

On the other hand, referring to most exposed people, it is worth noting that risk ($P_{(DI)}$) values pertaining to some of the individuals most at risk (Figure 9.3) is variously distributed, reaching values ranging between 10^{-4} /annum and 10^{-5} /annum, namely the thresholds established by the Geotechnical Engineering Office (1998) as tolerable and acceptable risk values for most exposed persons living at the toe of natural slopes.

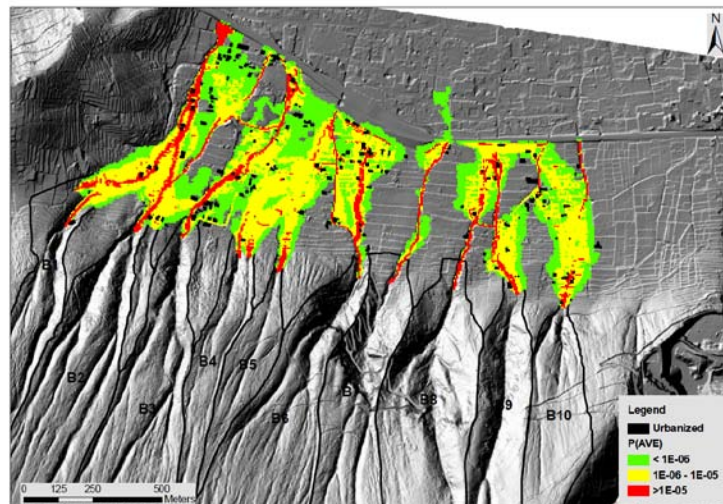


Figure 9.2 Individual total risk map for the average exposed people in open space posed by hyperconcentrated flows.

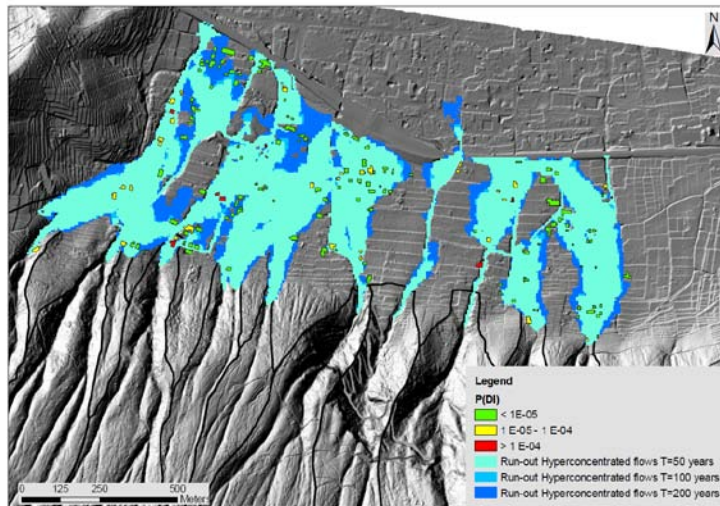


Figure 9.3 Individual total risk map for the most exposed people living within buildings potentially impacted by hyperconcentrated flows.

Further interesting considerations may derive from the estimate of risk to which groups of persons are exposed as it risk allows the achievement of different purposes, among which the ranking of the portions of a given urbanised territory at landslide risk and, thus, the prioritisation of the areas needing mitigation measures.

In order to pursue this aim for the problem at hand, the urbanised area at the toe of the Monte Albino massif was previously subdivided in 6 sectors (Figure 9.5) whose shape and size were simply established on the basis of both the run-out results (accomplished via the analyses explained in the section 8.5) and the geometrical path of the main roads. Then, on the basis of the QRA results obtained – for all the considered risk scenarios – in terms of annual probability of loss of life for the persons most at risk, the maximum number of equivalent victims (Wong et al. 1997) to be expected for each of the considered sectors was finally assessed. This allowed the ranking of the sectors at risk, as shown in Figure 9.5. It is worth noting that the most exposed sector is that labelled with symbols S5 where an equivalent number of victims per event equal to 1.03 can be expected (Table 9.5). Fractional results in Table 9.5 can be interpreted as 0–1 or 1–2 expected victims (Jakob et al., 2013 b).

Table 9.5. Average number of expected casualties per event for each of the considered urbanised sector at risk.

<i>Sector</i>	<i>Average number of expected casualties per event</i>	<i>Ranking</i>
<i>S1</i>	<i>0.08</i>	<i>3</i>
<i>S2</i>	<i>0.10</i>	<i>2</i>
<i>S3</i>	<i>0.01</i>	<i>6</i>
<i>S4</i>	<i>0.04</i>	<i>4</i>
<i>S5</i>	<i>1.03</i>	<i>1</i>
<i>S6</i>	<i>0.01</i>	<i>5</i>

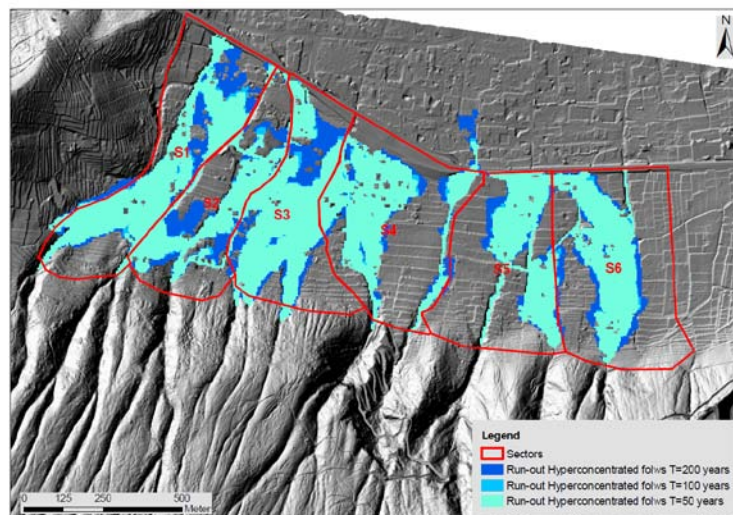


Figure 9.4 Urbanised sectors at risk.

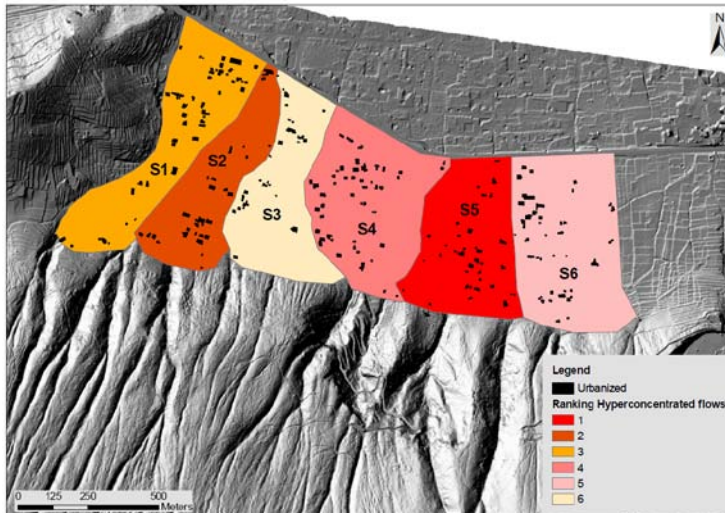


Figure 9.5 Ranking of the urbanised sectors at risk.

Considering that this is one of the first QRA's application in Italy, the obtained results prove to be useful from several points of views. In particular, they can allow to overcome the current limits in the official risk zoning maps that, being developed using basic methods, do not allow the ranking of the most at risk areas needing mitigation measures with reference to both: i) a given municipal territory (such as in the case study of Nocera Inferiore where areas potentially affected by hyperconcentrated flows are currently zoned at the same level of risk); ii) a number of municipal territories (such in the case of Campania region where tens of towns are threatened by hyperconcentrated flows). In this regard, the use of the quantitative estimation of the risk allow, on the one hand, to increase the level of knowledge in the zones defined (on the base of qualitative studies) at high risk, and second, to compare - in a simple and impartial way - the risk belonging to different areas as this can be expressed in terms of annual probability of loss of human life. It is important to note that this methodology can also set up a prioritisation of areas requiring urgent protective measures favouring, efficiently and effectively, the proper allocation of available financial resource. The QRA provides, where it is necessary and on the basis of the results of a cost-benefit analysis which cannot be performed using qualitative risk assessment procedures, the selection of the most suitable risk-mitigation

measures, which is able to respect economic and technical requirements (type, location and dimensions).

The results arising from the use of the QRA can be placed at the base of participatory processes in order to increase the risk awareness in people and to take into account, in the choice of the mitigation options, of technical, economic, environmental and social considerations. In this regard, it is worth noting that the QRA results for Monte Albino hillslope were used for a pioneering project of a deliberative participative processes, conceived within the framework of the European project SAFELAND (<http://www.safeland-fp7.eu>), where different packages of risk mitigation measures were evaluated also on the basis of the results of a cost-benefit analysis. The results can be found in SafeLand Deliverable D5.7 (2011).

10 CONCLUDING REMARKS

In the last decades, the growing increase all over the World of landslide events associated to huge consequences in terms of loss of life and properties, led several Central Authorities in charge of the landslide risk management to promote political actions aimed at forecasting and preventing the landslide risk. Focusing on Europe, some Countries (France, Italy, Norway and Switzerland) developed, on official bases, landslide hazard and risk zoning maps – at medium and large scales – where hazard and risk posed by both existing and potential landslides are ranked according to established criteria. Although the procedures adopted for hazard and risk analysis and zoning are different among the Countries, they are commonly based on qualitative methodological approaches.

As far as the case of Italy is concerned, it must be observed that hazard and risk zoning maps are available for the whole Country. These maps were produced within the so-called “Hydrogeological Setting Plans - Landslide risk (PsAI-Rf)” promoted by Laws promulgated immediately after the disaster occurred in Campania region on May 1998. The risk is differentiated in four classes (Very High R4, High R3, Medium R2 and Low R1) according to the criteria provided by the Central Government (D.P.C.M. 29/09/98).

It is worth observing that the landslide risk zoning maps, being developed by the River Basin Authorities at a preliminary level via the adoption of basic methods, are useful for land-use planning purposes – in this regard the zoning is legally binding – and allow the implementation of strategies for human life safeguarding through non-structural risk mitigation measures (i.e. warning systems and emergency plans). Conversely, the landslide risk zoning maps seem to be inadequate for the development of criteria aimed at defining, within a territory classified at very high risk: *i)* the prioritisation of areas needing mitigation measures, *ii)* the most appropriate risk reduction strategy (including type, location and sizes of stabilization and/or control works, in the cases

where they are chosen) and *iii*) its effectiveness with the aid of cost-benefit analyses.

All these goals can be pursued via quantitative risk analyses, as those carried out in the present thesis at both regional and site-specific scales.

At regional scale the research activities dealt with the case study of the Campania region where urban areas of 212 Municipalities – potentially affected by flow-like phenomena – were indiscriminately classified at very high risk (R4) by the “Extraordinary Plans” (L. 226/99). Anyway, a careful analysis of the contents of the historical documents allowed, with the aid of F-N curves (Cascini et al., 2008 b), the categorisation of the geological contexts according to the expected consequences in terms of number of victims posed by the occurrence of flow like phenomena (121 Municipalities). After that, a more in-depth analysis (in terms of rainfall characteristics, deposition areas, magnitude of the recorded consequences, etc.) of the contents of available historical documents regarding all the events (not necessarily causing fatalities) allows: *i*) the discrimination of the censored flow-like phenomena into two main classes, namely hyperconcentrated flows and debris flows; *ii*) the categorisation of the Municipalities where one class of the abovementioned flow-like phenomena is prevailing (i.e. 59 Municipalities affected by debris flows and 25 by hyperconcentrated flows). This latter result is of particular concern for Authorities in charge of the risk management as it can help them in planning and designing the actions for risk mitigation via non-structural measures taking into account the main aspects differentiating the initiation of debris flows from that of hyperconcentrated flows. This could promote an efficient and effective policy programme of economic and financial resources.

From a scientific point of view, the analysis of the temporal and spatial distributions of the phenomena allowed to make relevant considerations about initial (e.g. suction values) and boundary conditions (e.g. rainfall) leading to their occurrence as well as a deep understanding of the triggering mechanisms, so providing a detailed cognitive framework of aspects related to mechanics of the problem.

At detailed scale, the research activities focused on the application of a quantitative risk analysis (QRA) procedure to the case study of Nocera Inferiore (southern Italy) whose urbanised area is systematically affected by hyperconcentrated flows. The novelty of the proposed procedure consisted in conjugating the fundamentals of the risk theory with the geotechnical approach for solving practical problems.

In particular, as far as hazard analysis is concerned, the adopted QRA procedure firstly benefited of the availability of a reliable catalogue of incident data in estimating the hyperconcentrated flow frequency that drastically changed during the last centuries being strongly related to the explosive activity of Vesuvius volcano. Then, on the basis of data achieved via in-situ and laboratory tests on the potentially involved pyroclastic soils covering the Monte Albino (namely, the relief threatening the urbanised area of Nocera Inferiore), the propagation stage of the hyperconcentrated flows was numerically simulated for three different return period of the triggering rainfall thanks to the availability of an accurate DTM. In this regard, the knowledge of the areas historically flooded by the hyperconcentrated flows allowed a proper calibration of the rheological parameters of the flowing mixtures introduced in the adopted numerical model. As for exposed people, available data were used to estimate the expected consequences to both average exposed persons in open space and most exposed persons living within the impacted houses. The obtained results were finally represented in risk maps and later on used to rank the portions of the urbanised territory at hyperconcentrated flow risk.

Considering that this is one of the first QRA's application in Italy, the obtained results prove to be useful from several points of views. In particular, they could allow the overcoming of the current limits in the official risk zoning maps that, being developed using basic methods, do not allow the ranking of the most at risk areas needing mitigation measures with reference to both: *i*) a number of municipal territories (such in the case of Campania region where tens of towns are threatened by hyperconcentrated flows); *ii*) a given municipal territory (such as in the case study of Nocera Inferiore where areas potentially affected by hyperconcentrated flows are currently zoned at the same level of risk).

Furthermore, it must be observed that, among other things, QRA is well-suitable for society in increasing the awareness of existing risk levels as well as in appreciating the efficacy of the actions undertaken (Corominas et al., 2013). This is again the case of Nocera Inferiore, considering that QRA results were used in a pioneering participatory process where different packages of risk mitigation measures were evaluated also on the basis of the results of a cost-benefit analysis (SafeLand Deliverable 5.4, 2012) which cannot be performed using qualitative risk assessment procedures.

However, it must be stressed that the proposed procedure can be confidently applied in other contexts only if reliable input data are available and a proper calibration of the parameters to be introduced in advanced numerical models is carried out. Anyway, even in such a case, the due attention is necessary since additional information necessary to apply the QRA may be based on expert judgement or empirical data and the related uncertainties could be unknown. In such a case the analysis must be developed on the safe side and this is totally in charge of the person applying the QRA.

REFERENCES

- AGS Australian Geomechanics Society (2000). Landslide risk management concepts and guidelines. Australian Geomechanics Society, Sub-Committee on Landslide Risk Management. Australian Geomechanics 35, pp. 49-92.
- AGS Australian Geomechanics Society (2007). Guideline for Landslide Susceptibility, Hazard and Risk Zoning for Land Use Management. Australian Geomechanics Society Landslide Taskforce Landslide Zoning Working Group. Australian Geomechanics 42 (1), pp.13–36.
- Aleotti P. and Chowdhury R. (1999). Landslide hazard assessment: summary review and new perspectives. Bulletin of Engineering Geology and the Environment 58, pp. 21–44.
- Amarotta, A. (1994). L'alluvione del Salernitano. Un'esperienza disastrosa. Salerno, Italy. Arti Grafiche Boccia.
- Amatruda G., Bonnard C.H., Castelli M., Forlati F., Giacomelli L., Morelli M., Paro L., Piana F., Pirulli M., Polino R., Prat P., Ramasco M., Scavia C., Bellardone G., Campus S., Durville J.-L., Poisel R., Preh A., Roth W., Tentschert E.H. (2004). A key approach: the IMIRILAND project method. In: Identification and mitigation of large landslide risks in Europe. Ch. Bonnard, F. Forlati, C. Scavia (Ed.), pp. 13-43.
- Atkinson, P.M., Massari, R., 1998. Generalised linear modelling of susceptibility to landsliding in Central Apennines, Italy. Computers and Geosciences 24, pp. 373-385.
- Aucelli P.P.C., Cavinato G.P., Cinque A. (1996). Indizi geomorfologici di tettonica plio-quadernaria sul piedimonte adriatico dell'Appennino Abruzzese. IL QUATERNARIO, vol. 9, pp. 299-302, ISSN:0394-3356.
- Bagarello V. and Ferro V. (2006). Erosione e conservazione del suolo. The McGraw-Hill Companies, Milano, Italy. ISBN: 88-386-6311-4, pp. 123-171.
- Baeza, C., Corominas, J. (2001). Assessment of shallow landslide susceptibility by means of multivariate statistical techniques. Earth Surface Processes and Landforms 26, pp. 1251– 1263.
- Bakker J.P., Le Heux J.W.N. (1952). A remarkable new geomorphological law. Koninklijke Nederlandsche Akademie von Wetenschappen, 55, pp. 399-410 and pp. 554-562.
- Baum R.L., Savage W.Z., Godt J.W. (2008). TRIGRS—A Fortran program for transient rainfall infiltration and grid-based regional slope-stability analysis, Version 2.0. USGS open-file report 08–1159.
- Baynes F.J. and Lee M. (1998). Geomorphology in Landslide Risk Analysis, an Interim Report. In: Moore, D., Hungt, O. (Eds.), Proceedings of the Eight

- International Congress of the International Association of Engineering Geologists, Vancouver, Canada, pp. 1129–1136.
- Beasley D.B., Huggins L.F., Monke E.J. (1980). ANSWERS: a model for watershed planning. *Trans. ASAE*, 23 (4), pp. 938-944.
- Beguieria S., van Asch Th.W.J., Malet J.-P., Grondahl S. (2009). A GIS based numerical model for simulating the kinematics of mud and debris flows over complex terrain. *Natural Hazard and Earth System Sciences*, 9, pp. 1897-1909.
- Beguiniot C. (1957). La pianificazione urbanistica della Valle del Sarno: questioni di metodo per la valutazione dell'ambiente, Napoli.
- Bell R. and Glade T. (2004). Quantitative risk analysis for landslides - examples from Búdudalur, NW-Iceland. *Natural Hazards and Earth System Sciences*, vol. 15, pp.117-131.
- Belmans C., Wesseling J.G., Feddes R.A. (1983). Simulation model of the water balance of a cropped soil: SWATRE. *Journal of Hydrology* 63, pp. 271–286.
- Beverage J.P. and Culbertson J.K. (1964). Hyperconcentrations of suspended sediment. *Journal of Hydraulics Division, A.S.C.E.*, 90, pp. 117-128.
- Bilotta E., Cascini L., Foresta V., Sorbino G. (2005). Geotechnical characterisation of pyroclastic soils involved in huge flowslides. *Geotechnical and Geological Engineering* (2005) 23, pp. 365–402. DOI 10.1007/s10706-004-1607-3.
- Bingham, E.C. and Green, H. (1919). Paint, a plastic material and not a viscous liquid; the measurement of its mobility and yield value. *Proc. Am. Soc. Test. Mater.*, 19, pp. 640-664.
- Bonnard CH., Forlati F., Scavia C. (2004). Identification and mitigation of large landslides risks in Europe. *IMIRILAND PROJECT – European Commission – Fifth Framework Program*. A.A. Balkema Publishers, pp. 317.
- Bovolin V. (2012). Studio idraulico dell'evento alluvionale avvenuto ad Atrani (SA) il 9 settembre 2010. Parte I: ricostruzione dell'evento. *Cooperativa Universitaria Editrice Studi, Fisciano (Italy)*, pp 54.
- Brancaccio L., Cinque A., Sgrosso I. (1978). L'analisi morfologica dei versanti come strumento per la ricostruzione degli eventi neotettonici. *Memorie della Società Geologica Italiana, Volume 19*, pp. 621 - 626.
- Brancaccio L., Cinque A., Sgrosso I. (1979). Forma e genesi di alcuni versanti di faglia in rocce carbonatiche: il riscontro naturale di un modello teorico. *Rendiconto dell'Accademia di Scienze Fisiche e Matematiche della Società Nazionale di Scienze, Lettere e Arti in Napoli, serie IV, vol. 46*, pp. 1-21.
- Bull W.B. (1964). Alluvial fans and near-subsidence in western Fresno County, California. *Geol. Surv. Prof. Pap. (U.S.) 437-A*, pp. 1-71.
- Buono A. and Milone A. (2000). Un sottile filo. *Uomo e territorio nella piana del Sarno*. Nocera Inferiore, Italy.

- Calcaterra D., De Riso R., Evangelista A., Nicotera M.V., Santo A., Scotto Di Santolo A. (2004). Slope instabilities in the pyroclastic deposits of the Carbonate Apennine and the phlegrean district (Campania, Italy). In L. Picarelli (ed.). Proceedings of the International Workshop “Occurrence and Mechanisms of Flow-like Landslides in Natural Slopes and Earthfills”, Sorrento, Italy, May 14-16, Pàtron Editore, Bologna, pp. 61-75.
- Camera M. (1999). Memorie storico-diplomatiche dell’antica città e ducato di Amalfi. Amalfi 1999, Vol. I pp. IV-683; Vol. II pp. 710-LXVIII. Ristampa anastatica.
- Cascini L., Sorbino G. (2002). Soil suction measurements over large areas: a case study. In: 3rd Intern. Conf. on Unsaturated Soils, UNSAT 2002. vol. 2, pp. 829-834.
- Cascini L. and Ferlisi S. (2003). Occurrence and consequences of flowslides: a case study. In L. Picarelli (ed.), Proceedings of the International Conference on “Fast Slope Movements – Prediction and Prevention for Risk Mitigation”, Napoli, Napoli, Italy, May 11-13, Pàtron Editore, Bologna, Vol. I, pp. 85-92.
- Cascini L. (2004). The flowslides of May 1998 in the Campania region, Italy: the scientific emergency management. *Rivista Italiana di Geotecnica*, 2: pp. 11-44.
- Cascini L. (2005 a). La gestione scientifica dell’emergenza idrogeologica del maggio 1998 nella Regione Campania. Monografia, Rubbettino Editore, pp. 278. ISBN: 88-498-0964-6.
- Cascini L. (2005 b). Risk assessment of fast landslide—From theory to practice. General Report. Proceedings of the International Conference on “Fast Slope Movements – Prediction and Prevention for Risk Mitigation”. Naples (Italy). Pàtron Editore, 2, pp. 33-52.
- Cascini, L., Bonnard, Ch., Corominas, J., Jibson, R., Montero-Olarte, J. (2005). Landslide hazard and risk zoning for urban planning and development – State of the Art report. *Landslide Risk Management*. Hungr, Fell, Couture & Eberhardt (Eds.), A.A. Balkema Publishers, pp. 199-235.
- Cascini, L. (2008). Applicability of landslide susceptibility and hazard zoning at different scales. *Engineering Geology*, 102, pp. 164-177.
- Cascini L., Cuomo S., Guida D. (2008 a). Typical source areas of May 1998 flow-like mass movements in the Campania region, Southern Italy. *Engineering Geology* 96, pp. 107–125.
- Cascini L, Ferlisi S, Vitolo E (2008 b). Individual and societal risk owing to landslides in the Campania region (southern Italy). *Georisk* 2(3), pp.125-140.
- Cascini L. (ed.) (2012). Criteri di zonazione della suscettibilità e della pericolosità da frane innescate da eventi estremi (piogge e sisma). Comoservice S.r.l., Padova.

- Cascini L., Ferlisi S., Vitolo E. (2012). La valutazione dei PsAI-Rf alla luce delle linee guida del JTC-1. In: Cascini L. (ed.), *Criteri di zonazione della suscettibilità e della pericolosità da frane innescate da eventi estremi (piogge e sisma)*. Composervice S.r.l., Padova, pp. 50-51.
- Cascini L., Sorbino G., Cuomo S., Ferlisi S. (2013 a). Seasonal effects of rainfall on the shallow pyroclastic deposits of the Campania region (southern Italy). *Landslides* DOI 10.1007/s10346-013-0395-3.
- Cascini L., Di Nocera S., Calvello M., Cuomo S., Ferlisi S., Matano F. (2013 b). Hyperconcentrated flow susceptibility analysis and zoning at medium scale: methodological approach and case study. In *Landslide Science and Practice - Vol. 1: Landslide Inventory and Susceptibility and Hazard Zoning*, pp. 395-402.
- Castellanos Abella, E.A., van Westen, C.J. (2007). Generation of a landslide risk index map for Cuba using spatial multi-criteria evaluation. In: *Landslides : journal of the International Consortium on Landslides*, 4 (2007)4, pp. 311-325.
- Catenacci V. (1992). Il dissesto geologico e geoambientale in Italia dal dopoguerra al 1990. *Memorie Descrittive della Carta Geologica d'Italia*, XLVII, pp. 1-301.
- Celentano N. (2001). Sarno. Breve storia del Fiume e della Valle, Sarno, Italy.
- Celico, F., Celico, P., De Paola, P., Fabbrocino, S., Mozzarella, A., Petrella, E., (2003). Analisi preliminare delle possibilità di utilizzazione delle risorse idriche sotterranee ai fini della mitigazione dei fenomeni di siccità. *Atti Convegno Nazionale: "La risorsa acqua: il ruolo della Geologia"*, Firenze, 24 Ottobre.
- Chen H. and Lee C.F. (2004). Geohazards of slope mass movement and its prevention in Hong Kong. *Engineering Geology*, 76: 3 – 25.
- Chen J. and Lee C.F. (2007). Landslide mobility analysis using Madflow. In: *The 2007 International Forum on Landslide Disaster Management*. Ho & Li (Eds), ISBN 978-962-7619-30-7.
- Childs E.C., Collis-George N. (1950). The permeability of porous materials. *Proc. of Royal Soc., London, England, series A*, v-200, pp. 392-405.
- Chow V.T. (1959). *Open- Channel hydraulics*. McGraw-Hill, pp. 680.
- Chow V.T., Maidment D.R., Mays L.W. (1988). *Applied Hydrology*. McGraw-Hill, pp 572.
- Christen M., Kowalski J., Bartelt P. (2010). REMMS: Numerical simulation of dense snow avalanche in three-dimensional terrain. *Cold Regions Science*.
- Christian, J. (2004). Geotechnical Engineering Reliability: How Well Do We Know What We Are Doing?. *J. Geotech. Geoenviron. Eng.*, 130(10), pp. 985–1003 and *Technology* 63, pp. 1-14.

- Cinque A., Ascione A., Caiazzo C. (2000). Distribuzione spazio-temporale e caratterizzazione della fagliazione quaternaria in Appennino meridionale. GNDT, pp 16.
- Cinque A. and Robustelli G. (2009). Alluvial and coastal hazards caused by long-range effects of Plinian eruptions: the case of the Lattari Mts. After the AD 79 eruption of the Vesuvius. In: Violante C. (ed.), *Geohazard in Rocky Coastal Areas*. The Geological Society, London, Special Publications, 322, pp. 155-171.
- Committee on Methodologies for Predicting Mudflow Areas (1982). *Selecting a Methodology for Delineating Mudslides Hazard Areas for the National Flood Insurance Program*. Nat. Res. Council, Nat. Acad. Press, Washington, D.C.
- Corominas J. (1996). The angle of reach as a mobility index for small and large landslides. *Canadian Geotechnical Journal* 33, pp. 260-271.
- Corominas J. and Moya J. (2008). A review of assessing landslide frequency for hazard zoning purposes. *Engineering Geology*, 102: pp.193-213.
- Corominas, J., Mavrouli, O., (coordinators) (2010). Overview of landslide hazard and risk assessment practices. Deliverable 2.1 of the Work Package 2.1 - Harmonization and development of procedures for quantifying landslide hazard. SafeLand Project - 7th Framework Programme Cooperation Theme 6 Environment (including climate change) Sub-Activity 6.1.3 Natural Hazards.
- Corominas J., van Westen C., Frattini P., Cascini L., Malet J. P., Fotopoulou S., Catani F., Van Den Eeckhaut M., Mavrouli O., Agliardi F., Pitiakis K., Winter M.G., Pastor M., Ferlisi S., Tofani V., Hervás J., Smith, J.T. (2013). Recommendations for the quantitative analysis of landslide risk. *Bulletin of engineering geology and the environment*, pp. 1-55.
- Costa J.E. (1988). Rheologic, geomorphic, and sedimentologic differentiation of water floods, hyperconcentrated flows, and debris flows. In: Baker VR, Kochel RC, Patton PC (eds), *Flood Geomorphology*. John Wiley and Sons, Inc., New York, pp. 113-122.
- Coussot P. (1992). *Rheology of Debris Flows - Study of Concentrated dispersions and Suspensions*. Ph.D. Thesis. INPG. Grenoble, France. (in French).
- Coussot P. and Piau J.M. (1995). The effects of an addition of force-free particles on the rheological properties of fine suspensions. *Canadian Geotechnical Journal*, 32, pp. 263-270.
- Coussot P. and Meunier M. (1996). Recognition, classification and mechanical description of debris flows. *Earth-Science reviews*, 40, pp. 209-227.
- Coussot P. (1997). *Mudflow Rheology and Dynamics*. IAHR monograph. Balkema: Rotterdam; pp. 260.

- Cronin S.J., LeCointre J.A., Palmer A.S., Neall V.E. (2000). Transformation, internal stratification, and depositional processes within a channelized, multi-peaked lahar flow. *New Zealand Journal of Geology and Geophysics*, 43 pp. 117-128.
- Crosta G., Frattini P., Sterlacchini S. (2001). Valutazione e gestione del rischio da frana. Principi e Metodi. Volume 1. Milano: Regione Lombardia e Università di Milano Bicocca.
- Crosta G.B., Dal Negro P., Frattini P. (2003). Soil slips and debris flows on terraced slopes. *Natural Hazard and Earth System Sciences*, 3, pp. 31-42.
- Crozier M. J. and Glade T. (2005). *Landslide Hazard and Risk: Issues, Concepts and Approach*, *Landslide Hazard and Risk*, John Wiley and Sons, Chichester, West Sussex, UK pp. 1-40.
- Cruden D.M., Varnes D.J. (1996). Landslide types and processes. In Turner A.K. and Schuster R.L. eds., *Landslides Investigation and Mitigation*, Transportation Research Board, US National Research Council, Special Report 247, Washington, DC pp. 36-75.
- D'Ambrosio D., Di Gregorio S., Iovine G. (2003). Simulating debris flows through a hexagonal cellular automata: SCIDDICA S3-hex. *Natural Hazards and Earth System Sciences*, vol.3, pp. 545-559.
- Dai F.C., Lee C.F., Ngai Y.Y. (2002 a) Landslide risk assessment and management: an overview. *Eng Geol* 64(1) pp. 65–87.
- Dai, C.F., Lee, C.F. (2002 b). Terrain based mapping of landslide susceptibility using a geographic information system: a case study. *Canadian Geotechnical Journal* 38, pp. 911-923.
- De Luca C, Furcolo P, Rossi F, Villani P, Vitolo C. (2010). Extreme rainfall in the Mediterranean. *Proceedings of the International Workshop on Advances in Statistical Hydrology*, 23–25 May 2010 Taormina, Italy, pp 1–11. http://www.risorseidriche.dica.unict.it/Sito_STAHY2010_web/proceedings.htm
- De Luca C. (2013). Previsione e prevenzione di eventi idrologici estremi. PhD Thesis, University of Salerno (Italy).
- Del Prete M., Giaccardi E., Trisoro-Liuzzi G. (1992). Rischio da frane intermittenti a cinematica lenta nelle aree montuose e collinari urbanizzate della Basilicata. Pubbl. n. 841 GNDICI (Gruppo Nazionale per la Difesa delle Catastrofi Idrogeologiche). Potenza: Centro nazionale delle Ricerche.
- De Natale G., Troise C., Pingue F., Mastrolorenzo G., Pappalardo L. (2006). The Somma–Vesuvius volcano (Southern Italy): Structure, dynamics and hazard evaluation. *Earth-Science Reviews* 74, pp. 73-111.
- De Roo A.P.J., Wesseling C.G., Ritsema C.J. (1996 a). LISEM: a single-event physically based hydrological and soil erosion model for drainage basins. I: theory, input and output. *Hydrological Processes* Vol. 10, pp. 1021–1025.

- De Roo A.P.J., Offermans R.J.E., Cremers H.D.T. (1996 b). LISEM: a single-event physically based hydrological and soil erosion model for drainage basins. II: sensitivity analysis, validation and application. *Hydrological Processes* Vol. 10, pp. 1119–1126.
- De Roo A.P.J. and Jetten V.G. (1999). Calibrating and validating the LISEM model for two data sets from the Netherlands and South Africa. *CATENA* 37, pp. 477- 493.
- De Vita P., Agrello D., Ambrosino F. (2006). Landslide susceptibility assessment in ash-fall pyroclastic deposits surrounding Mount Somma-Vesuvius: Application of geophysical surveys for soil thickness mapping. *Journal of Applied Geophysics* vol. 59, pp.126 -139.
- De Vita P., Napolitano E., Godt J.W., Baum R.L. (2012) Deterministic estimation of hydrological thresholds for shallow landslide initiation and slope stability models: case study from the Somma-Vesuvius area of Southern Italy. *Landslides* pp. 1-16. ISSN:1612–5118, doi:10.1007/s10346-012-0348-2.
- Donati, L., Turrini, M.C. (2002). An objective method to rank the importance of the factors predisposing landslides with the GIS methodology application to an area of the Apennines (Valneria; Perugia, Italy), *Engineering Geology*, 63 pp. 277-290.
- DRM Delegation Aux Risques Majeurs (1990). Les études préliminaires à la cartographie réglementaire des risques naturels majeurs. Secrétariat d'Etat auprès du premier Ministre chargé de l'Environnement et de la Prévention des Risques technologiques et naturels majeurs. La Documentation Française, pp. 143.
- Düzgün, H.S.B., Lacasse, S. (2005). Vulnerability and acceptable risk in integrated risk assessment framework. *Atti della Conferenza su “Landslide Risk Management”*, O. Hungr, R. Fell, R. Couture, E. Eberhardt (eds.). Taylor and Francis, London, pp. 505-515.
- Einstein H.H. (1988). Special lecture, landslide risk assessment. *Proc. 5th Int. Symp. On Landslides, Lausanne, Switzerland*. A.A. Balkema, Rotterdam, 2, pp. 1075-1090.
- Ellison W.D. (1947). Soil erosion studies, part I. *Agric Eng* 28(4) pp.145-146.
- Evans, N.C., King, J.P. (1998). The natural terrain landslide study. Debris avalanche susceptibility. Technical Note TN 1/98, Geotechnical Engineering Office, Hong Kong.
- Fell R. (1994). Landslide risk assessment and acceptable risk. *Canadian Geotechnical Journal*, 31, pp. 261-272.
- Fell R. and Hartford, D. (1997). Landslide risk management. In D.M. Cruden, R. Fell (eds.), *Landslide Risk Assessment*, Balkema, Rotterdam, pp. 51-110.
- Fell R., Ho K.K.S., Lacasse S., Leroi E. (2005). A framework for landslide risk assessment and management. State of the Art Report (SOA1). *Proceedings*

- of the International Conference on “Landslide Risk Management”, Vancouver (Canada). O. Hungr, R. Fell, R. Couture and E. Eberthardt (eds.). Taylor and Francis, London, pp. 3-25.
- Fell R., Corominas J., Bonnard C., Cascini L., Leroi E., Savage W.Z. on behalf of the JTC-1 Joint Technical Committee on Landslides and Engineered Slopes (2008). Guidelines for landslide susceptibility, hazard and risk zoning for land-use planning. *Engineering Geology* 102, pp. 85–98.
- Finlay P.J., Mostyn G.R., Fell R. (1997). Vulnerability to landsliding. *Quarterly Journal of Engineering Geology, Geotechnical Society, Toronto, Canada*, 1, pp. 307-324.
- FLO-2D: Reference manual (2009). Available at: <http://www.flo-2d.com>.
- Gagoshidze M.S. (1969). Mudflows and floods and their control. *Sov Hydrol.* 4, pp. 410-422.
- Galadini F., Meletti C., Vittori E. (2000). Stato delle conoscenze sulle faglie attive in Italia: elementi geologici di superficie. Risultati del progetto 5.1.2 “Inventario delle faglie attive e dei terremoti ad esse associabili”. GNDT, pp. 30.
- GeoSlope (2005). User’s guide. GeoStudio 2004, versione 6.13. Geo-Slope Int. Ltd, Calgary.
- Geotechnical Engineering Office (1998). Landslides and Boulder Falls from Natural Terrain: Interim Risk Guidelines. GEO Report No. 75. Geotechnical Engineering Office, The Government of the Hong Kong Special Administrative Region.
- Gerson R. (1977). Sediment transport for desert watersheds in erodible materials. *Earth Surface Processes*, 2, pp. 343-361.
- Glade T. and Crozier M.J. (2005). The nature of landslide hazard impact. In: Glade et al. (eds.), *Landslide Hazard and Risk*, John Wiley & Sons, England. Pp. 43-74.
- Govers G. (1990). Empirical relationships on the transporting capacity of overland flow. *IAHS Publ.*, pp. 189, 45-63.
- Green W.H., Ampt G.A. (1911). Studies on soil physics: Part I. The flow of air and water through soils. *J. Agric. Sci.* 4-1., pp. 1-24.
- Gutenberg B., Richter C.F. (1956). Earthquake magnitude, intensity, energy and acceleration, *Bull. Seismol. Soc. Am.* 46, pp. 105-145.
- Guzzetti F., Carrara A., Cardinali M., Reichenbach P. (1999). Landslide hazard evaluation: a review of current techniques and their application in a multi-scale study, central Italy. *Geomorphology* 31, pp. 181-216.
- Guzzetti F. (2000). Landslide fatalities and evaluation of landslide risk in Italy. *Engineering Geology*, 58, pp. 89-107.
- Guzzetti F., Stark, C.P., Salvati, P. (2005). Evaluation of flood and landslide risk to the population in Italy. *Environmental Management*, 36(1), pp. 15-36.

- Herschel W.H. and Bulkley R. (1926). Über die viskosität und Elastizität von Solen. *Am. Soc. Test. Mater.*, 26, pp. 621-633.
- Ho K.K.S., Leroi E., Roberds W.J. (2000). Quantitative risk assessment applications, myths and future direction. *Proceedings GeoEng International Conference on Geotechnical and Geological Engineering*, Melbourne, pp. 269-312.
- Holtan H.N. (1961). A Concept of Infiltration Estimates in Watershed Engineering. ARS-41-51. USDA Agricultural Research Service, pp 25.
- Hong, Y., Adler, R., Huffman, G. (2007). Use of satellite remote sensing data in the mapping of global landslide susceptibility. *Natural Hazards* 43, pp. 245-256.
- Hungr O. (1992). Runout prediction for flow-slides and avalanches: Analytical methods. In: *Proceedings of the Geotechnical and Natural Hazards Symposium, Vancouver, British Columbia* (pp 139-144). Vancouver Geotechnical Society/Canadian Geotechnical Society and Bitech Publishers, Richmond, Canada.
- Hungr O. (1997). Some methods of landslide hazard intensity mapping. In: Cruden, D., Fell, R. (Eds.), *Landslide risk assessment*. A.A. Balkema, Rotterdam, pp. 215-226.
- Hungr O., Evans S.G., Bovis M.J., Hutchinson J.N. (2001). A review of the classification of landslides of the flow type. *Environ. & Eng. Geosci.*, VII (3), pp. 221-238.
- Hungr O., Corominas J., Eberhardt E. (2005). Estimating landslide motion mechanism, travel distance and velocity – State of the Art report. *Landslide Risk Management*. Hungr, Fell, Couture & Eberhardt (Eds.), A.A. Balkema Publishers, pp. 99-128.
- Hungr O., and McDougall S. (2009). Two numerical models for landslide dynamic analysis. *Computers & Geosciences* 35, pp. 978-992.
- Hungr O., Leroueil S., Picarelli L. (2012). Varnes classification of landslide types, an update. In: Eberhardt E, Froesse C, TurnerAK, Leroueil S (eds) *Landslides and engineered slopes: protecting society through improved understanding*, vol 1. CRC Press, Boca Raton, pp. 47–58.
- Hutchinson J.N. (1986). A sliding-consolidation model for flow slides. *Canadian Geotechnical Journal* 23, pp. 115-126.
- Hutchinson J.N. (1988). Morphological and Geotechnical parameters of Landslides in relation to Geology and Hydrogeology. State of the art Report. *Proc. V Int. Symposium on Landslides*, 1, pp. 3-35, Lausanne.
- Hutchinson J.N. (2003). Review of flow-like mass movements in granular and fine-grained materials. *Proc. of the Int. Workshop “Flows 2003 - Occurrence and Mechanisms of Flows in Natural Slopes and Earthfill”*, pp. 3-16, Sorrento.

- IUGS (1997). Quantitative risk assessment for slopes and landslides – the state of the art. IUGS working group on landslides, committee on risk assessment. Cruden and Fell (eds.), *Landslide Risk Assessment, Proceedings of the International Workshop on Landslide Risk Assessment*, Hawaii. Balkema, Rotterdam, pp. 3-12.
- Iverson R.M. (2005). Debris-flow mechanics. In: Jakob, M., Hungr, O. (Eds.), *Debris-flow Hazards and Related Phenomena*. Springer, Berlin, pp. 105-134.
- Jakob M. (2005). Debris-flow hazard analysis. In: Jakob, M., Hungr, O. (Eds.), *Debris-flow Hazards and Related Phenomena*. Springer, Berlin, pp. 411-443.
- Jakob M., McDougall S., Weatherly H., Ripley N. (2013 a). Debris-flow simulations on Cheekye River, British Columbia. *Landslide* Vol. 10, Issue 6, pp. 685-699.
- Jakob M, Holm K, Weatherly H, Liu S, Ripley N (2013 b) Debris flood risk assessment for Mosquito Creek, British Columbia, Canada. *Natural Hazards* 65(3): 1653-1681.
- Jetten V. (2002). LISEM user manual, version 2.x. Draft version January 2002. Utrecht. Centre for Environment and Landscape Dynamics, Utrecht University, The Netherlands. pp 48.
- Johnson A.M. (1970). *Physical Processes in Geology*. Freeman, Cooper, San Francisco.
- Jonkman S.N., Vrijling J.K., Vrouwenvelder A.C.W.M. (2008). Methods for the estimation of loss of life due to floods: a literature review and a proposal for a new method. *Natural Hazards* 46(3), pp. 353-389.
- Julien P. and Lan Y. (1991). Rheology of hyperconcentrations, *J. Hydrol. Eng.*, 117(3), pp. 346-353.
- Kaynia, A.M., Papatoma-Köhle, M., Neuhäuser, B., Ratzinger, K., Wenzel, H., Medina-Cetina, Z. (2008). Probabilistic assessment of vulnerability to landslide: Application to the village of Lichtenstein, Baden-Württemberg, Germany. *Engineering Geology* 101, pp. 33-48.
- Kelfoun K. and Druitt T.H. (2005). Numerical modeling of the emplacement of Socompa rock avalanche, Chile *J Geophys Res* 110: B 12202.1-12202.13 DOI:10.1029/2005JB003758.
- Knisel W. G. (1980). CREAMS: A field-scale models for Chemicals, Runoff and Erosion from Agricultural Management Systems, *Report No. 26*. U.S. Department of Agriculture, Washington, D.C.
- Kostaschuk R., James T., Rishi R. (2003). Suspended sediment transport during tropical cyclone floods in Fiji. *Hydrological Processes*, 17 pp. 1149-1164.
- Kurdir R.D. (1973). Classification of mudflows. *Sov. Hydrol.* 4, pp. 310-316.
- Kwan J.S.H. and Sun H.W. (2006). An improved landslide mobility model. *Canadian Geotechnical Journal*, vol. 43, pp. 531-539.
- Lane L.J., Nearing M.A., Laflen J.M., Foster G.R., Nichols M.H. (1992). Description of the US Department of Agriculture Water Erosion Prediction

- Project (WEPP) Model. In Parsons A. J. and Abrahams A. D. (Eds), *Overland Flow: Hydraulics and Erosion Mechanics*, UCL Press Limited, London. pp. 377-391.
- Laronne J.b., Reid I., Yitshak Y., Frostick L.E. (1994). The non-layering of gravel streambeds under ephemeral flood regimes. *Journal Of Hydrology*, 159 pp. 353-363.
- Lateltin O. (1997). Recommandations: prise en compte des dangers dus aux mouvements de terrain dans le cadres des activités de l'aménagement du territoire. OFAT, OFEE and OFEFP. Switzerland, pp 42.
- Lateltin O. (2002). Landslides, land-use planning and risk management: Switzerland as a case study. In: McInnes, R., Jakeways, J. (Eds.), *Instability Planning and Management*. Thomas Telford, pp. 89-96.
- Lawson D.E. (1982). Mobilization, movement and deposition of active subaerial sediment flows, Matanuska Glacier, Alaska. *J. Geol.* 90, pp. 279-300.
- Lee E.M. and Jones D.K.C. (2004). *Landslide Risk Assessment*. Thomas Telford Publishing, London.
- Lehmann O. (1933). Morphologische Theorie der Verwitterung von Steinschlagwänden. *Vierteljahrsschrift der Naturforschende Gesellschaft in Zurich*, 87, pp. 83-236.
- Leroi E. (1997). Landslide risk mapping: Problems, limitations and developments. In: D.M. Cruden and R. Fell (Editors), *Landslide risk assessment – Proceedings of the Workshop on Landslide Risk Assessment*. Honolulu, Hawaii, USA. Balkema, Rotterdam, pp. 239-249.
- Leroi E., Bonnard Ch., Fell R., McInnes R. (2005). Risk assessment and management – State of the Art report. *Proceeding of the International Conference on Landslide Risk Management*. Hungr, Fell, Couture & Eberhardt (Eds.), A.A. Balkema Publishers, pp. 159-198.
- Leroueil S., Vaunat J., Picarelli L., Locat J., Faure R. (1996). Geotechnical characterization of slope movements. *Proc. VII Int. Symp. on Landslides*; pp. 53-74. Trondheim.
- Li R.M. (1979). Water and sediment routing from watersheds. In: Shen, H.W. Ed., *Modeling of Rivers*, Chap. 9. Wiley.
- Linden D.R., Van Doren D.M., Jr., Allmaras R.R. (1988). A model of the effects of tillage-induced soil surface roughness on erosion. *Proceedings of the 11th International Conference of the International Soil Tillage Research Organisation*, Edinburgh, Vol. 1, pp. 373-378.
- Maizels J. (1989). Sedimentology, paleoflow dynamics and flood history of jökulhlaup deposits: Paleohydrology of Holocene sediment sequences in southern Iceland sandur deposits. *Journal of Sedimentary Petrology*, 59, pp. 204-223.

- Major J.J. and Pierson T.C. (1992). Debris flow rheology: Experimental analysis of fine-grained slurries. *Water Resour. Res.*, 28 pp. 841-857.
- Major J.J., Janda R.J., and Daag A.S. (1996). Wareshed disturbance and lahars on the east side of Mount Pinatubo during the mid-June 1991 eruptions. In: C.G. Newhall, and R.S. Punungbayan (eds), *Fire and Mud: Eruptions and Lahars of Mount Pinatubo, Philippines* pp. 895-919. Philippines Institute of Vulcanology and Seismology, Quezon City and University of Washington Press, Seattle.
- Major J.J., Iverson R.M., McTigue D.F., Macias S., Fiedorowicz B.K. (1997). Geotechnical properties of debris-flow sediments and slurries, in Chen, C.L., ed., *Debris-flow hazards mitigation: mechanics, prediction, and assessment: American Society of Civil Engineers, Proceedings of First International Conference, August 7-9, San Francisco*, pp. 249-259.
- Malet J.-P., Remaître A., Maquaire O. (2004). Runout modeling and extension of the threatened area associated with muddy debris flows. *Geomorphologie: relief, processus, environment* n.3, pp. 195-210.
- Malet J.-P., Thiery Y., Puissant A., Hervás J., Günther A., Grandjean G. (2009). Landslide susceptibility mapping at 1:1M scale over France: exploratory results with a heuristic model. In: Malet, J.-P., Remaître, A., Boogard, T. (Eds), *Proc. International Conference on Landslide Processes: from Geomorphologic Mapping to Dynamic Modelling, 6 -7 February 2009, Strasbourg, France*. CERG Editions, Strasbourg, pp. 315-320.
- Mansi L. (1912). *Cenni storici della città di Scala, Salerno, Italy*.
- Marciani, F. (1930). *Per la bonifica integrale dell'Agro Nocerino. Relazione presentata a S.E. il Prefetto di Salerno. 16.3.1930, Salerno 1930* (in "Il Picentino", giugno 1931) [BNN Misc B 42(24)].
- Martino R. (2003). Experimental analysis on the rheological properties of a debris flow deposit. *Proceedings of the 3rd International Conference on Debris-Flow Hazards Mitigation: Mechanics, Prediction, and Assessment, Davos, Switzerland*.
- Martino R. and Papa M. (2008). Variable-Concentration and Boundary Effects on Debris Flow Discharge Predictions. *J. Hydraul. Eng.*, 134(9), pp. 1294-1301.
- Mazza G. and Amendola E. (1999). *Storia liquida. Alluvioni e sistemazione idraulicomontana a Sarno dalla fine del '700 agli inizi del '900, Sarno, Italy*.
- Medina V., Hürlimann M., Bateman A. (2008). Application of FLATModel, a 2D finite volume code, to debris flows in the northeastern part of the Iberian Peninsula. *Landslides* 5, pp. 127-142.
- Migale L.S. (1998). *Eventi franosi della Costiera Amalfitana nel XIX secolo, MSc. Thesis, University of Salerno, Italy*.

- Migale L.S. and Milone A. (1998). Colate di fango in terreni piroclastici della Campania. Primi dati della ricerca storica. *Rassegna Storica Salernitana*, n.s., XV/2, n. 30, December, pp. 235-271.
- Montgomery D.R. and Dietrich W.E. (1994). A physically based model for the topographic control on shallow landsliding. *Water Resources Research*, 30 pp. 153-1171.
- Moore I.D. and Foster G.R. (1990). Hydraulics and overland flow. In Anderson, M. G. and Burt, T. P. (Eds) *Process Studies in Hillslope Hydrology*. John Wiley & Sons, Chichester. pp. 215-254.
- Morgan R.P.C., Quinton J.N., Rickson R. J. (1992). *EUROSEM Documentation Manual. Version I : June 1992*. Silsoe College, Silsoe.
- Morgan R.P.C. (1994). The European Soil Erosion Model an update on its structure and research base. In Rickson, R. J. (Ed.), *Conserving Soil Resources: European Perspectives*. CAB International, Cambridge. pp. 286-299.
- Morgenstern N.R. and Price V.E. (1965). The Analysis of the Stability of General Slip Surfaces. *Geotechnique*, Vol. 15, No. 1, pp. 79-93.
- Mostyn G.R. and Fell R. (1997). Quantitative and semiquantitative estimation of probability of landsliding. In: Cruden, D., Fell, R. (Eds.), *Landslide risk assessment*. A.A. Balkema, Rotterdam, pp. 297-315.
- Nadim, F., Einstein, H., Roberds, W. (2005). Probabilistic stability analysis for individual slopes in soil and rock – State of the Art report. *Landslide Risk Management*. Hungr, Fell, Couture & Eberhardt (Eds.), A.A. Balkema Publishers, pp. 63-98.
- Nadim, F., Kjekstad O., Peduzzi P., Herold C., Jaedicke C. (2006). Global landslide and avalanche hotspots. *Landslides*, Vol. 3, No. 2, pp. 159-174.
- Nadim, F., Kjekstad, O. (2009). Assessment of Global High-Risk Landslide Disaster Hotspots. In: Sassa, K., Canuti, P. (Eds.), *Landslides - Disaster Risk Reduction*. Springer, pp. 213-221.
- Napolitano R., Altobelli A., Feoli E., Bressan E. (2006). Stima della biomassa verde in diverse tipologie forestali del Friuli Venezia Giulia attraverso il satellite MODIS e misure indirette in campo di LAI. In *Ecologia. Atti del XV Congresso Nazionale della Società Italiana di Ecologia (Torino, 12-14 settembre 2005)* a cura di Claudio Comoglio, Elena Comino, e Francesca Bona.
- O'Brien, J.S. and Julien, P.Y. (1985). Physical processes of hyperconcentrated sediment flows. *Proc. of the ASCE Specialty Conf. on the Delineation of Landslides, Floods, and Debris Flow Hazards in Utah*, Utah Water Research Laboratory, Series UWRL/g-85/03, pp. 260-279.
- O'Brien, J.S. and Julien, P.Y. (1988). Laboratory analysis of mudflows properties. *J. Hydraul. Eng.*, I 14: 8777887.

- O' Brien J.S., Julien P.Y., Fullerton W.T. (1993). Two-dimensional water flood and mudflow simulation. *Journal of Hydraulic Engineering*, 119(2), pp. 244-261.
- O' Connor J.E., Hardison J.H. 3rd, Costa J.E. (2002). Debris flows from failure of neoglacial-age moraine dams in the Three Sisters and Mount Jefferson Wilderness areas, Oregon (USGS Professional Paper 1606, 93 pp.) US Geological Survey, reston, VA.
- Onstad C.A. (1984). Depressional storage on tilled soil surfaces. *Transactions of the ASAE* 27, pp. 729-732.
- Overton D.E. (1965). Mathematical refinement of an infiltration equation for watershed engineering. ARS-41- 99. Agricultural Research Service, U.S.D.A. pp 11.
- Papa M.N., Trentini G., Carbone A., Gallo A. (2011). An integrated approach for debris flow hazard assessment - a case study on the Amalfi coast - Campania, Italy. In: Genevois R, Douglas L. Hamilton DL, Alberto Prestininzi A. *Proceedings of the 5th International Conference on Debris-Flow Hazards Mitigation, Mechanics, Prediction and Assessment*. La Sapienza, Roma, pp. 983-992.
- Park S.W., Mitchell J.K., Bubenzer G.D. (1982). Splash erosion modeling: physical analyses. *Trans Am Soc Agric Eng* 25, pp. 357-361.
- Pastor M., Haddad B., Sorbino G., Cuomo S., Drempetic V. (2009). A depth-integrated, coupled SPH model for flow-like landslides and related phenomena. *Int. J. Numer. Anal. Meth. Geomech.* 33, pp. 143-172.
- Picarelli L., Oboni F., Evans S.G., Mostyn G., Fell, R. (2005). Hazard characterization and quantification. In: Hungr, O., Fell, R., Couture, R., Eberhardt, E. (Eds.), *Landslide Risk Management*. Taylor and Francis, London, pp. 27-61
- Pierson T.C. and Scott K.M.(1985). Downstream dilution of a lahar: transition from debris flow to hyperconcentrated streamflow. *Water Resources Research*, 21 pp. 1511-1524.
- Pierson T.C. (1986). Flow behavior of channalized debris flows, Mount St. Helens, Washington. In: A.D. Abrahams (ed.), *Hillslope Processes*, pp. 269-296. Allen & Unwin, Boston.
- Pierson T.C., Daag A.S., delos Reyes P.J., Regalado M.T.M., Solidum R., and Tubianosa B.S. (1996). Flow and deposition of posteruption hot lahars on the east side of Mount pinatubo, July-October 1991. In: C.G. Newhall, and R.S. Punungbayan (eds), *Fire and Mud: Eruptions and Lahars of Mount Pinatubo, Philippines* pp. 921-950. Philippines Institute of Vulcanology and Seismology, Quezon City and University of Washington Press, Seattle.
- Pierson T.C. (2005). Hyperconcentrated flow - transitional process between water flow and debris flow. In: Jakob, M., Hungr, O. (Eds.), *Debris-flow Hazards and Related Phenomena*. Springer, Berlin, pp. 159-202.

- Pirulli M. and Mangeney A. (2008). Results of back-analysis of the propagation of rock avalanches as a function of the assumed rheology. *Rock Mechanics and Rock Engineering*, 41 (1), pp 59-84.
- Pirulli M. and Sorbino G. (2008). Assessing potential debris flow runout: a comparison of two simulation models, *Natural Hazards and Earth System Sciences*, Vol. 8, pp. 961-971.
- Phillips, C.J. and Davies. T.R.H.. (1991). Determining rheological parameters of debris flow material. *Geomorphology*, 4, pp. 101-110.
- Pisciotta, G. (2008). Physical vulnerability of elements at risk in landslide prone areas. PhD Thesis, University of Salerno (Italy).
- Pitman B.E. and Le L. (2005). A two-fluid model for avalanche and debris flow. *Phil. Trans. R. Soc. A*. 363, pp. 1573-1601.
- Poisel R. and Preh H. (2007). Landslide detachment mechanisms. An overview of their mechanical models. In: *The 2007 International Forum on Landslide Disaster Management*. Ho & Li (Eds), ISBN 978-962-7619-30-7.
- Quan Luna B. (2012). Dynamic numerical run - out modelling for quantitative landslide risk assessment. Enschede, University of Twente Faculty of Geo-Information and Earth Observation (ITC). ITC Dissertation 206, ISBN: 978-90-6164-330-2.
- Rauws G. and Govers G. (1988). Hydraulic and soil mechanical aspects of rill generation on agricultural soils. *J. Soil Sci.*, 39, pp. 111 -124
- Reale O, Atlas R. (2001). Tropical cyclone-like vortices in the extratropics: observational evidence and synoptic analysis. *Weather Forecast* 16(1), pp. 7-34.
- Remondo, J., Bonachea, J., Cendrero, A. (2005). A statistical approach to landslide risk modelling at basin scale: from landslide susceptibility to quantitative risk assessment. *Landslides* 2, pp. 321-328.
- Renard K.G., Foster G.R., Weesies G.A., McCool D.K., Yoder D.C. coordinators (1997). *Predicting Soil Erosion By Water: A Guide to Conservation Planning with the Revised Universal Soil Loss Equation (RUSLE)*, 1997. US Department of Agriculture, Agriculture Handbook No. 703, pp 404.
- Richards L.A. (1931). Capillary conduction of liquids in porous mediums. *Physics*, vol. 1 (5), pp 318-333.
- Rickenmann D. (1999). Empirical relationships for debris flows. *Natural Hazards*, 19, pp. 47-77.
- Rickenmann M. (2005). Runout prediction methods. In: Jakob, M., Hungr, O. (Eds.), *Debris-flow Hazards and Related Phenomena*. Springer, Berlin, pp. 305-324.
- Roberds W. (2005). Estimating temporal and spatial variability and vulnerability. In: Hungr O, Fell R, Couture R, Eberhardt E (eds) *Landslide Risk Management*. Taylor and Francis, London, pp. 129-157.

- Rodolfo K.S., Umbal J.V., Alonso R.A., Remotigue C.T., Paladio-Melosantos M.L., Salvador J.H.G., Evangelista D., Miller Y. (1991). Two years of lahars on the western flank of Mount Pinatubo: Initiation, flow processes, deposits, and attendant geomorphic and hydraulic changes. In: C.G. Newhall, and R.S. Punungbayan (eds), *Fire and Mud: Eruptions and Lahars of Mount Pinatubo, Philippines* pp. 989-1013. Philippines Institute of Vulcanology and Seismology, Quezon City and University of Washington Press, Seattle.
- Rolandi G. (1997). The eruptive history of Somma-Vesuvius. In Cortini M. & De Vivo (eds.). *Volcanism and Archaeology in Mediterranean Area*, pp. 77-78.
- Rolandi G., Paone A., Di Lascio M., Stefani G. (2007). The 79 AD eruption of Somma: The relationship between the date of the eruption and the southeast tephra dispersion. *Journal of Volcanology and Geothermal Research* 169, pp. 87–98.
- Rossi F. and Villani P. (1995). Flood evaluation in Campania Region, Department of Civil Engineering, University of Salerno, GNDICI-CNR, Pubbl. N. 1470, 1995. (in Italian).
- SafeLand Deliverable D2.6 (2011). Methodology for evaluation of the socio-economic impact of landslides (societal vulnerability). Edited for the EU-funded SafeLand Project by Eidsvig U, McLean A, Kalsnes B and Vangelsten BV. Available at <http://www.safeland-fp7.eu>.
- SafeLand Deliverable D5.4 (2011). Quantification of uncertainties in the risk assessment and management process. Edited for the EU-funded SafeLand Project by Narasimhan H. and Faber M. Available at <http://www.safeland-fp7.eu>.
- SafeLand Deliverable D5.7 (2011). Design and testing: a risk communication strategy and a deliberative process for choosing a set of mitigation and prevention measures. Edited for the EU-funded SafeLand Project by Scolobig A and Bayer J. Available at <http://www.safeland-fp7.eu>.
- Sanglerat, G., Olivari, G. et Cambou, B. (1980). *Problèmes pratiques de mécanique des sols et de fondations* (Tomes 1 et 2); Dunod.
- Sassa K. (1985). The mechanism of debris flows. In *Proceedings 11th International Conference on oil Mechanics and Foundation Engineering*, San Francisco, Vol 1, pp. 1173-1176.
- Sassa K. and Wang F. (2000). A modified geotechnical simulation model for the areal prediction of landslide motion. *Annuals of Disas. Prev. Res. Inst.*, Kyoto Univ., No. 43 B-1.
- Savage W.Z., Godt J.W., Baum R.L. (2004). “Modeling time-dependent areal slope stability”. In: Lacerda WA, Erlich M, Fontoura SAB, Sayao ASF, (eds) *Landslides – Evaluation and Stabilization Proceedings of the 9th*

- International Symposium on Landslides, vol. 1 Balkema, Rotterdam, pp. 23-36.
- Scandone R., Giacomelli L., Fattori Speranza F. (2008). Persistent activity and violent strombolian eruptions at Vesuvius between 1631 and 1944. *Journal of Volcanology and Geothermal Research* 170, pp. 167-180.
- Schmidt J., Von Werner M., Michael A. (1999). Application of the EROSION3D model to the Catsopwatershed, The Netherlands. *CATENA* 37, pp. 449–456.
- Smith, R.E. (1981). A kinematic model for surface mine sediment yield. *Trans. ASAE*, 24, pp. 1508-1514.
- Soeters, R. and van Westen, C.J. (1996). Slope instability recognition, analysis and zonation. In: Turner, A.K., Schuster, R.L. (Eds.), *Landslides Investigation and Mitigation*. TRB Special Report 247. National Academy Press, Washington D.C., pp. 129–177.
- Sorbino G. and Foresta V. (2002). Unsaturated hydraulic characteristics of pyroclastic soils. In Juca, de Campos, Marinho Eds. *Unsaturated Soils*, pp. 405-410 , . ISBN:9058093719 ID:1002043.
- Sorbino G. and Foresta V. (2012). Personal communication.
- State Archive of Salerno. (2000). *Montagna assassina o vittima? Per una storia del territorio e delle alluvioni di Bracigliano, Quindici, Sarno e Siano (1756-1997)*, Salerno, Italy. A cura di Aversano V. e Ruggiero G..
- Svendsen J., Stollhofen H., Krapf C.B.E., Stanistreet I.G.(2003). Mass and hyperconcentrated flow deposits record, dune damming and catastrophic breakthrough of ephemeral rivers, Skeleton Coast Erg, Namibia. *Sedimentary Geology*, 160, pp. 7-31.
- Swanston, D. N. 1974. Slope stability problems associated with timber harvesting in mountainous regions of the western United States. Gen. Tech. Rep. PNW-21. Portland, OR: U.S. Department of Agriculture, Forest Service, Pacific Northwest Forest and Range Experiment Station. pp 14.
- Takahashi T. (1991). *Debris Flow (IAHR Monograph Series, pp. 165)*. International Association for Hydraulic Research, Ecole Polytechnique Fédérale, Lausanne, Switzerland and A.A. Balkema, Rotterdam.
- Taylor, D.W. (1948). *Fundamentals of Soil Mechanics*: New York, Wiley, pp. 700.
- Tropeano R, Furcolo P, Guida D, Rossi F, Villani P. (2005). The effect of orography on extreme rainfall: a simplified meteo-morphological model. *Geophysical Research Abstracts*, SRef-ID: 1607-7962/gra/EGU05-A-10298, Vol. 7.
- Unità Operativa 2.38. (1998). *Ricerca storica sulle colate di fango in terreni piroclastici della Campania*, G.N.D.C.I.-C.N.R. - Università di Salerno.

- Uzielli M., Nadim F., Lacasse S., Kaynia A.M. (2008). A conceptual framework for quantitative estimation of physical vulnerability to landslides. *Engineering Geology* 102, pp.251–256.
- Van Asch Th. W. J., Malet J.-P., van Beek L. P. H., and Ami-trano, D. (2007). Techniques, advances, problems and issues in numerical modelling of landslide hazard, *B. Soc. Geol. Fr.*, 178, pp. 65-88.
- Van Westen, C.J. (2004). Geo-information tools for landslide risk assessment: an overview of recent developments. In: Lacerda, W.A., Ehrlich, M., Fontoura, S.A.B., Sayão, A.S.F. (Eds.), *Proceedings 9th International Symposium on Landslides, Rio de Janeiro, Brasil, Vol. 1*. Balkema, pp. 39-56.
- Van Westen C.J., Van Asch T.W.J., Soeters R. (2006). Landslide hazard and risk zonation - why is still so difficult? *Bulletin of Engineering Geology and the Environment* 65, pp. 167-184.
- Van Westen C. J., Castellanos E., Kuriakose S. L. (2008). Spatial data for landslide susceptibility, hazard, and vulnerability assessment: An overview, *Eng. Geol.*, 102, pp. 112-131.
- Varnes D.J. (1978). Slope movements types and processes. *Landslides: analysis and Control*. Transportation Research Board, Nat. Acad. of Sciences, Transp. Res. Board, Washington, Special Report, 76, pp. 11-35.
- Varnes D.J. (1984). Landslide hazard zonation: A review of principles and practice. *The International Association of Engineering Geology Commission on Landslides and Other Mass Movements 1984. Natural Hazards*, pp. 3-63. Paris, France. UNESCO.
- Vitolo E. (2009). *Analisi degli effetti indotti dai fenomeni franosi di flusso rapido*. PhD Thesis, University of Salerno (Italy).
- Voellmy A. (1955). *Über die Zerstörungskraft von Lawinen (on breaking force of avalanches)*. *Schweizerische Bauzeitung* 73, pp. 212-285.
- Wang Z., Larsen P., Xiang W. (1994). Rheological properties of sediment suspensions and their implications. *J. Hydraul. Res.*, 32, pp. 560-580.
- Whipple K. and Dunne T. (1992). The influence of debris-flow rheology on fan morphology, Owens Valley, California. *Geol. Soc. Am. Bull.*, 104, pp. 887-900.
- Wong H.N., Ho K.K.S., Chan Y.C. (1997). Assessment of consequence of landslides. *Proceedings of the International Workshop on Landslide Risk Assessment, Honolulu, Hawaii, USA*, pp. 111- 149.
- Wong H.N. (2005). Landslide risk assessment for individual facilities. *State of the Art Report (SOA1)*. *Proceedings of the International Conference on "Landslide Risk Management"*, Vancouver (Canada). O. Hungr, R. Fell, R. Couture and E. Eberthardt (eds.). Taylor and Francis, London, pp. 237-296.

- Woolhiser D.A., Smith R.E., Goodrich D.C. (1990). KINEROS: A kinematic runoff and erosion model: documentation and user manual. *USDA-ARS, ARS-77*.
- Young R.A., Onstad C.A., Bosch D.D., Anderson W.P. (1989). AGNPS: A nonpoint source pollution model for evaluating agricultural watersheds. *J. Soil War. Conserv.*, 44, pp. 168-173.